Novel Biopolymers for the Activation and Expansion of T-cells: Towards 3D Scaffolds for Cell Therapy

A Thesis Submitted to University College London for the Degree of

Doctor of Engineering

by

Rebecca Gunn

Department of Biochemical Engineering

University College London

August 2022

Declaration

I, Rebecca Gunn, confirm that the work presented in this thesis is my own. Where information has been derived from other sources, I confirm that this has been indicated in the thesis.

Rebecca Gunn

August 2022

Abstract

Chimeric Antigen Receptor (CAR) T-cell therapy is an emerging immunotherapy that exhibits promising results against haematological malignancies. Activation is a crucial step in the manufacturing as it renders T-cells susceptible to transduction, initiates expansion, and the development of effector functions. *Ex vivo* activation is achieved through stimulation of the T-cell receptor complex and co-stimulation, typically provided by anti-CD3 and anti-CD28 antibodies. Antibody coated magnetic beads are currently the most common activation technology, however, they require an additional process step for removal and release testing for residual beads. Furthermore, the beads are expensive, non-biodegradable, and evidence suggests that they are not optimal for antibody presentation due to aggregation. SpheriTech's biopolymers are low-cost peptide-based polymers that can be cast into a 3D porous structure to which anti-CD3 and anti-CD28 can be bound. The porous structure allows T-cells to be passed through, eliminating the need for a removal step and increasing the surface area for antibody presentation.

This thesis aimed to establish SpheriTech's biopolymer as an alternative manufacturing option. Fundamental characterisation and initial proof-of-concept studies of two iterations of SpheriTech's biopolymers are presented; termed polymer A and B. Characterisation included structural characterisation, antibody distribution, and biocompatibility. The first polymer was found to possess a macro-porous structure with a median pore diameter of 7.8 ± 0.2 µm, when produced at densities of 0.04 to 0.07 g/cm^3; and polymer B was found to possess a super-macro-porous structure with a median pore diameter of 134 µm. aCD3 and aCD28 were successfully attached to both polymers and confirmed with fluorescence imaging. T-cell cultures stimulated with aCD3/aCD38 polymer A displayed a 19 % population expression of activation marker, CD69, 24 hours post-stimulation. Though polymer A demonstrated the potential for T-cell activation; it was limited by a low cell recovery of T-cells (51 %) from the structure.

Polymer B was subsequently investigated and exhibited an improved cell recovery of 97 %. Activation and expansion of primary human T-cells were demonstrated with polymer B in both a non-porous and a porous 3D scaffold format. T-cell cultures stimulated with non-porous aCD3/aCD28 polymer B

resulted in a 27 and 44 % expression of activation markers CD25 and CD69, respectively, 3 days post-stimulation. Stimulation resulted in an 8.3-fold expansion with > 90 % viability over 14 days, which was comparable to Dynabeads. Expanded T-cell populations were found to be skewed towards $CD8^+$ T-cells (CD4:CD8 ratio of 0.72), and exhibited a 3.6 % decrease in the expression of exhaustion marker, PD-1, than when activated with Dynabeads. The dominant sub-populations of $CD4^+$ and $CD8^+$ T-cells were found to be T_{EM} (40 %) and T_{CM} (38 %), respectively.

T-cell cultures expanded with a porous aCD3/aCD28 polymer B scaffold resulted in an 11-fold expansion with a viability of 88 % after 14 days. Expanded T-cell populations had a CD4:CD8 ratio of 1.2 and consisted predominantly of clinically relevant T_{CM} (50 - 84 %) within both $CD8^+$ and $CD4^+$ populations. Stimulation of T-cells with the polymer scaffold was found to induce IFNγ secretion, indicating the expansion of T-cells with an advantageous cytotoxic function. Hence, this thesis has demonstrated the proof-of-concept of a novel T-cell activation and expansion technology using SpheriTech's biopolymer matrices.

Impact Statement

Immunotherapy has become an important fourth pillar of cancer treatment, alongside surgery, chemotherapy, and radiotherapy. Significant therapies include chimeric antigen receptor (CAR) T-cells, which are T-cells that express a synthetic receptor which recognises and targets cancer. The manufacture of CAR T-cells entails removal of a patients T-cells, gene transfer, expansion, and re-infusion. T-cell activation is crucial as it renders T-cells susceptible to gene transfer, and initiates proliferation and the differentiation of resting T-cells into active sub-populations. Currently, activation in commercial manufacturing is dominated by the use of antibody-coated magnetic beads. These beads, however, present a significant cost through their requirement for additional process steps for removal and release testing for residual beads. Additionally, beads are not biodegradable and antibody presentation is not optimal due to aggregation.

This thesis aimed to address these shortcomings through the development of a low-cost peptide-based biopolymer as an alternative activation technology. The presented work has potential impacts within T-cell therapy manufacturing, with subsequent impacts in public health through improving accessibility by reducing costs, and improving the sustainability of production; as well as direct impacts within academia and the collaborating company, SpheriTech.

The current cost of CAR T-cell therapies is ~ £300,000 per dose. Lowering this cost is of upmost importance to improve the accessibility of T-cell therapies. Costs incurred during the manufacturing process contribute substantially to the final price and so a great focus has been placed on the optimisation of the manufacturing process to reduce the high cost. The ability to produce and utilise a polymer-based activation and expansion technology in a 3D porous format is envisaged to allow integration into a closed-automated process in which T-cells can be seeded, activated, expanded, and removed by flowing a cell suspension, media, or buffer through the polymer. This would reduce the number of open manual steps in the process, therefore reducing the risk of contamination and streamlining the manufacturing process. Removing the use of Dynabeads would also improve the process through the mitigation of a time-consuming bead-

removal step and the need for residual bead testing in the final product; allowing faster manufacturing and product release, and driving down costs.

There is also much interest in expanding specific T-cell populations to further improve therapy efficacy and cost effectiveness. Given the observed effect of activation with polymers in this thesis to impact resultant populations, these polymer technologies may have applications in controlling T-cell populations. Furthermore, the customisability of ligands that could be attached will allow stimulation signals to be adjusted and fine-tuned for further studies in this regard.

Furthermore, polymers are produced from poly-ε-lysine which is bio-degradable and of natural origin, in contrast to polystyrene coated beads - which are the current gold-standard activation technology. Hence, adoption of this technology would also improve sustainability of the manufacturing process as the use of non-biodegradable beads would be removed and replaced with a technology that can be broken down more readily into its natural components.

The 3D scaffold format explored in this thesis is not one that has been widely explored for T-cell activation and expansion, particularly for cell therapy applications. Therefore, the outputs of these studies provide important contributions to the limited body of literature in this field. This includes methods for live cell imaging of T-cells within a scaffold which could be implemented with other scaffolds with auto-fluorescent properties.

The knowledge gained whilst characterising and assessing the biopolymers described in this thesis is of direct importance to the industrial partner, SpheriTech, as it has allowed them to further characterise their polymer portfolio both materially and when applied practically in cell culture. The work undertaken here has demonstrated the feasibility of using their biopolymer in culture with primary human T-cells as an activation and expansion platform, which is an avenue of great interest. Furthermore, it has highlighted areas of inconsistency to be improved in the production process, such as the attachment of antibodies to the polymer. This knowledge will also be of importance to future collaborators of SpheriTech who may work with these polymers. Further, the work presented in this thesis provides a proof-of concept foundation on which future studies by SpheriTech may optimise and scale-up this activation technology.

Acknowledgements

There are endless amounts of people whom I should acknowledge for supporting me throughout this EngD journey, both academically and personally; in an attempt to be brief (believe it or not!) the list here is undoubtedly incomplete.

I am extremely grateful to have been given the opportunity to undertake an EngD and for this, I first and foremost have to thank my initial primary supervisor - Dr. Farlan Veraitch, and my industrial supervisor - Dr. Don Wellings. Thank you for your belief, support, and invaluable guidance and expertise. I would also like to thank Dr. Kenth Gustafsson, who took over as my primary supervisor in 2019, I'll be forever grateful for you taking me under your wing and providing me with the same level of invaluable guidance and support as before. I'd also like to take this opportunity to thank Prof. Dan Bracewell, my secondary supervisor. Though our interactions were few, each one contributed valuable input to the project and support was always there when I needed it.

I would like to thank the Engineering and Physical Sciences Research Council (EPSRC) and SpheriTech Ltd. for funding this research. Additionally, further thanks are owed to SpheriTech Ltd. for sharing their knowledge and portfolio of biomaterials, and for providing me with research materials. In particular I'd like to thank again Dr. Don Wellings, and Dr. Andy Gallagher, for welcoming me warmly on my visits and for your patience in teaching me.

This research was only made possible by tapping into the knowledge and skills of many amazing and talented people who I would like to thank greatly for giving me their time. Firstly, a special thanks goes to Ms. Ludmila Ruban for training me in cell culture and supporting me endlessly throughout my research. I would like to thank Dr. Dale Moulding for training and assistance with fluorescence microscopy, Mr. Jamie Evans for training in flow cytometry, Dr. Thomas Johnson for his expertise in x-ray computed tomography and for going above and beyond, Dr. Martin Pule and the Pule lab at the UCL Cancer Institute for their expert advice early in the project, and Dr. Toby Proctor for allowing me to use his lab at the Royal Free in my first year.

The administrative team both past and present have provided me with great support and a friendly face from the start of my research. I am grateful to Kate

Sym, Victor Diran, and Andrea Crammond for this, thank you for helping me with my many queries.

Thank you to “Farlan’s Lab” and the “Regen Med” group for giving me my first taste of a wholesome lab family, and to the “Gustafsson Lab” group for taking me in and giving me my second taste. I felt so at home from day one and I’ll never forget everyone’s kindness, friendship, and willingness to help. In particular, Vaques, Arman, Fair, Rana, Abeer, Gerry, Ana, Anthea, Jack, and Georg. It’s been an absolute pleasure to work with you all and I hope our paths cross again in the future.

To Alex, Vincent, Rosalía, Neha, Victoria, Darryl, Matt, Molly, Joe, Sofia, Jamie, Alex VDS, Maria, Mau, Artemis, Chile, Victor, Charnett, Bapi, Mark, others of the Vineyard office, and generally the whole Department of Biochemical Engineering. Not in a million years did I imagine developing the friendships that I have during the EngD and I find myself struggling to put into words the gratitude I feel for your support over the years and how happy I am to have met you all. Thank you also to UCLWFC for providing me with some relief from long days in the lab, and to the friends I made there for giving me a second place within UCL where I felt at home. These people, IOE bar, and Neos pizza got me through some of the toughest days.

I would like to thank my friends outside of UCL - you know who you are, and my family - my parents, sisters, and niece, for your unconditional love and encouragement, for keeping me grounded and humble, and for always being there when I needed you.

Finally to Lucy, your warmth, love, and support has meant more to me over the last few years than you can imagine. Thank you for being there to celebrate every little victory with me and for being an endless source of happiness.

Looking back on the last 6 years makes my heart swell with joy. How lucky was I to have been able to develop as a researcher on a fascinating project, mentored by incredible people, all the while surrounded and supported by some of the most beautiful and selfless people you could ever hope to meet? I am forever grateful to you all, I would not be who or where I am today without you.

Contents

List of Figures

Chapter 1

Chapter 2

Chapter 3

Chapter 4

Chapter 5

Chapter 6

Chapter 7

Appendix

List of Tables

Chapter 1

Chapter 2

Chapter 3

Chapter 4

Chapter 5

Appendix

Abbreviations, Acronyms, Symbols, and Nomenclature

$^-$	negative
$^+$	positive
ΔP	pressure drop
μ	liquid viscosity
aAPC	artificial antigen presenting cell
aCD28	anti-(cluster of differentiation-28)
aCD3	anti-(cluster of differentiation-3)
ACT	adoptive T-cell therapy
ANOVA	analysis of variance
AP-1	activator protein-1
APC	allophycocyanin
BSA	bovine serum albumin
BUV395	brilliant ultraviolet™ 395
BUV737	brilliant ultraviolet™ 737
BV421	brilliant violet 421™
CaN	calcineurin
CAR	chimeric antigen receptor
CCL19	chemokine (C-C motif) ligand-19
CCL21	chemokine (C-C motif) ligand-21
CCR7	C-C chemokine receptor-7
CD25	cluster of differentiation-25
CD28	cluster of differentiation-28
CD3	cluster of differentiation-3
CD4	cluster of differentiation-4
CD45RO	cluster of differentiation-45, isoform RO
CD62L	L-selectin
CD69	cluster of differentiation-69
CD8	cluster of differentiation-8
CD95	cluster of differentiation-95
CFSE	carboxyfluorescein succinimidyl ester
cGMP	current good manufacturing practice
CNP	carbon nanotube-polymer
CO_2	carbon dioxide

CPP	critical process parameter
CQA	critical quality attribute
CTLA-4	cytotoxic T lymphocyte antigen-4
DAPI	4′,6-diamidino-2-phenylindole
DAG	diacylglycerol
DC	dendritic cell
DNA	deoxyribonucleic acid
DoE	design of experiments
EA	ethanolamine
EDC	1-Ethyl-3-(3-dimethylaminopropyl)carbodiimide
EDTA	ethylenediaminetetraacetic acid
ELISA	enzyme-linked immunosorbent assay
EMA	European Medicines Agengy
ER	endoplasmic reticulum
Erk	extracellular signal-regulated kinase
Fab	fragment antigen binding
FBS	fetal bovine serum
FDA	Food and Drug Agency
FITC	fluorescein isothiocyanate
FOXP3	factor forkhead box P3
FSC	forward scatter
FSC-A	forward scatter, area
FSC-H	forward scatter, height
GMF	glass micro fiber
GMP	good manufacturing practice
GRex	gas-permeable rapid expansion
GSK-3	glycogen-synthase kinase 3
H_2SO_4	sulphuric acid
HEPES	4-(2-hydroxyethyl)-1-piperazineethanesulfonic acid
HIV	human immunodeficiency virus
HRP	horseradish peroxidase
HSC	haematopoietic stem cell
ICAM-1	intercellular adhesion molecule-1
ICH	International Council for Harmonisation of Technical Requirements for Pharmaceuticals for Human Use

ICOS	inducible co-stimulatory molecule
ID	inner diameter
IgG	Immunoglobulin G
IgG1κ	mouse immunoglobulin, class G, subclass 1, light chain κ
IgG2a	mouse immunoglobulin, class G, subclass 2a
IL	interleukin
IL-10	interleukin-10
IL-12	interleukin-12
IL-2	interleukin-2
INFγ	interferon-γ
IP3	inositol triphosphate
IP3R	inositol triphosphate receptor
ITAM	immunoreceptor tyrosine-based activation motif
Itk	interleukin-2-inducible kinase
IU	international units
K	chromatography bed permeability
L	chromatography bed length
LAG-3	lymphocyte activation gene-3
LAT	linker for the activation of T-cells
LFA-3	lymphocyte function associated antigen-3
LoG	laplacian of gaussian
MACs	magnetic-activated cell sorting
MAPK	mitogen-associated protein kinase
MD	minimum distance
MES	2-(N-morpholino)ethanesulfonic acid
MHC	major histocompatibility complex
mRNA	messenger ribonucleic acid
NaOH	sodium hydroxide
NFAT	nuclear factor of activated T-cells
NFκB	nuclear factor-κB
NHS	N-hydroxysuccinimide
NMM	4-methylmorpholine
OCT	optimal cutting temperature
PA	polyacrylamide
PBMC	peripheral blood mononuclear cell

PBS	phosphate buffered saline
PCL	polycaprolactone
PD-1	programmed cell death protien -1
PDMS	polydimethylsiloxane
PE	phycoerythrin
PE-Cy7	phycoerythrin-cyanine7
PEG-Hep	polyethylene glycol–heparin
PerCP-Cy5.5	peridinin chlorophyll protein-cyanine5.5
PFA	paraformaldehyde
PGLA	polylactide-co-glycolide
PI	propidium iodide
PIP2	phosphatidylinositol 4,5-bisphosphate
PIP3	phosphatidylinositol (3,4,5) trisphosphate
PKCθ	protein kinase Cθ
PLCγ1	anti-phospholipase C-γ1
pMHC	peptide-major histocompatibility complex
PTK	protein tyrosine kinase
Q	volume flow rate
QbD	quality by design
QTPP	quality target product profile
REC	Research Ethics Committee
RFU	relative fluorescence unit
RGD	arginylglycylaspartic acid
rIL-2	recombinant interleukin-2
RNA	ribonucleic acid
SAM	self-assembled monolayer
scFv	single chain variable fragment
SEM	scanning electron microscopy
SEM	scanning electron microscopy
SH2	src homology 2
SLP-76	leukocyte phosphoprotein of 76 kDa
SSC	side scatter
SSC-A	side scatter, area
SSC-H	side scatter, height
STAT3	signal transducer and activator of transcription 3

T_{CM}	central memory T-cell
T_{EFF}	effector T-cell
T_{EM}	effector memory T-cell
T_{EMRA}	terminally differentiated effector memory T-cell
Tfh	follicular helper T-cell
TGF	transforming growth factor
TGF-β	transforming growth factor- β
T_h	helper T-cell
TIL	tumour infiltrating lymphocytes
TIM-3	T-cell immunoglobulin and mucin domain-containing protein-3
TMB	3,3',5,5'-tetramethylbenzidine
T_N	naïve T-cell
TNFR	tumour necrosis factor receptor
T_{reg}	regulatory T-cell
T_{reg}^{CM}	regulatory central memory T-cell
T_{reg}^{EF}	regulatory effector T-cell
T_{reg}^{EM}	regulatory effector memory T-cell
T_{RM}	tissue-resident memory T-cells
ε-PL	poly-ε-lysine
λEm	emission bandwidth
λEx	excitation bandwidth

Chapter 1. Introduction

In recent decades massive advances have been made in the fields of cell and gene therapies, with treatments having being developed and approved for significant diseases. One of these treatments is known as CAR-T cell therapy and has been developed to treat B cell malignancies such as leukaemia and lymphoma. The primary focus of this thesis is on improving the manufacturing of CAR T-cell therapies. In particular, the activation step via development of a novel biopolymer-based activation technology. This following chapter presents a general introduction to cell and gene therapies against cancer, T-cells, CAR-T cells and their manufacturing process, T-cell activation and *ex vivo* activation methods, and the use of polymers within T-cell therapies.

1.1.1. Cell and Gene Therapy: A Brief History

Cell and gene therapies have long been of great interest and are now considered significant pillars of current medical research. Cell therapy refers to a therapy in which viable cells are injected, grafted, or implanted into a patient; gene therapy refers to a therapy in which cells are genetically modified. Cell and gene therapy is a combination of both therapies in which viable genetically modified cells are introduced into a patient for therapeutic purposes. In 1985, through the collaboration of the laboratories of Anderson and Blaese, it was demonstrated that white blood cells taken from a patient with an enzyme deficiency could be corrected in tissue culture by inserting the genes for producing said enzyme; adenosine deaminase (Kantoff *et al.,*1986). This proof-of-concept study paved the way for subsequent testing and on September 14, 1990 a four-year old child became the first cell and gene therapy patient. The patient's own cells were removed, corrected, and re-infused, resulting in the trial ending in tremendous success (Blaese *et al*., 1995). In 1989, on the road to this success, studies were

undertaken by Rosenberg and his laboratory, together with Anderson and Blaese, that demonstrated the safety of introducing virus mediated, genetically engineered cells into the body. Tumour-infiltrating lymphocytes (TIL) obtained genes conveying antibiotic resistance though transduction via retrovirus, before being infused back into patients as a treatment for metastatic melanoma (Rosenberg, 1990). The gene for antibiotic resistance was used as a marker and allowed the researchers to track the persistence of the lymphocytes. This study not only validated the safety of gene and cell therapy, but opened the door to the possibilities of genetic engineering in cell based immunotherapy against cancer.

1.1.2. Immunotherapy Against Cancer

Immunotherapy refers to treatment of a disease through induction, enhancement or suppression of immune responses. The first observations that immune system engagement exhibited anti-tumour effects are often attributed to William Coley in the early 1890's. Coley (1891) observed the regression of sarcoma following the injection of patients with streptococcal organisms to stimulate an immune response. It was not however, until the anti-leukemic effects of allogenic –donor sourced, bone marrow transplants were reported, that immune cells were definitively recognised as having potent anti-cancer activity (Weiden *et al.,* 1979). This effect was attributed to the action of T-cells (Korngold and Sprent, 1978) and spurred on the development of methods aiming to modulate the immune system to improve tumour targeting. At present, the spotlight is on a cell and gene therapy known as chimeric antigen receptor (CAR) T-cells, which are to be discussed further in more detail. In the last decade CAR T-cells have produced some extremely promising results against various stage leukaemia in clinical trials, sparking the interest of many notable pharmaceutical companies. In 2017 the first applications for FDA approval for CAR-T therapies from Novartis and Kite were

approved, marking a historical landmark in the fields of immuno-, cell-, and gene-therapy.

1.2. T-cells

1.2.1. Their Place in the Immune System

The human immune system can be largely split into two categories; the innate and the adaptive. The innate immune system consists of cells such as phagocytes, natural killer cells, mast cells, and dendritic cells (DCs). It is the body's first line of defence and produces a rapid and non-specific response to foreign material. The adaptive immune system takes longer to develop than the innate, however, it produces a highly specific response capable of memory. The adaptive immune system consists of the B- and the T-cells. Created in the thymus and matured mainly under the influence of bone marrow, B-cells give rise to a humoral immunity and produce antigen specific immunoglobulins, known as antibodies (Lydyard *et al.,* 2011).

T-cells, both created and matured in the thymus, give rise to cellular immunity when stimulated via major histocompatibility complex (MHC) molecules on antigen presenting cells (APCs). The innate and the adaptive immune system are often thought of as separate systems, but this is undeniably not the case. Interaction occurs continually between cells of both systems during infection via chemical mediators such as cytokines, chemokines, and antibodies (Lydyard *et al.,* 2011). During infection, foreign material is internalised and presented to T-cells by APCs, such as DCs or macrophages. Extracellular proteins are endocytosed and digested in lysosomes to produce epitopic peptide fragments. These fragments are then loaded onto MHC class-II molecules and presented on the cells surface (Robinson and Delvig, 2002). If a cell becomes infected it alerts the immune system through MHC class-I antigen presentation. MHC class-I

molecules are present on all nucleated cells. In an un-infected state, these molecules contain peptide fragments that have been derived from the cell's own 'house-keeping' proteins. Infected cells expressing foreign proteins will instead present foreign fragments (Hewitt, 2003).

1.2.2. Initial T-cell Differentiation

Both T- and B-cells originate from haematopoietic stem cells (HSCs). T-cells undergo a complex differentiation process that results in a plethora of subsets. T-cells in the periphery are predominantly divided into two groups dependent on the expression of the surface marker CD4 or CD8 (CD= cluster of differentiation). This differentiation occurs in the thymus. HSCs develop into haematopoietic/lymphoid progenitors which populate the thymus and produce a population of immature thymocytes. The most primitive thymocytes are double negative ($CD4^-CD8^-$), and as they develop become double positive ($CD4^+CD8^+$). Double positive thymocytes then react with cortical epithelial cells that express high levels of MHC class-I and-II molecules. The fate of the cell is dependent on this interaction and the strength of signal produced as a result. Assuming an appropriate level of response, thymocytes that are able to bind to MHC class-I complexes develop into single positive $CD8^+$ T-cells, commonly known as cytotoxic T-cells. Those that bind to MHC class-II complexes develop into single positive $CD4^+$ T-cells, known as helper T-cells (T_h), T-cells that produce a signalling response that is too weak or too strong are destroyed by delayed or acute apoptosis, respectively. This selection process enables control of the immunological response in the body as only T-cells that are able to bind and signal correctly are then released into the peripheral lymphoid sites (Germain, 2002).

1.2.3. $CD4^+$ T-cells

When an infection occurs, $CD4^+$ naïve T-cells (T_N) become activated via MHC class-II presentation. Recognition and binding to this complex by a naïve $CD4^+$ T-cell results in migration to the site of infection, proliferation, and differentiation of the T-cell into either a T_h or a regulatory T-cell (T_{reg}); both of which consist of further subsets (see **Figure 1.1**). The differential fate of a naïve T-cell is largely dependent on the cytokines present at the time of differentiation. Furthermore, once differentiated, each subset assumes a distinctive and diverse cytokine profile, commonly used to characterise the subsets (Golubovskaya and Wu, 2016). The primary role of T_h cells is to secrete cytokines at the site of infection that have either a pro- or anti-inflammatory, survival, or effector function. For example, T_{h1} secretes interferon-γ (IFNγ), a pro-inflammatory cytokine required for macrophage activation (Teixeira *et al*., 2005).

T_{regs}, originally termed 'suppressor cells' (Gershon *et al.*, 1972) are produced as a means of negative control of the T-cell immune response. They play an important role in preventing autoimmune diseases, such as type 1 diabetes, and restricting chronic inflammatory diseases, such as asthma (Pellerin *et al*., 2014). T_{reg} cells that are induced through the differentiation are antigen-specific, however, there is evidence that once activated they inhibit effective T-cells in an antigen-nonspecific manner (Thornton and Shevach, 2000). Induced T_{regs} suppress the immune response through the secretion of interleukin-10 (IL-10) and transforming growth factor-β (TGF-β) (Vignali *et al*., 2008). In addition to induced T_{regs}, another distinct population of naturally occurring T_{regs} exists. These T_{regs} are thymus derived and are distinguished though their expression of transcription factor forkhead box P3 (FOXP3). $FOXP3^+$ T_{reg} cells not only regulate through the secretion of IL-10 and TGF-β as induced T_{reg} cells, but also though

metabolic disruption, cytolysis, and the targeting of DCs. These mechanisms can be found- reviewed in more detail, elsewhere (Vignali *et al*., 2008).

As shown in **Figure 1.1**, $CD4^+$ effector cells, are capable of further differentiation into either effector or central memory T-cells. The term effector cell (T_{EFF}) is used here, and will be henceforth, as a blanket term for T-cells that have been activated; thereby expressing an effector function. T_{EFFs} are often short lived and their activity is antigen-specific stimulation-dependant, so do not persist following the clearance of infection. Differentiation of a small pool of T_{EFFs} into memory subtypes confers the potential of long-term survival, with the half-life of a memory T-cell being ~ 8 - 15 years (Hammarlung *et al*., 2003). Generally, memory T-cells are characterised by their persistence in the absence of antigen, and their increased and rapid activity upon re-exposure. The differentiation of T-cells into memory cells is thought to be driven by a combination of extracellular signals such as cytokines, length of activation, and antigen clearance/persistence. Effector memory T-cells (T_{EM}) are found located in recently infected tissue and possess the ability to perform an effector function if re-stimulated. T_{EMs} display a limited proliferation potential in contrast to central memory T-cells. T_{EMs}, found in secondary lymphoid organs, are permanently differentiated and display an increased persistence following antigen clearance. High levels of L-selectin (CD62L) and C-C chemokine receptor-7 (CCR7) expressed by T_{CMs} allow homing to secondary lymphoid organs, whereas the absence of these in T_{EMs} results in the migration through non-lymphoid tissues (Sallusto *et al.,* 1999; Pennock *et al*., 2013). Terminally differentiated effector memory T-cells (T_{EMRA}) are T-cells that, as the name indicates, are terminally differentiated. Although their exact role is unclear, it is thought that this sub-set of T-cells possesses cytotoxic abilities, are slightly more prevalent within aging populations and have been particularly

associated with dengue virus infection (Koch *et al.*, 2008; Tian *et al*., 2016; Tian *et al*., 2017).

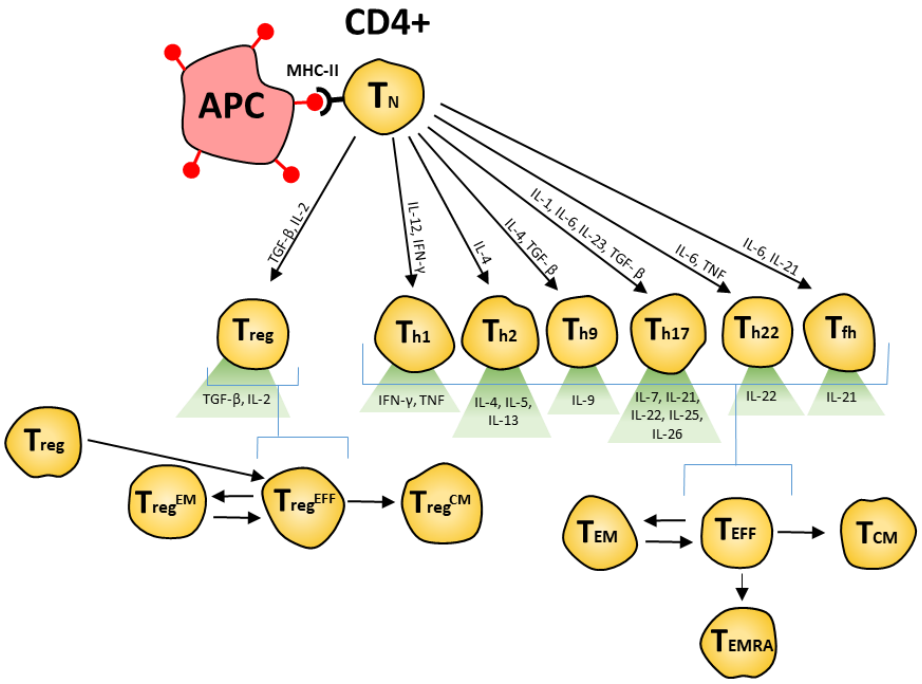

Figure 1.1. The differentiation of CD4+ T-cells. Upon stimulation, $CD4^+$ T-cells undergo rounds of division. The differentiation of T-cells is dependent on cytokines and molecular signal exposure. Differentiated T-cells then, in turn, secrete their own cytokines into the infection micro-environment. Regulatory T-cells differentiate as a means of negative immune response control. Helper T-cells are classified as effector T-cells; of these, some will differentiate into memory T-cells. Commonly defined populations of $CD4^+$ are shown in the figure. APC = antigen presenting cell. MHC-II = major histocompatibility complex class-II. IL = interleukin. IFN = interferon. TGF = transforming growth factor. T_N = naïve T-cell. T_h = helper T-cell. T_{fh} = follicular helper. T_{reg} = regulatory T-cell. T_{reg}^{EFF} = regulatory effector T-cell. T_{reg}^{EM} = regulatory effector memory T-cell. T_{reg}^{CM} = regulatory central memory T-cell. T_{EFF} = effector T-cell. T_{EM} = effector memory T-cell. T_{CM} = central memory T-cell. T_{EMRA} = terminally differentiated effector memory T-cell. Adapted from (Golubovskaya and Wu, 2016).

1.2.4. $CD8^+$ T-cells

$CD8^+$ naïve T-cells become activated via MHC class-I presentation and are understood to follow a linear differentiation through the subsets, shown in **Figure 1.2**. It is believed that as the T-cells undergo proliferation they decrease in

memory function and become more differentiated towards an effector role (Golubovskaya and Wu, 2016). $CD8^+$ T_{EFF} cells are commonly referred to as cytotoxic T-cells. Like $CD4^+$ T_h cells, $CD8^+$ T_{EFFs} are capable of producing various cytokines, however, it is their ability to eliminate pathogen-infected host cells by cytotoxic methods that is their predominant feature. This is achieved through the release of cytotoxic granules into the cytosol of the infected cell (Pennock *et al*., 2013). The two main memory subclasses of $CD8^+$ T-cells, T_{CM} and T_{EM}, are the same as those of $CD4^+$ and are defined by the same properties discussed previously.

In 2011 Gattinoni *et al.,* identified a memory T-cell subset with stem cell like properties, termed stem cell memory T-cells (T_{SCM}). These T-cells were found to comprise 2-3% of the total $CD4^+$ and $CD8^+$ circulating population (of 29 healthy donors) and exhibited a phenotype characteristic of T_N. They also, however, exhibited attributes characteristic of the memory subset, such as increased levels of CD95, IL-2Rβ, CXCR3, and LFA-1. Further investigation found $CD8^+$ T_{SCMs} to be a long-lived, self-renewing population with the multipotent capacity to differentiate into all memory and effector T-cells cells upon re-exposure of antigen, with specificity for multiple viral and self-tumour antigens. T_{SCM} was positioned between T_N and T_{CM} in the sequence of $CD8^+$ differentiation (**Figure 1.2**).

As with $CD4^+$ T_{EMRA}, $CD8^+$ T_{EMRA} are highly differentiated and cytotoxic T-cells that are associated with accumulating with age - even more so than $CD4^+$, and in situations of chronic viral stimulation such as cytomegalovirus and Epstein-Barr virus (Koch *et al., 2008;* Newell *et al*., 2012). Furthermore, studies undertaken with $CD8^+$ T_{EMRA} have reported shortened telomeres and the loss of the co-stimulatory receptor, CD28, which indicates proliferative senescence within this

population (Plunkett *et al*., 2007; Akbar *et al*., 2016; Najarro *et al*., 2015; Goronzy and Weyand, 2017).

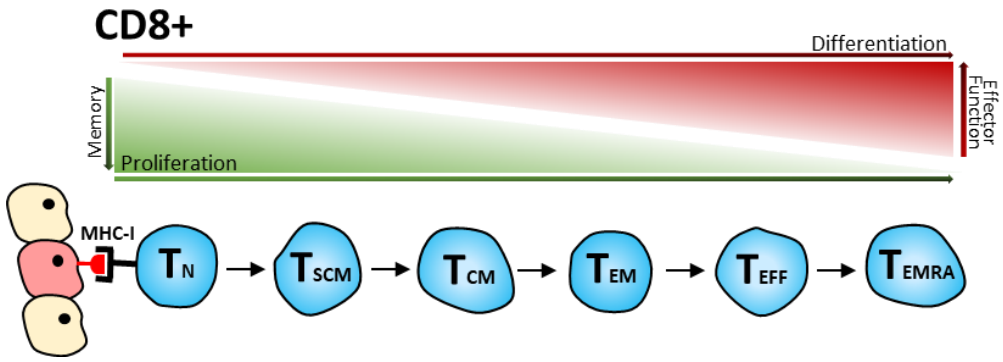

Figure 1.2. The differentiation of CD8+ T-cells. Upon stimulation, $CD8^+$ T-cells progress through rounds of division which results in T-cell differentiation. As the state of differentiation state progresses, T-cells experience a loss of memory and proliferative state in exchange for an increase in effector function. Commonly defined populations of $CD8^+$ are shown in the figure. T_N = naïve T-cell. T_{SCM} = stem cell memory. T_{CM} = central memory T-cell. T_{EM} = effector memory T-cell. T_{EFF} = effector T-cell. T_{EMRA} = terminally differentiated effector memory T-cell. Adapted from (Golubovskaya and Wu, 2016).

1.2.5. T-cell Exhaustion

Exhaustion is a state of T-cell dysfunction that occurs during persistent antigen exposure and/or inflammation, such as chronic infection and cancer. It is characterised through the progressive loss of effector functions, expression of multiple inhibitory receptors, altered expression of key transcription factors, and a failure to differentiate into memory-type T-cells (Wherry and Kurachi, 2015). The co-expression of inhibitory receptors, such as programmed cell death protein-1 (PD-1), lymphocyte activation gene-3 (LAG-3), cytotoxic T lymphocyte antigen-4 (CTLA-4), and T-cell immunoglobulin and mucin domain-containing protein-3 (TIM-3) are often used to distinguish T-cells in an exhaustive state (Yi *et al.*, 2010). Moreover, inhibition of these receptors has been demonstrated to

aid in the reversal of dysfunction and restore immunogenic responses (Wei *et al*., 2018; Wolf *et al.*, 2019; Maruhashi *et al.*, 2020).

1.2.6. T-cells used in this Thesis

1.2.6.1. Cell Line - Jurkat T-cells

Some studies within this thesis are performed using a derivative of the human T-cell line: Jurkat, Clone E6-1. This cell line consists of $CD4^+$ T-cells which were derived from 14 year old male with acute T-cell leukaemia. They are widely used as a model for studying T-cell biology and function, as well as for investigating various diseases that affect T-cells as they express many of the same surface markers and cytokines as normal T-cells.

1.2.6.2. Primary Human T-cells

Primary human T-cells are also used in this thesis as this was the target cell population of the final activation technology. These T-cells were isolated from the blood of healthy donors on the basis of CD3 expression. Cells used were therefore a combination of both $CD4^+$ and $CD8^+$ T-cells.

1.3 T-Cell Therapy Against Cancer

1.3.1. History

Cancers/tumours are the result of uncontrolled division of abnormal own cells. Unfortunately cancers often possess mechanisms that allow them to manipulate the tumour environment by excreting pro-inflammatory signals and immuno-inhibitory factors, ultimately avoiding immune system recognition and destruction. One key mechanism is the ability to down-regulate antigen processing machinery therefore downregulating MHC antigen presentation (Hicklin *et al*., 1999). Tumour antigen presentation may also become lost through an accumulation of mutational changes acquired through continuous cell division, a process known as “immunoediting” (Vinay *et al*., 2015). As discussed previously, T-cells

recognise infected cells through MHC antigen presentation and so suppression of antigen display allows the cancerous cells to remain largely undetected by T-cells.

Tumour biopsies lead to the discovery of TILs, which, as their name suggests, are able to recognise and infiltrate the tumours from which they were isolated (Sadelain *et al*., 2003). This discovery brought to light the possibility of using the natural immune system to fight cancers. Early cancer immunotherapies focused predominantly on TIL therapies, where TILs were isolated from tumour tissue, expanded, and infused back into the patient with the hope that they will recognise and attack the tumour (Maus *et al.,* 2014). More recently the field of adoptive T-cell therapy (ACT) has shifted towards the use of CAR T-cells. These are T-cells that have been genetically engineered to allow them to recognise and respond to cancerous cells independent of MHC antigen presentation.

1.3.2. A Focus on CAR T-cells

1.3.2.1. CAR Overview

CARs fundamentally consist of 3 domains; an extracellular targeting domain, a transmembrane domain, and an intracellular signalling domain (**Figure 1.3**). The extracellular targeting domain contains a moiety that is able to recognise and bind to antigen. Ideally, target antigens are those which are expressed exclusively on the dysfunctional/cancerous cells which are the target of the therapy. The targeting domain consists of either a single chain variable fragment (scFv), a fragment antigen binding (Fab) fragment, or an invariant human ligand. ScFv's are most commonly used in CARs as they can be easily produced from well characterised monoclonal antibodies (Sadelain *et al.,* 2013) They are derived from murine immunoglobulins and comprise of a heavy chain and a light chain

connected by a linker (Ahmad *et al*., 2012). The moiety is connected to the transmembrane domain via a spacer/hinge.

The transmembrane domain is a protein that anchors the CAR into the T-cell membrane and allows transmission of a signal from extracellular to intracellular. Type I single-pass membrane proteins, such as CD3ζ, CD4, CD8, or CD28, are used for this role (Shirasu and Kuroki, 2012).The intracellular signalling domain consists of domains that transmit signals for the activation of the T-cell once the CAR is bound to an antigen. Initially in first generation CARs, this domain consisted of just one signalling domain; the signalling domain of the T-cell receptor (TCR), CD3ζ. Second and third generation CARs saw the addition of one or more co-stimulatory domains (**Figure 1.3**) to enhance activation signalling within the cell.

Common co-stimulatory domains include CD28, OX44, and 4-1BB. Finney *et al.* (1998) found that a CAR consisting of a CD28 co-signalling and a CD3ζ signalling domain produced a response of up to 20-fold higher interleukin-2 (IL-2) production upon stimulation with Jurkat cells, in comparison to a CAR with the CD3ζ signalling domain alone. Using primary T-cells, Maher *et al.* (2002) found that CAR T-cells without a co-signalling domain underwent limited expansion upon initial stimulation moreover, re-stimulation resulted in a dramatic decline. CARs with the addition of a CD28 co-signalling domain permitted sequential rounds of re-stimulation. Addition of a co-stimulatory domain raised the prospect of a CAR that would allow expansion *in vitro*, before infusion, and then again upon encounter of the complementary antigen of the extracellular target domain *in vivo*. Addition of a 4-1BB co-signalling domain has also been found to confer an enhanced cytotoxic response, increasing expansion and IL-2 production (Imai *et*

al., 2004). Addition of at least one co-stimulatory domain is now commonplace in CAR design (van der Stegen *et al*., 2015).

Fourth generation CARs introduced a cytokine inducer. This was to further enhance T-cell killing capabilities through the secretion of a cytokine, such as interleukin 12 (IL-12), upon activation. This generation of CARs are referred to as “TRUCKs” - T-cells redirected for universal cytokine-mediated killing (Chmielewski and Abken, 2020). Most recently, fifth generation CARs have also been developed and comprise a truncated intracellular domain of a cytokine receptor, such as IL-2Rβ, in place of the cytokine inducer in the fourth generation (**Figure 1.3**). These domains contain a motif for binding transcription factors, such as STAT-3/5 which enhances T-cell activation, survival, and memory generation, in addition to reactivating and stimulating the immune system (Kagoya *et al*., 2018; Mehrabadi *et al.*, 2022).

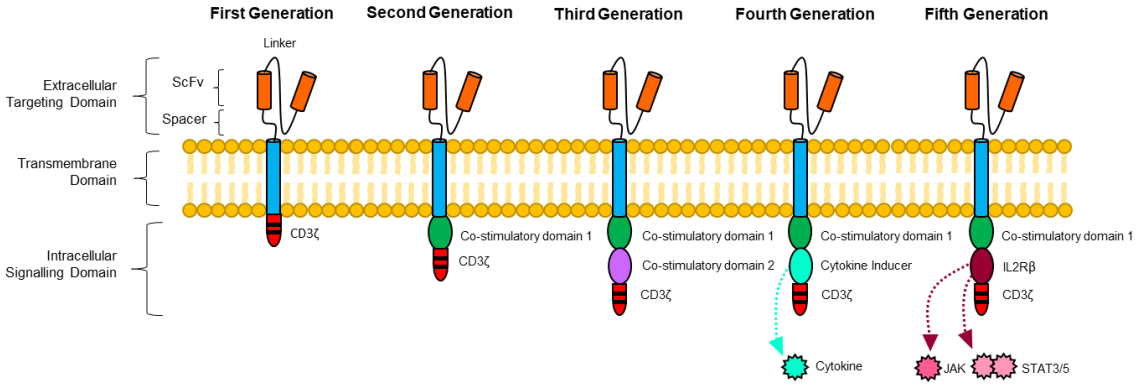

Figure 1.3. The generations of chimeric antigen receptors (CARs). All CARs consist of an extracellular targeting domain, a transmembrane domain, and an intracellular signalling domain. The intracellular signalling domain of first generation cars contained a CD3ζ signalling domain only. Second generation CARs contained an additional co-stimulatory domain. Third generation CARs contained a second additional co-stimulatory domain. Fourth generation CARs are based on second generation CARs with the addition of a cytokine inducer, there are also known as T-cells redirected for universal cytokine-mediated killing (TRUCKs). Fifth generation CARs are also based on the second generation with the addition of an intracellular domain of a cytokine receptor with a STAT3/5 binding motif, such as IL-2Rβ. ScFv = single chain variable fragment. Figure Adapted from Tokarew *et al*. (2019).

1.3.2.2. CAR T-cells

Genes which encode for the various domains of the CAR are inserted into and consequently transcribed and translated in T-cells, resulting in the expression of the CAR. Introduction of the CAR genes into the T-cell is most commonly achieved through transduction, where the CAR gene is inserted directly into the DNA of the T-cell. In clinical applications this is usually facilitated by γ-retroviral vectors, lentiviral vectors, and the transposon/transposase system; these are described in more detail in **Section 1.4.4.** Most recently, the CRISPR/Cas9 system has also been reported as a tool to integrate the CAR gene into the genome of T-cells in clinical trials, however, it is yet to be utilised in an approved product (Mueller *et al*., 2022).

The expression of the CAR construct by T-cells is fundamental to CAR T-cell therapy. When re-infused back into the patient, the CAR recognises and binds specifically to the complementary antigen of the extracellular signalling domain, this is an antigen expressed by the cancerous cells. The binding event then transmits a signal through the transmembrane domain into the intracellular signalling domain. The intracellular signalling domain then transmits signals to the T-cell which mimic those induced in the natural activation of T-cells upon the recognition of the TCR with its cognate antigen. These signals ultimately result in the proliferation of the CAR T-cells and the generation of CAR T-cell populations with cytotoxic capabilities which enable the destruction of the cancerous cells. The extracellular signalling domain of the CAR can be modified to target different antigens, which allows the therapy to be tailored to target cancers arising in various tissues (Tokarew *et al*. (2019).

A combination of both $CD4^+$ and $CD8^+$ T-cells are used in CAR T-cell therapy. Whilst CD8+ CAR T-cells directly kill the cancer cells, CD4+ CAR T-cells produce cytokines that support the immune response and can promote the formation of memory cells which may confer longer term protection. Therefore both are desirable for therapies.

1.3.3. Clinical Significance of CAR T-cells

Most CAR therapies to date are autologous and have focused on the treatment of B cell malignancies such as leukaemia and lymphoma. This is due to the availability of surface antigens that are specific to infected cells in these diseases. CD19 for example, is the most investigated target in CAR-T therapies. Although CD19 is expressed on both cancerous and healthy T-cells, expression is limited to B-cells only. Whilst this does not prevent the destruction of all B-cells during treatment, the on-target off-tumour effects are significantly reduced in

comparison to other possible target antigens which may also be present on additional cell types (Ivica and Young, 2021).

In February 2018, Novartis published results from its CTL019 (tisagenlecleucel; KYMIRAH®) ELIANA phase 2 clinical study, a CD19 CAR T-cell therapy to treat B-cell acute lymphoblastic leukaemia. Of 75 patients treated, 81 % remained in complete remission within 3 months, and 76 % overall survival at 12 months. Furthermore, tisagenlecleucel was observed in blood for as long as 20 months post infusion, demonstrating long-term persistence (Maude *et al*., 2018). These remarkable results were followed by the announcement of results from another CTL019 phase 2 clinical trial (JULIET), in which tisagenlecleucel was used to treat diffuse large B-cell lymphoma. Of 93 patients treated, 12 % showed a partial response and 40 % remained in complete remission three months post treatment with an 81 % probability of remaining relapse-free at 12 months (Schuster *et al*., 2019). Similarly, Kite Pharma have also reported impressive results using their CD19-CAR therapy, KTE-C19 (axicabtagene ciloleucel; YESCARTA®). From its phase 3 trial against large B-cell lymphoma, they have reported a 41 % 2-year event-free survival rate, which was 25 % higher than with standard care (Locke *et al*., 2022). In a historic action, KYMIRAH® and YESCARTA® became the first approved CAR T-cell therapies by the Food and Drug Agency (FDA) in August 2017 and October 2017, respectively. Currently, there are 6 CAR T-cell therapies that have been FDA approved, all of which are autologous, these are summarised in **Table 1.1**. To date, no allogenic CAR T-cell therapies have yet been FDA approved.

Table 1.1. FDA Approved CAR T-cell Therapies

Company	Therapy Name	Brand Name	Target	Dose	Min Dose Number	Max Dose Number
Novartis	Tisagenlecleucel	KYMIRAH®	B-cell acute lymphoblastic leukemia	0.2 to 5 x 10^6 per kg	1	4
			B-cell non-Hodgkin lymphoma	0.6 to 6.0 x 10^8		
Kite Pharma/ Gilead Sciences	Axicabtagene ciloleucel	YESCARTA®	B-cell non-Hodgkin lymphoma	2 × 10^6 per kg	1	4
			Follicular lymphoma			
	Brexucabtagene autoleucel	TECARTUS®	Mantle cell lymphoma	2 × 10^6 per kg	1	4
			B-cell acute lymphoblastic leukemia	1 × 10^6 per kg		
Juno Therapeutics/ Bristol Myers Squibb	Lisocabtagene maraleucel	BREYANZI®	B-cell non-Hodgkin lymphoma	9 to 11 × 10^7	1	4
bluebird bio/ Bristol Myers Squibb	Idecabtagene vicleucel	ABECMA®	Multiple myeloma	3 to 4.6 × 10^8	1	4
Janssen Pharmaceuticals/ Johnson & Johnson	Ciltacabtagene autoleucel	CARVYKTI®	Multiple myeloma	0.5 to 1.0 × 10^6 per kg	1	4

Source: National Cancer Institute (2022). Correct as of April 2022.

1.4. Autologous CAR T-cell Manufacturing Process

1.4.1. Process Overview

Figure 1.4 shows an overview of the autologous CAR T-cell manufacturing process. Briefly, the process consists of 6 steps: leukapheresis, T-cell purification and selection, activation, CAR gene transductions, expansion, and infusion. These steps are described in more detail in the sections below.

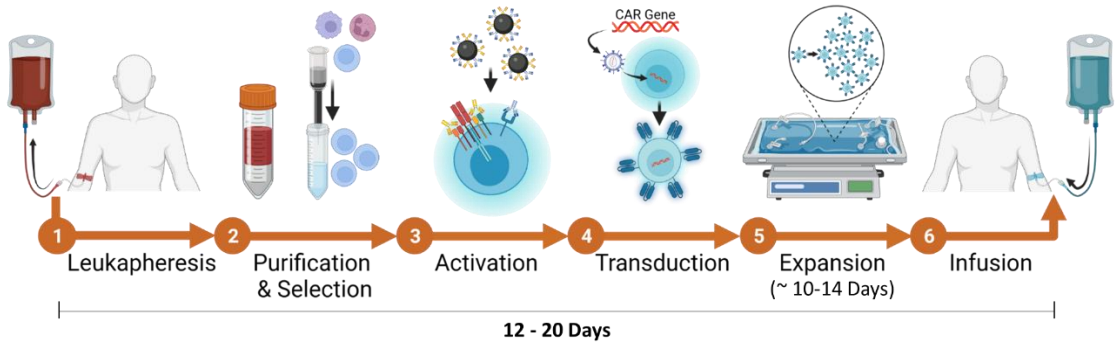

Figure 1.4. An overview of the autologous CAR T-cell manufacturing process. Most common methods for each step are displayed. (1) A patients leukocytes are removed from their blood in a process called leukapheresis. (2) The leukapheresis produce is purified to remove remaining contaminants such as red blood cells, this is often done through density based separation to purify peripheral blood mononuclear cells (PBMCs). T-cells are then selected from PBMCs, generally through magnetic-activated cell sorting. (3) T-cells are then activated. This is most commonly achieved through the use of anti-CD3 and anti-CD28 coated magnetic beads. Anti-CD3 stimulates the CD3 domain of the T-cell receptor and anti-CD28 targets the CD28 receptor to provide co-stimulation which results in T-cell activation. (4) T-cells are transduced with the chimeric antigen receptor (CAR) gene. Most commonly this is achieved through the use of a lentivirus. (5) CAR T-cells are expanded. A rocking motion bioreactor - a popular expansion platform, is displayed in the figure. (6) CAR T-cells are infused into the patient for treatment. Most common methods are those reported by Vormittag *et al*. (2018).

1.4.1. Leukapheresis

Manufacture of CAR T-cells begins with a leukapheresis step. Leukapheresis is a type of apheresis that specifically targets leukocytes. The process involves whole blood being taken from a patient and separated into layers of different

components by centrifugal force (Smith, 1997). The layer containing the peripheral blood mononuclear cells (PBMCs), also known as the ‘buffy coat’, is removed and the remainder of the blood components are returned to the patient. This process is usually performed continuously or semi-continuously and involves the addition of anti-coagulants, such as citrates to the blood to prevent clotting (Lee and Arepally, 2012). Anti-coagulants and other contaminants still remaining in the leukapheresis product can be removed through a washing step. Automated cell-washers, such as the Haemonetics Cell Saver (Haemonetics Corp), COBE2991 Cell Processor (TerumoBCT), and the Lovo Cell Processing System (Fresenius Kabi), can be used to wash out the collection buffer, and the bulk of red blood cells and platelet contaminants. Further isolation of lymphocytes can then be achieved through purification and enrichment steps.

1.4.2. Purification, Selection, and Enrichment

Purification of the leukapherisis product is achieved through methods of cell separation predominantly based on density, size, and immunophenotypic differences of the cells. Once separated, specific cell populations within T-cells, can be selected for or depleted, depending on the final desired composition. Specific T-cell populations include $CD8^+$ T-cells which may be desired for their enhanced cytotoxic potential, and γδT-cells which may be desired for their ability to mediate natural tumour responses (Rozenbaum *et al*., 2020). Purification can be done with or without the washing step previous. One method used for purification of whole-blood, based on cell density, is Ficoll-Hypaque density centrifugation. Ficoll-Hypaque is a sedimentation agent that is denser than lymphocytes, monocytes, and platelets, but is less dense than red blood cells and granulocytes; addition therefore allows highly efficient depletion of red blood cells and granulocytes (Thong *et al.*, *1983*). Traditionally Ficoll-Hypaque is an open

process that requires extensive manipulation; the blood is layered on top of the Ficoll-Hypaque media and centrifuged. This results in layers of separation: red blood cells and granulocytes, Ficoll-Hypaque, PBMCs, and plasma. The PBMC layer is then manually extracted via careful pipetting so as to not disturb the layers. Devices have been developed that are able to perform this technique in a closed-system, Good manufacturing practice (GMP)-compliant manner, such as the SepaxTM and the Haemonetics Cell Saver5 (Janssen *et al*., 2010). These devices separate cell populations based on their density through centrifugation.

A major drawback in the use of Ficoll-Hypaque density centrifugation is that the density gradient alone is not sufficient to separate monocytes from lymphocytes. Monocytes contaminants may inhibit T-cell activation and expansion and so other methods to further isolate lymphocytes are necessary (Bryn *et al.,* 2007). Elutriation is a purification method that can be applied instead of Ficoll-Hypaque density. It is a method that combines centrifugal force with a counter-flowing fluid that is able to separate cells on the basis of both size and density. As elutriation takes into account cell size, it allows the separation of monocytes and lymphocytes. The process can be performed using a GMP-compliant closed system device, such as the Elutra Cell Separation System (ThermoBST inc).

The third approach, separation by immunophenotypic differences, is performed post-washing/elutriation and involves the use of monoclonal antibodies attached to 50 nm magnetic beads, known as magnetic-activated cell sorting (MACs). The antibodies are specific for certain markers, such as CD3, CD4, and CD8. Once the target population, $CD3^+$, $CD4^+$, or $CD8^+$ T-cells, is attached, the cell-bound beads are separated via magnet. These beads do not activate T-cells and do not have to be removed. This technique allows for the separation/enrichment or

depletion of certain T-cell subsets. A wide array of good-manufacturing-practice (GMP)-grade antibody-conjugated beads are available (Miltenyi Biotec).

GMP compliance is important during each step in the manufacturing of CAR T-cells to be used as a therapy as it ensures consistent product quality and efficacy, and ultimately, the safety of the patient. Considerations for GMP manufacture include: facility and equipment design - to minimise the risk of contamination and ensure the validation and accuracy of the process, raw materials and reagents - must be sourced from qualified suppliers and tested for quality and purity, and process validation - to certify that the process is robust and that the final product meets the required quality standards.

1.4.3. Activation

Once the T-cells have been selected and successfully isolated, they must then be activated in order to proceed with the CAR T-cell manufacturing process. T-cell activation requires a primary signal generated through engagement of the TCR, and a co-stimulatory signal, generated though the engagement of receptors, such as CD28, 4-1BB, or OX40 (Wang and Riviere, 2016). One of the most widely used technologies is anti-CD3/anti-CD28 (aCD3/aCD28) coated paramagnetic beads, Dynabeads (Thermo Fisher Scientific). The activation of T-cells and the methods developed for activation in T-cell therapy manufacturing will be discussed further below.

1.4.4. Transduction

Activated T-cells are transduced with a vector containing the CAR transgene. There are three major gene delivery methods used for clinical applications; γ-retroviral vectors, lentiviral vectors, and the transposon/transposase system. Lentiviral vectors and γ-retroviral vectors are both members of the Retroviridae family. Both work by retro-transcribing their RNA genome into a complementary

DNA copy which is then permanently integrated into the host cell's genome (Vannucci *et al*., 2013). Both are widely used in the production of CAR T-cell therapies as they mediate high gene transfer efficiency and provide a stable CAR expression, however, each are not without their disadvantages. γ-retroviral vectors are only able to transduce dividing cells, whereas lentivirus vectors can transduce both dividing and non-dividing cells (Miller *et al.,* 1990; Freed and Martin, 1994). Theoretically, lentiviruses also convey a lower risk of oncogenicity through insertional mutagenesis as they tend to integrate DNA away from promoters, though it remains a risk nonetheless (Levine, 2015). The level of transduction efficiency with both lentiviral and γ-retroviral vectors varies depending on the specific process but has been reported to be between 25 - 80 % in optimised GMP protocols (Wagner *et al*., 2022).

An alternative to viral methods of transduction is a transposon/transposase system, such as the PiggyBac or the Sleeping Beauty transposon systems. Transposon-based systems are plasmids that contain a gene for transposase and the CAR transgene as the transposon. The plasmid is introduced to the cells via electroporation and the transposase is transcribed. Transposase "cuts" the transposon/ CAR transgene from the plasmid and "pastes" it into a new site in the host cell's genome (Morgan and Boyerinas, 2016). Transposons are integrated intact, eliminating the risks of random mutations or rearrangements associated with the reverse transcription of viral vectors. Integration, however, is still reasonably random and so the risk of oncogenesis via insertional mutagenesis is still present (Izsvák *et al*., 2010). Electroporation of messenger ribonucleic acid (mRNA) is a transfection method that has recently gained interest due to lack of genomic integration resulting in very low risk of international mutagenesis. This method is limited by the unstable and short-lived nature of

mRNA resulting in only transient expression, though this may prove advantageous if a non-permanent CAR expression is desired; potentially as a means to reduce long-term off target effects (Morgan and Boyerinas, 2016).

1.4.5. Expansion

Once the T-cells are transduced with the CAR gene, they are expanded to the cell number required for patient infusion. The CAR gene will be copied into daughter of cells resulting in an expanded population of CAR expressing T-cells. T-cells grow in suspension as opposed to adherent cells; expansion of CAR T-cells was traditionally achieved via static cell culture systems, a labour intensive open system that involves frequent manipulation. Although semi-closed systems of static culture have been developed (Tumaini *et al.*, 2013; Castella *et al*., 2020), WAVE and Gas-permeable Rapid Expansion Flasks (GRex) bioreactors still confer considerable advantages. The WAVE is a closed system rocking motion bioreactor that is capable of automated media perfusion and waste removal. Cells are expanded within a single use Cellbag that is placed on a rocking platform to allow for gentle but rapid gas transfer and mixing. The homogenous and highly oxygenated environment allows T-cells to rapidly expand from 0.5 - 1 x 10^6 to more than 10^7 per mL. The WAVE system can support up to 25 L and is widely used to support clinical trials, phases 1-2, and by academic centres (Wang and Riviere, 2016). The GRex system is a cell culture flask with a gas permeable membrane at the base that allows efficient gas exchange at high cell densities. The flask can be seeded at a low density and media is added only once, dramatically reducing the number of media exchange steps when compared with traditional culture in flasks. GRex flasks are compatible with standard incubators and can be easily scaled up with the addition of more flasks (Somerville and Dudley, 2012).

These systems, however, are also not without their disadvantages. The WAVE bioreactor represents a large up-front capital cost, an additional re-occurring cost of the Cellbag, and lacks a culture monitoring system (Meng *et al*., 2018). Scale up with GRex flasks is limited by the surface area available for gas transfer, which in turn limits the volume per flask. Additionally, drawbacks arise in the potential for automation, as seeding and removing cells from a GRex requires the transfer of a large volumes to and from the flask (Ganeeva *et al*., 2022).

Recently the possibility of expanding CAR T-cells in an automated stirred tank bioreactor such as the ambr® (Sartorius) has been also been demonstrated (Costariol *et al*., 2020). This confers benefits as stirred tank bioreactors are common within biotech companies and may remove the need for purchasing additional specialist equipment. Furthermore, fully closed systems automated platforms such as the CliniMACS Prodigy® (Miltenyi Biotech), and the Cocoon® (Lonza) have been developed and are capable of performing all manufacturing steps in a closed system, including expansion. The CliniMACs Prodigy is an automated cell processing platform that enables the manufacturing of CAR T-cells in a closed, sterile, GMP-compliant manner; and has been used to produce CAR T-cell therapies for clinical trials (Jackson *et al*., 2020). So far literature on manufacturing with the Cocoon is limited, however, it has been reported that four patients have been treated with a CAR T-cell therapy manufactured using the platform (Lonza, 2021).

1.4.6. Formulation, Preservation, and Delivery to the Patient

Once the CAR T-cells have been expanded they must be formulated into a product that is ready to be delivered to the patient. Depending on the manufacturing route chosen this may first consist of purification steps to select for the CAR T-cells or remove residual beads. Generally, the expanded product

is harvested from the cell culture vessel, concentrated, washed to remove the cell culture medium and replace it with formulation buffer, and then filled into cryobags at the required patient dose (Iyer *et al*., 2018). For a de-centralised model of CAR T-cell manufacturing, where the manufacturing centre is not attached to the clinic, the final CAR T-cell product will require cryopreservation. Options for cryopreservation include controlled rate freezers with liquid nitrogen and automated liquid nitrogen free freezers such as the Asymptote VIA Quad (GE Healthcare) (Buhl *et al*., 2012). Frozen bags are then delivered to the clinic where they are thawed using an automated dry-thawing device, such as the Asymptote VIA Thaw CB1000 (GE Healthcare). Once thawed the CAR T-cell dose can be administered to the patient by intravenous infusion.

1.5. Activation

The fundamental goal of this thesis was to develop a novel activation technology to activate and expand T-cells for use in cell and gene therapies. It was therefore important to further understand the mechanisms behind T-cell activation, why it is necessary, and what technologies are already available. Briefly, activation of T-cells is essential in T-cell therapies as it induces proliferation, differentiation, and effector functions. The following sections take a more in-depth look into the process of T-cell activation, *ex vivo* activation methods, and markers of activation.

1.5.1. Primary Stimulation

In vivo, T-cell activation is initiated through the engagement of the TCR with MHC molecules on APCs. The TCR is a complex that consists of variable α and β chains non-covalently associated with non-polymorphic CD3 proteins. The α and β chains form a single heterodimer, whereas the CD3 proteins exist as a series of dimers, including γε, δε, and ζζ. Following unsuccessful attempts to create cell

lines expressing αβ without CD3 and vice versa, it was accepted that there is an obligatory co-expression of αβ with CD3 (Saito and Germain, 1987). Inferred by their morphology of long cytoplasmic tails, CD3 proteins are critical for signal transduction. Stimulation of the TCR complex instigates the initial series of biochemical reactions necessary for cellular activation. Signalling, however, is not a straightforward linear event but is instead governed by a complex feedback and feedforward regulatory system, an overview is shown in **Figure 1.5**.

Engagement of the TCR leads to src protein tyrosine kinase (PTK) activity that results in the phosphorylation of CD3ζ and other immunoreceptor tyrine-based activation motifs (ITAMs). This then triggers a cascade of phosphorylation events. ITAM phosphorylation leading to the recruitment of ZAP-70 converts the TCR into an active PTK that is able to phosphorylate a wide array of substrates that result in a myriad of signals downstream that eventually result in T-cell activation (Smith-Garvin *et al*., 2009).

Amongst the targets of ZAP-70 are two adapter proteins that form the backbone of the complex responsible for organising effector molecules in the correct spatiotemporal arrangement necessary for the activation of multiple signalling pathways. The transmembrane adapter protein linker for the activation of T-cells (LAT), and the cytosolic adapter protein src homology 2 (SH2) domain-containing leukocyte phosphoprotein of 76 kDa (SLP-76) (Zhang *et al*., 1998; Wardenburg *et al*., 1996). Anti-phospholipase C-γ1 (PLCγ1) binds to SLP-76 and LAT and is phosphorylated and activated by interleukin-2-inducible kinase (Itk). Activated PLCγ1 then hydrolyses a membrane lipid to produce the secondary messengers, diacylglycerol (DAG) and inositol triphosphate (IP3), both of which are essential for T-cell function (Smith-Garvin *et al*., 2009).

The production of DAG activates two major pathways that involve Ras and selective protein kinase Cθ (PKCθ). Ras is required for the activation of serine-threonine kinase Raf-1 which, in turn, activates mitogen-associated protein kinases (MAPKs) extracellular signal-regulated kinase (Erk) 1 and 2. Elk1, and signal transducer and activator of transcription 3 (STAT3) are transcriptionally activated as a result of the activation of the MAPK pathway. Furthermore, Ras plays a role in the activation of the activator protein-1 (AP-1) transcription complex and the upregulation of CD69 expression (d'Ambrosio *et al*., 1994). The second major pathway regulated by DAG is mediated by PKCθ. PKCθ regulates the critical pathway of nuclear factor-κB (NFκB) activation. NFκB is a family of transcription factors that, when translocated to the nucleus, activate the transcription of genes required for effector function, survival, and homeostasis of the activated T-cell (Roose and Weiss, 2000).

Production of the secondary messenger IP3 stimulates Ca2+ permeable ion channel receptors (inositol triphosphate receptor (IP3R)) on the endoplasmic reticulum (ER) membrane. ER stored Ca2+ is released into the cytoplasm and an influx of extracellular Ca2+ is triggered by the change in gradient. The increase of intracellular Ca2+ results in the activation of a myriad of transcription factors and signalling proteins. Of high significance is the activation of signalling protein phosphatase calcineurin (CaN). Activated CaN dephosphorylates members of the nuclear factor of activated T-cells (NFAT). Dephosphorylation of NFAT allows for translocation to the nucleus where they are able to facilitate a variety of different transcriptions. Notably, NFAT is responsible for transcription that results in IL-2 production (Chow *et al*., 1999).

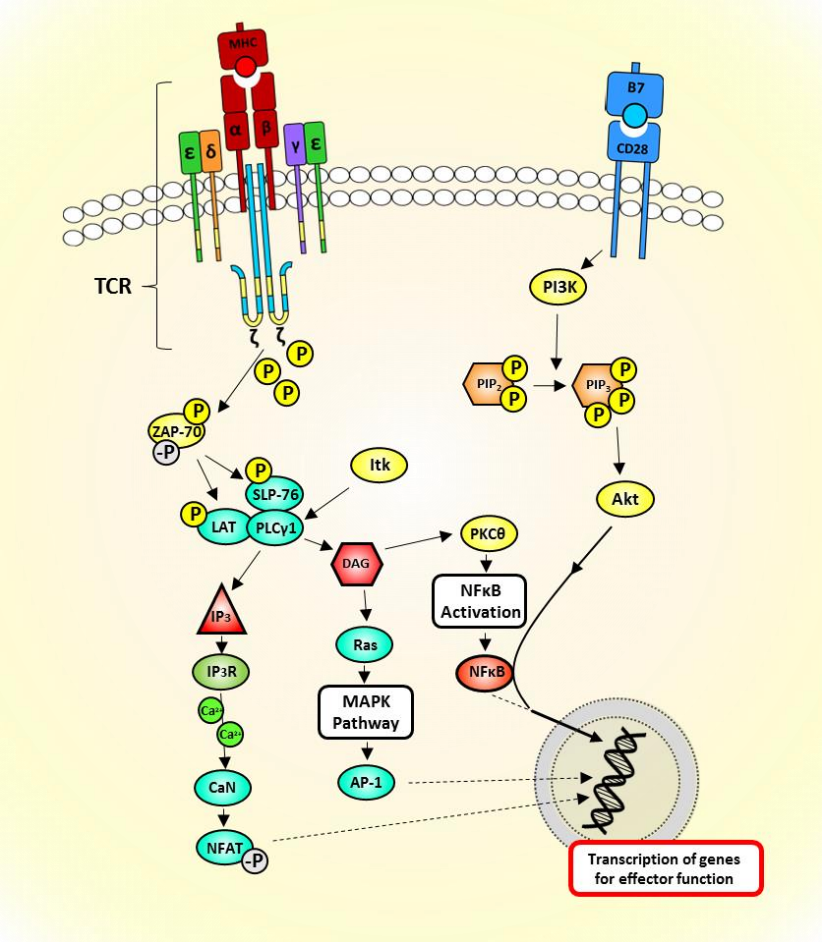

Figure 1.5. Intracellular T-cell Activation Pathway

1.5.2. Co-stimulation

Stimulation of the TCR alone is not enough to sufficiently activate a T-cell, but instead can lead to a state of unresponsiveness, also known as anergy. Co-stimulation of the T-cell is necessary to provide the adequate activation needed for an effective response and proliferation (Liu, 1994). Co-stimulation can be provided through stimulation of various cell surface receptors, such as CD2, CD5, CD30, CD28, OX40 (CD134) and, 4-1BB (CD147). Of these, CD28 has been recognised to play a key function in T-cell activation, providing a robust co-stimulatory signal that promotes proliferation, cytokine production, cellular metabolism, and survival (Smith-Garvin *et al*., 2009). *In vivo* CD28 is stimulated though interaction with B7 ligands on APCs (Chen and Flies, 2013).

Engagement of CD28 results in the association of the p85 subunit of phosphoinositide 3-kinase (PI3K) to a motif in the cytoplasmic tail of CD28. The p85 subunit then recruits p110, a catalytic subunit of PI3K that converts phosphatidylinositol 4,5-bisphosphate (PIP2) to phosphatidylinositol (3,4,5) trisphosphate (PIP3). Akt is recruited to the membrane though interaction with PIP3 where it become activated. Akt is responsible for the phosphorylation of several proteins, effecting multiple responses. Activated Akt enhances nuclear translocation of NFκB and optimises NFAT mediated transcription, which, as mentioned previously, results in the transcription of essential effector and survival genes. Additionally, Akt inhibits transcription factors promoting cell cycle arrest (Xu, 2012), such as glycogen-synthase kinase 3 (GSK-3). GSK-3 promotes the nuclear exportation of NFAT. Inhibition of GSK-3 results in prolonged nuclear internalisation and therefore, prolonged transcription of IL-2 and other NFAT induced transcriptions (Ohteki *et al*., 2000).

Members of the tumour necrosis factor receptors (TNFRs), OX40 and 4-1BB are also known to provide co-stimulation upon engagement with their complementary ligands, OX40L and 4-1BBL, respectively. As with stimulation of CD28, OX40 and 4-1BB ligation results in the activation of PI3K/Akt, NFκB, and MAPK pathways. These pathways, however, are activated through downstream signalling mediated by TNFR-associated factor adapter proteins, whereas with CD28 pathways are associated with protein kinases (Smith-Garvin et al., 2009). This is shown in **Figure 1.5**.

1.5.3. Extracellular Events

T-cell activation is a complex process which involves a multitude of extracellular events. Activation itself is initiated though antigen recognition by the TCR and co-stimulation, as described above. In addition to this, T-cells react and bind to

other immune system cells, the extracellular matrix proteins in tissues, and cytokines: small signalling proteins released by APCs and other cells in response to inflammation. These extracellular cell-cell, cell-matrix and cell-cytokine interactions result in downstream signalling pathways which can ultimately influence the function and differentiation of activated T-cells (Golubovskaya and Wu, 2016).

1.5.4. Requirement for Activation in CAR T-cell manufacture

Activation of T-cells prior to gene transfer is essential for successful gene transfer by γ-retroviral or lentiviral vectors. Due to γ-retroviral vectors only being able to transduce dividing cells, the T-cell must be activated to induce cell division before gene delivery (Miller *et al.,* 1990). Though lentiviral vectors are able to transduce non-dividing cells they still require the T-cell activation to be effective. In 1998, Korin and Zack found that progression to the G1b phase of the cell cycle was required for the completion of human immunodeficiency virus-1 (HIV-1) DNA synthesis in T-cells. G1b is a sub-compartment of the G1 phase in which the RNA within the cell is above the level required for cells to initiate DNA replication; G1a is when then RNA is below this critical level (Darzynkiewicz *et al*., 1980). The lentivirus is a HIV-vector based system and so progression of the cell cycle to G1b is also required for successful synthesis of a CAR gene delivered via lentiviral vector. Korin and Zack (1998), also found that stimulation through the TCR alone was only sufficient to progress the cell cycle to G1a. Additional co-stimulation provided through CD28 engagement was necessary to progress to G1b. Moreover, T-cell activation is necessary to induce proliferation which is essential to expand CAR T-cells to clinically relevant numbers for treatments.

1.6. *Ex Vivo* Methods of Activation

A myriad of methods and technologies exist and are been developed to address the demand for *ex vivo* activation of T-cells for T-cell therapy purposes, with a key goal being to expand T-cells. In keeping with the topic of this thesis, the below activation methods are those which have been developed with T-cell therapy processing in mind. Additional methods of activation can be found in the literature, however, these have predominantly been used as a tools to investigate activation conditions rather than developed for expansion and commercial use – these will not be discussed here. Most *ex vivo* methods of activation involve the use of aCD3 and aCD28 antibodies. aCD3 stimulates the CD3 domain of the T-cell receptor (TCR) and aCD28 targets the CD28 receptor to provide co-stimulation which results in activation (**Figure 1.6**).

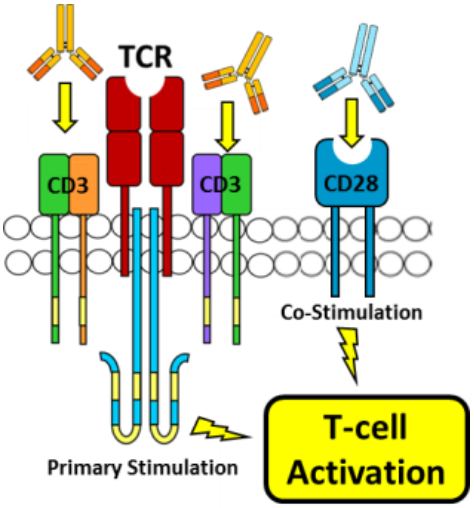

Figure 1.6. *Ex vivo* activation of T-cells with anti-CD3 and anti-CD28. Anti-CD3 stimulates the CD3 domain of the T-cell receptor (TCR). Anti-CD28 stimulates the CD28 co-stimulatory domain. The downstream signals from this stimulation results in T-cell activation.

1.6.1. Soluble Antibodies and Interleukins

The addition of monoclonal antibodies and interleukins to stimulate T-cell activation is a method that was commonly used in early clinical trials. One of the

earliest methods for the ex-vivo activation and expansion was to culture TILs with soluble aCD3 monoclonal antibody (clone OKT3), IL-2, and irradiated allogenic PBMCs (Dudley *et al*., 2003). The irradiated allogenic PBMCs, also known as feeder cells, are loaded with specific antigens to facilitate selective expansion. This method is referred to as the 'Rapid Expansion Protocol' (Levine, 2015).

1.6.2. Cell Based Artificial Antigen Presenting Cells

Another cell-based method of activation is the genetic modification of irradiated cells to present antigens capable of T-cell activation, such as aCD3 and aCD28, or peptide-MHC (pMHC). These are known as cell based artificial antigen presenting cells (aAPCs). A common cell line chosen for modification is K562 as they do no express MHC molecules and therefore, do not provoke an allogenic response (Suhoski *et al*, 2007). Additionally, K562 cells are easily manipulated to stably express genes and have a track record of being used safely in humans (Butler and Hirano, 2014). Cells can also be engineered to secrete cytokines, such as IL-2, further promoting T-cell activation and expansion.

Whilst both this method and the 'Rapid Expansion Protocol' above did allow the successful *ex vivo* expansion of T-cells, its use in GMP manufacturing of T-cell therapies was not ideal due to the additional development and regulatory requirements involved with the use of live cells as an activation tool. This resulted in the need to develop non-cell based activation methods, such as the ones described below.

1.6.3. Bead Based Artificial Antigen Presenting Cells

Bead based aAPCs are not cells but are, instead, synthetic beads which mimic antigen presenting cells; these are arguably the most popular of method of *ex vivo* T-cell activation. In particular, magnetic antibody-coated microbeads are used extensively in both laboratory research and clinical trials. Initially, non-

magnetic spherical polystyrene beads were coated with antibodies against CD3 and CD28. Microbeads were sized at 4 to 5 µm, which was found to be optimal for T-cell activation (Mescher, 1992). These beads successfully activated T lymphocytes against a range of targets (Turtle and Riddell, 2010) and circumvented the issues which arose with using cell-based activation methods, however, a significant issue was presented in that the beads are not biodegradable and must be removed before expanded T-cells can be infused into patients.

1.6.3.1. Magnetic aCD3/aCD28 Microbeads – Dynabeads®

Magnetic antibody-coated beads were developed to enable a more convenient removal of the beads once the T-cells have been activated. An iron oxide core in the beads allows removal with a magnet. Importantly aCD3/aCD28 coated magnetic beads have been applied to activate and expand T-cells infused into patients in many clinical trials, demonstrating safety in activating using this method (Eggermont *et al*., 2014). As with the non-magnetic beads, antibody coated magnetic beads are readily available with off-the-shelf cGMP standard products such as CD3/CD28 Dynabeads® (Thermo Fisher Scientific). Dynabeads are the current preferred activation technology in CAR-T clinical trials (Vormittag *et al*., 2018).

1.6.3.2. aCD3/aCD28 Nanobeads – TransAct™

Nanobeads, such as TransAct™ beads (Miltenyi Biotech), have also been developed to address the issue of bead removal. TransAct consists of iron oxide crystals embedded into a polymeric nanomatrix (~100 nm diameter beads) coated with aCD3 and aCD28. The small size of these beads allows removal to be achieved through either washing/centrifugation, or sterile filtration (Mauer *et al*., 2014). A comparison study between TransAct beads and Dynabeads

concluded that TransAct beads displayed equivalent activation potential and would be a viable alternative in the event of a Dynabead supply limitation (Wang *et al*., 2016). Furthermore, TransAct is also available off-the-shelf, cGMP ready, and can be found used in recent clinical trials confirming safety and ability to be used clinically (Castella *et al*., 2020; Ortiz-Maldonado *et al*., 2022).

1.6.3.3. aCD3/aCD28 Hydrogel Beads – Cloudz™

One of the most recent activating technologies, Cloudz™ (Bio-Techne), was released to the market in May 2020. Cloudz consist of aCD3/aCD28 microspheres that are made from a hydrogel referred to as “Quickgel”. Microspheres are removed through the addition of a non-enzymatic release buffer that instigates dissolution of the Cloudz (Bio-Techne, 2022). Cloudz can be supplied in a cGMP format, however, there is currently no literature available referring to its use in the production of CAR-T cell therapies in either a research setting or within GMP manufacturing facility.

1.6.4. Expamer™/ CD3/CD28 Streptamer®

Expamers™, developed by Juno Therapeutics, utilises Streptamer® technology which was developed by Iba Life Sciences. Briefly, Streptamer technology can be described as a backbone of engineered streptavidin, Strep-Tactin®, to which a peptide sequence, the Strep-Tag®, binds. aCD3 and aCD28 Fab fragments are bound to a Strep-Tag which is then attached to a Strap-Tactin core and used to active T-cells (Poltorak *et al*., 2020). The Streptamer is then dissociated to terminate the activation signal through the addition of biotin and then is removed via centrifugation. This platform has been demonstrated to expand human T-cells in a research setting and offers the potential of tuning activation signals through adjusting the stoichiometry and density of bound Fab ligands. Furthermore, the

components to produce this technology are available commercially as a CD3/CD28 Streptamer Kit (Iba Life Sciences).

1.6.5. ImmunoCult™

ImmunoCult™ by STEMCELL Technologies is an activating reagent containing aCD3 and aCD28 tetrameric antibody complexes. A key advantage is that it is provided in a medium that is serum free which is desirable in production processes. The use of ImmunoCult in a research setting is well documented and its ability to expand human T-cells has been demonstrated (Batchu *et al.,* 2018; MacDonald *et al*., 2019; Walsh *et al*., 2020), however, at the time of writing, no literature was found on its use within a GMP manufacturing facility.

1.6.6. Activation Methods Under Development

1.6.6.1. Cytokine Releasing Beads

An additional bead based aAPC has been reported within the literature. Steenblock and Fahmy (2008) describe biodegradable micro (8 µm) and nano (130 nm) particles that were prepared using polylactide-co-glycolide (PGLA). Similar to other bead based methods, these beads offer a surface to which aCD3/aCD28 or peptide-loaded MHC proteins can be attached through avidin-biotin binding. A notable feature of these beads is the capability to encapsulate IL-2 within the bead that is then released locally to T-cells as degradation occurs. To date the literature available on this method is limited to murine T-cell expansions, however these demonstrated proof-of-concept (Steenblock *et al.,*2011).

1.6.6.2. Hydrogel Coated Magnetic Beads

In 2016, Jesuraj *et al*. (2016) reported a novel phase-change substrate that was capable of activating and expanding T-cells. The substrate was an alginate-calcium based hydrogel which was coated onto magnetic beads of ~10 µm

diameter. Hydrogel coated beads were conjugated to streptavidin and bound to biotinylated aCD3 and aCD28. To remove the beads, cells were first detached by adding a calcium chelating agent to dissolve the hydrogel coating by binding and removing the calcium from the alginate-calcium hydrogel. Beads were ten removed via magnet. This method has been reported to be successful with human T-cells.

1.6.6.3. Carbon Nanotube-Polymer

Carbon nanotube-polymer (CNP) is an innovative method of T-cell activation that was developed by Fadel *et al*. in 2014. Initially, carbon nanotubes were produced with dimensions of ~0.8 nm diameter x ~0.5 – 5 µm length. Nanotubes were bundled and bound together through the addition of neutravidin. Stimulating ligands (either MHC-1 and aCD28, or aCD3 and aCD28), were then attached through the neutravidin. Finally, PLGA nanoparticles (~150 – 200 nm) encasing IL-2 for slow release were also attached. The resultant structure was termed a CNP. As with many other methods, CNP removal was achieved through the use of a magnet. The group reported successful expansions of both murine and human T-cells, both for specific and polyclonal expansion.

1.6.6.4. 3D Scaffold of Microrods

Another novel method recently described is a 3D scaffold capable of releasing soluble paracrine cues locally to T-cells, similar to PGLA beads described above (Cheung *et al*., 2018). Mesoporous silica micro-rods, pre-absorbed with IL-2, were coated with a fluid lipid bi-layer to which aCD3/aCD28, or a MHC proteins can be attached. IL-2 is released as the silica micro-rod degrades by hydroxyl ions in the media attacking Si-O binds within the rods. These micro-rods are 70 um length, 4.5 um diameter, and assemble into a 3D scaffold in culture through the random settling and stacking of rods. This method has been shown to be

effective in the expansion of both murine and human T-cells, resulting in significantly increased polyclonal expansions compared to the current gold standard CD3/CD28 Dynabeads.

1.6.6.5. 3D Printed Lattice

Finally, also of note is a novel activation technology reported by Delalat *et al*. (2017). Melt electrospinning writing with medical-grade polycaprolactone (PCL) was employed to produce a lattice structure with 200 µm spacing. Lattices were coated with a functional polymer to which aCD3/aCD28 was attached. Expansion was demonstrated with human T-cells, and interestingly this method was found to be both compatible and enhanced with a G-rex bioreactor.

1.6.7. Dynabead Limitations

Whilst Dynabeads represent the current industry gold standard in current activation technologies, they are not without their disadvantages. Dynabeads remaining in the final formulation may result in an adverse immune reaction by the patient and so they must be removed. Bead removal is facilitated through the use of a magnet, however, complete bead removal is not guaranteed. Hollyman *et al*. (2009) suggest a product release criteria of < 100 beads per 2 x 10^6 cells, however a residual of 0 would be preferred. Moreover, they describe a protocol in which cultures of 1.2 L were passed over 2 magnets at a maximum of 200 mL per run, indicating that bead removal is a time consuming step.

Residual bead count by microscopy is a critical product release specification of the FDA approved CAR-T-cell therapy Tisangenlecleucel (CTL019 – Kymriah tm), with the limit set at ≤ 50 beads per 3 x 10^6 cells (Committee for Medicinal Products for Human Use, 2018). Determination of this attribute represents an additional step in safety release testing and an additional juncture at which the product may fail. There has been at least one reported manufacturing failure due

to an out of specification (high) Dynabead count in the final product (Rossoff *et el*., 2021).

Furthermore, it was found by Chin *et al*. (2020) that the available surface area of Dynabeads is not fully utilised by T-cells in culture. This was due to bead aggregation, multiple beads bound to a single cell, or failure to make contact with a cell. Thus indicating that beads may not in fact be the most optimal and cost effective format in which to present stimulating antibodies to T-cells.

One of the major pitfalls in CAR T-cell therapy currently is the manufacturing costs. It is estimated that regardless of the manufacturing model chosen, the raw cost of production will likely be $25,000-35,000 per patient (Walker and Johnson, 2016). Wholesale acquisition costs of FDA approved therapies presently range from $373,000 – 475,000, these are exclusive of preparation, administration, and follow up costs (Borgert, 2021). To reduce the total costs of T-cell therapies it will be crucial to minimise the costs of goods and to streamline the manufacturing process through a move from manual open processes, to closed-automated ones (van der Walle *et al*., 2021). Dynabeads, due to their commercial licencing, will be a significant expense in the manufacturing costs. Moreover, they are not biodegradable and their inclusion in the manufacturing process requires open processing for their addition, removal, and sampling for residual bead release testing which increases manufacturing complexity and the risk of contamination. In an attempt to optimise, simplify, and drive down the cost of manufacturing, alternative activation technologies should continue to be explored.

A summary of advantages and disadvantages of all mentioned *ex vivo* T-cell activation technologies can be found below in **Table 1.2**.

Table 1.2. Advantages and Disadvantages of *ex vivo* T-cell Activation Methods

	Activation Method	Advantages	Disadvantages
Cell Based	Soluble antibodies and interleukins + Antigen-loaded irradiated allogenic PBMCS	• "Natural" activation • Potent activation of T-cells	• Expensive • Labour intensive • Need to source autologous cells • Additional regulatory requirements for cells
	Antigen loaded- K562 cells	• Easily modified to express antigens • Antigens are customisable • GMP compliant	• Cell banking necessary • Time consuming • Cells may express inhibitory molecules • Additional regulatory requirements for cells
Bead Based	aCD3/aCD28 microbeads	• Enhanced activation over soluble antibodies • Can be produced consistently • Beads are available off-the-shelf	• Non-biodegradable • Not easily removed
	Magnetic aCD3/aCD28 microbeads (Dynabeads™)	• GMP compliant • Available off-the-shelf • Potent activation • Removed via magnet • Efficacy demonstrated clinical trials and products	• Expensive • Exclusively licensed • Need for time-consuming removal • Additional release testing for residual beads • Non-biodegradable
	aCD3/aCD28 nanobeads (TransAct™)	• GMP compliant • Can be removed via centrifugation • Comparable activation to Dynabeads	• Removal via centrifugation can be difficult at larger scale • Non-biodegradable
	aCD3/aCD28 Hydrogel Beads (Cloudz™)	• Detachable from cells via reagent addition • Core of beads can be removed via magnet • GMP compliant	• No reported use in a clinical setting • Limited literature available
	Cytokine releasing microbeads	• Biodegradable • Localised release of cytokines better mimics natural APCs • Encapsulated cytokine can be tailored	• No reported use in a clinical setting • Only reported use is with murine T-cells • No protocol for removal

	Hydrogel coated magnetic	• Detachable from cells via reagent addition • Core of beads can be removed via magnet	• No reported use in a clinical setting • Core is non-biodegradable • Additional step in the removal process compared to Dynabeads
Complex Based	aCD3/aCD28 - Streptamer® complexes (Expamer™)	• Soluble reagent results in even distribution • Can be removed via centrifugation • Can be detached from cells	• No reported use in a clinical setting • Not available off-the-shelf • Safety of use not confirmed by clinical trials • Limited literature on its use
	aCD3 and aCD28 tetrameric antibody complexes (ImmunoCult™)	• GMP compliant • Available off-the-shelf • Easy to use • Soluble reagent results in even distribution • Provided in a defined and serum-free media • Removed through centrifugation	• Expensive • Removal via centrifugation can be difficult at larger scale
Scaffold Based	Carbon nanotube-polymer	• Can be removed via magnet • Localised release of cytokines better mimics natural APCs • Significantly less IL-2 required • Large surface area for antibody presentation	• No reported use in a clinical setting • Non-biodegradable • Only reported use is with murine T-cells
	3D scaffold of microrods	• Localised release of IL-2 • Significantly increased expansion compared to Dynabeads	• No reported use in a clinical setting • Not available off-the-shelf • Difficult to remove
	3D printed lattice	• Large surface area for antibody presentation • Compatible with the G-rex	• No reported use in a clinical setting • Not available off-the-shelf • Requires specialist equipment to produce • Not easily scalable

1.7. Measurements of Activation

The activation of T-cells is an event which results in physiological changes of the cell. These changes can be monitored and assessed within cell cultures to infer the activation status of T-cells. The key measurements of activation utilised in this thesis were: the expression of activation markers CD25 and CD69; proliferation assessed through cell number, cell cycle progression, and the succinimidyl ester of carboxyfluorescein diacetate (CFSE) membrane staining; and cell size. These are described further below.

1.7.1 Activation markers

Populations of T-cells are defined by their expression of extracellular markers, for example naïve T-cells can be defined by the expression of CD45RA, CD62L and CCR7 (Tumeh *et al*., 2010). Once activated, T-cells begin to express other markers which allow them to be distinguished from T_N. Upregulated molecules include receptor proteins, adhesion molecules, and chemokine receptors (Shipkova and Wieland, 2012). CD25 (the IL-2 receptor), for example, is essential for proliferation and is expressed transiently at high levels on T-cells once they have been activated (Malek, 2008). CD25 and other extracellular activation markers can be detected easily through the use of fluorescence-labelled antibodies and a flow cytometer, to assess T-cell activation. Another example of a commonly evaluated activation marker is CD69 (a C-lectin receptor). CD69 is also known as the early activation marker and can be detected as early as 30 minutes post-activation (Cibrián and Sánchez-Madrid, 2017).

1.7.2 Cell Size

Activated T-cells are also known to increase in size. This is due to an increase in cytoplasmic RNA and protein content as the T-cells are driven in phase G1 of the cell cycle and begin transforming into lymphoblasts. Image/video based analysis

of the mean cell sizes of T-cells have been used to discriminate between activated and non-activated T-cells (Teague *et al*., 1993; Renner *et al*., 2014*)*. Alternatively, this phenomenon can also be observed and more easily analysed through an increase in forward and side light scatter using a flow cytometer (MacDonald and Zaech, 1982; Böhmer *et al*., 2011).

1.7.3 Proliferation

Proliferation is another characteristic of stimulated T-cells that can be exploited to determine activation status. Activation of a T-cell initiates progression of the cell cycle out of the resting G0 and into a state of division. The proliferation of T-cells can be assessed in a number of different ways. Most simply, proliferation can be determined via a cell count to determine if cells are actively dividing. Other assays are often based on: the incorporation of a labelled nucleoside, such as ^{3}H-thymidine; the expression of nuclear antigens, such as proliferating cell nuclear antigen; mitochondrial activity; or the use of a dye that becomes diluted in daughter cells, such as CFSE (Shipkova and Weiland, 2012). Additionally, the proliferation status of T-cells can be assessed through a cell cycle assay to determine if cells are in a state of division.

1.8. 3D Scaffolds in Cancer Immunotherapy

1.8.1. Overview

Cell cultures can be performed on a 2D surface such as that of cell culture dish, or supported by 3D scaffold. 3D cultures offer many benefits and additional avenues of research as they can influence mechanical, physiochemical, and biochemical cues microenvironment that cells are exposed to and may facilitate cell to cell interactions and better mimic their natural microenvironments. 3D scaffolds have already widely been applied in many areas such tissue engineering, cancer modelling and drug validation (Unnikrishnan *et al*., 2021).

Moreover, 3D scaffolds present themselves as exciting tools for use in cancer immunotherapy as delivery vectors and stimulation technologies. These are discussed briefly below but can be found reviewed extensively elsewhere (Han and Wu, 2022).

1.8.2. Localised Stimulation and Delivery Vectors

A key application of biomaterial based scaffolds within cancer immunotherapy is their use as treatment delivery vectors, as they allow they localised delivery and stimulation of immune cells. One such application is the use of scaffolds as a cancer vaccine delivery system which recruits and stimulates DCs through the release of cancer antigens and adjuvants *in vivo*. Here scaffolds such as PGLA matrices, alginate cryogels, or silica microrods were either implanted or injected in mouse models (Ali *et al*.,2009; Bencherif *et al*., 2015; Li *et al*., 2018). Alternatively, a hydrogel scaffold may be implanted to release a chemotherapy drug in combination with ligands targeted at the inhibiting the immune checkpoint blockade (Wang *et al*., 2018). Most recently scaffolds have also been reported as delivery vectors for pre-activated DCs, T-cells, and CAR T-cells (Stephan *et al*., *2015; Weiden et al*., 2018; Lin *et al*., 2019; Agarwalla *et al*., 2020; Ahn *et al*., 2020; Hu *et al*., 2021).

1.8.3. *Ex vivo* T-cell Stimulation with 3D Scaffolds

As discussed in **Section 1.6.7**, the gold standard of T-cell activation in ACT (magnetic beads) has major disadvantages in that 1) the available antibody presenting surface is not fully utilised due to aggregation, 2) bead removal is required representing in an additional processing step - with inadequate removal resulting in a failure of quality standards, 3) they are not biodegradable, and 4) they present a significant processing cost. Alongside the advantages of 3D cell culture and the demonstrated potential of using 3D matrices as delivery systems

discussed above, 3D scaffolds possess additional benefits that may alleviate some of the problems presented with magnetic beads. A scaffold that is highly porous would allow an increase in surface area available to present stimulating ligands to T-cells. The structure may then serve a dual function as the expansion platform, with the potential for expanded cells to be removed through flow, eliminating the need for a bead removal step. Furthermore, such a scaffold could be produced from a low-cost biodegradable material which would both increase the sustainability of the process, and drive down costs. Implementation of such as scaffold as an expansion platform for T-cells would require further engineering considerations such as the perfusion of fresh media through the scaffold and a flow applied to ensure T-cells remain in suspension and able contact the scaffold.

Currently, research into 3D scaffolds as both a T-cell activation and expansion platform is limited, however examples have been reported and include electrospun polydimethylsiloxane (PDMS) (Dang *et al*., 2018), 3D printed polycaprolactone (PCL) lattices (Delalat *et al*., 2017), and silica micro-rods which settle in culture to form a "scaffold" (Cheung *et al.,*2018; Zhang *et al.,* 2020). Other studies describe the use of a scaffold where T-cells were pre-activated and transferred into scaffolds for expansion. These include a polystyrene scaffold, Matrigel™ (Pérez del Río *et al*., 2018), a polyethylene glycol – heparin (PEG-Hep) hydrogel (Pérez del Río *et al*., 2020), and alginate scaffolds (Majedi *et al*., 2020).

1.9. Polymers

1.9.1. Overview

Polymers generally fall within 3 groups: synthetic polymers, biopolymers, or a combination of both – also known as biocomposites. Within the literature some disparities exist in the use of the word biopolymer; for the purpose of this thesis, biopolymers are defined as materials with a natural origin, such as plants, animals, or micro-organisms, and synthetic polymers are defined as man-made. Biopolymers can be further classified into 3 groups: polysaccharides, polypeptides, or polynucleotides (Reddy *et al*., 2021). In most cases natural biopolymers confer major advantages over synthetic polymers in that they are biodegradable, biocompatible, and are derived from renewable sources (Gowthaman *et al*., 2021; Mtibe *et al*., 2021).

1.9.2. Hydrogels

Hydrogels are polymers that contain a large amount of water within their 3D structure; this is due to the network of polymer chains being hydrophilic. The composition of the hydrogel can be adjusted to result in a range of physical and chemical properties, such as stiffness and porosity. Due to high water content, soft consistency, and porosity, hydrogels have been applied widely in drug delivery, tissue engineering, and wound healing, as they closely simulate living tissue (Caló and Khutoryanskiy *et al*., 2014).

Common methods for characterising hydrogels include: assessing their swelling behaviour by measuring the weight or size both before and after water saturation, assessing stiffness and elasticity via tensile testing/ compression testing i.e. with atomic force microscopy, structural assessment using imaging techniques such as scanning electron microscopy (SEM) or transmission electron microscopy, chemical composition analysis using techniques such as

nuclear magnetic resonance (NMR) spectroscopy, and biocompatibility via cytotoxicity assays (Ahmed., 2015).

Both synthetic and biopolymer based hydrogels can also be found applied in the context of T-cell activation studies (**Table 1.3**). Here, hydrogels generally have antibodies, such as aCD3 and aCD28 attached to their surface. The exact method used to immobilise antibodies to the hydrogel depends on the chemical properties of the hydrogel. Two commonly applied methods include: the attachment of streptavidin to the hydrogel to bind to biotinylated antibodies, and the addition/exploitation of functional groups on the hydrogels surface to attach antibodies via carboxyl-amine crosslinking.

Table 1.3. Examples of Applications of Polymers in T-cell Therapy

	Material	Format	Application	Reference
Synthetic Polymer	Polystyrene	Microbeads	T-cell activation and expansion	Thermo Fisher Scientific (2022)
	Polylactide-co-glycolide	Micro and nano beads	T-cell activation and expansion	Steenblock and Fahmy (2008)
	Polycaprolactone	3D printed lattice	T-cell activation and expansion	Delalat *et al*. (2017)
	Synthetic silica	Microrods	T-cell activation and expansion	Cheung *et al*. 2018
	Polyisocyanopeptide	Porous hydrogel	T-cell expansion and delivery	Weiden *et al*. (2018)
		2D hydrogel surface	Research into receptors and forces in T-cell activation	Zhang *et al*. (2021)
	Polyacrylamide	2D hydrogel surface	Research into physiochemical cues in T-cell activation	Chin *et al*. (2020)
Synthetic Polymer + Biopolymer	Polyethylene-glycol-diacrylate + thiolated hyaluronic acid	2D hydrogel surface	Research into T-cell mechanosencing in activation	Hickey *et al*. (2019)
	Polyethylene-glycol + chitosan	3D porous hydrogel	T-cell delivery	Tsao *et al*. (2014)
	Poly-β-amino ester + polyglutamic acid*	mRNA nanocarriers	T-cell transduction	Moffett *et al.* (2017)
Biopolymer	Alginate	3D hydrogel scaffold	Research into the effect of the 3D microenvironment on T-cell activation	Majedi *et al*. (2020)
			T-cell delivery	Stephan *et al*. (2015)
			T-cell and adjuvant delivery	Smith *et al.* (2017)
			T-cell transduction and delivery	Agarwalla *et al*. (2020)
		Hydrogel coated on microbeads	T-cell activation and expansion	Jesuraj et al. (2016)
	Matrigel®	3D porous hydrogel	T-cell expansion	Pérez Del Río *et al*. (2018)

*Formed separate components of the final format.

1.10. Knowledge Gap

The use of hydrogels for biomedical applications has proved useful in many areas including contact lenses, hygiene products, wound dressings, tissue engineering scaffolds, and drug delivery systems. These can be found reviewed elsewhere (Caló and Khutoryanskiy, 2015). More specifically in the field of T-cell immunotherapy, hydrogels have most often been employed either as a delivery vector or to study the impact of mechanical properties, such as stiffness, on T-cell functionality and immune synapse formation, examples of these are shown in **Table 1.3.** (Judokusumo *et al*., 2012; Singh and Peppas, 2014; Basu *et al.,* 2016; Weiden *et al*., 2018; Wahl *et al*., 2019; Majedi *et al*., 2020).

T-cell activation and expansion studies employing a 2D or 3D hydrogel focus either on activation alone, or expansion where activation is provided externally (Stephan *at al.,* 2015; Smith *et al*., 2017; Pérez del Río *et al*.; 2018; Weiden *et al*., 2018; Chin *et al*., 2020; Majedi *et al*., 2020; Zhang *et al.,* 2021). Furthermore, reported expansion studies tend to last a maximum of 7 days. To the best of my knowledge at the time of writing, the literature available on the activation and expansion of primary human T-cells both with and on a 2D or 3D hydrogel scaffold is extremely limited. There is, therefore, a gap in knowledge and a need to explore this further, particularly with a longer term culture that is more representative of current CAR T-cell manufacturing practices.

Furthermore, the use of a porous scaffold provides the opportunity to explore a simplified method of T-cell seeding and removal which has not yet been reported and is not available with other activation technologies; by flowing T-cells into and out of the scaffold when required. This novel technology could ultimately provide

a 3D activation technology which could be integrated into a closed automated manufacturing system.

1.11. SpheriTech's Biopolymer

1.11.1. SpheriTech Biopolymer Chemistry

SpheriTech is a company that specialises in polymer technologies. One of their patented technologies is a biopolymer hydrogel consisting of poly-ε-lysine (ε-PL) cross-linked with a dicarboxylic acid, achieved through carbodiimide cross-linker chemistry (see **Figures 1.6** and **1.7**). ε-PL is a poly amino acid consisting of 25-35 repeated units of L-lysine in which polymerisation has occurred between the ε-NH_2 and the α-COOH. Fermented by bacteria in the genus Streptomyces, it is one of only 3 poly amino acids to be produced naturally; the other 2 being y-poly-glutamic acid and cyanophycin (Bajaj and Singhall, 2011). ε-PL is biodegradable, water-soluble, non-toxic, and displays a wide range of antimicrobial qualities (Yoshida and Nagasawa, 2003). These qualities have made it an attractive target for the food, medical, and bioelectronics industries. Most notable is its application as a food preservative in Japan, where it has been produced and used commercially from as early as 2000 (Hiraki, 2000). More recently, the cross-linking of ε-PL to produce a hydrogel/ biocompatible matrix and the potential applications of this have been investigated (Hua *et al*., 2016; Gallagher *et al*., 2018).

ε-PL contains an amine (NH_2) terminal group that allows it to be cross-linked with a carboxyl functional group (–COOH) of a dicarboxylic acid. A dicarboxylic acid is an organic compound that contains two carboxyl functional groups. Cross-linking is mediated using carbodiimide compound, 1-Ethyl-3-(3-dimethylaminopropyl)carbodiimide (EDC), and N-hydroxysuccinimide (NHS). EDC is known as a zero-length linker as no trace of it is left in the resulting

compound after the reaction has been completed. In the first step of this reaction, EDC reacts with the carboxylic acid to produce an unstable o-Acylisourea intermediate. Addition of NHS results in the unstable o-acylicourea intermediate becoming a stable NHS ester that is able to efficiently bond to the free amines of the ε-PL. An overview of carbodiimide cross-linking is shown in **Figure 1.7.**

Quantities of ε-PL and the dicarboxylic acid can be altered so that the completed reaction results in not all COOH's or NH2's bonded together. This results in a polymer that has either free carboxyl functional groups or free amines. When the polymer is created with free COOH's, the same 2-step reaction with EDC and NHS can again be utilised to immobilise proteins, such as antibodies, or other biomolecules that contain a free NH_2 terminal group on the polymer.

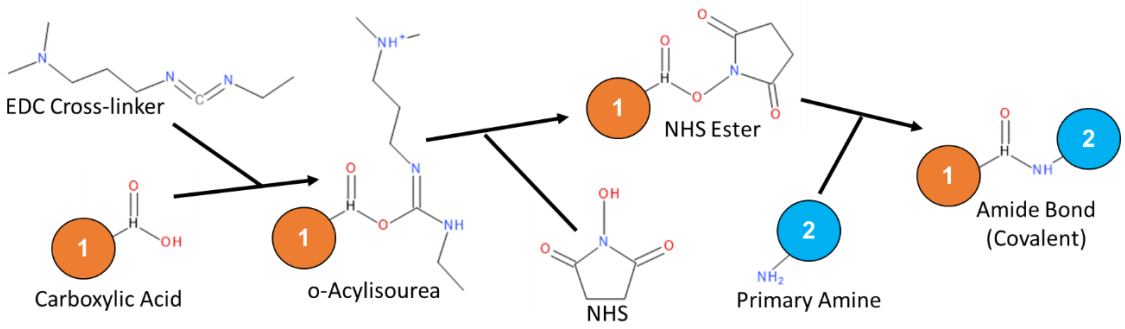

Figure 1.7. Carbodiimide mediated cross-linking chemistry. EDC reacts with a carboxylic acid to form an o-Acylisourea intermediate. NHS reacts with this intermediate to form an amine reactive NHS ester. A primary amine is then added which results in the formation of a covalent amide bond between the carboxylic acid and the primary amine. EDC = 1-Ethyl-3-(3-dimethylaminopropyl) Carbodiimide. NHS = N-hydroxysuccinimide.

Furthermore, by utilising dicarboxylic acids that consist of differing lengths of carbon chains as a cross-linker, final properties of the produced polymer, such as rigidity, porosity, and clarity can be altered (Gallagher *et al*., 2017). The studies performed in this thesis were first based on a self-assembling porous polymer

structure produced from the cross-linking of ε-PL with brassylic acid (tridecanedioic acid, $C_{13}H_{22}O_4$); this was termed polymer A (**Figure 1.8**). Secondly, studies were performed using a second biopolymer hydrogel produced in a non-porous and porous format through the cross-linking of ε-PL and suberic acid (octanedioic acid, $C_8H_{14}O_2$) (**Figure 1.8**). Porosity was achieved through the introduction of an additive (patent pending) during polymerisation.

Polymer A was recommended for use by SpheriTech following a discussion of the requirements of a material for this study: porous, cell culture compatible, able to bind antibodies to the surface, and structurally sound enough to implement a flow through. Once it became apparent that Polymer A may not be suitable, Polymer B was recommended as it met the same requirements.

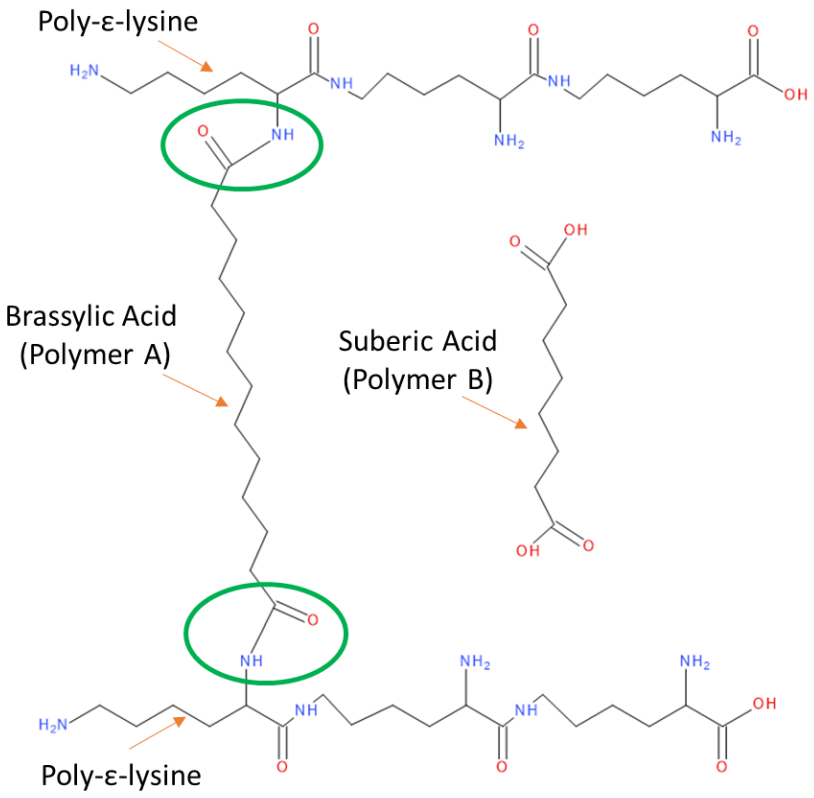

Figure 1.8. Cross-linking of poly-ε-lysine with dicarboxylic acids to produce SpheriTech's biopolymers. Polymer A was created through the cross-linking of poly-ε-lysine with brassylic acid. Polymer B was created through the cross-linking of poly-ε-lysine with suberic acid. Amide bonds are circled.

1.12. Thesis Aims

The overarching aim of this thesis is to demonstrate and characterise the activation and expansion of primary human T-cells using SpheriTech's biopolymer technologies as a platform. Further, this thesis seeks to develop this novel technology in a 3D format to maximise the surface area presenting stimulating ligands to cells, and to simplify processing through the mitigation of the bead removal step which is currently necessary when activating with antibody coated beads; ultimately with the aim of reducing processing costs in T-cell therapies.

This thesis comprises of 5 results chapters in which the specific aims are as follows:

Chapter 3 – To characterise a first biopolymer, termed polymer A. This is assessed in regards to: its porous structure and the impact of polymer density on pore size, porosity, and tortuosity; antibody attachment; biocompatibility; and auto-fluorescence properties.

Chapter 4 – Primarily, to evaluate the use of polymer A as a 3D T-cell activating scaffold through the demonstration of activation with polymer A, and the assessment of cell recovery of T-cells from a polymer A scaffold. Investigations into non-specific binding and flow through conditions are undertaken with the aim of improving cell recovery. Additionally, to characterise various activation technologies and to compare activation read outs of both cell line Jurkats and primary human T-cells as a foundation for further studies

Chapter 5 – To characterise a second biopolymer, termed polymer B, in both a porous and non-porous format. This is assessed in regards to: its surface

topology (non-porous) or porous structure/pore size (porous format); antibody attachment, biocompatibility; and auto-fluorescence properties.

Chapter 6 – To assess the interaction of T-cells with polymer B. Specifically, to demonstrate seeding and removal of cells into the porous format, to characterise the migration of T-cells on polymer B, to validate the ability of T-cells to expand on the surface, and to investigate if expansion on polymer B impacts T-cell growth.

Chapter 7 – To demonstrate and characterise activation and expansion of primary human T-cells with polymer B in both a non-porous and porous scaffold format. To investigate the impact of polymer B expansion on the resultant populations of T-cells. To compare expansion via polymer B with expansion via aCD3/aCD28 magnetic beads (Dynabeads). Finally, to visualise the growth of T-cells on polymer B.

1.13. Thesis Hypothesis

It is hypothesised that primary human T-cell activation and expansion can be achieved with aCD3/aCD28 coated SpheriTech biopolymer matrices, and that the expansion will be comparable to that with aCD3/aCD28 coated magnetic beads. T-cell exhaustion may also be reduced when activating with aCD3/aCD28 polymer, possibly as a result of less TCR stimulation than with multiple beads interacting with a single cell. It is further hypothesised that this can be achieved with polymer in the format of a porous 3D scaffold and that this will remove the need for a bead removal step and the risk associated with residual beads.

Chapter 2. Materials and Methods

2.1. General Methods

2.1.1. Cell Culturing Methods

2.1.1.1. Complete RPMI Media

Complete RPMI media was prepared by supplementing plain RPMI 1640 medium (Gibco; Thermo Fisher Scientific, Paisley, UK) with 10 % fetal bovine serum (FBS) (Gibco) and 2 mM L-glutamine (Sigma-Aldrich, Dorset, UK). Both Jurkat and primary sourced T-cells were cultured in complete RPMI.

2.1.1.2. Jurkat Cell Culturing

Jurkat, clone E6-1, cells were purchased from the American Type Culture Collection (Virginia, USA). Cells were cultured in complete RPMI media at 37 °C with 5 % CO_2. Flasks were subcultured every 2-4 days by removing the cells in spent media, centrifuging at 400 G for 5 minutes to pellet the cells, removing the spent media, and re-suspending the cells in fresh media. The cells were then counted and diluted as appropriate with fresh media in new flasks, to a seeding density of $1 \times 10^5 – 5 \times 10^5$ cells/mL.

2.1.1.3. Human Blood Procurement

Whole blood in sodium citrate, from healthy donors aged 18 – 60 years old, was purchased from Cambridge Bioscience (Cambridge, UK). Blood samples were collected under a comprehensive informed consent permitting the use of blood for research applications. Research Ethics Committee (REC) favourable opinion was obtained (REC reference: 17/SW/0189) prior to commencing the study. Blood was received and processed on the same day as collection.

2.1.1.4. PBMC Isolation from Whole Blood

Whole blood in sodium citrate was mixed at a 1:1 ratio with plain RPMI 1640 medium supplemented with 2 % FBS (v/v). (both Gibco). For each 30 mL of blood, 15 mL Lymphoprep™ (STEMCELLTechnologies, Vancouver, Canada) was added to a SepMate™ tube (STEMCELL Technologies) and the sample was centrifuged at 1,200 G for 10 minutes with breaks on setting 9. PBMCs were collected from the buffy coat and diluted 1:3 with RPMI, 2 % FBS (v/v), before being transferred to a centrifuge tube (Corning, New York, USA) and centrifuged at 500 G for 10 minutes with breaks on setting 3. Supernatant was discarded and PBMCs were re-suspended in complete RPMI supplemented with 1 % Antibiotic-Antimycotic (v/v) (Gibco).

2.1.1.5. $CD3^+$ T-cell Isolation from PBMCs using a MACS® Column

PBMCs were centrifuged at 400 G for 5 minutes. Supernatant was removed and PBMCs were re-suspended in 40 µL de-gassed buffer per 1 x 10^7 cells, consisting of MACS® BSA Stock Solution 1:20 MACS® Rinsing Solution (both Miltenyi Biotech, Bergisch Gladbach, Germany). 10 µL of Pan T-cell Biotin-Antibody Cocktail (Miltenyi Biotech) per 1 x 10^7 cells was added to the cell suspension and incubated at 4 °C for 5 minutes. Pan T-cell Biotin-Antibody Cocktail contained biotinylated antibodies against CD14, CD15, CD16, CD19, CD34, CD36, CD56, CD123, and CD235a, which label non-T-cells in the cell suspension. 30 µL buffer and 20 µL Pan T-cell MicroBead Cocktail per 1 x 10^7 cells was added and incubated at 4 °C for 5 minutes. Pan T-cell MicroBead Cocktail contained magnetic beads which bound to the antibodies from the antibody cocktail. LS MACS® columns were placed on a magnetic cell separator (both Miltenyi Biotech) and rinsed with 3 mL buffer. Cell suspension was added, followed by 3 mL buffer which separated. Antibody/magnetic bead labelled cells were retained

in the column and $CD3^+$ T-cells were collected at the base of the column and cryopreserved using Cryostor CS10 (STEMCELL Technologies) cryopreservation media. Purity was confirmed by staining cells for CD3 and analysing by Flow Cytometry, as per **Methods 2.1.3.1** and **2.1.5.8** using the panel detailed in **Table 2.5**.

2.1.1.6. Primary T-cell Culturing

Primary $CD3^+$ T-cells were cultured in complete RPMI media supplemented with 1 % Antibiotic-Antimycotic (v/v) (Gibco) at 37 °C with 5 % CO_2. Cells were thawed as required from frozen and left in culture media at 37 °C with 5 % CO_2 for 24 hours before being seeded into experiments.

2.1.1.7. Cryopreservation

Cells to be cryopreserved were centrifuged at 400 G for 5 minutes. Media was removed and the cell pellet was re-suspended to 1 x 10^6 - 5 x 10^6 cells/mL with CryoStor® CS10 (STEMCELL Technologies). 1mL cell suspension was aliquoted into cryogenic vials (Nalgene; Thermo Fisher Scientific, Massachusetts, USA). Vials were then transferred into a Mr. Frosty™ Cryo-Freezer (Nalgene; Thermo Fisher Scientific) and stored at -80 °C to be frozen at a rate of -1 °C/min for 24 hours. Vials were then transferred to liquid nitrogen containers for long-term storage.

2.1.2. T-cell Stimulation Methods

2.1.2.1. Dynabeads® Human T-Activator CD3/CD28

Dynabeads ® (Gibco) were supplied as a suspension containing 4 x 10^7 beads/mL. The required volume, corresponding to the required quantity of Dynbeads, was calculated. Dynabeads were re-suspended in the vial via vortexing and the desired volume of Dynabead suspension was transferred to a tube. Dynabeads were washed with 1 mL sterile phosphate-buffered saline (PBS)

(Gibco) before being re-suspended in RPMI cell culture medium. Dynabeads were added to cell cultures at a 1:1 cell to bead ratio. T-cell cultures stimulated with Dynabeads were supplemented with 30 IU/mL rIL-2 (Miltenyi Biotech) and incubated at 37 °C with 5 % CO_2. Additional media supplemented with 30 IU/mL rIL-2 was added or media was changed every 2-3 days. Dynabeads remained in cultures for the entirety of the culture.

2.1.2.2. T Cell TransAct™

T Cell TransAct™ (Miltenyi Biotech) was added to cell culture suspensions as per the volume recommended by the manufacturer (**Table 2.1**). The volume of TransAct added to cultures that contained less than the total T-cell number for the corresponding culture plate format remained the same as recommended for the well plate size. T-cell cultures were supplemented with 30 IU/mL rIL-2 (Miltenyi Biotech) and incubated at 37 °C with 5 % CO_2. Additional media supplemented with 30 IU/mL rIL-2 was added or media was changed every 2-3 days. TransAct remained in cultures for the entirety of the culture.

Table 2.1. Manufacture Recommendations for T Cell TransAct™

Culture Plate	Total T-cell Number	T Cell TransAct™ to Add Per Well	Max Total Volume
96-well	0.3×10^6	2 µL	0.2 mL
48-well	1×10^6	10 µL	1 mL
24-well	2×10^6	20 µL	2 mL

2.1.2.3. aCD3/aCD28 Coated Wells

Antibody was diluted in sterile PBS (Gibco) to the desired concentration of 1 µg aCD3, 1 µg aCD28 /mL (either Miltenyi Biotec or BioLegend, London, UK). In 96-well plates, 100 µL of antibody solution was added and incubated at 4 °C

overnight. Antibody solution was removed and wells were washed 3 times with sterile PBS before exposure to cells. Cells were exposed to antibody coated wells for the entirety of the culture.

2.1.3. Cell Staining Methods

2.1.3.1. Extracellular Immunostaining for Flow Cytometry

Cell suspensions were centrifuged at 400 G for 5 minutes. Supernatant was removed and the cells were re-suspended in brilliant stain buffer (BD Biosciences). The cell suspension was then centrifuged at 400 G for 5 minutes, supernatant removed, and re-suspended in 50 µL brilliant stain buffer. Test volumes of antibodies and viability dyes, displayed in **Section 2.1.5.9**, were added to each sample and incubated in the dark for 20 minutes at room temperature. Cells were washed with brilliant stain buffer, centrifuged at 400 G for 5 minutes and supernatant removed; this was repeated twice. Cells were then re-suspended in 400 µL brilliant stain buffer and filtered through a 40 µm cell strainer (pluriSelect, El Cajon, USA). Cells were then either analysed live within 1 hour of staining, or fixed.

Cells that were fixed were re-suspended in 4 % PFA (w/v) (Sigma Aldrich). Cells were incubated at 4 °C for 15 minutes, then centrifuged at 400 G for 5 minutes and the supernatant removed. Cells were washed with brilliant stain buffer, centrifuged at 400 G for 5 minutes, and the supernatant was removed. Cells were re-suspended in 400 µL brilliant stain buffer. Fixed samples were then stored at 4 °C in the dark and analysed within 3 days.

2.1.3.2. CellTracker™ Staining

1 x 50 µg vial of CellTracker™ Red CMTPX Dye (Invitrogen) was re-constituted to a 10 mM stock solution in 7.3 µL DMSO (Sigma-Aldrich). 0.4 µL stock solution was then diluted in 4 mL HEPES RPMI 1640 medium (Gibco) supplemented with

2 mM L-glutamine (Sigma-Aldrich) to a 1 µM concentration. 10 mL of cell suspension at 5 x 10^5 cells/mL were centrifuged at 400 G for 5 minutes, supernatant removed, re-suspended in 4mL CellTracker solution and incubated for 45 minutes at 37 °C with 5 % CO_2. Cells were washed 3 times by centrifugation at 400 G for 5 minutes, supernatant removal, and re-suspension in complete HEPES RPMI media.

2.1.3.3. Rapid Red Staining for Incucyte®

1 x vial of Incucyte® Cytolight Rapid Red Dye (Sartorius) was re-constituted in 20 µL DMSO (Sigma-Aldrich) and added to 180 µL sterile PBS (Gibco) to give a 100 µM solution. Cell suspensions were centrifuged at 500 G for 5 mins, supernatant removed, cells washed with 10 mL sterile PBS, centrifugation repeated, supernatant removed, and cells re-suspended in sterile PBS to a concentration of 1 x 10^5 cells/mL. Rapid red solution was added at 1:99 and incubated for 20 minutes at 37 °C with 5 % CO_2. 6 times the cell suspension volume of complete RPMI media was added. Cell suspension was centrifuged at 500 G for 5 minutes, supernatant removed, and re-suspended in complete RPMI media.

2.1.3.4. Live Nuclear Staining

1 x vial of SYTO™ Deep Red Nucleic Acid Stain for live cells (Invitrogen) was re-constituted in 50 µL DMSO (Sigma-Aldrich). This was then diluted to 2 µM in the same medium as the cell culture to which it will be added. Stain solution was added to cells in culture to give a final concentration of 0.67 µM. Cells were stained for 1 hour at 37 °C with 5 % CO_2.

2.1.3.5. CFSE Staining

Cell suspensions were centrifuged at 400 G for 5 minutes, supernatant was removed, and the cells were re-suspended in and washed with sterile PBS

(Gibco) – twice. Cell suspensions were then centrifuged at 400 G for 5 minutes, supernatant removed, and cells were re-suspended in sterile PBS to a concentration of 1 x 10^6 cells/mL. An equal volume of 10 µM CFSE (Insight Biotechnology, London, UK) dissolved in sterile PBS was added and mixed via vortex, giving a final CFSE concentration of 5 µM. The cell suspension was incubated for 20 minutes at room temperature in the dark. 5 times the volume of the cell suspension was added of cold media and incubated for 5 minutes on ice in the dark. This was then centrifuged at 400 G for 5 minutes, supernatant was removed, and cells were re-suspended in complete RPMI media. Centrifugation and supernatant removal was repeated with cells being re-suspended in complete RPMI media supplemented with 1 % Antibiotic-Antimycotic (v/v) (Gibco).

2.1.4. Polymer Production Methods

2.1.4.1. Polymer A Production

Polymer was produced in accordance to the patent owned by SpheriTech Ltd. A 200 mL stock of ε-PL solution was prepared by dissolving 40.9 g ε-PL (Handary, Belgium) in 200 mL MilliQ water on a roller shaker (IKA-Werke) for 1 hour. The pH of the solution was adjusted to 7.1 using 5 M NaOH (Fluka Analytical, Czech Republic) before being filtered through a 0.45 µm Nylon + GMF 25 mm syringe filter (Whatman, Maidstone, UK) into a clean 200 mL glass flask (Duran, USA). A stock of brassylic acid solution was prepared by adding 24.4 g brassylic acid (supplied by SpheriTech, lot no. 13213110105) to 21.15 g NMM, 99% (Alfa Aesar, UK) and 20 mL MilliQ water in a 200 mL glass flask. The solution was placed in a Branson 2510 ultrasonic cleaner (Branson Ultrasonics Corporation, Connecticut, USA) for 30 minutes with gentle mixing occurring every 10 minutes. MilliQ water was added to the solution so that the total volume was 200 mL before

being filtered through a 0.45 µm Nylon + GMF 25 mm syringe filter (Whatman) into a clean 200 mL glass flask.

In a 50 mL centrifuge tube (Corning), a monomer solution was prepared. ε-PL stock solution, brassylic acid stock solution, and 30 µL 5 % TWEEN® 80 (v/v) (Sigma-Aldrich, Dorset, UK) was added to the centrifuge tube. MilliQ water was added so that the total volume of the solution was 25 mL and the solution was mixed gently. In a separate 50 mL centrifuge tube NHS 98+ % (Alfa Aesar) and EDC (AnaSpec, Freemont) were dissolved in MilliQ water to make a total volume of 25 mL. Both solutions were mixed together and inverted 3 times to produce a polymer solution.

Quantities of ε-PL stock solution, brassylic acid stock solution, NHS, and EDC were varied according to the density and NH_2:COOH ratio required. Brassylic acid and ε-PL was provided so that the NH_2:COOH ratio was 1:1.05; resulting in unreacted COOH functional groups in the final polymer. NHS and EDC were provided in excess to ensure efficient bond formation. EDC reacts with the –COOH groups in brassylic acid to produce an unstable o-acylicourea intermediate. Addition of NHS stabilises the intermediate to form an active NHS ester that is then able to form a covalent bond with the NH_2 groups present in ε-PL.

Quantities used for each requirement can be found in **Table 2.2**. Densities of polymer A were recommended my SpheriTech Ltd and represented a range in which the pore size was expected to be large enough to allow T-cells to pass through and in which the density was high enough for the polymer to retain its structure.

Table 2.2. Details of Polymer A Produced

Density (g/cm^3)	Total Volume (mL)	Poly-ε-lysine Stock Solution (mL)	Brassylic Acid Stock Solution (mL)	NH_2:COOH ratio	EDC (g)	NHS (g)
0.067	50	12.00	15.00	1:1:05	7.18	0.164
0.050	50	9.00	11.25	1:1.05	5.39	0.123
0.040	50	7.20	9.00	1:1.05	4.31	0.100
0.033	50	6.00	7.50	1:1.05	3.59	0.082

2.1.4.2. Polymer A Syringe Casting

Initially, solutions of polymer are liquid and set over time, taking the shape of their container; therefore, polymer solution must be placed into a mould of an appropriate shape. For polymer cast in plastic syringes, polymer solution was taken up by syringe (BD Biosciences, UK) whilst still in liquid form (**Figure 2.1**). In 5 mL or 10 mL syringes, 2 ml of polymer solution was taken up. The polymer was left to set overnight at room temperature. The syringe plunger was removed and the polymer was washed through with de-ionised water 5 times. For polymer that was not to undergo further antibody attachment, 1 M ethanolamine (EA) (Sigma-Aldrich) in 0.1 M 2-(N-Morpholino)ethanesulfonic acid (MES) was added and left to soak for 30 minutes at room temperature to cap un-reacted carboxyl, before being washed 3 times with MilliQ water. All polymer in syringes were filled with MilliQ water or PBS (Gibco), sealed with a luer plug (Bio-Rad, California, USA) and parafilm® (Heathrow Scientific, Vernon Hills, USA) and stored at 4 °C.

Figure 2.1. Polymer A cast into a cylindrical format using a syringe. Image shows 2 mL of polymer solution taken into a 5 mL syringe.

2.1.4.3. Polymer A Disc Production

7.5 mL of polymer solution was pipetted into a 100 mm (width) x 100 mm (length) x 20 mm (depth) square petri dish (Sarstedt, Nümbrecht Germany). The polymer solution was left to set overnight, covered and on a flat surface at room temperature. Set polymer was washed 5 times with de-ionised water. Discs of polymer were then cut from the sheet using a 6 mm inner diameter (ID) cork borer (Thermo Fisher Scientific) (**Figure 2.2**). For polymer that was not to undergo further antibody attachment, 1 M EA (Sigma-Aldrich) in 0.1 M MES was added, left to soak for 30 minutes at room temperature, before being washed 3 times with MilliQ water. All polymer discs were stored and then stored in MilliQ water or sterile PBS (Gibco) at 4 °C.

Figure 2.2. Disc production from polymer A. Image shows polymer A cast into a 100 mm (width) x 100 mm (length) x 20 mm (depth) square petri dish - left. The cork borer used to cut discs from the polymer sheet – centre. Resultant 6 mm diameter polymer A discs – right.

2.1.4.4. Polymer A Silicon Tubing Casting

Platinum cured 15 mm ID silicon tubing (SILEX Ltd., Hampshire, UK) was cut into sections 25 cm in length. One end of each section was plugged using a tubing connector (VWR International, Pennsylvania, USA) wrapped in parafilm® (Heathrow Scientific). 15 mL polymer solution was transferred into each section and covered with parafilm®. Tubing was held in a vertical position using a clamp stand and polymer was let to set overnight, see **Figure 2.3**. Set polymer was removed and cut into cylindrical sections 1.5 cm in length using an carbon steel cutting wire (Kitchen Craft, Winnipeg, Canada) whilst being hydrated with MilliQ water. Polymer sections were washed 5 times with MIlilQ water on a roller shaker (IKA-Werke). Polymer was then submerged in PBS, 1 % BSA (w/v), 0.5 M ethylenediaminetetraacetic acid (EDTA) (all Gibco) and stored at 4 °C.

Figure 2.3. Polymer A cast into a 15 mm diameter cylindrical format using silicon tubing. Image shows sections of silicon tubing plugged with a tubing connector, suspended vertically using a clamp stand, and partially filled with polymer A solution.

2.1.4.5. 3D Printed Mould

A mould was designed using Paint 3D (Microsoft) consisting of 24 hollow cylinders 15 mm diameter x 500 mm height. This design was produced via 3D printing using white resin (Formlabs, USA) by Dr. Marco Marques (Department

of Biochemical Engineering, UCL) (**Figure 2.4**). 2 mL polymer solution was pipetted into each “well” and was left to set overnight, covered and on a flat surface at room temperature. Set polymer was removed using tweezers (Knipex, Germany) and a Pasteur pipette (Appleton Woods Ltd, Birmingham). Polymer was washed 5 times with MilliQ water on a roller shaker (IKA-Werke). Polymer was then submerged in PBS, 1 % BSA (w/v), 0.5 M EDTA (all Gibco) and stored at 4 °C.

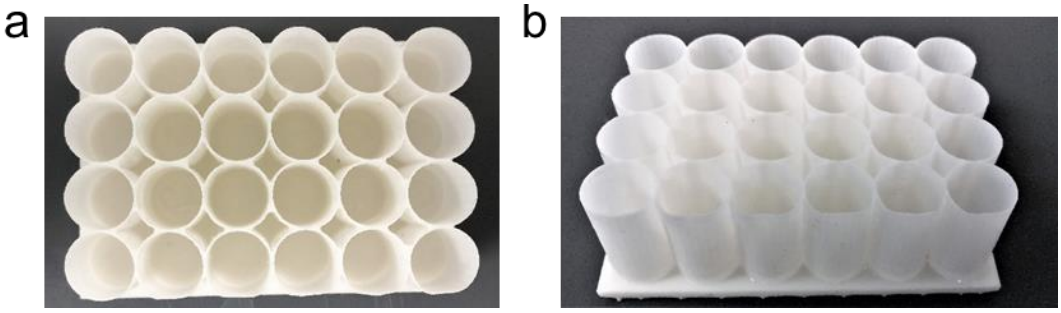

Figure 2.4. 3D printed mould to cast polymer A in a 15 mm diameter cylindrical format. Mould contains 24 x hollow cylinders with a 15 mm inner diameter. **a.** Top view of mould. **b.** Angled side view of mould.

2.1.4.6. Attachment of Antibody to SpheriTech’s Carboxyl-Functionalised Polymer A in Disc Format

Polymer discs were washed with 0.1 M MES, pH 5.5 (Sigma-Aldrich) twice. 20 x polymer discs were soaked in 2 mL MES + 0.078 g EDC + 0.057 g NHS in a 2 mL centrifuge tube (Eppendorf, Hamburg, Germany) for 30 minutes at room temperature on a tube rotator (Thermo Fisher Scientific). Polymer was washed 5 times with MES. Antibody solution was prepared by diluting antibody in MES to give a final concentration of 40 µg aCD3, 40 µg aCD28 /mL. 100 µL antibody solution per 0.5 mL centrifuge tube containing 4 polymer discs was added and left overnight at room temperature on a tube rotator. Antibody solution was removed and 500 µL 1 M EA (Sigma-Aldrich) in MES was added to each tube for

30 minutes at room temperature. EA was then removed. Polymer discs to be used in cell culture and polymer characterisation investigations were then washed 3 times with, and stored in sterile PBS (Gibco) at 4 °C.

2.1.4.7. Polymer B Formats

Polymer B, both with aCD3 and aCD28 attached and without, was produced and provided by SpheriTech Ltd. at a density of 0.071 g/cm^3. Polymer was provided in the following formats: non-porous discs, either 6 or 10 mm diameter x 1 mm height (**Figure 2.5**); or porous cylinders encased within a plastic casing, 7 mm diameter x 30 mm height (**Figure 2.6**). Porous polymer discs, 6 mm diameter x 30 mm height (**Figure 2.7**), were produced from the porous cylinders. Porous cylinders were sliced into sections using a sterile disposable scalpel (VWR International), and then cut to a 6 mm diameter using a 6 mm ID cork borer (Thermo Fisher Scientific).

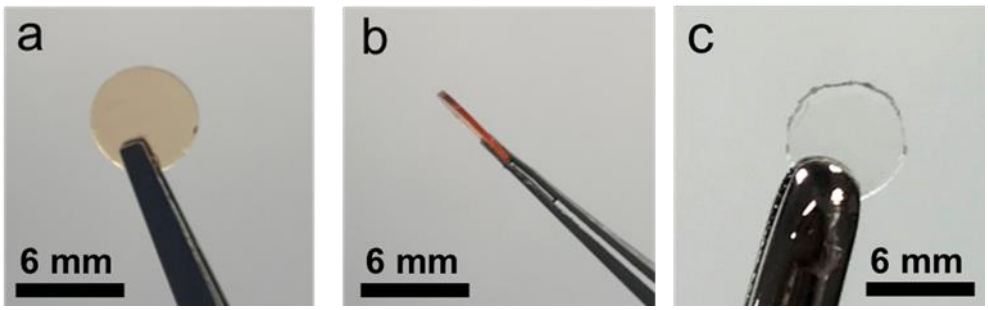

Figure 2.5. Non-porous polymer B disc. A transparent disc which has been pre-soaked in RPMI media in order to image it. **a.** Top view of disc. **b.** Side view of disc. **c.** A transparent disc pre-media soaking. Scale bars = 6 mm.

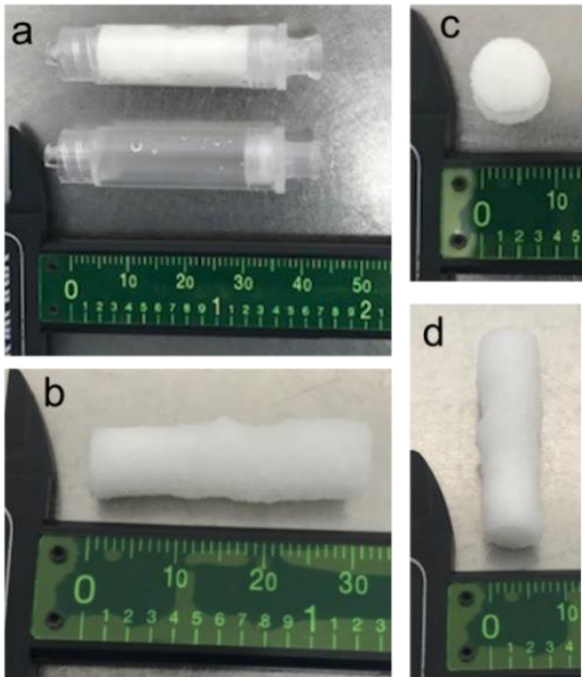

Figure 2.6. Porous polymer B in a cylindrical format. a. Polymer cylinder encased within a plastic casing – top. Empty plastic casing - bottom. **b.** Size view of polymer cylinder showing height. **c.** Top view of polymer cylinder showing circular face. **d.** Side view of polymer cylinder showing width. Top line of ruler shows values in mm.

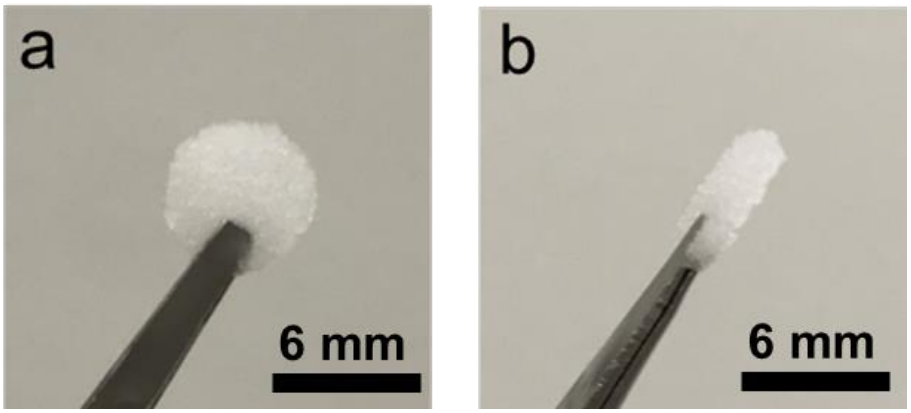

Figure 2.7. Porous polymer B in a disc format. a. Top view of disc. **b.** Side view of disc. Scale bar = 6 mm.

Calculations were performed to estimate the volumes of aCD3 and aCD28 required to cover the surface area of the polymers, an overview is shown in **Table 2.3**. For the purposes of these calculations, pores within the porous cylinder format of polymer B were assumed to be straight line channels and the outer surface was assumed to be solid and the top and bottom were excluded. The surface area of all channels within the porous cylinder was determined using ***Equation 1***. The outer surface area for porous cylinders was determined using ***Equation 2***. The outer surface area for discs was determined using **Equation 3.** The quantity of either aCD3 or aCD28 at a 1:1 ration to cover the polymer was calculated using ***Equation 4***.

$$Surface\ Area\ of\ Channels = Number\ of\ Channels \cdot 2\pi rh$$

Where r is the radius, and h is the height.

(Eq. 1)

$$Outer\ Surface\ Area\ of\ Porous\ Cylinder = 2\pi rh$$

(Eq. 2)

$$Outer\ Surface\ Area\ of\ Discs = (2\pi rh) + (2\pi r^2)$$

(Eq. 3)

.

$$Quantity\ of\ Antibody\ (\mu g) = \frac{\left(\frac{Total\ Surface\ Area\ of\ Polymer}{Surface\ Area\ of\ Antibody}\right) \cdot 0.5}{No.\ of\ Antibody\ in\ 1\ \mu g}$$

(Eq. 4)

For batch 3, antibody quantities for the porous cylinder were increased ~10-fold and for discs were increased >100-fold in an attempt to improve antibody attachment. Final volumes of aCD3 and aCD28 used for each batch are displayed in **Table 2.4**.

Table 2.3. An Overview of Calculated Values to Determine Antibody Quantities used for Attachment.

	Porous Cylinder	Non-Porous Disc 10 mm	Non-porous Disc 6 mm
Cartridge Height (µm)	25000	1000	1000
Cartridge Diameter (µm)	9000	10000	6250
Channel Diameter (µm)	250	N/A	N/A
No. of Channels	1007	N/A	N/A
Surface Area of all Channels (μm^2)	1.58E+10	N/A	N/A
Outer Surface Area (μm^2)	7.07E+08	1.88E+08	8.10E+07
Total Surface Area	1.65E+10	1.88E+08	8.10E+07
Antibody Width (µm)		0.014	
Antibody Height (µm)		0.008	
Antibody Area (µm2)		1.12E-04	
No. of Antibodies to Cover Total Surface Area	1.48E+14	1.68E+12	7.23E+11
aCD3:aCD28 at 1:1 Coverage			
No. of anti-CD3 required	7.38E+13	8.41E+11	3.62E+11
No. of aCD3 antibodies in 1µg		1.08E+13	
aCD3 required (µg)	6.830	0.078	0.033
No. of anti-CD28 required	7.38E+13	8.41E+11	3.62E+11
No. of aCD28 antibodies in 1µg		2.62E+13	
aCD28 required (µg)	2.820	0.032	0.014

Table 2.4. Details of aCD3 and aCD28 quantities used for antibody attachment.

		Antibody Quantity (µg, 2 SF)	
Batch	**Polymer Format**	**aCD3**	**aCD28**
1	Porous Cylinder, 6mm Diameter x 3 mm height	6.8	2.8
2	Non-porous Disc, 6 mm Diameter	0.034	0.014
	Non-porous Disc, 10 mm Diameter	0.078	0.032
	Porous Cylinder, 6mm Diameter x 3 mm height	6.8	2.8
3	Non-porous Disc, 6 mm Diameter	4.0	2.0
	Non-porous Disc, 10 mm Diameter	8.0	4.0
	Porous Cylinder, 6mm Diameter x 3 mm height	70	35

2.1.4.8. Sterilisation of Polymer

Prior to exposure to cell cultures, polymer required sterilisation. Polymer was soaked in PBS (Gibco) for 30 minutes. PBS was removed and replaced with 70 % (v/v) aqueous ethanol solution. Polymer was soaked in ethanol for 3 hours. Polymer was then transferred to a cell culture cabinet. In the case of movable discs or scaffolds, the polymer was transferred using sterile tweezers (Thermo Fisher Scientific) into a sterile well plate containing sterile PBS. Polymer was soaked in the sterile PBS for 30 minutes on an IKA HS 260 Basic rocker (IKA-Werke, Staufen, Germany). The PBS wash step was repeated 3 times, removing and replacing the PBS each time. After the final PBS wash, the PBS was removed and replaced with complete RPMI media. Polymer was then incubated in the cell culture media at 37 °C overnight. Media was inspected for contamination prior to use in cell culture studies.

2.1.4.9. Freeze Drying of Polymer for Scanning Electron Microscopy

Polymer was freeze dried using an Edwards Super Modulyo Freeze Dryer (Edwards Lifesciences, California, USA) with a temperature transition of -30 to 26 °C, at SpheriTech Ltd. laboratories**.** Polymer was stored dried at room temperature for 1 day before imaging.

2.1.4.10. Freeze Drying of Polymer for X-Ray Computed Tomography

Polymer set in syringes were freeze dried using a VirTis Genesis 25EL Lyophilizer (VirTis, New York, USA) with a temperature transition of -30 to 26 °C. Polymer was stored dried at room temperature for up to 3 months.

2.1.5. Analytical Techniques

2.1.5.1. Cell Counting and Viability

Cell counting was performed using a Vi-CELL™ automated cell counter (Beckman Coulter, California, USA), or a NucleoCounter® NC-3000™ system

with a Via1-Cassette™ (ChemoMetec, Allerod, Denmark); these required a 0.5 mL or a 60 µL cell suspension sample, respectively. Both cell counting systems provided a live cell count, a dead cell count, and therefore, a total population cell viability.

2.1.5.2. Cell Diameter

The diameter of cells were measured using a NucleoCounter® NC-3000™ system (ChemoMetec) which provided an average cell diameter per 60 µL sample.

2.1.5.3. Apoptosis Assay

Cell suspensions of a volume corresponding to 2-4 x 10^5 cells were centrifuged at 400 G for 5 minutes and the supernatant was discarded. Cells were then re-suspended in 300 µL PBS (Gibco), centrifuged at 400 G for 5 minutes, and the supernatant discarded. 200,000 – 400,000 cells were re-suspended in 100 µL Annexin V binding buffer (Biotium California, USA). 2 µL Annexin V-CF®488A (Biotium) and 2 µL 500 µg/mL Hoechst 33342 (Solution 15, ChemoMetec) were added and mixed via pipetting. Cells were incubated at 37 °C for 15 minutes before being centrifuged at 400 G for 5 minutes at room temperature. Supernatant was removed, cells were re-suspended in 300 µL Annexin V binding buffer and centrifuged at 400 G for 5 minutes – this was repeated once. Cells were then re-suspended in 100 µL Annexin V binding buffer and 2 µL 500 µg/mL propidium iodide (PI) (Solution 16, ChemoMetec), to give a final concentration of 10 µg/mL PI. 30 µL of each sample was loaded onto a NC-Slide A2™ (ChemoMetec), and processed using the “Annexin V Assay” setting on the NucleoCounter® NC-3000™ (ChemoMetec). Data was then analysed using FlowJo™ software V10.7.2. (BD Biosciences). This assay was validated through the running of positive controls in which cultures of Jurkat or primary human T-

cells were exposed to the camptothecin, an apoptosis inducer, were ran and are shown in **Appendices D.1** and **D.2**.

2.1.5.4. Cell Cycle Assay

Cell suspension of a volume corresponding to 5 x 10^5 – 1 x 10^6 cells were centrifuged at 400 G for 5 minutes at room temperature and the supernatant removed. Cells were re-suspended in 500 µL PBS (Gibco), centrifuged at 400 G for 5 minutes, supernatant removed, and re-suspended in 250 µL lysis buffer (Solution 10, ChemoMetec) supplemented with 500 µg/mL 4′,6-diamidino-2-phenylindole (DAPI) (Solution 12, ChemoMetec) to give a final concentration of 10 µg/mL DAPI. Cell suspension was incubated at 37 °C for 5 minutes before adding 250 µL stabilisation buffer (Solution 11, ChemoMetec). Either 30 µL, or 10 µL of each sample was loaded onto a NC-Slide A2™, or a NC-Slide A8™ (both ChemoMetec), respectively. Slides were processed using the "2-Step Cell Cycle Assay" setting on the NucleoCounter® NC-3000™ (ChemoMetec) in which the fluorescence intensity of DAPI was measured. Data was then analysed using FlowJo™ software V10.7.2 (BD Biosciences).

2.1.5.5. aCD3/aCD28 ELISA

An ELISA assay was developed to assess anti-CD3 and anti-CD28 content of polymers (**Figure 2.8**). Wells in a 96-well plate contained either polymer samples with aCD3 and aCD28 attached, or Dynabeads held in place with a magnet. Wells were washed 3 times with 0.1 % TWEEN® 20 (v/v) (Arco Organics). To block, 200 µl 2 % bovine serum albumin (BSA) (w/v) (Sigma-Aldrich) was added to each well for 1 hour at room temperature. Wells were washed 5 times with 0.1 % TWEEN 20 (v/v). Secondary antibody, horse radish peroxidase (HRP) conjugated anti-murine (Dako; Agilent, California, USA), was diluted in PBS (Gibco) 1:2000 before adding 100 µL to each well for 30 minutes at room

temperature. Wells were washed 3 times with 0.1 % TWEEN 20 (v/v). 100 µL 3,3',5,5'-tetramethylbenzidine (TMB) substrate solution (Biolegend, California, USA) was added to each well and allowed to develop for 2 minutes. To halt development, 100 µL 1M H_2SO_4 was added to each well. Developed solution was removed and transferred into a new plate for spectrophotometer analysis. The plate was analysed using or Safire II plate reader (Tecan, Männedorf, Switzerland) with Magellan™ software (Tecan). Detection wavelength = 450 nm. Reference wavelength = 655 nm. Negative controls were empty wells or contained polymer without antibody attached.

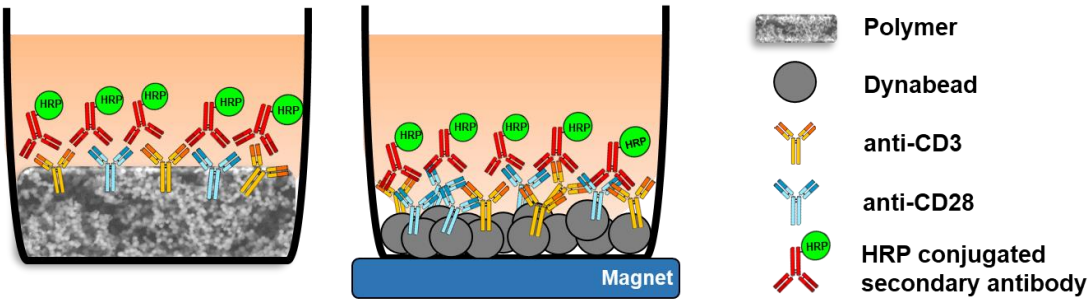

Figure 2.8. ELISA developed to assess anti-CD3 and anti-CD28 content. Wells contained either polymer samples with aCD3 and aCD28 attached, or Dynabeads held in place using a magnet. A secondary antibody conjugated to horse radish peroxidase (HRP) was added which bound to aCD3 and aCD28 in samples. Substrate solution was added and detected via plate reader at 450 nm.

2.1.5.6. IFNγ ELISA

An IFNγ ELISA was performed to quantify IFNγ secreted by T-cells into the cell culture medium. An IFNγ human ELISA kit was purchased (Invitrogen; Thermo Fisher Scientific) in which all solutions in the following method were provided. 50 µL of Incubation Buffer was added to each well, followed by 50 µL of either standards or cell culture supernatant, and then 50 µL Hu IFNγ Biotin Conjugate solution. Wells were mixed by gentle tapping of the plate. The plate was covered

and incubated for 1 hour 30 minutes at room temperature, before wells were washed 4 times with 1X Wash Buffer. 100 µL 1X Streptavidin-HRP was added to each well before being incubated for 45 minutes at room temperature. Wells were then washed 4 times with 1X Wash Buffer. 100 µL Stabilised Chromogen was added to each well and incubated for 30 minutes at room temperature in the dark. 100 µL Stop Solution was added and the plate was analysed using a CLARIOstar® Plus plate reader (BMG Labtec, Aylesbury, UK). All samples, standards, chromogen blanks, and controls were performed in duplicates.

2.1.5.7. Media Analysis

Samples of spent media from cell culture and activation studied described in **Sections 2.2.2.1**, **2.2.4.1**, and **2.2.4.3** were frozen and stored at -20 °C before being thawed at room temperature and analysed for lactate, ammonia, glucose, and glutamine content using a CuBiAn HT270 bio analyser (Optocell; GmbH. & Co. KG, Bielefeld, Germany).

2.1.5.8. Flow Cytometry

Flow cytometry of T-cells was performed either on a BD Accuri C6 flow cytometer (BD Biosciences) at the UCL Biochemical Engineering Department, or a BD LSRFortessa X-20 flow cytometer (BD Biosciences) at the Flow Cytometry Core Facility at the Great Ormond Street Institute of Child Health. Analysis of data was performed using FlowJo V.10.7.2 (BD Biosciences). OneComp eBeads (Invitrogen; Thermo Fisher Scientific) stained with the relevant fluorophore-conjugated antibodies and ARC Amine Reactive Compensation Beads (Invitrogen; Thermo Fisher Scientific) stained with the relevant viability stain, were used to perform single-colour compensation. Compensation matrices were then calculated either using BD FACSDiva software (BD Biosciences) or FlowJo V.10.7.2. For all samples, events were identified and a first gate was set using a

SSC-A vs FSC-A plot. Following this, doublets were excluded by identifying and setting a gate around single-cell events using a FSC-A vs FSC-H plot. Unless otherwise stated, 10,000 events within the second gate were collected for each sample. For samples stained with CD3, 10,000 $CD3^+$ events were collected. Unstained and isotype controls were ran for each study and are shown in **Appendix E.**

2.1.5.9. Flow Cytometry Antibody Panels

Table 2.5. Antibody Panel for Determining the Purity of Isolated T-cells.

	Antigen/ Target	Conjugate	Volume per 1 x 10^6 cells (µL)	Supplier
Panel	CD3	APC	4	BD Biosciences
	Live/Dead	Fixable Viability Stain 520	1	BD Biosciences
Isotypes	IgG1κ	APC	4	BD Biosciences

Table 2.6. Antibody Panel for Distinguishing between CD4 and CD8 T-cells.

	Antigen/ Target	Conjugate	Volume per 1 x 10^6 cells (µL)	Supplier
Panel	CD3	APC	4	BD Biosciences
	CD4	PE	4	BD Biosciences
	CD8	PE-Cy7	2	BD Biosciences
	Live/Dead	Fixable Viability Stain 520	1	BD Biosciences
Isotypes	IgG1κ	APC	4	BD Biosciences
	IgG1κ	PE	4	BD Biosciences
	IgG1κ	PE-Cy7	2	BD Biosciences

Table 2.7. Antibody Panel for Determining the Activation of T-cells.

	Antigen/ Target	Conjugate	Volume per 1 x 10^6 cells (µL)	Supplier
Panel	CD3	APC	4	BD Biosciences
	CD69	PerCP-Cy5.5	4	BD Biosciences
	CD25	PE	2	BD Biosciences
	Live/Dead	Fixable Viability Stain 520	1	BD Biosciences
Isotypes	IgG1κ	APC	4	BD Biosciences
	IgG1κ	PerCP-Cy 5.5	4	BD Biosciences
	IgG1κ	PE	2	BD Biosciences

Table 2.8. Antibody Panel for Determining T-cell Populations.

	Antigen/ Target	Conjugate	Volume per 1 x 10^6 cells (µL)	Supplier
Panel	CD3	BUV395	0.63	BD Biosciences
	CD8	BUV737	0.63	BD Biosciences
	CD4	FITC	2.50	BD Biosciences
	CCR7	BV421	2.50	BD Biosciences
	CD45RO	PE-Cy7	1.25	BD Biosciences
	Live/Dead	Fixable LIVE/DEAD Aqua	1.00	Invitrogen
Isotypes	IgG1κ	BUV395	0.63	BD Biosciences
	IgG1κ	BUV737	0.63	BD Biosciences
	IgG1κ	FITC	2.50	BD Biosciences
	IgG2a	BV421	2.50	BD Biosciences
	IgG2a	PE-Cy7	1.25	BD Biosciences

Table 2.9. Antibody Panel for Determining T-cell Exhaustion.

	Antigen/ Target	Conjugate	Volume per 1 x 10^6 cells (µL)	Supplier
Panel	CD3	APC	4	BD Biosciences
	LAG-3	PE	2	BD Biosciences
	PD-1	PE-Cy7	2	BD Biosciences
	Live/Dead	Fixable Viability Stain 520	1	BD Biosciences
Isotypes	IgG1κ	APC	4	BD Biosciences
	IgG1κ	PE	2	BD Biosciences
	IgG1κ	PE-Cy7	2	BD Biosciences

2.1.5.10. Confocal Microscopy

Confocal imaging was performed on an EVOS® Cell imaging system (Thermo Fisher Scientific).

2.1.5.11. Time-Lapse Imaging

Time-lapse imaging was performed on a confocal microscope; the EVOS® cell imaging system (Thermo Fisher Scientific) using the “time-lapse” feature. Time-lapses were performed over 4 hours with images taken at intervals of 10 seconds at room temperature.

2.1.5.12. Analysis of Time-Lapses

Time-lapses were analysed in 30 minute intervals on the Fiji software developed by Schindelin *et al*., 2012. Images were stacked into z-stacks using the macro in **Appendix B.4**. If necessary, drift in the z-stack was corrected using the plugin “Correct 3D drift”. The plugin TrackMate v5.2.0 developed by Tinevez, J.Y *et al.* 2017. was used to track cells throughout the stack using the “LoG” detector with of an estimated “blob” diameter of 4.7 – 6 µm and a threshold of 1.35 µm. Spots detected on the image scale bar were excluded through the use of a maximal

intensity filter. Tracks with < 25 spots were also excluded through a number of spots in track filter. Track statistics giving data on displacement and velocity were exported. From this data the percentage of mobile cells was calculated with cells with a track displacement of < 2.5 µm classified as stationary. Cell mobility was used to indication T-cell stimulation.

2.1.5.13. Z-Stack Fluorescent Confocal Microscopy

Fluorescent z-stack imaging of polymer sections was performed on a Zeiss LSM 710 confocal microscope (Zeiss, Oberkochen, Germany) at the imaging facilities at the Great Ormond Street Institute of Child Health.

2.1.5.14. 3D Z-stack Image Reconstruction

3D reconstruction of z-stack images was performed using Fiji software (Schindelin *et al*., 2012) and ZEN Blue v3.3 (Zeiss).

2.1.5.15. Analysis of Fluorescence Intensity of Z-stacks

Fluorescent z-stack images were analysed using Fiji software (Schindelin *et al*., 2012). z-stack channels were split and the channel displaying stained antibody was projected using a mean intensity projection. Regions of interest were drawn across the projection using the line tool and grey-values, which correspond to fluorescence intensity, were obtained and exported. Mean background fluoresce was calculated and subtracted from all values obtained.

2.1.5.16. Scanning Electron Microscopy

Scanning electron microscopy (SEM) of polymer was performed on a Hitachi TM3030 tabletop microscope (Hitachi, Tokyo, Japan) at SpheriTech Ltd. laboratories.

2.1.5.17. X-Ray Computed Tomography

X-Ray computed tomography was performed by Dr. Thomas F Johnson (Department of Biochemical Engineering, UCL) using a Nikon XT H 225 ST (Nikon, Tring, UK) at the UCL Electrochemical Innovation Lab. Following optimisation of the process parameters, > 2,000 X-ray scans for each sample were collected and re-constructed using Nikon X-Tek software to form a 2 mm x 2 mm 3D render of each sample. Analysis of 3D renders was also performed by Dr. Thomas F Johnson using Avizo™ software (FEI, Hillsboro, USA) to analyse 500 sub-volumes of each 3D reconstruction, producing values for porosity and tortuosity.

2.1.5.18. Excitation/Emission Scanning

Polymer samples were placed into a black CELLSTAR® 96-well plate (Greiner Bio-One, Stonehouse, UK) with 100 µL PBS (Gibco). A well containing only PBS was used as a control. 3D wavelength scans were performed on a Safire II plate reader with Magellan™ software (both Tecan). The scan parameters can be found in **Table 2.10**. The z-position for each scan was determined as per the application note “Improved Fluorescence Top Measurements” (Tecan, 2010). Obtained data was trimmed according to the technical note “Optimizing the acquisition of 3D fluorescence spectra” (Tecan, 2012), using ***Equation 5***.

$$\lambda Ex > \lambda Em - MD$$

(Eq. 5)

Where λEx is the excitation bandwidth, λEx is the emission bandwidth, and MD is the minimum distance between the excitation and emission maxima- so that the spectra does not overlap.

Minimum distance (MD) was calculated using ***Equation 6***.

$$MD = \lambda Ex + \lambda Em$$

(Eq. 6)

Values where ***Equation 5*** was not true were excluded from analysis.

Additionally, values that were negative after correction using the negative control were excluded.

Table 2.10. Excitation/Emission Scanning Plate Reader Parameters

Parameter	Setting
Measurement Mode	Fluorescence Top
Wavelength Scan Type	3D
Excitation Wavelength	230 – 850 nm
Excitation Step Size	5 nm
Emission Wavelength	280 – 850 nm
Emission Step Size	5 nm
Excitation Bandwidth	10 nm
Emission Bandwidth	10 nm
Gain (Manual)	100
Integration Time	40 µs

2.1.5.19. Incucyte® Live Cell Analyser

An Incucyte® live cell analyser (on loan from Sartorius) was set up inside of an incubator at 37 °C with 5 % CO_2. The Incucyte is an imaging system in which well plates containing cells are placed and images are taken periodically to visualise cell growth over time without removing the cells from the incubator. The Incucyte was set-up with the parameters detailed in **Table 2.11**.

Table 2.11. Incucyte Imaging Settings

Parameter	Setting
Vessel Type	96-well Essen ImageLock
Scan Type	Standard (With Lock)
Channel Selection	Phase and Fluorescence
Objective	10 X
Scan Interval	2 Hours
Images per Well	3
Total Run Period	7.6 Days

2.1.5.20. Analysis of Incucyte Images

Images taken on the Incucyte were analysed using the Incucyte software using a pre-set programme to analyse confluency. Analysis parameters were set to: 0.6 segmentation adjustment, edge split on. Due to the edges of polymer discs in many images distorting the analysis, only images taken at the centre of wells were analysed (**Figure 2.9**). Additionally, images that were blurry were also removed from analysis. Time points in which an average could only be provided for 1 of 3 donors were removed from the final data set so that data points were at least n = 2.

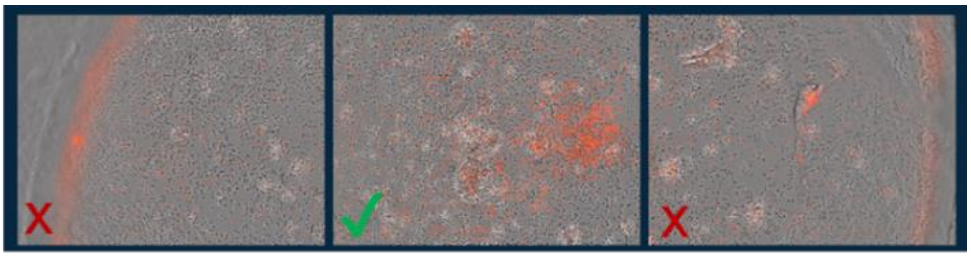

Figure 2.9. Three images taken by an Incucyte® live cell analyser across a well containing a polymer B disc and primary human T-cells. Images on the left and right show how data is distorted by images containing the edges of the polymer disc. Central well images were used for analysis.

2.2. Specific Methods

2.2.1. Polymer Characterisation

2.2.1.1. Surface and Pore Characterisation

20 mL of 067, 0.050, and 0.040 g/cm^3 polymer A solution was cast in a square cell culture as in **Method 2.1.4.3**. Quantities of reagents for each density are detailed in **Table 2.2**. Polymer B was produced by SpheriTech Ltd. Polymer was set in a freeze dryer overnight as per **Method 2.1.4.9**. A cross section of the polymer was cut using a scalpel and imaged by SEM as per **Method 2.1.5.17**. Polymer B was produced, freeze dried, and SEM imaging was performed by Josh Greenwood at SpheriTech Ltd.

Three images of one sample of porous polymer of each density were analysed using Fiji software (Schindelin *et al*., 2012) using the macros in **Appendices B.1** and **B.3**. This produced individual values for “ferret’s diameter” and area for each pore.

2.2.1.2. Polymer A Structure, Porosity, and Tortuosity

2 mL of 0.067, 0.050, 0.040, 0.033 g/cm^3 polymer A solution was produced and cast within 5 mL syringes as per **Methods 2.1.4.1** and **2.1.4.2**. Quantities of reagents for each density are detailed in **Table 2.2**. One sample of each density of polymer was sealed within the plastic syringe casing and freeze dried as per **Method 2.1.4.10**. X-Ray tomography and the analysis of the resultant 3D renders were performed by Dr. Thomas F Johnson as outlined in **Method 2.1.5.17**.

2.2.1.3. Confirmation of aCD3 and aCD28 Attachment to Polymer

An aCD3/aCD28 ELISA assay as described in **Method 2.1.5.5** was performed on both polymer A and B samples in 6 mm diameter circular disc format that had undergone the aCD3 and aCD28 attachment. Samples that had not undergone

antibody attachment, empty wells, and wells coated with aCD3 and aCD28 were ran as controls. All conditions were assayed in triplicate wells.

2.2.1.4. Visualising Attached aCD3 and aCD28

0.067 g/cm^3 polymer A discs were produced as per **Method 2.1.4.1** and **2.1.4.3** using reagent quantities detailed in **Table 2.2**. aCD3/aCD28 attachment was performed as per **Method 2.1.4.6**. Polymer B was produced and provided having undergone aCD3/aCD28 attachment by SpheriTech Ltd. Polymer A and B samples in 6 mm diameter circular disc format, were soaked in PBS, 1 % BSA (w/v) (both Gibco) for 1 hour. Secondary antibody, goat anti-mouse IgG H&L conjugated to Alexa Flour® 594 (Abcam, Cambridge, UK), was added according to the manufacturer to a give a final dilution of 1:500. Samples were left on a rocker in the dark for 1 hour at room temperature. Polymer was then submerged in PBS for 45 minutes on a rocker in the dark, with the PBS being removed and replaced every 15 minutes. Polymer samples were then stored in the dark at 4 °C before being imaged on a Zeiss LSM 710 confocal microscope (Zeiss). Excitation = 405 nm, emission = 493 nm (DAPI channel) was used to visualise the polymer. Excitation = 594 nm, emission = 493 nm was used to visualise Alexa Flour® 594.

Control samples were also processed: polymer that had not undergone antibody attachment – both stained with secondary antibody and unstained; polymer that had undergone antibody attachment- unstained by secondary antibody. These can be found in **Appendices C.1**, **C.2**, and **C.3.**

Z-stack images to give a top view were reconstructed using Fiji software (Schindelin *et al*., 2012). Z-stack images to give an angular side view were reconstructed using ZEN Blue v3.3 (Zeiss).

2.2.1.5. Biocompatibility

0.067 g/cm^3 polymer A discs (6 mm diameter), were produced as per **Method 2.1.4.1** and **2.1.4.3** using reagent quantities detailed in **Table 2.2**. Polymer B discs (6 mm diameter) were produced and provided by SpheriTech Ltd. Polymer was sterilised according to **Method 2.1.4.8**, and 1 x disc was placed at the base of a 96-well plate. 2 x 10^5 Jurkat T-cells in 200 µL complete RPMI supplemented with 1 % Antibiotic-Antimycotic (v/v) (Gibco), were seeded into each well. This seeding density ensured that were enough cells to perform an apoptosis assay on day 1 (2 - 4 x 10^5 cells). On day 3, an additional 100 uL complete RPMI media supplemented with 1 % Antibiotic-Antimycotic (v/v) was added to each well. Every day for 6 days, cell suspensions from wells in triplicate were harvested. Harvesting the cells involved first re-suspending the cells via gentle pipetting, followed by a wash of the well and polymer with 200 µL PBS (Gibco). Cells were then counted and assessed for viability using a NucleoCounter® NC-3000™ system (ChemoMetec), and subject to an Annexin V assay to assess early and late apoptosis within the culture as per **Method 2.1.5.3**. Control wells that did not contain any polymer were set up and processed in an identical manner.

2.2.2. Evaluation of Polymer A

2.2.2.1. Jurkat vs Primary T-cell Activation

Jurkat T-cells were acquired as detailed in **Method 2.1.1.2**. Primary human CD3$^+$ T-cells were isolated from whole human blood as per **Methods 2.1.1.4** and **2.1.1.5**. 4 x 10^5 Jurkat or primary T-cells in 500 µL complete RPMI media supplemented with 30 IU/mL rIL-2 (Miltenyi Biotech) were added to wells in a 48-well plate. T-cells were stimulated with either Dynabeads, TransAct, or an aCD3/aCD28 coated well as described in **Methods 2.1.2.1**, **2.1.2.2**, and **2.1.2.3**. Stimulation remained present in cultures for the entirety of the culture length as

is done in industrial processes. On day 3, an additional 500 µL RPMI supplemented with 30 IU/mL rIL-2 was added to each well. On day 5, 500 µL spent media was removed from the top of the wells to minimise culture disruption, and replaced with 500 µL fresh RPMI supplemented with 30 IU/mL rIL-2. At time points of 0 hours, 3 hours, 1 day, 3 days, 5 days, and 7 days, cell suspensions from an entire well (1 mL) of Jurkat and primary T-cells for each method of stimulation were harvested. Cells were counted and analysed for viability and cell diameter using a NucleoCounter® NC-3000™ system (ChemoMetec) as per **Methods 2.1.5.1** and **2.1.5.2**. Cell suspensions were then centrifuged and the spent media was removed and frozen at -20 °C, before media composition was analysed using a CuBiAn HT270 bio analyser (Optocell GmbH. & Co. KG) as per **Method 2.1.5.7**. Cell pellets were re-suspended in brilliant stain buffer (BD Biosciences) and stained for activation markers CD69 and CD25 as per **Method 2.1.3.1**, using the antibody panel described in **Table 2.7**. Stained cells were analysed live on a BD Accuri C6 flow cytometer (BD Biosciences) as per **Method 2.1.5.8**. For both Jurkat and primary T-cells at each time point, each stimulation method was performed in triplicate in independent wells.

2.2.2.2. Activation of T-cells with aCD3/aCD28 Polymer A

0.067 g/cm^3 polymer A in 6 mm diameter circular disc format were made according to **Methods 2.1.4.1** and **2.1.4.3**, using reagent quantities detailed in **Table 2.2**. aCD3 and aCD28 were attached as described in **Method 2.1.4.6**. Primary human CD3$^+$ T-cells were isolated from whole human blood as per **Methods 2.1.1.4** and **2.1.1.5**. Polymer discs were sterilised as per **Method 2.1.4.6** and washed 3 times with sterile PBS (Gibco) on a roller shaker (IKA-Werke) before being soaked and incubated in complete RPMI supplemented with 1 % Antibiotic-Antimycotic (v/v) (Gibco) at 4 °C overnight. 1 x polymer disc was

placed at the base of 3 wells in a 96-well plate. Due to concerns of an ineffective T-cell removal caused by specific and non-specific binding to the polymer, an increased seeding density was used to maximise the number of T-cells that could be removed for analysis 24 hours post stimulation. 2.5 x 10^5 T-cells in 200 µL complete RPMI supplemented with 1 % Antibiotic-Antimycotic (v/v) were added to each well before being centrifuged at 200 G for 5 minutes to ensure cell-polymer contact. A second polymer disc was added to the top of each culture and again centrifuged at 200 G for 5 minutes. Cells and polymer were incubated for 24 hours at 37 °C with 5 % CO_2. 24 hours was previously found to be sufficient to determine activation using immobilised aCD3 and aCD23. Cells were then harvested from wells via gentle pipetting and a wash with sterile PBS. The wash was performed by removing the polymer discs, submerging them in 200 µL sterile PBS in a centrifuge tube (Eppendorf), and placing them on a tube rotator (Thermo Fisher Scientific) in “agitate” mode for 10 minutes. The cell suspension was removed and added to the original supernatant. Harvested cells were then stained according to **Method 2.1.3.1** using activation marker panel in **Table 2.7**. Cells were analysed live on a BD Accuri C6 flow cytometer (BD Biosciences) as per **Method 2.1.5.8**.

Wells containing polymer without antibody attached, and without polymer were used as negative controls. aCD3/aCD28 coated wells prepared as per **Method 2.1.2.3**, and wells with T-cells stimulated with Dynabeads as per **Method 2.1.2.1** were used as positive controls and to compare methods. Each condition was replicated 3 times in individual wells per T-cell donor for a total of 3 donors.

2.2.2.3. Non-specific Binding - Supernatant-derived Counts

An initial cell count was performed using a NucleoCounter® NC-3000™ automated cell counter (ChemoMetec) as in **Method 2.1.5.1**. Jurkat T-cells in

complete RPMI media were incubated with 1 x polymer A in 6 mm diameter circular disc format- prepared as per **Methods 2.1.4.1** and **2.1.4.3** at a density of 0.040 g/cm^3 to mimic that used in the initial testing set-up, or polymer B in a 6 mm diameter circular disc format- produced and provided by SpheriTech Ltd. in a 1.5 mL centrifuge tube (Eppendorf). Disc formats were used here to maximise external polymer surface area and so that studies to take place in 1.5 mL tubes compatible with the rotator. Tubes were rotated on a tube rotator (Thermo Fisher Scientific) for 30 minutes. Supernatant was then collected and cells counted again. The final cell count was deducted from the initial cell count to give a value for the number of cells bound. Controls without polymer were used to provide an average cell number lost through processing which was also deducted from the final cell count. This was done for a total of 5 individual discs per polymer.

2.2.2.4. Non-specific Binding - Confocal-derived Counts

Jurkat T-cells were stained with CellTracker™ Red CMTPX Dye (Invitrogen) as per **Method 2.1.3.2**. The experimental method was repeated as above in **Method 2.2.2.3**, excluding collection and cell counting of supernatant post polymer exposure. Polymer discs instead were removed and imaged using the Texas Red filter of an EVOS FL fluorescent microscope (Thermo Fisher Scientific).

With polymer A, a second condition was also ran in which cells were both originally suspended in and washed with PBS, 1 % BSA (w/v), 0.5 M EDTA (all Gibco).

For each polymer discs of each experimental condition, 10 images were taken (5 on either side of the disc). These images were analysed to give an average cell count per mm^2 using the macro in **Appendix B.2** ran on Fiji software (Schindelin *et al*., 2012).

2.2.2.5. Flow of cells through polymer

All methods described in this section were performed at room temperature. Jurkat T-cells were used for these experiments as it was found that their size is representative of an activated primary human T-cell and so could be used as a as an appropriate model for size.

2.2.2.5.1. Initial Set-Up – Flow Rates

2 mL of 0.040 g/cm^3 polymer A was cast into a 5 mL syringe according to **Methods 2.1.4.1** and **2.1.4.2**, using reagent quantities detailed in **Table 2.2**. This density of polymer was used following results that indicated that pore sizes at this density would likely be sufficient to allow T-cells to pass through. Polymer within the syringe was suspended vertically using a clamp stand. A 20 mL syringe (BD Biosciences) fixed within a neMESYS syringe pump (CETONI; GmbH & Co. KG, Germany) was connected to the hub of the syringe using 2 mm ID silicon tubing (BRAND™; GmbH & Co. KG), as shown in **Figure 2.10**. The syringe pump was used to draw liquid through at the desired flow rate - set by the neMESYS user interface software v 2017.10.10.2 (CETONI; GmbH & Co. KG) - 5 mL of PBS (Gibco), followed by 5 mL Jurkat T-cells in complete RPMI media at 1.5 x 10^6 cells/mL, followed by an additional 5 mL of PBS. A cell count and viability analysis was performed using a Vi-CELL™ automated cell counter (Beckman Coulter) as per **Method 2.1.5.1**, both pre and post flow through of the polymer. Cell recovery was calculated using ***Equation 7***. Viability Reduction was calculated using ***Equation 8***. Flow rates of 6; 12; 24; 36; and 48 mL/minute were investigated. For each flow rate this method was repeated 3 times, each time replacing the polymer sample and syringe.

$$Cell\ Recovery\ (\%) = \frac{Final\ Cell\ Count}{Initial\ Cell\ Count} \times 100$$

(Eq. 7)

$$Viability\ Reduction\ (\%) = Initial\ Viability - Final\ Viability$$

(Eq. 8)

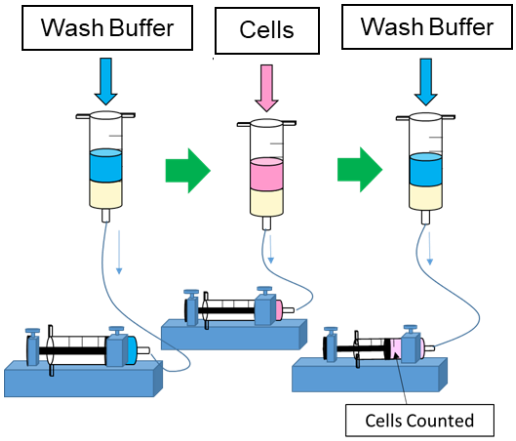

Figure 2.10. Initial set up to investigate the flow of T-cells through Polymer A. Polymer A was cast within 5 mL syringes which were suspended vertically with syringe pumps connected to the hub. Polymer was first washed with wash buffer (PBS) before cells in suspension were passed through, followed by additional wash buffer. Collected cells were counted to determine cell recovery.

2.2.2.5.2. Improved Set Up - Cell density and Flow Rates

Through experimentation, various adjustments were made to the set-up outlined in **Method 2.2.2.5.1**: polymer density was decreased from 0.040 to 0.033 g/cm^3 to increase pore sizes, polymer diameter was increased thereby decreasing the length by casting in a 10 mL syringe, cell suspension and wash buffer was changed to PBS, 1 % BSA (w/v), 0.5 M EDTA to decrease non-specific binding, wash buffer volume was increased to 10 mL to improve cell elution, a support frit was added to the bottom of the set up to prevent the polymer being pulled into the hub of the syringe, and flow rates were reduced to a range of 0.5 - 3 mL/min.

2 mL of 0.033 g/cm^3 polymer A was cast into a 10 mL syringe, according to **Methods 2.1.4.1** and **2.1.4.2**, using reagent quantities detailed in **Table 2.2**. Once set and washed the polymer was removed from the syringe. A circular nylon

mesh with 100 µM pores was cut from cell strainer (Thermo Fisher Scientific). The mesh was placed at the base of the syringe and the polymer was placed back into the syringe. PBS, 1 % BSA (w/v), 0.5 M EDTA (all Gibco) was used as the buffer both pre and post flow through of cell suspension, with both wash volumes increasing to 10 mL.

Using this improved set up, 1 x 10^7 Jurkat T-cells in cell suspension densities of 1 x 10^6, 5 x 10^6, and 1 x 10^7 cells/mL, at flow rates of 0.5, 1.5, and 3 mL/minute were investigated. The polymer sample was replaced for each run. The whole experiment was repeated 3 times. A control consisting of an empty syringe without polymer was also processed for each experiment. Cells were counted and analysed for viability using a Vi-CELL™ automated cell counter (Beckman Coulter) both pre and post flow through, from which cell recovery and viability reduction were calculated using ***Equation 7*** and ***Equation 8***.

2.2.2.5.3. Addition of a Trypsin Step

2 mL of 0.033 g/cm^3 polymer in a 10 mL syringe was set up as per **Method 2.2.2.5.1**, with the adjustments described in **Method 2.2.2.5.2**. Polymer was initially washed with 10 mL wash buffer (PBS, 1 % BSA (w/v), 0.5 M EDTA (all Gibco)). 10 x 10^6 Jurkat T-cells, suspended in wash buffer, at 5 x 10^6 cells/mL were flown into the column, followed by 2 mL 0.25 % trypsin (Gibco). Trypsin was held suspended in the polymer for 2 minutes at room temperature. 4 mL of complete RPMI media was passed through to deactivate the trypsin, followed by 10 mL wash buffer. The syringe pump was set to 3 mL/minute for all steps. As above, cell recovery and viability reduction were calculated using ***Equation 7*** and ***Equation 8***, from cell count and viability data obtained through a Vi-CELL™ automated cell counter (Beckman Coulter).

2.2.2.5.4. Chromatography-Based Set Up

An Omnifit™ EZ Chromatography Column with Adjustable End-pieces, 15 x 100 mm (Diba, Danbury, UK) was purchased. The column was suspended vertically using a clamp stand and adjusted to the size of the polymer sample. Polymer A was inserted into the column. The inlet and outlet of the column were both connected to a pressure gauge (Swagelock, Ohio, USA) with tubing provided with the column. The inlet pressure gauge was connected to a 50 mL syringe (BD Biosciences) within a neMESYS syringe pump system (CETONI; GmbH. & Co. KG). Both the pressure gauge and syringe pump at the inlet were elevated so that they were level with the top height of the column. Tubing connected to the outlet pressure gauge ran into a cylinder (Corning) which was used to collect liquid. **Figure 2.11.** shows an overview of this set up. This chromatography based set-up allowed the controlled flow of cells and buffer from the syringe pump through the column, and into a collection tube, whilst assessing the pressure difference over the column.

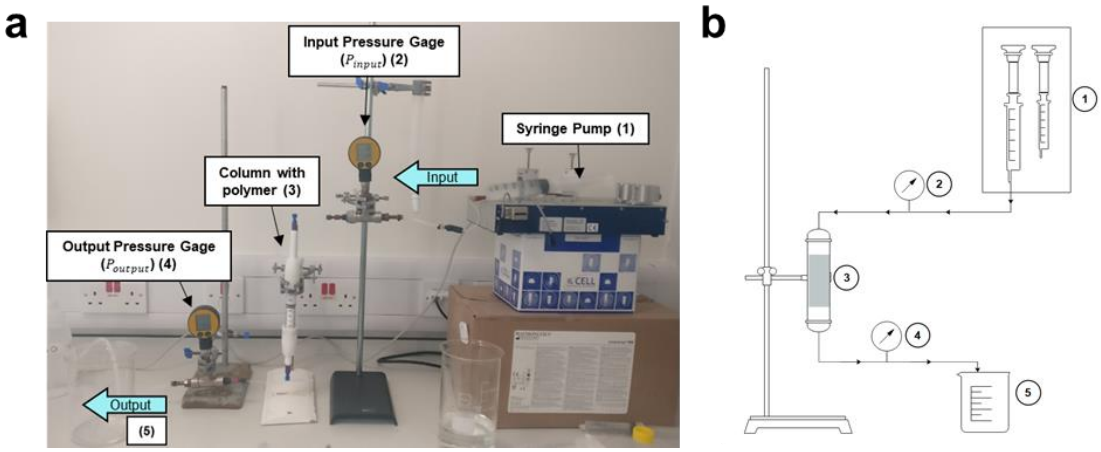

Figure 2.11. Chromatography based set-up to investigate the differential pressure and the flow of T-cells through polymer A. Polymer A was inserted into an adjustable chromatography column. Cells were pumped from a syringe pump (1), through an inlet pressure gauge (2), into the column (3), through the outlet pressure gauge (4), and collected in a cylinder (5). **a.** A labelled photographic image of the set up. **b.** A diagram of the set-up. Created by Karen Trippler (Department of Biochemical Engineering, UCL) on Edraw Max, reproduced with permission.

2.2.2.5.5. Differential Pressure of Polymer

An Omnifit™ EZ Chromatography Column (Diba) was set up as described in **Method 2.2.2.5.4**. 2 mL of 0.033 g/cm^3 polymer A was produced as per **Methods 2.1.4.1** with reagent quantities detailed in **Table 2.2**, and cast in a 15 mm diameter cylinder format using **Method 2.1.4.4**. 1 x polymer cylinder was placed inside the column with the end-pieces adjusted to equal the height of the polymer. 0.033 g/cm^3 polymer A was used as this density was found to allow T-cells to pass through the polymer. MilliQ water was passed through the column at flow rates set by the syringe pump. Differential pressure within the column was calculated using ***Equation 9***:

$$\Delta P = P_{input} - P_{output}$$

(Eq. 9)

Where ΔP is the differential pressure within the column, P_{input} is the input pressure, and $P_{output}$is the output pressure.

A large value of differential pressure indicated a blockage within the column/polymer.

This was performed at flow rates of 5 to 100 mL/min at intervals of 5, and was repeated on 3 separate occasions replacing the polymer each time. A control was performed with an empty column following the same method.

2.2.2.5.6. Cell Recovery Using Chromatography Based Set Up

An Omnifit™ EZ Chromatography Column (Diba Industries, Cambridge, UK) was set up as described in **Method 2.2.2.5.4**. 2 mL of 0.033 g/cm^3 polymer A was produced as per **Method 2.1.4.1**, with reagent quantities detailed in **Table 2.2**, and cast in a 15 mm diameter cylinder format using **Method 2.1.4.5**. 1 x polymer

cylinder was placed inside the column with the end-pieces adjusted to equal the height of the polymer. 0.033 g/cm^3 polymer A was used as this density was previously found to allow T-cells to pass through the polymer. The syringe pump was stood so that the syringes within it were vertical. The column and tubing were primed with wash buffer: PBS, 1 % BSA (w/v), 0.5 M EDTA (all Gibco). 1 x 10^7 Jurkat T-cells suspended in 10 mL wash buffer were passed into the system, followed by a further 29 mL of wash buffer (9 mL dead volume + 10 x column volume). Output liquid was collected and analysed for cell count and cell viability using a ViCELL™ automated cell counter (Beckman Coulter) as per **Method 2.1.5.1**. Differential pressure within the column was also measured during each step, as described above in **Method 2.2.2.5.5**.

This was performed at flow rates of 10; 20; and 30 mL/min, and was repeated on 3 separate occasions replacing the polymer each time. A control was performed with an empty column following the same method. The whole system was flushed with 50 mL wash buffer at 50 mL/min at the start of and between each run, additionally, the system was regularly cleaned with 70 % v/v ethanol.

2.2.2.6. Collaborative Work Disclosure

The studies described in **Methods 2.2.2.5.3**, **2.2.2.5.5,** and **2.2.2.2.6** were performed in collaboration with Karen Trippler (Department of Biochemical Engineering, UCL) as part of an undergraduate final year project supervised by myself. The experimental set-up and design, and polymer stock solution preparation was completed by myself. Polymer production and design of the experiment procedure was performed together. The experimental procedure was executed by Karen Trippler under my supervision. The data processing, analysis, and statistical tests presented in this thesis were performed by myself.

2.2.3. T-cell Interaction with Polymer B

2.2.3.1. Flow of Cells through Scaffold

Polymer B in a cylindrical format, both with and without aCD3/aCD28 attached, were provided by SpheriTech Ltd. pre-cased inside of plastic casing as shown in **Method 2.1.4.7**, **Figure 2.6**. PBS, 1 % BSA (w/v), 0.5 M EDTA buffer was made by mixing MACS® BSA Stock Solution 1:20 MACS® Rinsing Solution (both Miltenyi Biotech). Polymer was washed with 10 mL buffer by connecting a 10 mL syringe filled with buffer to one end of the casing and an empty 10 mL to the other. Buffer was passed through the polymer by emptying the filled syringe so that it passed through the polymer and filled the empty syringe; this was repeated 10 times. Syringes were removed and polymer in casing was suspended vertically using a clamp stand. A 10 mL syringe with a luer lock connection (BD Biosciences) with the plunger removed was attached to the top end of the casing. 10 mL buffer was pipetted into the syringe opening so that it passed through the polymer via gravity and was collected in a 50 mL centrifuge tube (Corning) placed underneath. As in the methods above, Jurkat T-cells were used for these experiments as it was found that their size is representative of an activated primary human T-cell and so could be used as a as an appropriate model for size. 1 x 10^7 Jurkat T-cells in 10 mL buffer were pipetted into the syringe, passed through the polymer and collected in another 50 mL centrifuge tube. A sample of 100 µL supernatant was collected and processed with a NucleoCounter® NC-3000™ automated cell counter (ChemoMetec) to give a cell count and viability. The remaining cell suspension was then mixed by gentle pipetting, re-transferred into the open syringe, and the sampling process repeated again. This was repeated for a total of 10 passes through the polymer.

Both conditions, with aCD3/aCD28 attached and without, were repeated 3 times replacing the whole set-up each time.

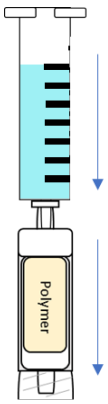

Figure 2.12. Set-up to investigate the flow of T-cells though porous polymer B. Cylindrical sections of porous polymer B were encased within plastic housing with a female and male luer lock and suspended vertically. A 10 mL syringe without the plunger was attached to the top and used to funnel T-cells in suspension through the polymer by gravity.

2.2.3.2. T-cell Growth on Polymer B Assessed via Incucyte

Polymer discs (**Figure 2.5**), 6 mm diameter, were provided by SpheriTech Ltd. Primary human $CD3^+$ T-cells were isolated from whole human blood as per **Methods 2.1.1.4** and **2.1.1.5**. T-cells were stained with Incucyte Rapid Red membrane dye as per **Method 2.1.3.3**. 1 x polymer disc, pre-soaked in complete RPMI supplemented with 1 % Antibiotic-Antimycotic (v/v) (Gibco), was placed at the base of the relevant wells in a 96-well Essen ImageLock plate (Sartorius). Non-porous polymer discs were used due to their transparency, allowing cells to be visualised via confocal microscopy. T-cells were suspended in complete RPMI supplemented with 1 % Antibiotic-Antimycotic (v/v) (Gibco), 30 IU/mL rIL-2 (Miltenyi Biotech) at 5 x 10^7 cells/mL.

Experimental conditions were: T-cells stimulated with Dynabeads, with and without polymer; T-cells stimulated with TransAct, with and without polymer. Wells containing unstimulated T-cells were used as controls, both with and

without polymer. T-cells to be stimulated with Dynabeads were stimulated at a 1:1 ratio, as per **Method 2.1.2.1**, in a 50 mL centrifuge tube (Corning). T-cells to be stimulated with TransAct were stimulated with volumes that would result in the appropriate amount when transferred to the well-plate, as per **Method 2.1.2.2** and volumes detailed in **Table 2.1**. 100 µL aliquots of cell suspension containing 5 x 10^5 T-cells were transferred to the appropriate wells. Each condition was replicated 3 times in individual wells per T-cell donor, for a total of 3 donors. Well plates were placed into an Incucyte live cell analyser (Sartorius) set up as per **Method 2.1.5.19** and imaged over the course of 182 hours (7.6 days). 100 µL complete RPMI supplemented with 1 % Antibiotic-Antimycotic, 30 IU/mL rIL-2 was added to each well at 63 hours, and 50 µL was added at 135 hours.

Images were analysed as per **Method 2.1.5.20**.

2.2.3.3. Migration of T-cells

Polymer discs (**Figure 2.5**), 6 mm diameter, were provided by SpheriTech Ltd. Primary human $CD3^+$ T-cells were isolated from whole human blood as per **Methods 2.1.1.4** and **2.1.1.5**. 1 x polymer disc, either with or without aCD3 and aCD28 attached, was placed into the bottom of a 48-well plate (Thermo Fisher Scientific). Non-porous polymer discs were used due to their transparency, allowing cells to be visualised via confocal microscopy. 1 x 10^5 primary human T-cells suspended in 250 µL of complete RPMI media supplemented with 1 % Antibiotic-Antimycotic (v/v) (Gibco) were pipetted into the well. This low seeding density ensured that single cells on the polymer could be distinguished in images. Wells were left stationary for 5 minutes before time-lapse imaging on an EVOS® Cell imaging system (Thermo Fisher Scientific) as per **Method 2.1.5.11**. For the control, wells contained no polymer. Each condition was replicated 3 times per T-cell donor for a total of 3 donors. Images were grouped into time intervals of 30

minutes and analysed using the TrackMate plugin on Fiji software (Tineves *et al*., 2012) as per **Method 2.1.5.12**.

2.2.4. T-cell Activation and Expansion with Polymer B

2.2.4.1. Activation Expansion with Non-porous Polymer B

Non-porous polymer B in a 10 mm diameter disc format (**Figure 2.5**), with and without aCD3 and aCD28 antibodies attached (3rd batch), were produced and provided by SpheriTech Ltd. Discs were washed 3 times with sterile PBS (Gibco) on a shaker (IKA-Werke), and then soaked and incubated in complete RPMI supplemented with 1 % Antibiotic-Antimycotic (v/v) (Gibco) at 4 °C overnight. Primary human $CD3^+$ T-cells were isolated from whole human blood as per **Methods 2.1.1.4** and **2.1.1.5**. The general term media for the remainder of this method refers to complete RPMI supplemented with 1 % Antibiotic-Antimycotic (v/v) (Gibco) and 30 IU/mL rIL-2 (Miltenyi Biotech).

For relevant wells, 1 x polymer disc was placed at the base of a well in a 48-well plate. A high seeding was used to ensure that there was enough T-cells for analysis of unstimulated controls and at early time-points as the number of available polymer discs was limited. 5 x 10^5 T-cells in 500 µL media were transferred into wells, including wells not containing polymer as an unstimulated control. T-cells stimulated with Dynabeads were stimulated at a 1:1 bead to cell ratio as per **Method 2.1.2.1**, in a centrifuge tube. 500 µL T-cell-Dynabeads suspension containing 5 x 10^5 T-cells was then transferred to relevant wells. On day 3, 500 µL fresh media was added to each well. On day 5, 7, 9, 10, and 14, spent media was removed from the top of the wells to minimise culture disruption, and replaced with 500 µL fresh media. Stimulation remained present in cultures for the entirety of the culture length as is done in industrial processes.

T-cells in wells were imaged as per **Method 2.1.5.10** on day 0, 1, 3, 5, 7, 10, and 14. On day 0, 3, 5, 7, 10, and 14, T-cells were harvested by gently pipetting media up and down before removing the cell suspension, followed by an additional wash with 100 µL PBS, 1 % BSA (w/v), 0.5 M EDTA (all Gibco). Time points analysed were chosen to best see early activation signals and then to provide a regular assessment of cultures over the 14 days, whilst considering the limited number of discs available. Cell suspensions were analysed using a NucleoCounter® NC-3000™ automated cell counter (ChemoMetec) as per **Methods 2.1.5.1** and **2.1.5.2** to give values for cell count, viability, and cell diameter. On days 0, 3, 7, 14, T-cells were also stained and analysed for activation markers using a BD Accuri C6 flow cytometer (BD Biosciences) as per **Methods 2.1.3.1** and **2.1.5.8**, using the antibody panel in **Table 2.7**. On day 0 and 14, T-cells were additionally stained and analysed for phenotypic markers using the antibody panel indicated in **Table 2.8** with a BD LSRFortessa X-20 flow cytometer (BD Biosciences), for exhaustion markers using the antibody panel indicated in **Table 2.9** with a BD Accuri C6 flow cytometer, and subject to cell cycle analysis as per **Method 2.1.5.8**. For flow cytometry analysis, cells were fixed and 10,000 events within the $CD3^+$ gate were collected for fully stained samples (full gating strategy shown in **Figure 7.4**). All analysis mentioned was also performed pre-experiment on day 0. Each experimental condition was replicated 3 times in individual wells per T-cell donor, for a total of 3 donors.

2.2.4.2. Early Proliferation with Non-porous Polymer B

Set up was performed identically to above (**Method 2.2.4.1**), with T-cells having being pre-stained with CFSE as per **Method 2.1.3.5**. On day 4, all cells were harvested – again as above in **Method 2.1.3.5**, stained according to **Method 2.1.3.1** using the antibody panel indicated in **Table 2.6**, and processed using a

BD LSRFortessa X-20 flow cytometer (BD Biosciences) as per **Method 2.1.5.8**. For flow cytometry analysis, cells were fixed and 10,000 events within the $CD3^+$ gate were collected for fully stained samples. Each experimental condition was replicated 3 times in individual wells per T-cell donor, for a total of 3 donors.

2.2.4.3. Expansion with Porous Polymer B Scaffold

Porous polymer B in a cylindrical format (**Figure 2.6**), with and without aCD3 and aCD28 antibodies attached (1^{st} batch), were produced and provided by SpheriTech Ltd. and cut into 6 mm diameter discs to allow them to fit into a well, as per **Method 2.1.4.7**. These will further be referred to as scaffolds. Scaffolds were washed 3 times with sterile PBS (Gibco) on a roller shaker (IKA-Werke), and then soaked and incubated in complete RPMI supplemented with 1 % Antibiotic-Antimycotic (v/v) (Gibco) at 4 °C overnight. Primary human $CD3^+$ T-cells were isolated from whole human blood as per **Methods 2.1.1.4** and **2.1.1.5**. The general term media for the remainder of this method refers to complete RPMI supplemented with 1 % Antibiotic-Antimycotic (v/v) (Gibco) and 30 IU/mL rIL-2 (Miltenyi Biotech).

For relevant wells, 1 x scaffold was placed at the base of a Falcon® cell culture insert with 1 uM pores (Corning) and inserted into a 24-well cell culture insert companion plate (Corning). The seeding density used here was the same as above with non-porous polymer, and was used so that the expansions could be compared. This cell seeding density was concentrated even further during the first seeding of cells into the scaffold to promote cell-scaffold interaction. 5×10^5 T-cells in 50 µL media were seeded into aCD3/aCD28 scaffolds and incubated at 37 °C with 5 % CO_2 for 3 hours. T-cells stimulated at a 1:1 bead to cell ratio with Dynabeads, as per **Method 2.1.2.1**, were similarly incubated for 3 hours in a centrifuge tube (Corning). For the unstimulated control, 5×10^5 unstimulated T-

cells in 100 µL media were seeded into cell culture inserts and also incubated for 3 hours. After 3 hours, 50 µL additional media was added to each insert containing an aCD3/aCD28 scaffold. 100 µL T-cell-Dynabeads suspension containing 5 x 10^5 T-cells was transferred into relevant well plate inserts, either with or without a scaffold. 500 µL media was added to each of the outer wells. Spent media from the outer well was completely removed and replaced with fresh 500 µL media on day 3 and 5, and 1 mL on day 7, 9, 11, and 13. Spent media was frozen at – 20 °C and subsequently analysed as per **Method 2.1.5.7**. Stimulation remained present in cultures for the entirety of the culture length as is done in industrial processes.

Here, cells were only harvested and analysed on the final day of the culture due to the limited availability of aCD3/aCD28 scaffolds. On day 14, cells were harvested by transferring 500 µL spent media from the outer well into the cell culture insert and gently pipetting to re-suspend cells before removal. T-cells were then subject to the following analysis: cell count, viability, and cell diameter, using a NucleoCounter® NC-3000™ automated cell counter (ChemoMetec) as per **Methods 2.1.5.1** and **2.1.5.2**; phenotypic analysis as per **Methods 2.1.3.1** and **2.1.5.8**, using the antibody panel indicated in **Table 2.7**, and processed using a BD LSRFortessa X-20 flow cytometer (BD Biosciences); an apoptosis assay as per **Method 2.1.5.3**; and a cell cycle assay as per **Method 2.1.5.4**. For flow cytometry analysis, cells were fixed and 10,000 events within the $CD3^+$ gate were collected for fully stained samples (full gating strategy shown in **Figure 7.4**). All analysis mentioned was also performed pre-experiment on day 0. Each experimental condition was replicated 3 times in individual wells per T-cell donor, for a total of 3 donors.

2.2.4.4. Live Staining and Imaging of T-cells in Culture with Polymer B Scaffold

aCD3/aCD28 scaffolds, as described above in **Method 2.1.4.7**, were washed 5 times with sterile PBS before being soaked and incubated in RPMI 1640 medium, HEPES, no glutamine (Gibco) supplemented with 10 % FBS (v/v) (Gibco), 2 mM L-glutamine (Sigma-Aldrich), and 1 % Antibiotic-Antimycotic (v/v) (Gibco), overnight at 4 °C overnight. Primary T-cells were stained with CellTracker™ Red CMTPX Dye (Invitrogen) as per **Method 2.1.3.2**. T-cells were washed and re-suspended in RPMI 1640 medium, HEPES, no glutamine supplemented with 10 % FBS, 2 mM L-glutamine, 1 % Antibiotic-Antimycotic, and 30 IU/mL rIL-2 (Miltenyi Biotech) at 1 x 10^7 cells/mL.

aCD3/aCD28 scaffolds were placed in a 35 mm glass bottomed FlouroDish™ (Thermo Fisher Scientific). 50 µL cell suspension, containing 5 x 10^5 T-cells, was added to each scaffold and incubated at 37 °C with 5 % CO_2 for 3 hours. 500 µL additional media was added to each dish and cell cultures were incubated at 37 °C, 5 % CO_2 until they were imaged. 1 hour prior to imaging T-cells were stained with SYTO™ Deep Red Nucleic Acid Stain for live cells (Invitrogen) as per **Method 2.1.3.4**. Dishes were sealed with parafilm® (Heathrow Scientific) and transported to the Great Ormond Street Institute of Child Health for imaging using a Zeiss LSM 710 confocal microscope (Zeiss) as per **Method 2.1.5.13**. Z-stack images were re-constructed as per **Method 2.1.5.14**. Unstained and samples incubated with SYTO™ membrane dye were imaged as controls, shown in **Appendix C.4.** Due to absorbance of dyes by the polymer scaffold, T-cells were identified through red fluorescence channels accompanied by the absence of fluorescence in the DAPI channel.

2.2.5. Summary of Assays

A summary of the assays undertaken with each polymer and their purpose is shown in **Table 2.12**. The assays performed vary due to limiting factors such as polymer and T-cell availability during experiments and physical characteristics of polymer - such as polymer A being opaque and therefore unable to be imaged via confocal microscopy or by the Incucyte live cell imager. Additional assays were also performed whilst characterising the flow through of T-cells with polymer A due to the low recovery of cells. These assays were not necessary with porous polymer B as polymer B did not demonstrate the same issue.

2.3. Statistical Analysis

All statistical analysis was performed on IBM SPSS Statistics 27 (IBM, Chicago, USA). For the comparison of 2 means, a two-tailed T-test or a Tukey's honest significant difference test was performed. A Levene's test was performed prior to T-tests to determine the equality of variances, a significance value of > 0.05 was deemed as equal variance. For the comparison of > 2 means with one independent variable, a one-way analysis of variance (ANOVA) was performed followed by a post-hoc Tukey's test if significance was indicated. For skewed and exponentially distributed data sets, significance of difference between medians was determined using a non-parametric Mann-Whitney U test. For the evaluation of influence and interaction of 2 independent variables on a dependant variable, a two-way ANOVA was performed. *A* p-value of ≤ 0.05 was considered statistically significant.

Table 2.12. Summary of Assays and Methods Used for Polymer A and B.

Assay/Method	Purpose	Polymer A	Polymer B Non-porous	Polymer B Porous
Excitation/emission Scan	Auto-fluorescence	✓	✓	
aCD3/aCD28 ELISA	Antibody attachment	✓	✓	✓
IFNγ ELISA	IFNγ secretion of T-cells post stimulation			✓
Cell count, viability, and cell diameter	Biocompatibility	✓	✓	✓
	T-cell proliferation post stimulation		✓	✓
	T-cell recovery post flow-through polymer	✓		✓
Annexin V/PI apoptosis	Biocompatibility	✓	✓	✓
	Activation characterisation			✓
SEM imaging	Pore size	✓		✓
	Topology	✓	✓	✓
X-Ray computed tomography	Porosity, tortuosity, structure	✓		
Differential pressure	Flow-through characterisation	✓		
Incucyte live cell analyser	T-cell proliferation on polymer		✓	
Fluorescence confocal microscopy	Polymer Structure	✓		✓
	Bound antibody visualisation	✓	✓	✓
	T-cell proliferation on polymer			✓
Confocal microscopy	T-cell proliferation		✓	
	T-cell mobility		✓	
Cell cycle	Activation characterisation		✓	✓
Flow cytometry	Activation markers	✓	✓	✓
	Phenotypic characterisation		✓	✓
	Exhaustion markers		✓	
	Proliferation		✓	
Metabolites	Activation characterisation			✓

Chapter 3. Polymer A Characterisation

3.1. Introduction

In order to be a successful candidate for use in this project, SpheriTech's polymer A must have the following requirements: the ability to be produced with a porous structure, the capacity to attach antibodies to its surface, and biocompatibility with T-cells in culture. Additionally, it is known that other formats of SpheriTech's polymer auto-fluoresce, resulting in complications with immunostaining. In view of this, characterisation in this chapter broadly falls into the categories of: structure and porosity, antibody attachment, biocompatibility, and auto-fluorescence.

3.1.1. Polymer A

Polymer A is a, biodegradable, macroporous, hydrophilic (also referred to as a hydrogel) biopolymer created through the cross-linking of ε-PL with brassylic acid (also known as tridecanedioic acid, $C_{13}H_{24}O_4$). The patent to create this polymer is owned by SpheriTech Ltd. This polymer was investigated due to its ability to form a monolithic porous structure, and other iterations formed with an additional or alternative di-carboxylic acids having previously demonstrating compatibility in cell culture methods and *in vivo* rat models (Hosseinzadeh *et* al., 2021).

3.1.2. Auto-fluorescence

The auto-fluorescence of SpheriTech's polymer in other formats has previously been reported (Weil, 2016). This is a phenomenon that is not unique to SpheriTech's polymer but has also been observed in other polymers such as polyurethanes, polyethylenes, polyethers, and nylon (Asfour *et al*., 2020). Auto-fluorescence of polymer A was important to characterise due to its potential to interfere with future immunostaining and cell-polymer visualisation techniques.

Additionally, the identification of auto-fluorescence has allowed it to be exploited to visualise this opaque polymer by fluorescent microscopy without staining.

3.1.3. Structure and Porosity

The final structure of the polymer, specifically the porosity, is a critical feature of a 3D cell culture scaffold. In order to maximise the surface area available to T-cells, the structure must contain pores that are sufficiently big throughout the scaffold to allow T-cells to enter into and interact with the surfaces in a 3D manner. Insoluble scaffolds, such as polymer A must also have a structure which allows cells to be removed - this could be achieved by applying a flow through to potentially simplify and automate removal in the future. Through adjusting the quantities of ε-PL and brassylic acid during production, the final density of the polymer can be altered. This in turn alters the final structure. Structural characterisation and the impact of polymer density on the pore structure of the final scaffold was investigated.

3.1.4. Antibody Attachment

Through the adjustment of polymer chemistry, followed by carbodiimide-mediated cross-linking, proteins, such as antibodies can be attached to the surface of the polymer. Antibodies that target specific cell receptors are able to activate T-cells and are of particular interest in this study.

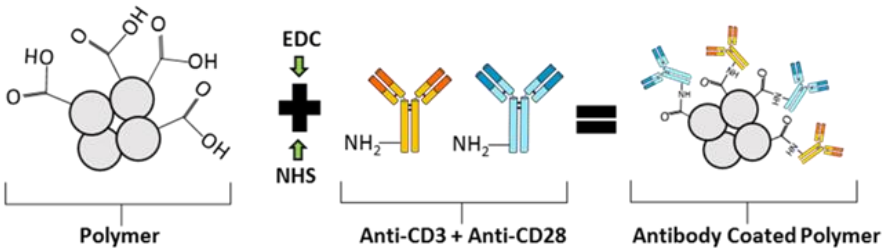

Figure 3.1. Carbodiimide-mediated attachment of antibodies to SpheriTech's Polymer A.

When producing the polymer, the ratio of ε-PL to brassylic acid can be adjusted as such that free carboxyl functional groups (-COOH) remain unreacted on the surface of the polymerised polymer. Antibodies can then be attached to the free –COOH group via free amine (NH_2) terminal groups on the antibody. This attachment is facilitated by EDC and NHS. EDC reacts with the –COOH group to produce an unstable o-acylicourea intermediate. Addition of NHS stabilises the intermediate to form an active NHS ester that is then able to form a covalent bond with the NH_2 group present on the antibody (**Figure 3.1**).

aCD3 and aCD28 antibodies were attached to the surface of SpheriTech's polymer A. aCD3 is an antibody that stimulates T-cells though the binding to the CD3 section of the TCR. aCD28 is an antibody that provides co-stimulation to positively promote T-cell activation. It was essential for this project that both of these antibodies attach to the polymer in sufficient amounts in order to activate T-cells that interact with them.

3.1.5. Biocompatibility

Within this study, biocompatibility refers to the characteristic of the polymer of allowing T-cells to interact with and grow in contact with the material without detrimental impact to growth or viability. This was investigated using an apoptosis assay to identify apoptotic and necrotic cells. Apoptotic cells are cells that are undergoing programmed cell death. Apoptosis can be triggered extrinsically through signals from other cells, or intrinsically due to cellular stress. Necrotic cells are cells that have auto-lysed due to cellular injury (Majno and Joris, 1995).

3.2. Aims and Hypotheses

3.2.1. Chapter aims

- To evaluate the structure of polymer A in terms of pore size, porosity and tortuosity – specifically the relationship between these characteristics and polymer density.
- To develop a method to confirm and evaluate the attachment of aCD3 and aCD28 to SpheriTech's polymer A.
- To evaluate the biocompatibility of polymer A with T-cells.
- To characterise the auto-fluorescent properties of polymer A.

3.2.2. Hypotheses

It is hypothesised that the structural properties of pore size, porosity, and tortuosity, can be controlled through the adjustment of polymer density. It is expected that decreasing the density, by varying concentrations of poly-ε-lysine and brassylic acid, will increase the pore size. As the polymer chemistry is well characterised it is expected that aCD3 and aCD28 antibodies can be attached to the surface of the polymer. As other poly-ε-lysine hydrogels and other isotypes of poly-lysine are commonly used in cell cultures, it is hypothesised that polymer A will demonstrate a good level of biocompatibility. It is also anticipated that Polymer A will fluoresce when exposed to light at certain wavelengths.

3.3. Results and Discussion

3.3.1. Auto-fluorescence

Fluorescence of polymer A through excitation at 358 nm and emission at 461 nm (pre-set DAPI microscope channel) was previously identified and used to visualise the polymer as mentioned earlier in this chapter. To fully characterise the auto-fluorescence spectrum of the polymer, samples were subject to an

excitation/emission scan, as per **Method 2.1.5.18**. The scan was performed with an excitation wavelength range of 230 – 850 nm and an emission wavelength range of 280 – 850 nm.

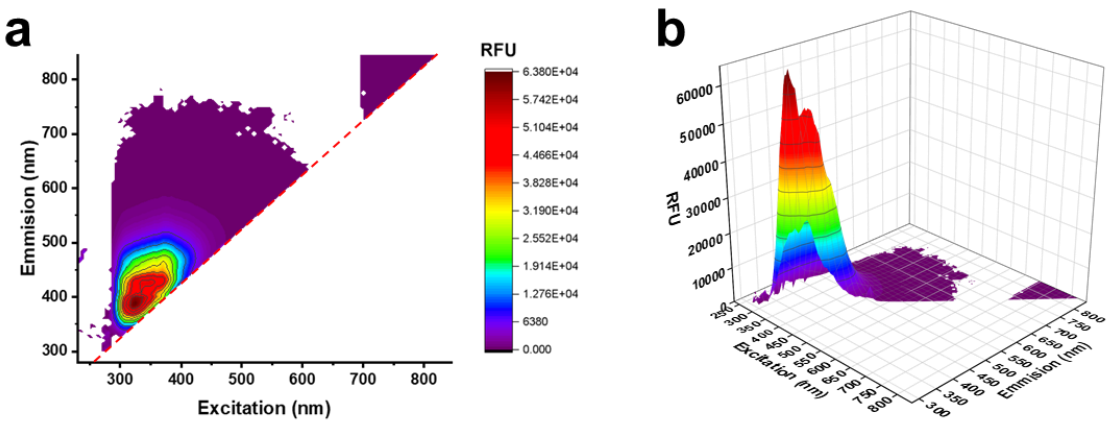

Figure 3.2. Excitation/emission spectrum of polymer A. Fluorescence intensity was measured over a range of 230 – 850 nm excitation and 280 – 850 nm emission wavelengths, with a step size of 5 nm for both. **a.** 2D top-view of excitation/emission spectrum. Red dashed line represents the data trimming limit. **b.** 3D surface graph of excitation/emission spectrum. RFU = relative fluorescence units. n = 1 scan.

Excluded values below the visible diagonal cut off line (**Figure 3.2a**) were excluded through data trimming described in **Method 2.1.5.18**. Excluded values above this line were removed due to a negative value being obtained when subtracting the negative control. With this in mind, it was accepted that there was no fluorescence observed at points with no data presented above the trimming line.

Two main peaks of auto-fluorescence were highlighted through scanning (**Figure 3.1**).The most intense peak, with a relative fluorescence of 63,788 units was observed at an excitation of 325 nm and produced an emission at 390 nm. A second peak, of 52,971 relative fluorescence units (RFU), was observed at an excitation of 345 nm and resulted in an emission at 425 nm. A range of excitation wavelengths resulted in a fluorescence, however, excitation wavelengths above

450 nm resulted in lower or no emission intensity. Excitation wavelengths < 450 nm produced emissions of wavelength ≤ 550 nm.

As a result of this auto-fluorescence characterisation, cell-polymer and antibody-polymer fluorescent imaging methods will use stains or antibodies bound to fluorophores that are excited and emit at higher wavelengths; to minimise interference. Moreover, this information can also be used to further optimise fluorescent microscope excitation laser and emission filter settings when using auto-fluorescence to image the polymer.

3.3.2. Polymer Structure and Topology

To initially assess the structure of Polymer A and evaluate the impact of varying the polymer density, polymer A at densities of 0.067, 0.050, 0.040 g/cm^3 were produced and imaged by SEM, as described in **Method 2.2.1.1** . These densities were suggested for use by SpheriTech Ltd. Polymer surface topology was viewed at magnifications of x100 and x1,000. These magnifications represent the scale at which an operator and cell would interact with the polymer.

SEM images displayed in **Figure 3.3**, show that polymer produced at all densities displayed an uneven surface and that the overall structure had numerous visible pores, this was particularly observed when viewed at x100. When viewed at x1,000 it appeared that polymer at lower densities contained larger cavities. Images taken at x1,000 also revealed that the structure that formed as a result of cross-linking ε-PL resembled one of many smaller polymer spheres fused together. These spheres had an approximate 4 µm diameter, determined visually. This is smaller than the average T-cell and so consequently, T-cells interacting with this polymer will do so in a non-planar manner. Additionally, the spheres that comprise the polymer appeared smooth and without holes allowing cell interaction to occur only on the surface.

Mescher (1992) investigated the optimal micro-particle diameter for the activation of T-cells, studying bead sizes of 1 ± 0.02 µm to 5 ± 0.66 µm. Here it was found that sizes of 4 ± 0.26 µm and 5 ± 0.66 µm were the optimum. Although particles with diameters up to 10 µm have reported successful activation (Steenblock and Fahmy, 2008; Lambert *et al*., 2017), it is widely acknowledged that a dimeter of 4 – 5 µm is most desirable (Sunshine and Green, 2013), with Dynabeads® having a diameter of 4.5 µm. From the SEM images it appears that all spherical particles forming the polymer possess a diameter sufficient to activate T-cells. However, to confirm this it would be suggested that future work be done to quantify the diameters of each sphere, perhaps through the use of image processing software such as Fiji. A limitation of using this method to infer structure is that the 2 dimensional view lacks depth information. To provide additional surface topology information and confirm the structure inferred here, further 3D fluorescent imaging was employed.

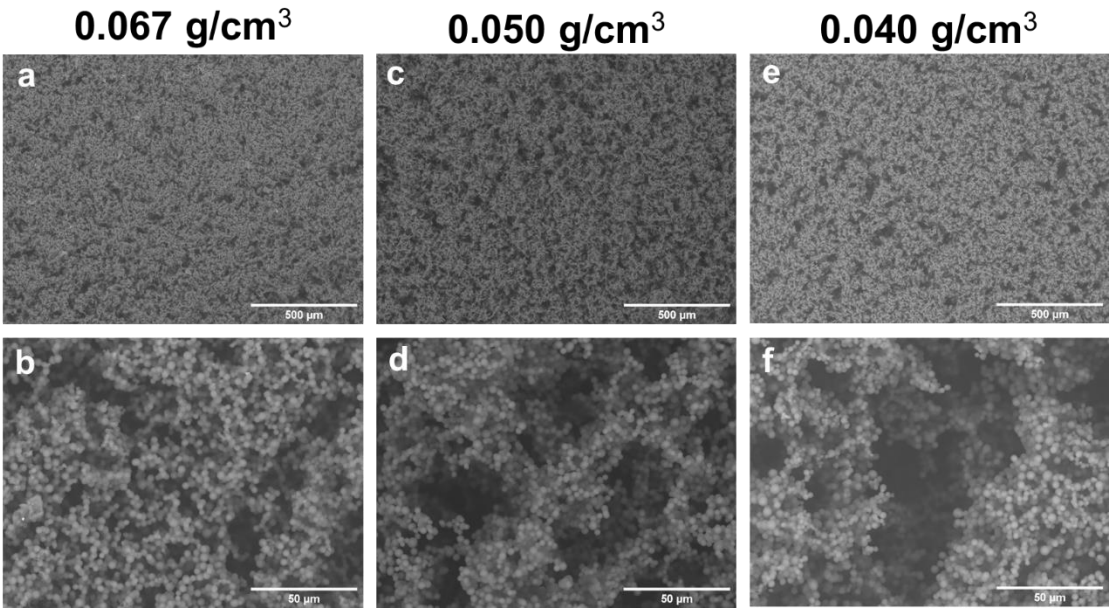

Figure 3.3. Scanning electron microscopy images of Polymer A at densities of **a** and **b.** 0.067 g/cm^3, **c** and **d.** 0.050 g/cm^3, and **e** and **f.** 0.040 g/cm^3. Top row images (**a, c** and **e.**) = x100. Scale bars = 500 µm. Bottom row images (**b, d** and **f**) = x1,000. Scale bars = 50 µm

3.3.3. 3D Surface Reconstruction

To enable visualisation in a 3D manner, the “DAPI” setting of a fluorescent confocal microscope (excitation = 405 nm, emission = 493 nm) was used as this was found to allow visualisation of the polymer through its auto-fluorescence, as per **Methods 2.1.5.13** and **2.1.5.14**. Images were taken through a z-stack to a depth of 100 µm. These images were then re-constructed to produce an interactive 3D model of the polymer surface showing its structure in more detail.

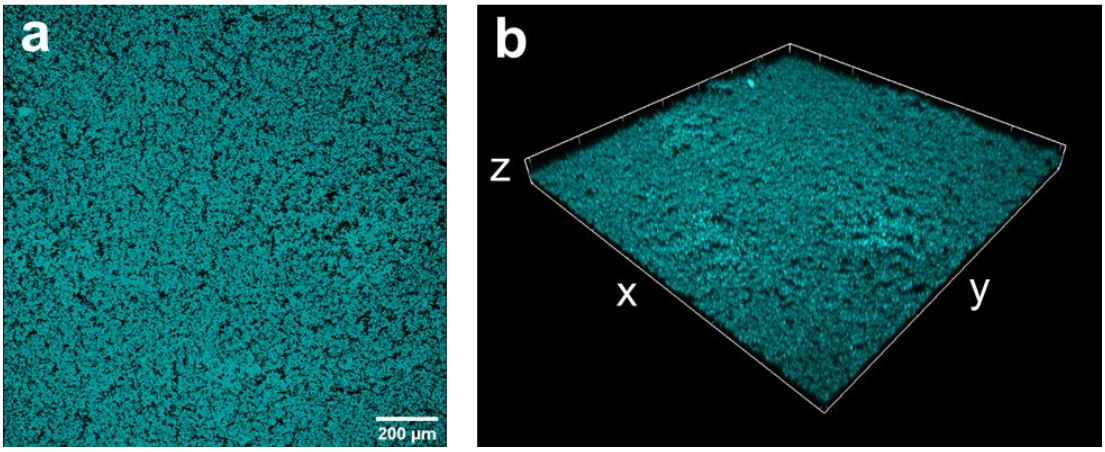

Figure 3.4. Reconstructed 3D z-stack fluorescent confocal microscopy images of polymer A. Polymer A was visualised through the DAPI channel and pseudo-coloured cyan. **a.** Top view. Scale bar = 200 µm. **b.** Angled side view. Scale bar = 100 µm (Z) x 1400 µm (Y) x 1400 µm (X).

Clearly defined pores were seen within the top layer of the polymer, confirming the highly porous 3D structure previously inferred from **Figure 3.3**. Alternative views of the polymers topology were visualised using the 3D reconstruction, providing additional visual depth information of the uneven surface (**Figure 3.4**). This allowed confirmation of the structure previously observed. This method of imaging provided an increase in contrast between the polymer and background, giving a more clear and defined depiction of the polymers structure, compared to previous SEM imaging, further confirming the structure described previously in **Section 3.3.2**.

3.3.4. Pore Diameter and Area

To further evaluate the pores generated within the structure of polymer A, SEM images of polymer at densities of 0.067, 0.050, 0.040 g/cm^3 were processed using Fiji software (Tinevez *et al*., 2012) to quantify pore diameter and area, as described in **Method 2.2.1.1**. Here diameter refers to the "feret" diameter which is the distance between the two furthest points of the pore.

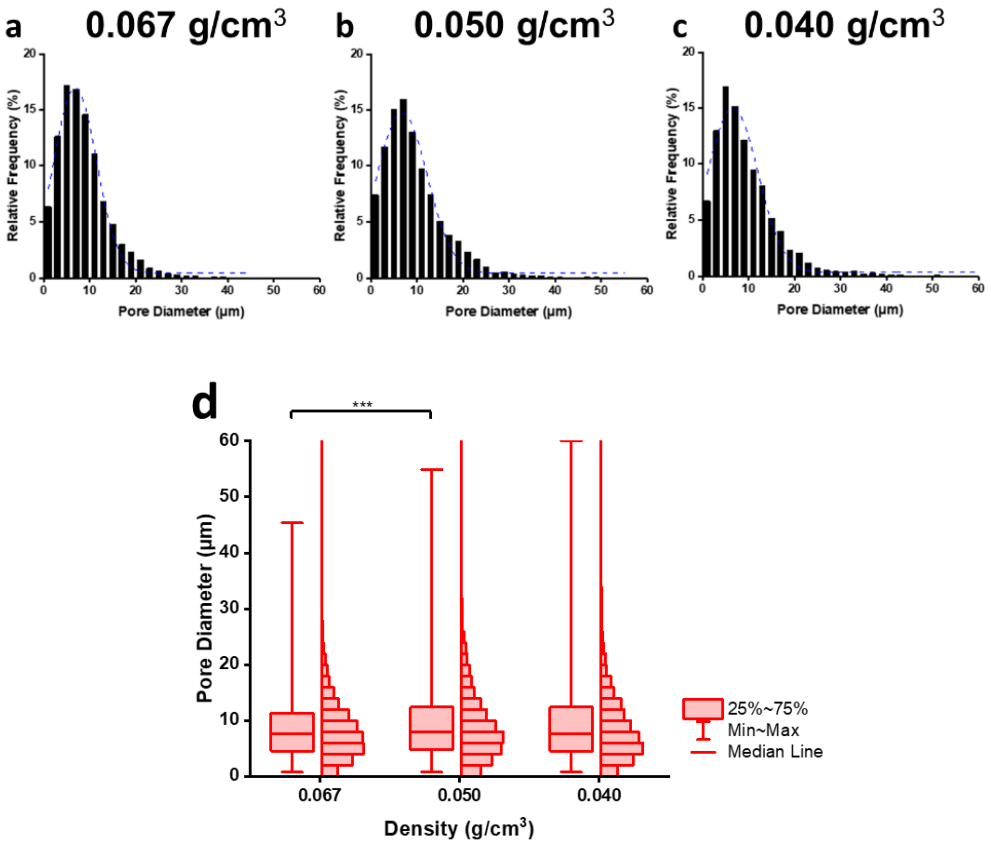

Figure 3.5. Diameter of pores in polymer A at varied polymer densities. Individual frequency distribution graphs for polymer A at densities of **a.** 0.067 g/cm^3. n = 1 image, 3005 pores. **b.** 0.050 g/cm^3. n = 1 image, 3113 pores. and **c.** 0.040 g/cm^3. n = 1 image, 3719 pores. **d.** Box and whisker graph for pore diameter at each polymer density. Statistical significance was determined by a Mann-Whitney-U test. *** = $p \leq .001$.

Figures 3.5a, **b**, and **c**. revealed that at each polymer density investigated, the distribution of pore diameters displayed a skewed distribution. Significant difference was only observed between the medians of 0.067 g/cm^3 (7.57 µm) and 0.050 g/cm^3 (7.94 µm). For all densities of polymer, pore diameter displayed a

lower quartile of 4.6 ±0.2 µm, and an upper quartile of 11.8 ±0.6 µm. This highlights that the majority of pore diameters fall within this range, regardless of polymer density. Further, **Figure 3.5d**. also showed that as the polymer density decreases, the overall range increase increases. This suggests that although the median value and interquartile range do not show a large increase, a small proportion of the pores increase to a larger maximum diameter, as the density decreases.

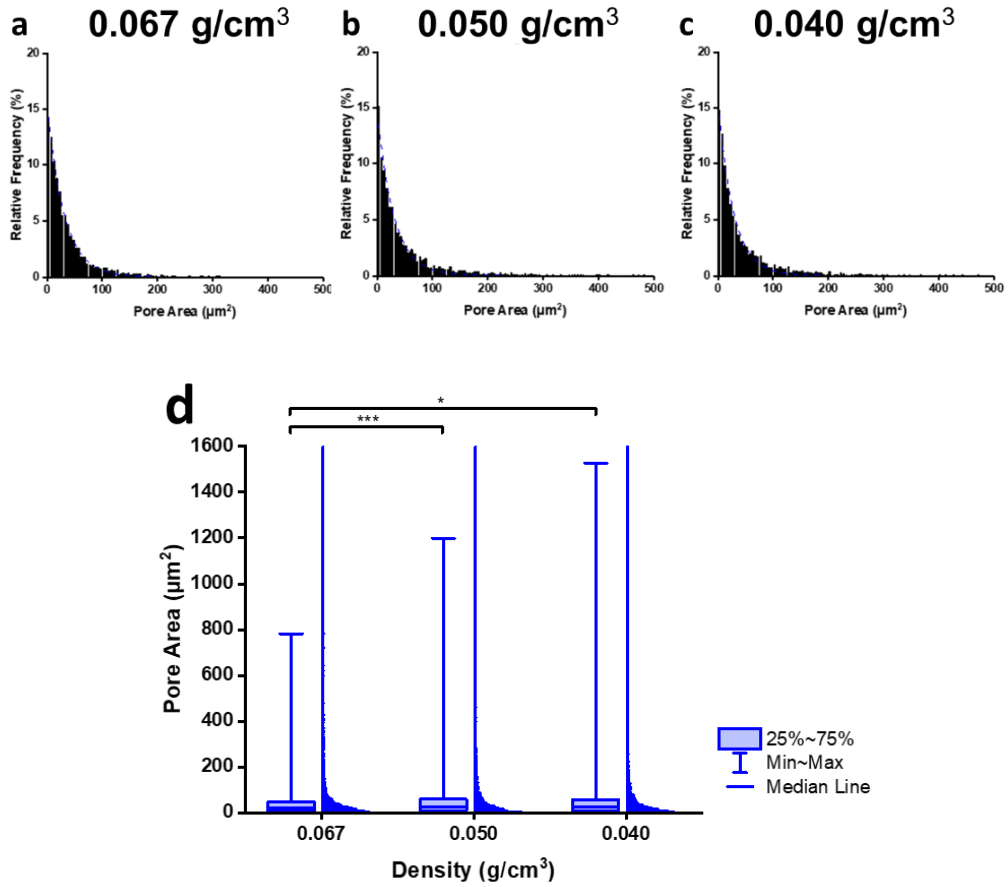

Figure 3.6. Area of pores in polymer A at varied polymer densities. Individual frequency distribution graphs for polymer A at densities of **a.** 0.067 g/cm^3. n = 3005. **b.** 0.050 g/cm^3. n = 3113. and **c.** 0.040 g/cm^3. n = 3719. **d.** Box and whisker graph for pore area at each polymer density. Statistical significance was determined by a Mann-Whitney-U test. * = $p \leq .050$. *** = $p \leq .001$.

Figures 3.6a, **b**, and **c**. revealed that at each polymer density investigated, the distribution of pore areas displayed an exponential distribution. Significant

differences between pore area were observed between the medians of 0.067 g/cm^3 (22.40 µm^2) and 0.050 g/cm^3 (26.04 µm^2); and 0.067 g/cm^3 (22.40 µm^2) and 0.040 g/cm^3 (23.80 µm^2) (**Figure 3.6d**). It was not possible to deduce from this data whether there was a difference in the median pore area between 0.050 and 0.040 g/cm^3. Additionally, the interquartile range increased from 38.9 µm^2 at 0.067 g/cm^3 to 50.9 µm^2 at 0.05 g/cm^3 showing an increase in variation of pore area with a decrease in density. This however, does not occur when the density is decreased from 0.050 to 0.040 g/cm^3. As with the pore diameter, the overall range was seen to increase as the polymer density decreases, over all densities tested. This suggests that a small proportion of the pores increase to a larger maximum area, as the density decreases.

It was expected that decreasing the density would increase the pore size within the polymer, however, this was not entirely found to be the case. Median pore diameter increased marginally only between densities of 0.067 and 0.050 g/cm^3 and median pore area was found to be significantly increased between 0.067 and 0.050 g/cm^3, and 0.067 and 0.040 g/cm^3. A reason for the lack of significant differences found between 0.050 and 0.040 g/cm^3 may be the smaller interval of 0.010 g/cm^3, compared to 0.017 g/cm^3 between .067 and 0.050 g/cm^3. This interval was investigated as a result of the initial density being measured in mL of polymer solution per gram. As the polymer was initially in a liquid solution, the volume in mL was adjusted to control the density. Hence densities of 0.067, 0.050, and 0.040 g/cm^3 correspond to 15, 20, and 25 mL/g.

Resting T-cells possess an average diameter of 7.3 µm (Kuse *et al*., 1985). Given this is smaller than the results found for median pore diameter it is anticipated that T-cells will be able to fit through the majority of pores in all densities of polymer investigated. Additionally, migrating T-cells are known to display an

elastic nature, changing their morphology to that similar of an amoeboid (Wolf *et al*., 2003; Lämmermann *et al*., 2008). In the body this allows T-cells to squeeze through gaps as small as that between cells in an endothelial cell monolayer (Weninger *et* al., 2014), in regards to polymer interaction this suggests T-cells may be able to migrate through pores of all diameters in this scaffold.

To complement this work, a further exploration into the 3D pore structure and its connectivity was undertaken through the use of X-ray computed tomography.

3.3.5. Porosity and Tortuosity

2 mL of 0.067, 0.050, 0.040, 0.033 g/cm^3 polymer A solution was produced and cast within 5 mL syringes. Samples were freeze dried and imaged via X-ray computed tomography, as described in **Method 2.1.5.17**. 3D renders were produced and analysed using Avizo™ software (FEI, Hillsboro, USA) to analyse 500 sub-volumes of each 3D reconstruction, producing values for porosity and tortuosity. The work in this section was performed in collaboration with Dr. Thomas F Johnson (University College London). Specific details of the collaboration are given in **Methods 2.1.5.17.** The porosity value represents the percentage of void volume within a given area. The tortuosity value represents the ratio of the line of flow between two points in the polymer and the straight line distance, therefore values closest to 1 represent a least torturous path with 1 being the lowest possible value. 1 sample of each density was analysed using x-ray computed tomography.

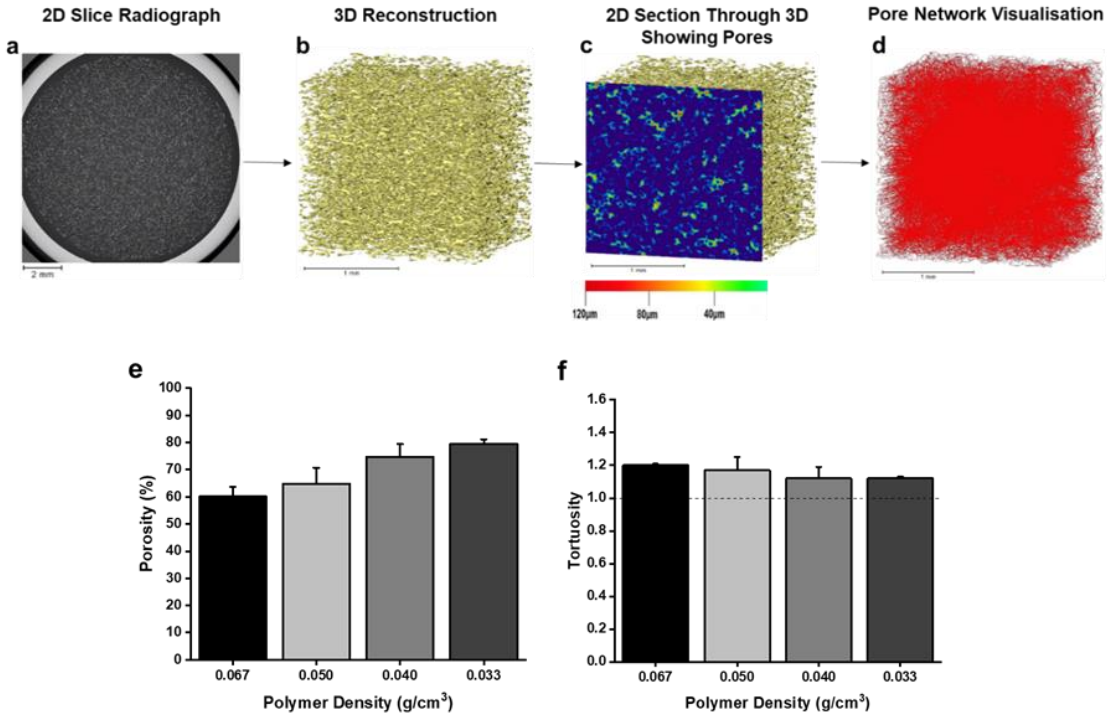

Figure 3.7. Porosity and tortuosity determined by X-ray computed tomography. a - **d.** show the process of pore analysis. **a.** A single 2D radiograph of polymer A. Scale bar = 2 mm. **b.** 3D reconstruction of polymer A constructed from multiple radiographs, 2 mm (H) x 2 mm (W) x 2 mm (L). **c.** A 2D section through a 3D reconstruction, showing internal pores. **d.** Pore network within the polymer. **b - d.** Scale bars = 1 mm. **e.** Porosity at various polymer densities. **f.** Tortuosity at various polymer densities. **e** and **f.** n = 1 polymer sample per density, 500 re-constructions analysed for each sample. Error bars = ± 1SD.

Through the visualisation of 3D reconstructions (**Figures 3.7a - d**) it was found that polymer, at all tested densities, displayed not only a highly porous structure but also one that is highly interconnected throughout the material. This suggests that there is sufficient flow through the polymer with a low number of “dead end” pores restricting flow through. Analysis of 3D reconstructions provided values for porosity and tortuosity (**Figures 3.7e** and **f**). Individual data was unavailable for analysis therefore statistical tests were unable to be performed. However, general trends supported by relatively small values of standard deviation were still able to be inferred and provided important insights.

Porosity was found to increase as polymer density decreased (**Figure 3.7e**), increasing from 60.1 % at a polymer density of 0.067 g/cm^3 to 79.5 % at 0.033 g/cm^3. This was expected as a decreased density results in less material within the same volume, causing more of the space to consist of air which constitutes pores. This strongly supports the hypothesis that porosity is able to be controlled through the adjustment of polymer density.

Tortuosity was found to decrease as polymer density decreased from 0.067 g/cm^3 (1.2) to 0.040 g/cm^3 (1.12). A decrease in tortuosity was not observed when the polymer density was decreased from 0.040 to 0.033 g/cm^3, with both giving a tortuosity value of 1.12. Generally tortuosity is known to decrease with increasing porosity (Kärger *et al*., 2012). The results here suggest that the tortuosity of polymer A can be controlled by the adjustment of polymer density but to a lower value limit.

Polymer at all densities tested displayed low values for tortuosity suggesting that the structure is a good candidate for the unhindered flow of substances in and out of the polymer. Thus providing a potential pathway for cell seeding into the scaffold and later removal. This method provides a good indicator of low tortuosity, however, it is limited in that the values of tortuosity are calculated assuming the flow through of water and not suspensions containing cells. Therefore, the values for tortuosity would be expected to increase with the introduction of cells.

3.3.6 Confirmation of Antibody Attachment

aCD3 and aCD28 antibodies were attached to polymer A as detailed in **Method 2.1.4.6**. To provide a quick semi-qualitative method to confirm successful attachment to the polymer, an ELISA was developed (see **Figure 2.8** in **Materials and Methods**).

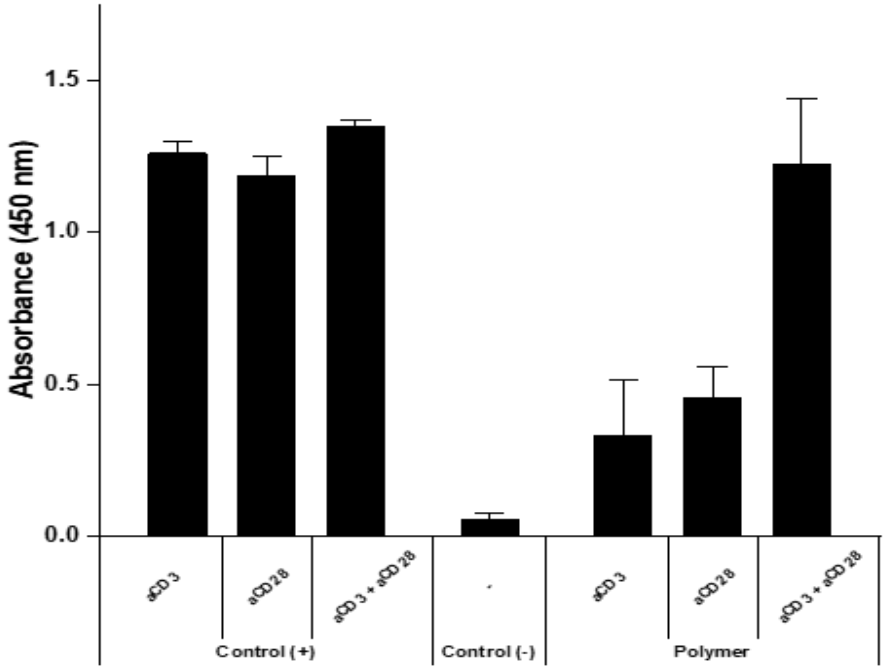

Figure 3.8. ELISA results confirming anti-CD3 and anti-CD28 presence in polymer A. n = 1 assay with triplicate wells for all conditions. Error bars = ± 1SD. Results for polymer samples have been adjusted using the negative polymer controls to account for background.

Absorbance was detected in all polymer samples that were subject to the antibody attachment protocol (**Figure 3.8**). Polymer subject to antibody solution containing either aCD3 or aCD28 only, displayed similar mean absorbance values of 0.42 and 0.45, respectively. Polymer subject to antibody solution containing both aCD3 and aCD28 displayed the highest mean value for absorbance, 1.23. This was expected due to the antibody solution containing double the total amount of antibody available for attachment than when the solution was contained either aCD3 or aCD28 only.

The result of this assay confirms that aCD3 and aCD28, both separately and combined, was present within the polymer matrix. This strongly indicates that the antibody has attached to the polymer.

3.3.7. Antibody Distribution

To further characterise antibody attachment to polymer A, polymer was incubated with a secondary anti-murine antibody to attach to aCD3 and aCD28. This secondary antibody was bound to a fluorophore which allowed visualisation of the distribution of attached aCD3 and aCD28 using a fluorescent confocal microscope, as per **Method 2.2.1.4**. As in **Section 3.1**, the auto-fluorescence of the polymer was utilised to visualise the polymer. Controls are shown in **Appendix C.1**.

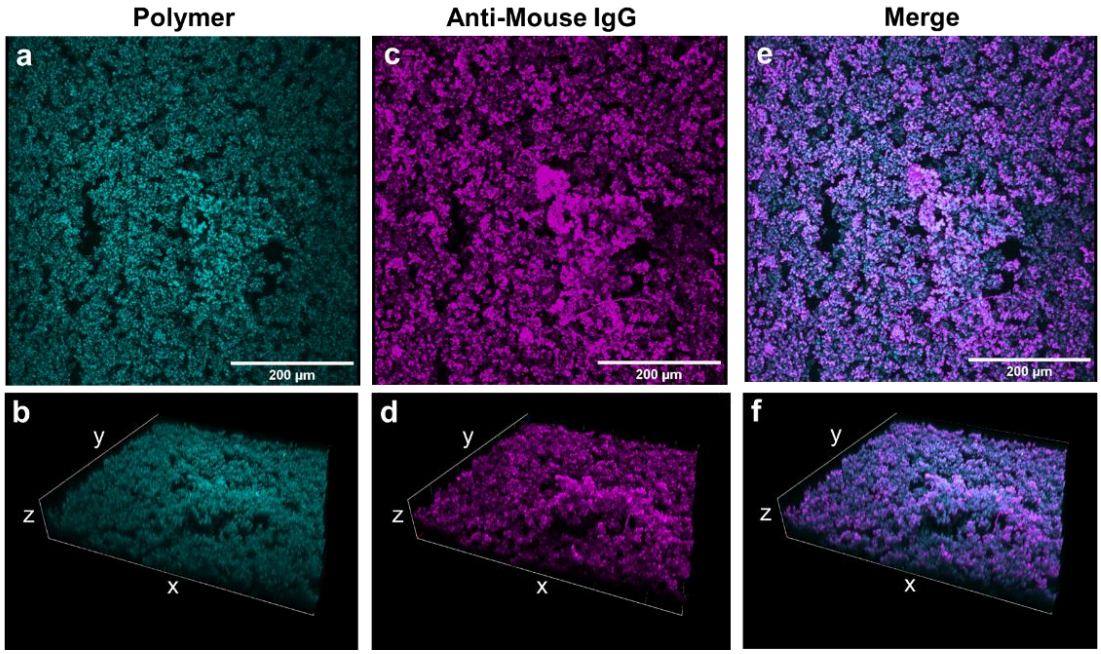

Figure 3.9. Reconstructed 3D fluorescent confocal microscopy images of polymer A showing the distribution of attached anti-CD3 and anti-CD28. a and **b.** Polymer A, visualised through the DAPI channel, pseudo-coloured cyan. **c and d.** aCD3 and aCD28, stained with anti-mouse IgG AlexaFlour® 594, pseudo-coloured magenta. **e and f.** Merged channels. Top row images (**a, c** and **d**) show a top view. Scale bars = 200 µm. Bottom row images (**b, d** and **f**) show an angled side view. Scale bars = 100 µm (Z) x 567 µm (Y) x 567 µm (X).

Secondary staining of aCD3 and aCD28 was successful in allowing the visualisation of antibodies attached to the polymer. Reconstructed 3D images provided additional confirmation of the attachment of aCD3 and aCD28, and

further revealed a dense and equal distribution of antibodies over the polymers surface (**Figure 3.9**). Antibody was observed at all levels within the 3D reconstruction indicating that the antibody is able to distribute though the 3D structure and attach throughout. Ideally this would be confirmed by imaging deeper into the polymer, however, imaging depth with polymer A was limited by spherical aberration. This is a process in which resolution is lost due to the thickness of the sample distorting light rays as they pass through regions of differing refractive index (North, 2006).

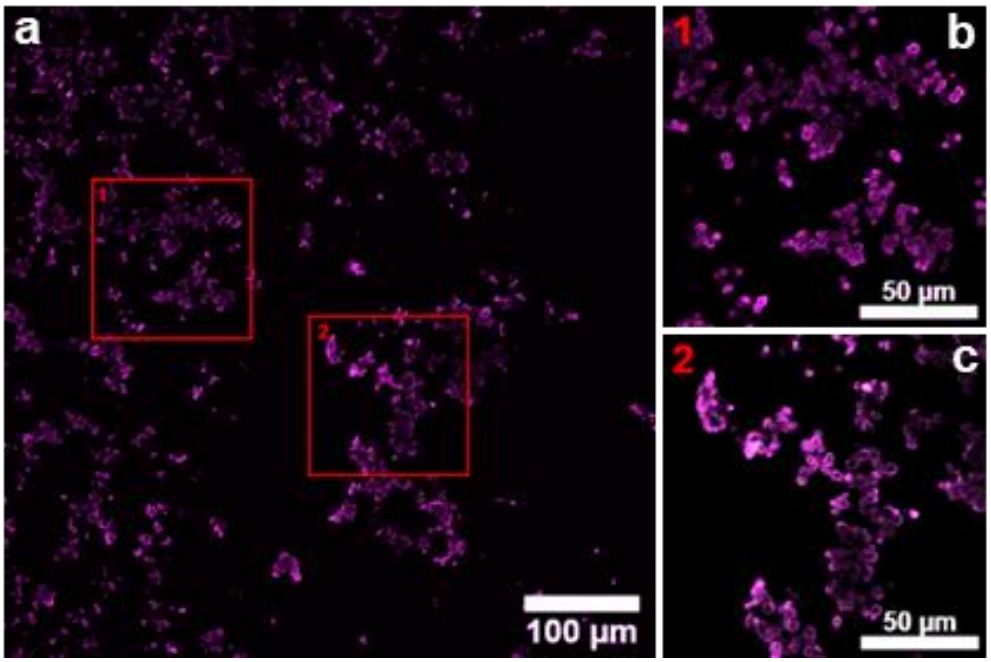

Figure 3.10. Single slice from a z-stack showing aCD3 and aCD28 attachment on Polymer A surface. aCD3 and aCD28 has been stained with anti-mouse IgG AlexaFlour® 594 and pseudo-coloured magenta. **a.** A single slice taken from a z-stack image. Scale bar = 100 µm. **b.** Region 1 magnified. **c.** Region 2 magnified. **b.** and **c.** Scale bars = 50 µm.

To minimise waste and reduce the cost of production, it is desirable that antibody does not permeate inside of the polymer. To investigate this images representing single slices through the z-stack, showing a view through the centre of spheres, were examined. Intense bands of fluorescence were observed around the

perimeter of the spheres that constitute the polymers structure, with minimal/ no fluorescence observed in the centre (**Figure 3.10**). This suggests that antibody diffusion into the polymer particles is minimal.

The importance of antibody density and spacing in regards to their effects on T-cell stimulation has been highlighted in previous studies (Deeg *et al*., 2013; Matic *et al*., 2013; Hickey *et al*., 2019). Taking this into consideration it would be recommended that future work should be completed with the aim of quantifying antibody density on the polymer surface. This could be achieved through the further optimisation of fluorescence microscopy settings so that fluorescence intensity could be used to infer antibody density. Additionally, secondary labelling of aCD3 and aCD28 with antibodies attached to gold particles combined with high magnification SEM could allow individual antibodies to be visualised and quantified in a given area.

3.3.8. Biocompatibility

Biocompatibility of the polymer with T-cells was investigated through the co-culture of discs of polymer A without antibody attached and Jurkat T-cells over 6 days, as described in **Method 2.2.1.5**. Each day, T-cell cultures were analysed for cell number and viability, then stained with annexin V and PI to identify viable, apoptotic, and necrotic cells.

Annexin V stains phosphatidylserines, phospholipids that occur in the inner membrane of a healthy cell. PI stains DNA, only passing into cells when membrane integrity is compromised, therefore indicating a non-viable cell. Viable cells will not be stained by either dye. During the early stages of apoptosis, phosphatidylserines are flipped onto the outer membrane of a cell with the membrane remaining intact, thus being profiled as annexin $V^{+}PI^{-}$. In the absence

of phagocytic cells, apoptotic bodies progress to late-stage apoptosis and begin to lose membrane integrity, and may therefore be stained by PI in addition to annexin V. Necrotic cells with their compromised membrane may also be stained with both dyes. Annexin V^+PI^+ cells were defined as either late-stage apoptosis or necrotic. Annexin V^-PI^+ were defined as necrotic (**Figure 3.12b**).

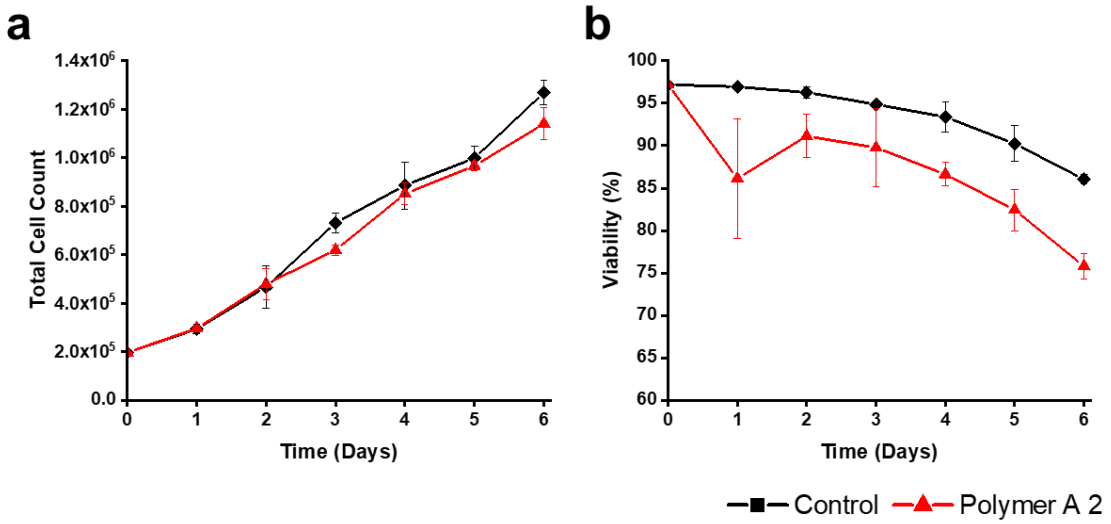

Figure 3.11. Jurkat T-cells in culture with polymer A over 6 days. a. Total culture cell count. **b.** Culture viability. n = 1 with triplicate technical repeats. Error bars = ± 1SD.

Table 3.1. *p*-values for the Total Cell Count and Viability of T-cells cultured with Polymer A over 6 Days.

Control vs Polymer A (*p-value, 3 d.p*)						
	Day					
	1	2	3	4	5	6
Total Cell Count	.999	.994	.007**	.886	.991	.039*
Viability	.048*	.032*	.225	.002**	.002**	*p*<.000***

Significance was determined by a one-way ANOVA with a post hoc Tukey's Test.
* = $p \leq .050$. ** = $p \leq .010$. *** = $p \leq .001$.

The total cell count of cells cultured with polymer A was similar to the control over the 6 days (**Figure 3.10a**). Significant differences were seen at days 3 and 6 where cultures containing polymer A showed a small decrease in total cell count

when compared to the control of 1.1 x 10^4 and 1.3 x 10^4, respectively. Cell growth over time was observed to increase in a linear manner from day 1, suggesting cells were in an exponential phase of growth. Analysis of total population viability (**Figure 3.10b**) revealed that although the total cell count remained similar over the 6 day period, the viability did not. T-cells in culture with polymer A showed a decreased population viability compared to the control at each time point. These differences were found to be statistically significant at every time point excluding day 3 (**Table 3.1**). A sharp decline in viability, from 97 to 86 %, is displayed after culture with polymer A for 1 day (from day 0 to day 1). This value, however, also shows a large standard deviation of ± 7 % and so it may not be entirely accurate to conclude that a large initial decline in viability was the case. From day 2 to 6, both the control and T-cells cultures with polymer A show a steady decline in viability to 86 and 76 %, respectively.

To further explore the effect of culturing T-cells with polymer A, an annexin V/PI assay was performed. **Figure 3.12a** shows representative annexin V vs PI graphs obtained from the NucleoCounter® NC-3000™. From the scatter graphs alone it was observed that both cells cultured with polymer A and the control displayed an increase in events in the top right quadrant by day 6, classified as either late/stage apoptotic or necrotic. The gating strategy shown in **Figure 3.12b**. was applied to further categorise events in all quadrants.

A significant decrease in the percentage of viable, and an increase in the percentage of late-stage apoptotic/necrotic, cells on days 5 and 6 was observed (**Figures 3.12c** and **e**). Furthermore, a significant increase was observed in the percentage of early-stage apoptotic cells of cells cultured with polymer A when compared to the control, at every point excluding day 1.

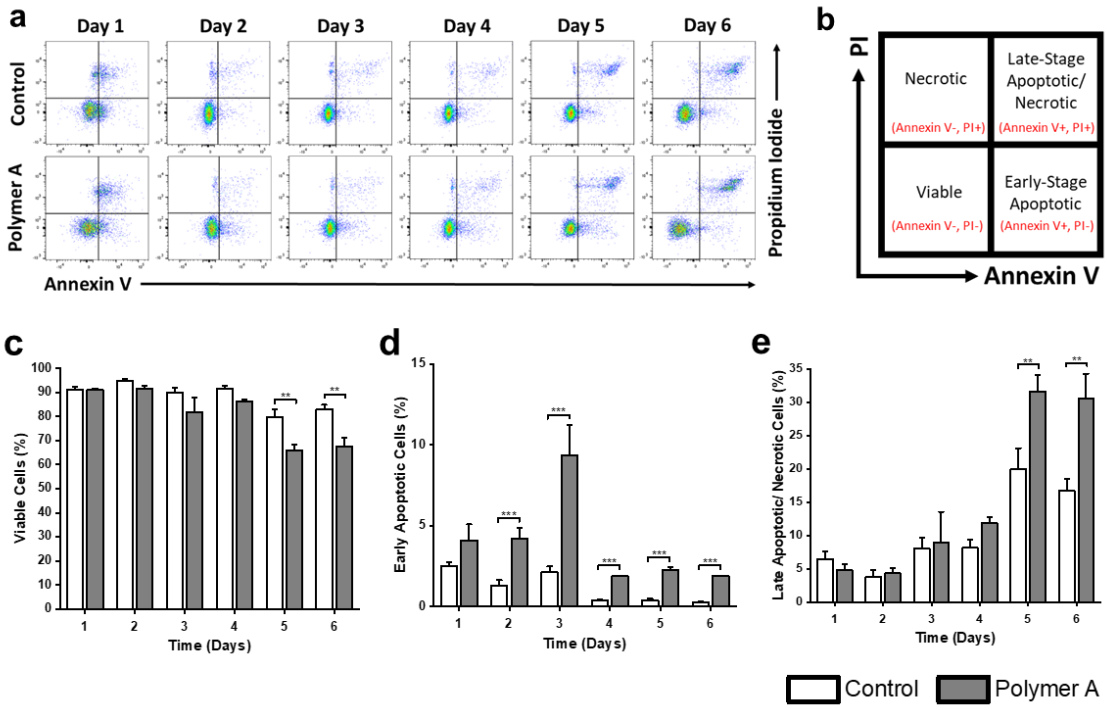

Figure 3.12. Apoptosis assay performed on Jurkat T-cells in culture with polymer A over 6 days. a. Representative scatter graphs with propidium iodide (PI) on the y-axis and annexin V on the x-axis. **b.** Gating strategy for the classification of viable (annexin V^-PI^-), early-stage apoptotic (annexin V^+PI^-), either late-stage apoptotic or necrotic (annexin V+, PI+), and necrotic (annexin V^-PI^+) T-cells. **c.** Percentage of viable cells in the total population (annexin V^-PI^-). **d.** Percentage of early-stage apoptotic cells in the total population (annexin V^+PI^-). **e.** Percentage of either late stage apoptotic or necrotic (annexin V^+PI^+) combined with necrotic (annexin V^-PI^+) cells in the total population. n = 1 with triplicate technical repeats. Error bars = ± 1SD. *p*-values were determined by a two-tailed T-test. ** = $p \leq .010$. *** = $p \leq .001$.

Although it is not possible to say what the cause of death of cells classified as necrotic was; the consistently increased percentage of early-stage apoptotic cells suggests that polymer A is inducing low-levels of apoptosis. This was surprising as other variations of hydrogels and structures made from cross-linked poly-ε-lysine have been used previously in culture with other cell types with no reports of toxicity (Wang *et al*., 2016; Kennedy *et al*., 2019; Lace *et* al., 2021). In fact, biocompatibility of poly-ε-lysine has been confirmed as such that it is being considered for use in drug delivery vectors (Shi *et al*., 2019).

Apoptosis can be triggered either by interactions with other immune system cells or environmental stress such pH or temperature (Zhou *et al*., 2019). As this is a pure culture of T-cells, the latter is more probable. Caló and Khutoryanskiy (2015) describe how 3D polymerisation often results in residual monomers which may leach out from hydrogels if not sufficiently washed. However, given the generally accepted biocompatibility of ε-PL discussed previously, even if it were to leach it would be unlikely to induce apoptosis. A more likely suggestion may be that insufficient washing may have led to either unreacted acid or ethanol used in sterilisation of the polymer remaining within the polymer; causing stress to T-cells as it leaches out. The reduction of viable cells when cultured with polymer A was - 15 % on day 6, it is important that polymers used in cell cultures be rinsed thoroughly to minimise this. Furthermore, it would be of interest to investigate the effect of different wash techniques and times on the resultant biocompatibility.

Discrepancies in the culture viability obtained from the NucleoCounter® NC-3000™ and the percentage of viable cells determined from the apoptosis assay are worth addressing here. This can largely be explained by the classification of early-stage apoptotic cells as viable in the first method. This method uses staining by DAPI to identify non-viable cells. Early-stage apoptotic cells retain an in-tact membrane resulting in them not being stained by DAPI and grouped as viable, despite their commitment to dying.

Both the decrease in culture viability and increase in dead or dying cells by day 6 demonstrated by the control suggests that the culture conditions were already not optimal for cell culture over the 6 days. To better separate and determine the effect of culturing with polymer A, it would be beneficial to optimise culture conditions to minimise the effect on culture health.

Additionally, the apoptosis assay utilised here is limited by an over simplification of the classification of cell death. Although it can differentiate between early-stage apoptotic and necrotic cells, it is not possible to further determine the pathway of cell death that occurred in the necrotic cells with this assay alone. Moreover, it has been reported that during the early stages of oncosis, oncotic cells stain annexin V^+PI^- (Lecoeur *et al*., 2001). Therefore cells determined as early-stage apoptotic using this assay may also be oncotic. For determining the level of general cell death in this early stage biocompatibility study, this method alone was suitable. However, differentiation of the pathway of cell death may be important in the future as oncotic cells swell causing an inflammatory immune response, whereas apoptotic cells do not, thus having implications for cells to be used in cell therapies (Majno and Joris, 1995). Future studies may consider validation of the cell death pathway using complimentary techniques such as microscopy (Balvan *et al*., 2015) or flow cytometry with antibody panels of increased specificity (Vossenkamper and Warnes, 2019).

3.4. Conclusion

The following characteristics of polymer A were evaluated to further understand and asses it's suitability for use in this project: the structure and topology, particularly the ability to form a porous structure in which T-cells could enter into; the ability to immobilise aCD3 and aCD28 antibodies on its surface; biocompatibility in culture with T-cells; and the auto-fluorescence profile.

Auto-fluorescence was previously noted and exploited to image polymer A through fluorescent imaging. This was characterised to minimise interference in immunostaining. Auto-fluorescence was found to be most intense at excitation wavelengths of < 450 nm producing emission wavelengths of ≤ 550 nm. Therefore, fluorescent imaging techniques should use stains or fluorophore

conjugated antibodies which are visualised though excitation wavelengths higher than 450 nm and emission wavelengths higher than 500 nm to minimise background fluorescence.

Surface topology, analysed through the use of SEM and 3D reconstructions by fluorescent confocal microscopy structure, was revealed to be uneven, highly porous, and structurally comprising of many spherical particles fused together.

Further characterisation of pores was achieved through the measurement of pore diameter and area with consideration of the impact of varying polymer density. Median pore diameter increased marginally only between the highest and middle density ranging from 7.57 µm to 7.94 µm. Similarly median pore area increased only marginally between the highest (22.50 μm^2) and middle (26.04 μm^2), and highest and lowest (23.80 μm^2) density. For both diameter and area it was found that a small proportion of the pores increase to a larger maximum size, as the density decreases.

Pore characteristics in regards to flow through the polymer in a 3D structure were investigated over varying polymer densities. 3D reconstructions confirmed that the polymer was highly porous throughout and consisted of a vastly interconnected pore network. It was also observed that porosity increased as density decreased, and that tortuosity decreased as density decreased. Tortuosity values for all polymer densities tested were low proving the polymer an ideal candidate for the implementation of flow through.

An aCD3/aCD28 ELISA was developed and confirmed the presence of aCD3 and aCD28 within the polymer matrix. The attachment of antibodies was further confirmed through the visualisation of aCD3 and aCD28 on the surface of polymer A by z-stack fluorescent confocal microscopy. Antibody was observed to

be distributed throughout the surface of the 3D structure, with minimal diffusion into the polymer structure itself.

Contrary to the previously reported good biocompatibility of ε-PL structures, polymer A was found to convey minor toxicity to T-cells in culture, inducing slightly increased levels of apoptosis over 6 days, and ~10 % decrease in viable cells on day 5 and 6. This is thought to be likely due to insufficient washing post ethanol sterilisation and future polymers will be washed extensively to minimise leaching.

Overall, characteristics of polymer A such as its macro-porous structure and ability to successfully bind aCD3 and aCD28 to its surface indicate that it is a promising candidate material for this thesis. The next steps towards evaluating the suitability of polymer A focused on the functionality and practicality of using polymer A to activate T-cells, namely a proof-of-concept of activating T-cells with the polymer, and the ability to seed and remove T-cells from its porous structure. These studies are described below in **Chapter 4**.

Chapter 4. Evaluation of Polymer A

4.1. Introduction

The characterisation of the macro-porous structure and confirmation of antibody attachment in **Chapter 3** suggest that polymer A is a suitable material for use as a 3D structure capable of activating T-cells. In this chapter the suitability is further investigated with a focus on: the ability of polymer A to activate T-cells, and capacity in which T-cells can be seeded into the polymer structure and then subsequently removed.

4.1.1. T-cell Activation

In vivo, T-cell activation occurs through the stimulation of the MHC complex and other co-stimulatory receptors. *Ex vivo*, this stimulation can be replicated through the use of an aCD3 antibody, which targets the CD3 motif of the MHC complex, and co-stimulation can be provided by an aCD28 antibody. Efficient stimulation results in the activation of a T-cell which switches it from a resting state to a proliferative state, exhibiting differentiation and effector functions. Successful T-cell activation can be assessed through numerous different outputs, with the ones investigated here being; cell proliferation, cell diameter, culture morphology, expression of activation markers CD69 and CD25, and metabolic profile. A key aim of this project is to establish a material that is capable of activating T-cells. It was therefore of great significance to investigate the activation of T-cells using current methods and with aCD3 and aCD28 attached to polymer A. Furthermore, cell lines are often used as models in preliminary studies as they are relatively less complex and variable than primary material, with the Jurkat T-cell line having been employed widely to model signalling events during activation (Montano, 2014). Therefore, it was also of interest to determine the role that Jurkat T-cells could play in investigating the activation of T-cells in this present study.

4.1.2. Cell Columns

As polymer A possesses a macro-porous structure and displays good flow through properties, a natural suggestion as a means to seed and remove T-cells in and from the 3D structure was to design a set-up in which a flow runs through the polymer; to flow cells both in and then out. Set-ups like this are used widely in chromatography for component separation of mixtures. The use of cell columns, however, is less reported, with the most well-known being a MACs column used for cell sorting. To assess the suitability of polymer A for use in a cell column format, multiple set-ups were explored each with the objective of incorporating enhancements and improving on the previous. These set-ups were used to investigate optimal running parameters for flow rate and cell density, and to examine the pressure drop within the system.

4.1.3. Pressure Drop

A pressure drop can be defined as the differential pressure between two points in which there is a flow through. A drop in pressure arises from resistance to flow which causes frictional forces. In chromatography this usually occurs as liquid enters the column and flows through the chromatography media. This can be problematic as a medium of high resistance results in high back pressure within the system. When flow through a porous material is in a laminar state, the relationship between flow rate and pressure drop is governed by Darcy's law:

$$\Delta P = \frac{Q \; x \; \mu \; x \; L}{K}$$

(Eq. 6)

Where ∆P is the pressure drop, Q is the volume flow rate, μ is the liquid viscosity, L is the chromatography bed length, and K is the chromatography bed permeability.

If liquid viscosity, bed length, and bed permeability remain constant, a linear relationship between flow rate and pressure drop should be observed. In order to assess polymer A as a material for use in a column format, it was important to characterise critical parameters in the set-up such as the pressure drop to allow behavioural predictions for future use.

4.2. Aims and Hypotheses

4.2.1. Chapter Aims

- To characterise T-cell activation readouts with different stimulation methods.
- To compare T-cell activation characteristics between cell-line derived and primary-sourced human T-cells.
- To demonstrate the activation of T-cells with polymer A.
- To evaluate and reduce non-specific binding to polymer A.
- To investigate flow through conditions in order to optimise the recovery and viability of cells flown into polymer A – specifically testing different set-ups, and evaluating the impact of flow rates and cell suspension density.
- To characterise the pressure drop within a chromatography-like system.

4.2.2. Hypotheses

Due to their use in other T-cell activation studies it is expected that, when stimulated, cell-line derived Jurkat T-cells will exhibit similar culture characteristics to activated primary T-cells. It is hypothesised that polymer A with aCD3 and aCD28 attached will activate T-cells that interact with it. As pores sizes are characterised and polymer A has previously demonstrated good flow though characteristics, it is expected that T-cells will be able to be enter into and be removed from the polymer by applying flow. It is further anticipated that an optimal

flow rate will be highlighted that will successfully allow T-cells to be passed into and then out of polymer A with minimal effect on cell viability. Additionally, characterisation of the pressure drop will allow future behavioural predictions of polymer A within a chromatography style set up.

4.3. Results and Discussion

4.3.1. T-cell Activation

Initially, it was of interest to characterise activation with 3 different activation methods, Dynabeads, TransAct, and an aCD3/aCD28 coated well plate, as per **Method 2.1.2**. These represent activation via micro-bead, nano-bead, and a flat surface respectively. Bead based methods can be found described further in **Section 1.6**. Additionally, at the time of this study Dynabeads were considered the gold standard in T-cell activation for T-cell therapies, with TransAct being one of the only available alternatives manufactured to GMP standards. Whilst also providing a comparison between various activation methods, it was of particular interest to compare the cell-line derived Jurkat T-cells to primary-sourced T-cells to assess the role that Jurkat T-cells to be useful in in future studies. This was followed by a preliminary assessment of T-cell activation by aCD3/aCD23 polymer A.

4.3.1.1. Jurkat vs Primary T-cell Activation

Primary and Jurkat T-cells were suspended in complete RPMI media supplemented with 30 IU/mL rIL-2, seeded into wells, and left unstimulated or stimulated with Dynabeads, TransAct, or an aCD3/aCD28 coated well. Cells were imaged via confocal microscope before being harvested at time points of 0 hours, 3 hours, 1 day, 3 days, 5 days, and 7 days. Harvested cells were subject to a cell count, viability analysis, cell diameter analysis, and activation marker expression analysis. Additionally, spent media at each time point was collected and analysed

for glucose, glutamine, lactate, and ammonia content. On day 3, the media volume was doubled. On day 5, half of the media volume was removed and replaced with fresh media. This method is descried in more detail in **Method 2.2.2.1**.

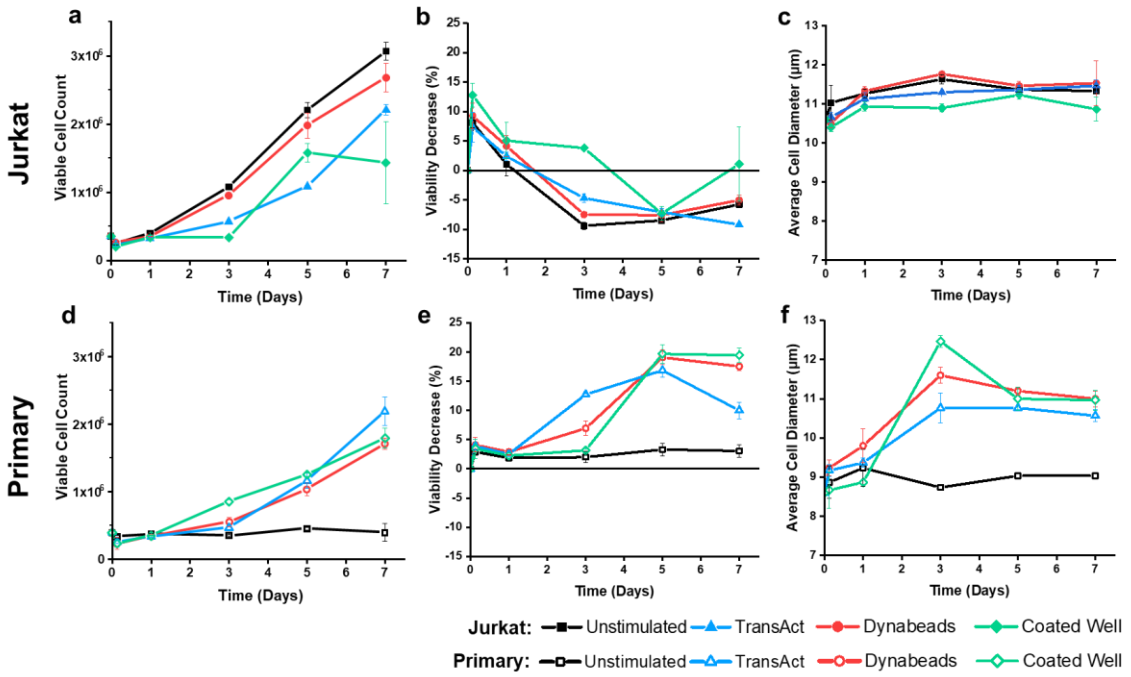

Figure 4.1. Culture dynamics of Jurkat and primary human T-cells stimulated with Dynabeads, TransAct, or an aCD3/aCD28 coated well over 7 days. a and **d.** Viable cell count. **b** and **e.** Viability Decrease. **c** and **f.** Average cell diameter. Top row (**a - c**) = Jurkat T-cells. Bottom Row (**d - f**) = Primary T-cells. n = 1 with 3 technical replicates. n = 1 donor for primary T-cells. Mean values are plotted. Error bars = ± 1SD.

For Jurkat T-cells from day 0 to day 7, unstimulated T-cells increased by 7.4-fold, Dynabead stimulated by 6.5-fold, TransAct stimulated by 5.3-fold, and coated well stimulated by 3.5-fold (**Figure 4.1a**). From day 5 and 6 it was observed that unstimulated Jurkat T-cells had an increase in viable cell count over all stimulation methods (**Table 4.1**). **Figure 4.1d** shows that with primary T-cells from 0 to day 7, Dynabead stimulated T-cells increased by 4.3-fold, TransAct stimulated by 5.6-fold, and coated well stimulated by 4.6-fold; unstimulated primary T-cells did not proliferate. By day 7 the differences in viable cell count

between primary T-cells stimulated with Dynabeads or TransAct were not significant (**Table 4.1**), and therefore resulted in both of these stimulation methods being determined as giving the largest increase in viable cell count.

Figure 4.1b displays the decrease in viability normalised to the starting viability. Jurkat T-cells exhibited generally similar behaviour over 7 days for all methods, with slight variations found with coated well stimulation. For unstimulated, Dynabeads, and TransAct, culture viability decreased an average 8.2 % from seeding to 3 hours, followed by a recovery and overall increase in viability by day 7. Unstimulated and Dynabead cultures displayed a maximum increase in viability at day 3 followed by a small decline, whereas TransAct displayed a gradual increase in viability from 3 hours to 7 days. From **Figure 4.1e** it can be seen that for primary T-cells, the viability of unstimulated cells remained stable over the 7 days. For all stimulated cultures, compared to unstimulated, a significant decrease in viability was observed for all by day 5, with the largest decrease for all occurring on day 5. Interestingly, of the stimulated cultures, TransAct shows a significant recovery in viability from day 5 to 7 compared to Dynabeads and coated well (**Table 4.1**).

The cell diameter of Jurkat T-cells remained between 10.4 and 11.8 µm for all methods investigated (**Figure 4.1c**), with the only significant differences between methods found at day 5 between all except unstimulated vs Dynabeads (**Table 4.1**). **Figure 4.1f** shows that unstimulated primary T-cells remained between 8.7 and 9.2 µm over 7 days, whereas all stimulated T-cells showed a significant increase in diameter in comparison by day 3 (**Table 4.1**). All stimulated primary T-cells displayed the maximum diameter at day 3 before a small decline. Dynabeads displayed a mean of 11.3 µm between day 3 and 7, TransAct 10.7

µm, and coated well 11.4 µm. This suggests that in regards to cell diameter, unstimulated Jurkat T-cells exhibit characteristics comparable to of that of an activated primary T-cell.

Overall, key differences were observed between Jurkat and primary T-cells that were unstimulated in regards to viable cell count, viability decrease, and average cell diameter. Unstimulated Jurkat T-cells increased by 7.4-fold in contrast to unstimulated primary T-cells which did not show an increase in cell number from day 0 to day 7. Viability decrease for unstimulated Jurkat T-cells highly resembled that of cells which were stimulated with Dynabeads and TransAct; a sharp decrease in viability of 8.1 % from 0 to 3 hours, followed by an increase of 17.5% from 3 hours to 3 days, and then a smaller decrease of 3.6 % by day 7. For unstimulated primary T-cells a smaller initial decrease in viability of 2.9 % was recorded from 0 to 3 hours which then remained relatively stable giving a range of 1.9 % to 3.3 % viability decrease over the 7 days. As with viability, the cell diameter of unstimulated Jurkat T-cells resembled that of those which were stimulated (**Figure 4.1c**), ranging between 10.6 and 11.6 µm over the 7 days. Unstimulated primary T-cells not only differed to Jurkats in cell size, ranging from 8.6 to 9.2 over 7 days, but also in that they did not resemble their stimulated counterparts. From day 3 unstimulated primary T-cells were significantly ($p \leq .001$) smaller than all stimulated primary T-cells (**Figure 4.1f** and **Table 4.1**).

These results indicate that as unstimulated Jurkat and primary T-cells differ significantly in proliferation, viability, and cell diameter, these readouts cannot be assessed to infer T-cell activation in Jurkats T-cell cultures. The diameter of Jurkats, however, was found to be comparable to that of activated primary T-cells and so Jurkats may be useful as a model for physical size; as was done in further studies in this thesis.

Table 4.1. *p*-values for the Comparison of Different Stimulation Methods in Regards to Viable Cell Count, Viability Decrease, and Cell Diameter for Primary Human, and Jurkat T-cells.

p-value (3 d.p)

		Primary					Jurkat				
		Day					Day				
Dependant Variable	**Group Comparison**	**0.125**	**1**	**3**	**5**	**7**	**0.125**	**1**	**3**	**5**	**7**
Viable Cell Count	Unstimulated vs Dynabeads	.296	.185	.006**	<.001***	<.001***	.845	.047*	.025*	.368	.659
	Unstimulated vs TransAct	.477	.104	.087	<.001***	<.001***	.708	.004**	<.001***	<.001***	.116
	Unstimulated vs Coated Well	.293	.449	<.001***	<.001***	<.001***	.114	.013*	<.001***	.006**	.005**
	Dynabeads vs TransAct	.976	.974	.293	.375	.048*	.300	.310	<.001***	<.001***	.514
	Dynabeads vs Coated Well	1.000	.891	<.001***	.070	.942	.045*	.773	<.001***	.060	.023*
	TransAct vs Coated Well	.975	.687	<.001***	.621	.105	.550	.799	<.001***	.020*	.168
Viability Decrease	Unstimulated vs Dynabeads	.561	.064	<.001***	<.001***	<.001***	.897	.336	<.001***	.616	.992
	Unstimulated vs TransAct	.707	.281	<.001***	<.001***	<.001***	.964	.859	<.001***	.268	.580
	Unstimulated vs Coated Well	.929	.660	.353	<.001***	<.001***	.082	.163	<.001***	.421	.114
	Dynabeads vs TransAct	.993	.714	<.001***	.223	<.001***	.666	.742	.001**	.878	.433
	Dynabeads vs Coated Well	.874	.318	.002**	.938	.233	.214	.944	<.001***	.981	.169
	TransAct vs Coated Well	.960	.861	<.001***	.102	<.001***	.042*	.443	<.001***	.981	.018*
Cell Diameter	Unstimulated vs Dynabeads	.569	.227	<.001***	<.001***	<.001***	.104	.913	.264	.657	.890
	Unstimulated vs TransAct	.704	.957	<.001***	.000***	<.001***	.321	.589	.005**	1.000	.963
	Unstimulated vs Coated Well	.883	.549	<.001***	.000***	<.001***	.051	.047*	<.001***	.445	.401
	Dynabeads vs TransAct	.995	.421	.009**	.047*	.072	.835	.283	.001**	.657	.995
	Dynabeads vs Coated Well	.244	.034*	.007**	.480	.996	.956	.019*	<.001***	.095	.160
	TransAct vs Coated Well	.332	.312	<.001***	.361	.099	.564	.283	.001**	.445	.221

Significance was determined by a one-way ANOVA followed by a post hoc Tukey's Test.
* = p ≤ .050. ** = p ≤ .010. *** = p ≤ .001.

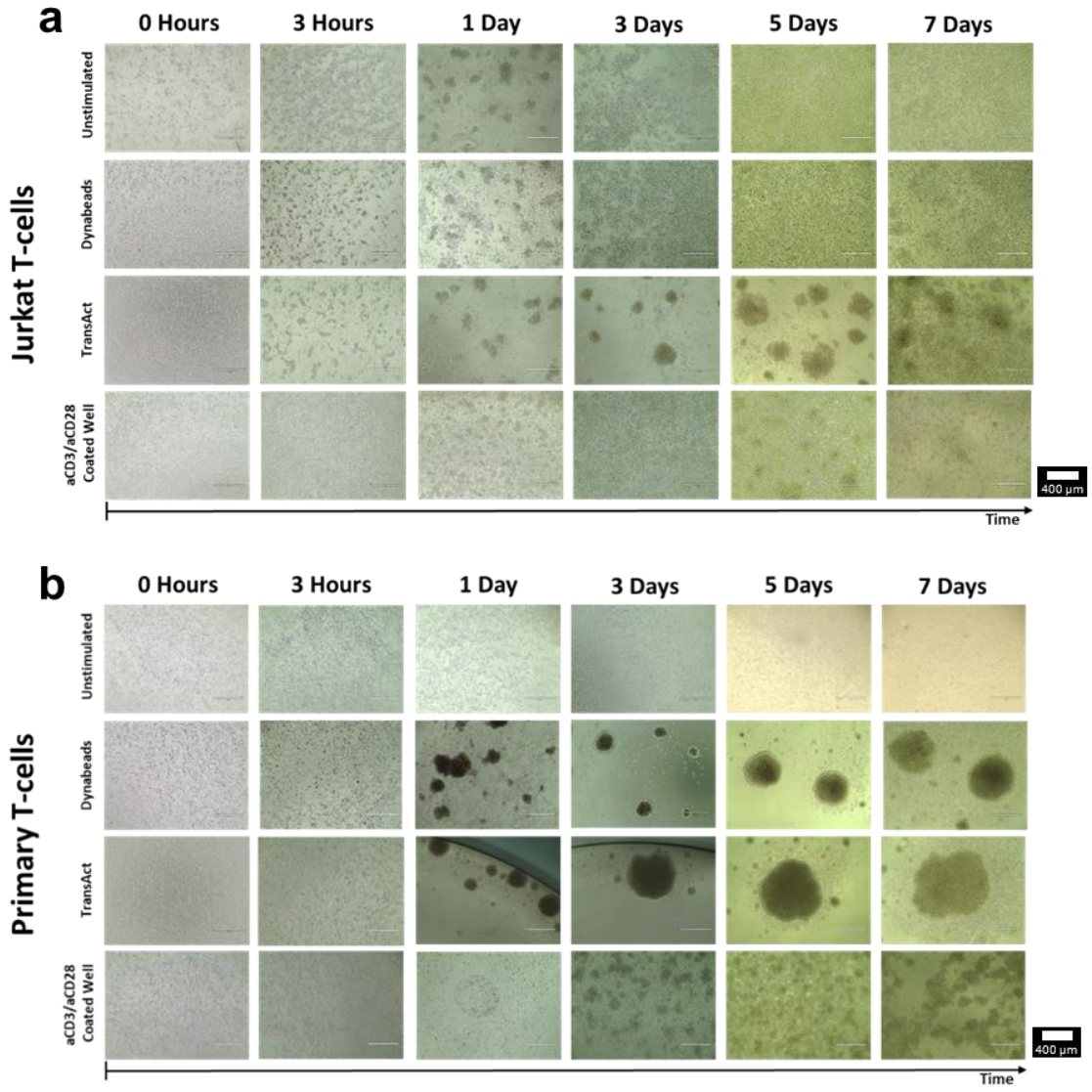

Figure 4.2. Confocal images showing culture morphology of Jurkat and primary human T-cells stimulated with Dynabeads, TransAct, or an aCD3/aCD28 coated well over 7 days. a. Jurkat T-cells. 1st row = unstimulated. 2nd row = Dynabeads. 3rd row = TransAct. 4th Row = aCD3/aCD28 coated well. Scale bar = 400 µm. **b.** Primary T-cells. 1st row = unstimulated. 2nd row = Dynabeads. 3rd row = TransAct. 4th Row = aCD3/aCD28 coated well. Scale bar = 400 µm. Images are representative of 3 technical repeats.

Figure 4.2a shows confocal images of Jurkat T-cells stimulated with different methods over 7 days. Up to day 1 all culture conditions display similar culture morphologies with the formation of defined T-cell clusters. With Dynabeads, these clusters are visibly formed of bead and T-cell aggregates. From day 3 to 7, unstimulated and Dynabead cultures became a mono-layer of T-cells with

clusters no longer defined. TransAct cultures still displayed visible clusters which have expanded in size. Jurkat clusters in coated well cultures were visible until day 5, though smaller than with transact. The clusters then become a monolayer by day 7.

Differences in the culture morphology observed with TransAct and coated well stimulated Jurkat cells may be explained by the lower cell count at day 5 and 7 highlighted previously (**Figure 4.1a**). As cell numbers increase, colonies merge and clusters lose their definition and become visible as monolayers. As there were less T-cells in TransAct and coated well cultures this process may have occurred more slowly.

With primary T-cells (**Figure 4.2b**) it was observed that unstimulated cultures remained largely as single cells over the 7 days. Dynabead and TransAct stimulated cultures displayed visible clusters by day 3, and coated well stimulated cultures by day 3. Dynabeads and T-cells are observed to be interacting by 3 hours, and clusters visibly consisted of cell and bead aggregates. Large clusters, were visible from day 1 to 7 with both Dynabeads and TransAct, with larger clusters in TransAct cultures. Clusters in coated well stimulated cultures remained visible and comparatively small from day 3 to 7.

The apparent reduction in size of primary T-cell clusters when stimulated with a coated well, in comparison to Dynabeads and TransAct, is likely due to the format of aCD3/aCD28 presentation. Both Dynabeads and TransAct represent bead based antibody presentation to T-cells, which are able to be transported by T-cells to form larger cell-bead aggregations. A coated well, on the other hand, presents aCD3 and aCD28 in a fixed 2D format, restricting the mobility of activated T-cell and resulting in the formation of smaller clusters.

The images discussed here suggest that analysing T-cell cluster formation would not infer T-cell activation when using Jurkat T-cells, as unstimulated T-cells also form clusters. However, this technique could prove useful with primary T-cells as a means of a quick evaluation of activation. To further improve the use of this suggested method, further quantitative analysis of clusters using images and an automated cluster counter may be recommended, though it is accepted that this may be challenging to automate due to irregular cluster sizes and ill-defined borders.

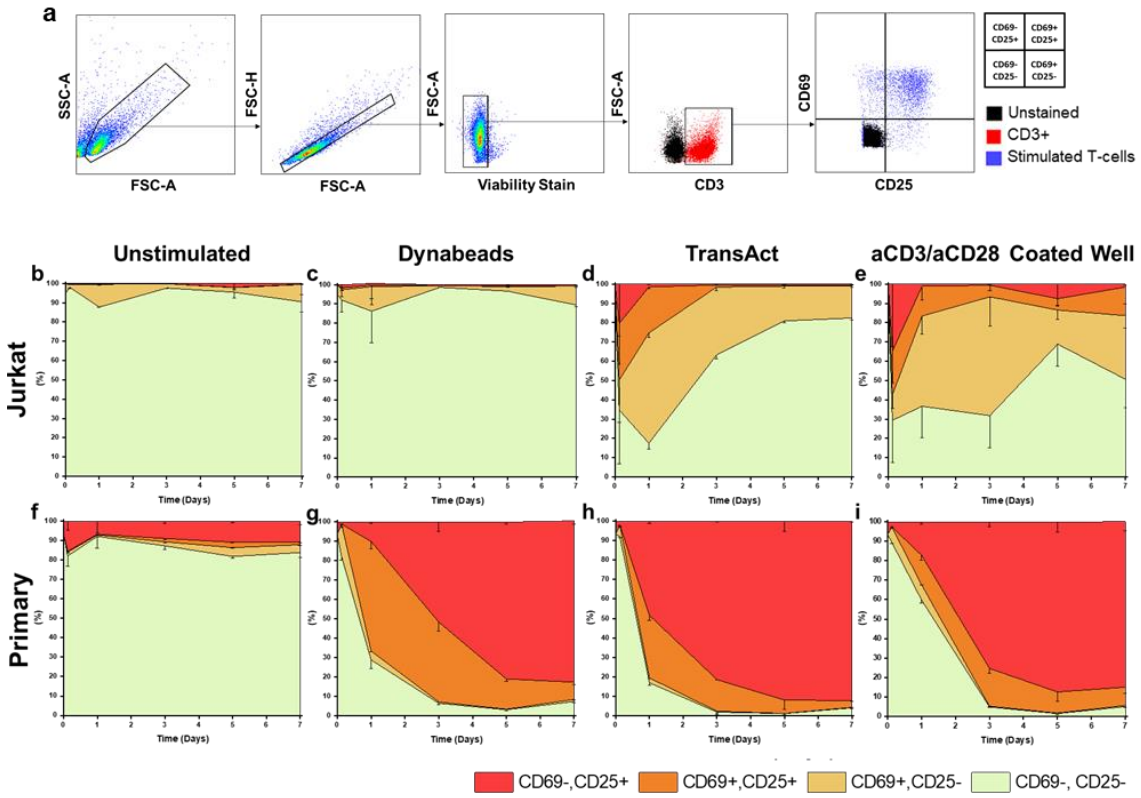

Figure 4.3. Combined expression of activation markers CD69 and CD25 by Jurkat and primary human T-cells stimulated with Dynabeads, TransAct, or an aCD3/aCD28 coated well over 7 days. a. Gating strategy used to identify CD69 and CD25 positive T-cells. **b** and **e.** CD69 and CD25 profile of unstimulated T-cells. **c** and **g.** CD69 and CD25 profile of T-cells stimulated with Dynabeads. **d** and **h.** CD69 and CD25 profile of T-cells stimulated with TransAct. **e** and **i.** CD69 and CD25 profile of T-cells stimulated with an aCD3/aCD28 coated well. **b - e.** = Jurkat T-cells. **f - i.** = Primary T-cells. n = 1 with triplicate technical replicates. n = 1 donor for primary T-cells. Mean values are plotted. Error bars = 1SD.

The expression of activation markers CD69 and CD25 over 7 days (**Figure 4.3**) revealed the dynamics of expression for each stimulation method for both Jurkat and primary T-cells. Representative scatter graphs, and unstained and isotype controls are shown in **Appendices F.1, F.2** and **E.1**.

Within Jurkat T-cell cultures, unstimulated and Dynabeads stimulated cultures (**Figures 4.3b** and **c**) displayed similar profiles, with low (~6 %) to no expression of CD69 or CD25 over the 7 days. With TransAct stimulated cultures (**Figure 4.3d**), the largest peak of all populations, $CD69^{+}CD25^{-}$ T-cells (57.2 %) was observed at day 1. Smaller maximums of $CD69^{+}CD25^{+}$ T-cells (29.4 %) and $CD69^{-}CD25^{+}$ T-cells (20.4 %) occurred earlier at 3 hours, before reducing by day 3 to 1.1 and 0.4 %, respectively. A percentage of $CD69^{+}CD25^{-}$ T-cells persisted throughout the experiment, with 16.6 % remaining at day 7. Coated well simulated Jurkat cultures (**Figure 4.3e**) displayed a more erratic expression over the 7 days. As with TransAct stimulation, $CD69^{-}CD25^{+}$ expression peaked at 34.7 % at 3 hours before it declined again to 1.1 % at day 1. A relatively small percentage of T-cells remained $CD69^{+}CD25^{+}$ throughout ranging from 0.1 % to 22.6 %. The largest percentage of $CD69^{+}CD25^{-}$ (61.6 %) occurred at day 3, which reduced to 17.7 % at day 5, and increased again to 33 % at day 7.

The most abundant phenotype in unstimulated primary T-cell cultures (**Figure 4.3f**) was found to be $CD69^{-}CD25^{-}$, ranging from 81.8 % to 92.1 %. However, a low percentage of $CD69^{-}CD25^{+}$ expressing T-cells were also highlighted throughout, ranging from 6.7 % to 15.6 %. Dynabead stimulated primary cultures (**Figure 4.3g**) displayed an initial increase in $CD69^{+}CD25^{-}$ of 16.4 % from 0 to 3 hours. On day 1, $CD69^{+}CD25^{+}$ became the most dominant expression profile of T-cells at 56.5 %, which then was surpassed by $CD69^{-}CD25^{+}$ T-cells at day 3. $CD69^{-}CD25^{+}$ T-cells then remained the most dominant expression type for the

remainder of the experiment, ranging from 51.6 % to 83.2 %, from day 3 to day 7. TransAct stimulated primary T-cells (**Figure 4.3h**) displayed a very similar expression profile for CD69 and CD25 to Dynabeads, with the key difference being a lower percentage of $CD69^{+}CD25^{+}$ T-cells. By day 1, $CD69^{-}CD25^{+}$ T-cells (48.2%) were the most dominant expression profile, closely seconded by $CD69^{+}CD25^{+}$ T-cells (32.2 %). From day 3 to day 7, $CD69^{-}CD25^{+}$ T-cells remained the dominant profile, as it increased substantially to 92.3 %. Primary T-cell cultures stimulated with a coated well (**Figure 4.3i**) appeared to take longer to express activation markers. A small increase from day 0 in $CD69^{+}CD25^{-}$ T-cells (7.6 %) at 3 hours, and in $CD69^{+}CD25^{+}$ T-cells (15.1 %) and $CD69^{-}CD25^{+}$ T-cells (10.8 %) at day 1 was observed, however $CD69^{-}CD25^{-}$ remained the prevailing profile. From day 3, the expression profile resembled that of the other stimulated cultures, with $CD69^{-}CD25^{+}$ T-cells becoming and persisting as the most dominant for the remainder of the experiment, ranging from 75.4 - 87.4 % from day 3 to 7.

Separate plotting of the expression of CD69 and CD25 (**Figure 4.4**) allowed further comparisions between the expression of individual markers and the differences in expression profiles between Jurkat and primary T-cells.

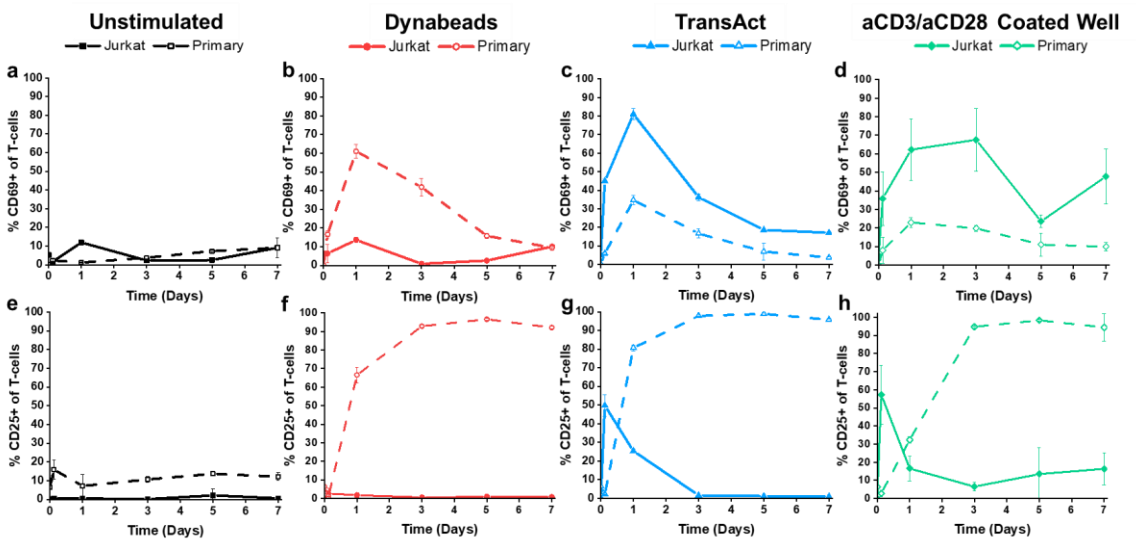

Figure 4.4. Separated expression of activation markers CD69 and CD25 on Jurkat and primary human T-cells stimulated with Dynabeads, TransAct, or an aCD3/aCD28 coated well over 7 days. a and **e.** Unstimulated T-cells. **b** and **f.** T-cells stimulated with Dynabeads. **c** and **g.** T-cells stimulated with TransAct. **d** and **h.** T-cells stimulated with an aCD3/aCD28 coated well. Top row (**a - d**) = CD69 expression. Bottom Row (**e - h**) = CD25 expression. Solid lines = Jurkat T-cells. Dashed lines = Primary human T-cells. n = 1 with triplicate technical replicates. n = 1 donor for primary T-cells. Mean values are plotted. Error bars = ± 1SD.

Both unstimulated Jurkat and primary T-cell cultures (**Figure 4.4a**) contained a low percentage of $CD69^+$ T-cells over 7 days, with primary ranging from 0.1 to 9.1 %, and Jurkat ranging from 1.63 to 11.9 %. All stimulated Jurkat cultures (**Figures 4.4b**, **c**, and **d**) increased in $CD69^+$ T-cells from 3 hours, with Dynabeads peaking at 13.6 % on day 1, TransAct at 81.1 % on day 1, and coated well at 67.6 % on day 3. An increase in the percentange of CD69 expressing primary T-cells with stimulated cultures (**Figures 4.4b**, **c**, and **d**) was detected from 3 hours, peaking at 1 day. Peak percentage expression varied according to stimulation method, Dynabeads 61.1 %, TransAct 34.7 %, and coated well 23.0 %. From day 1 to day 7 the percentage of $CD69^+$ primary T-cells then continually decreased.

In regards to CD25 expression, unstimulated primary T-cell cultures presented a mean increased expression of 10.3 % over Jurkat cultures (**Figure 4.4e**). However, both displayed similar patterns in expression as $CD25^+$ percantages largely remained constant over the 7 days. Jurkat T-cell cultures behaved similarly when stimulated with Dynabeads (**Figure 4.4f**), expressing a consistantly negligible percentage of $CD25^+$ T-cells throughout. When stimulated with TransAct or a coated well (**Figures 4.4g** and **h**), $CD25^+$ Jurkat T-cells increased to the highest levels at 3 hours, 49.7 and 57.3 %, respectively. Both cultures then displayed a decline by day 1, TransAct cultures then returned to the baseline expression of ~1 % at day 3, and coated well cultures remained between 6.5 and 16.3 % $CD25^+$ from day 3 to day 7. It was observed that all stimulated primary T-cell cultures (**Figures 4.4f**, **g**, and **h**) contunially increased in $CD25^+$ T-cells from 3 hours before peaking at day 5. Primary Dynabead cultures presented a maximum of 96.6 % $CD25^+$ T-cells, TransAct 98.9 %, and coated well 98.2 %. A small decline was then observed from day 5 to day 7.

The increases in $CD69^+$ and $CD25^+$ T-cells in TransAct and coated well stimulated Jurkat cultures suggests that there is potential for the upregulation of these markers to be used to indicate T-cell activation in Jurkats, as has been done in previous studies (Fernández-Riejos *et al*., 2008; Kamiya *et al.,*2018) However, the results here also demonstrate that the expression of CD69 and CD25 is also dependant on the stimulation method. Jurkats stimulated with Dynabeads displayed a very low expression of both markers, with the expression profile being almost identicle to unstimlated Jurkats. Therefore, using CD69 and CD25 expression as an indicator of activation when stimulating Jurkat T-cells with Dynabeads will be problematic. Particularly as Dynabeads are the current gold

standard in GMP T-cell activation, it it is expected they will comprise a key control in future experiments.

Concurrent with the results reported here Reddy *et al*., 2004 demonstrated that a culture of unstimulated human PBMCs expressed low to no CD69 and a moderate baseline expression of CD25. Additionally, they stimulated cultures with various stimulating additives, including a low and high concentration of soluble and plate bound aCD3 and aCD28. As indicated in this present study, it was also determined that the peak and persistence of CD69 and CD25 in primary T-cells was largely dependent on the stimulation method.

Table 4.2 shows that when comparing the expression of CD69 between Jurkat and primary T-cell cultures, significant differences were found at almost every time point for each experimental condition. Similar was observed with the expression of CD25. This strongly indicates that the level of CD69 and CD25 expression in both unstimulated and all stimulated cultures was highly dissimilar between Jurkat and primary T-cell cultures.

Table 4.2. *p*-values for the Comparison of Primary Human, and Jurkat T-cells in Regards to % CD69$^+$ and % CD25$^+$ for Different Stimulation Methods.

		Primary vs Jurkat (*p-value, 3 d.p)*				
		Day				
Dependant Variable	**Group**	**0.125**	**1**	**3**	**5**	**7**
% CD69+	Unstimulated	.183	<.001***	.029*	<.001***	.337
	Dynabeads	.026*	<.001***	.004**	<.001***	.478
	TransAct	<.001***	<.001***	<.001***	.045*	<.001***
	Coated Well	.039**	.051	.008**	.037**	.044*
% CD25+	Unstimulated	.006**	.204	<.001***	.005**	.001**
	Dynabeads	.418	.001**	<.001***	<.001***	<.001***
	TransAct	.005**	<.001***	<.001***	<.001***	<.001***
	Coated Well	.027**	.050*	<.001***	.010**	<.001***

Significance was determined by a one-way ANOVA followed by a post hoc Tukey's Test.
* = $p \leq .050$. ** = $p \leq .010$. *** = $p \leq .001$.

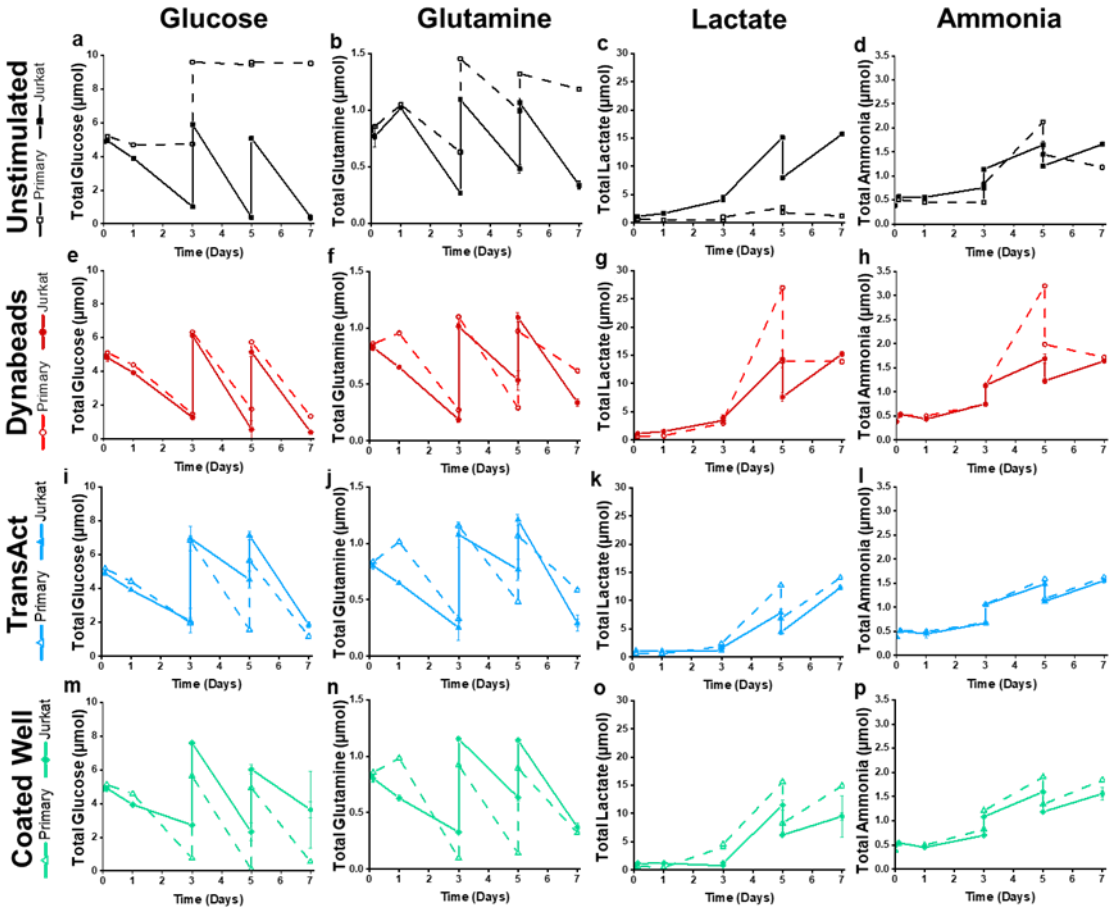

Figure 4.5. Metabolite profiles of cultures of Jurkat and primary human T-cells stimulated with Dynabeads, TransAct, or an aCD3/aCD28 coated well over 7 days. 1st row (**a - d**) = Unstimulated T-cells. 2nd row (**e - h**) = T-cells stimulated with Dynabeads. 3rd row (**i - l**) = T-cells stimulated with TransAct. 4th row (**m - p**) = T-cells stimulated with an aCD3/aCD28 coated well. 1st column (**a, e, I** and **m**) = Glucose profiles. 2nd column (**b, f, j** and **n.**) = Glutamine profiles. 3rd column (**c, g, k** and **o**) = Lactate profiles. 4th column (**d, h. l** and **p**) = Ammonia profiles. For all conditions media volume was doubled at day 3, then on day 5 half the media volume was removed and replaced with fresh. Solid lines = Jurkat T-cells. Dashed lines = Primary T-cells. n = 1 with triplicate technical replicates. n = 1 donor for primary T-cells. Mean values are plotted. Error bars = ± 1SD.

The metabolic profiles of glucose, glutamine, lactate, and ammonia concentrations in Jurkat and primary T-cell cultures are shown in **Figure 4.5**. From these it was observed that when stimulated with TransAct or a coated well, Jurkat and primary cultures displayed similar profile patterns for all metabolites analysed. When stimulated with Dynabeads, Jurkat and primary T-cells cultures produced similar patterns of all metabolites, with key differences of increased

concentrations of lactate (6.3 µmol) and ammonia (1.5 µmol) in primary T-cell cultures at day 5. The highest discrepancies between primary and Jurkat T-cell cultures were seen with unstimulated cell cultures, particularly with glucose and lactate concentrations where unstimulated primary T-cell cultures only fluctuated at points of external supplementation and removal.

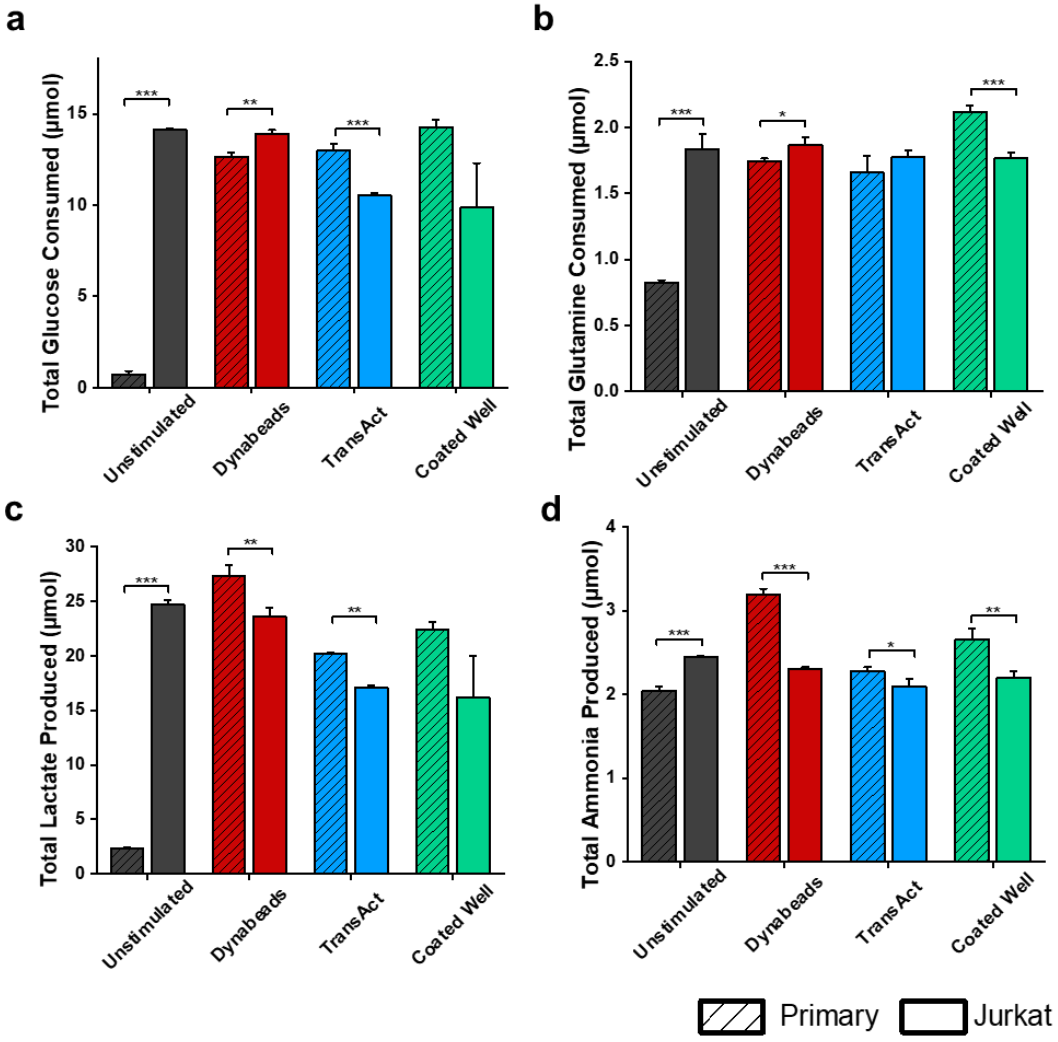

Figure 4.6. Total metabolite consumption and production for Jurkat and primary human T-cells stimulated with Dynabeads, TransAct, or an aCD3/aCD28 coated well. a. Total glucose consumed. **b.** Total glutamine consumed. **c.** Total lactate produced. **d.** Total ammonia produced. All totals are from a culture of 7 days. Solid fill = Jurkat T-cells. Striped lines = Primary T-cells. n = 1 with triplicate technical replicates. n = 1 donor for primary T-cells. Mean values are plotted. Error bars = 1SD.

Differences in metabolite profiles over the 7 day culture are summarised in **Figure 4.6**, showing the total amount of glucose and glutamine consumption, and lactate and ammonia production. In regards to total glucose consumption (**Figure 4.6a**) significant differences were found between Jurkat and primary T-cell cultures with unstimulated, Dynabead, and TransAct cultures. Jurkat cultures consumed a total increase of 13.4 µmol glucose compared to primary cultures when unstimulated, an increase of 1.3 µmol with Dynabead stimulation, and a decrease of 2.4 µmol with TransAct stimulation. In regards to total glutamine consumption (**Figure 4.6b**), Jukat cultures displayed a significant increase of 1 µmol when unstimulated, 0.1 µmol with Dynabead stimulation, and a significant decrease of 0.4 µmol with coated well stimulation.

Lactate production (**Figure 4.6c**) in both Dynabead and TransAct stimulated cultures was found to be significantly higher in primary T-cell cultures compared to Jurkat cultures, with an increase of 3.7 and 3.1 µmol, respectively. With unstimulated T-cells the opposite was found, Jurkat T-cell cultures produced a much larger and significant increase of 13.8 µmol, compared to primary T-cell cultures. In regards to ammonia production (**Figure 4.6d**) a similar pattern of results was observed, with primary cultures showing a significant increase compared to Jurkat in all stimulated cultures. Furthermore, this observation was again reversed for unstimulated cultures where it was displayed that Jurkat cultures produced a significant increase of 0.3 µmol ammonia when compared to primary cultures.

As the metabolic pathway in activated T-cells shifts to an increased rate of glycolysis, a large increase in the consumption of glucose in stimulated T-cells was expected. Additionally a smaller increase in glutamine consumption was expected as the rate of glutaminolysis increases to a lesser extent. Increased

consumption of both glucose and glutamine in stimulated primary T-cells compared to unstimulated was observed accordingly.

A consequent increase in glycolysis waste product lactate, and glutaminolysis waste product ammonia, was also anticipated. This increase in lactate and ammonia was detected in stimulated primary T-cells, however it was surprising that the stimulation methods that resulted in the greatest consumption of glucose did not correspond to the greatest production of lactate. Dynabead stimulated primary T-cells were observed to consume the least glucose yet produced the most lactate. This suggests that T-cells stimulated with Dynabeads have shifted more towards glycolysis, therefore producing more lactate, compared to TransAct or a coated well. Ammonia production remained low in all stimulated T-cells, thus indicating favourable growth conditions.

The consumption of glucose and glutamine, and production of lactate and ammonia in unstimulated Jurkat T-cells was significantly increased compared to unstimulated primary T-cells. This was anticipated as Jurkat T-cells are a cancerous cell line and as such constantly proliferate, requiring an increased metabolic activity. Consequently, change in metabolic activity of these metabolites cannot confidently be used to infer activation in Jurkat T-cells. However, unstimulated Jurkat T-cells may be considered in place of an activated primary T-cell to model metabolite usage.

4.3.1.2. Activation with Polymer A

To initially assess the capability of polymer A to activate T-cells, primary sourced human T-cells were cultured with polymer A with aCD3/aCD28 attached, henceforth referred to as aCD3/aCD28 polymer A. T-cells were exposed to aCD3/aCD28 polymer A discs for 24 hours before being evaluated for the expression of activation markers, CD69 and CD25. T-cell cultures were also

exposed to polymer A without antibody attached, Dynabeads at a 1:1 ratio, and an aCD3/aCD28 coated well. Unstimulated T-cells were analysed as a negative control. T-cells stimulated with Dynabeads and a coated well were treated both comparatively and as positive controls. Representative histograms, and unstained and isotype controls are shown in **Appendices F.3** and **E.2**.

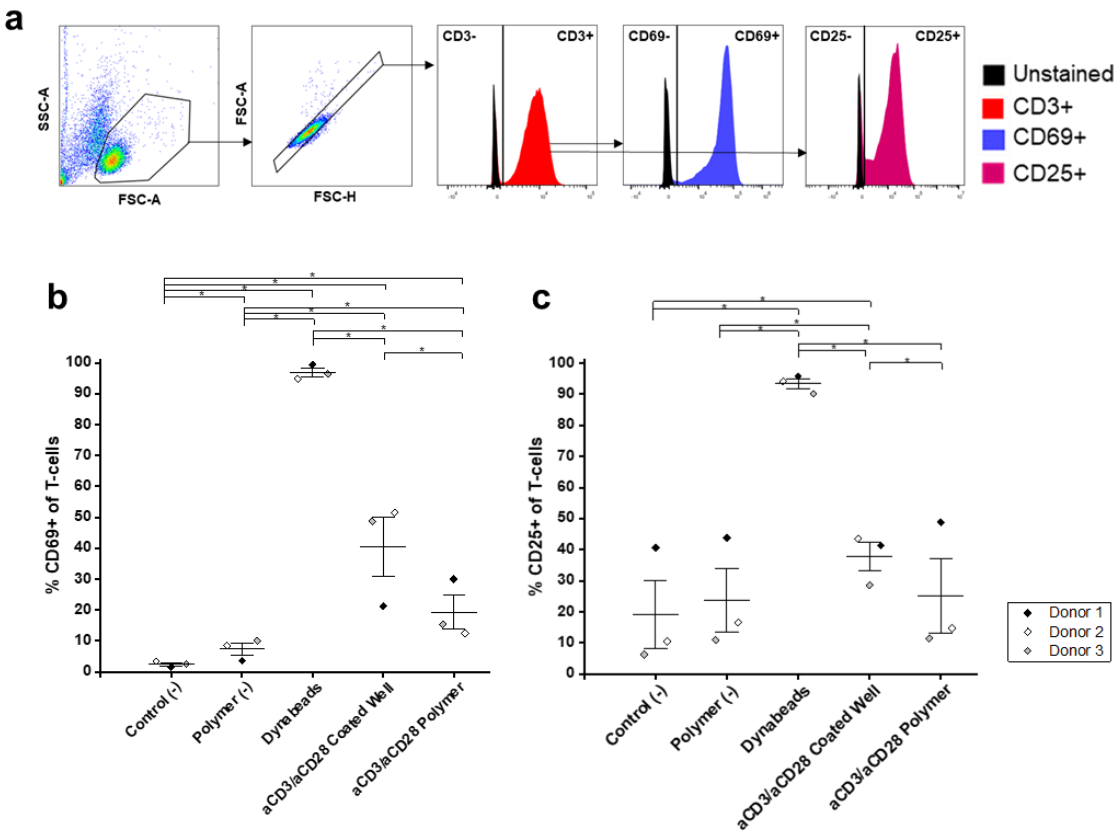

Figure 4.7. Expression of activation markers CD69 and CD25 by primary human T-cells cultured with aCD3/aCD28 polymer A for 1 day. a. Gating strategy used to identify CD69 and CD25 positive T-cells. **b.** CD69 expression. **c.** CD25 expression. Unstimulated samples= Control (-), no addition to well; polymer (-), polymer A without antibody attached. Stimulated samples = Dynabeads; aCD3/aCD28 coated well. n = 3 biological repeats with 3 donors with 3 technical replicates each. Individual markers = mean of 3 technical repeats for each donor. Centre bar = mean of 3 donors. Error bars = ± 1SD. *p*-values were determined by a one-way ANOVA with a post hoc Tukey's test. * = $p \leq .050$.

It was observed that T-cells cultures stimulated with aCD3/aCD28 polymer displayed a mean of 19.2 % $CD69^+$ T-cells (**Figure 4.7b**). This is an increase of

16.8 % when compared to control (-), and 11.9 % when compared to polymer (-). Both increases were found to be statistically significant ($p \leq .050$). aCD3/aCD28 polymer stimulation resulted in a significantly lower expression of CD69 than both Dynabeads (94.9 %) and aCD3/aCD28 coated well (40.5 %). Additionally, T-cells exposed to polymer (-) displayed a $CD69^+$ T-cell population of 7.3 %, representing a small statistically significant increase of 4.8 % compared to control (-).

Figure 4.7c shows that exposure to a CD3/aCD28 polymer resulted in a CD25 expression in 25.0 % of T-cells. This was found to be a minor increase from control (-) (19.1 %), and polymer (-) (23.8%). The differences between these three conditions, however, were not found to be statistically significant. Moreover, the standard deviation for these conditions was found to be relatively large compared to Dynabeads and aCD3/aCD28 coated well. As with CD69, T-cells stimulated with Dynabeads displayed the highest percentage of CD25 expressing cells (93.3 %), seconded by aCD3/aCD28 coated well (37.8 %), with both being a significant increase over aCD3/aCD28 polymer.

It was predicted that exposure to aCD3/aCD28 polymer A would result in the activation of primary T-cells. The results here show that exposure to aCD3/aCD28 polymer A for 1 day resulted in an increase in CD69 expressing T-cells but not CD25. As CD69 is an early activation marker and CD25 a late one, this suggests that T-cells have in fact been activated, however, the activation is still in the early stages at 24 hours post exposure. The effect of aCD3/aCD28 polymer stimulation appeared to be weaker than both Dynabeads and aCD3/aCD28 coated well, as stimulation resulted in a lower expression of both markers.

It was not anticipated that polymer without antibody (polymer (-)) would also result in an increase in activation marker CD69 when compared to control (-). Presently,

it is known that CD69 is expressed either in activated T-cells or in tissue-resident memory T-cells (T_{RM}) (Cibrián and Sánchez-Madrid, 2017). As no known activating agents were present in the culture, it was considered whether the CD69 increase could be due to T_{RM} cells. T_{RM} cells differentiate from circulating effector T-cells (T_{EFF}) that have migrated into a tissue and are exposed to the appropriate stimuli (Yang and Kallies, 2021). Type 1 T_{regs} are able to generate one such stimuli, TGF-β, and as such promote the generation of T_{RM} cells (Ferreira *et al.,* 2020). Therefore, it may be plausible that if samples contained both populations of T_{eff} cells and type 1 T_{reg} cells, that when introduced into the tissue-like environment of polymer A, that the effector cells could differentiate into CD69 expressing T_{RM} cells. To further explore this possibility, $CD69^+$ T-cells should be confirmed as T_{RM} cells; this could be done by additional staining for T_{RM} cell markers such as CD103 (Zheng and Wakim, 2021).

Also worth briefly discussing is the variability displayed in **Figure 4.7c**, with control (-), polymer (-), and aCD3/aCD28 polymer. The variability arises from the data point of donor 1, which appears to display a greater baseline level of $CD25^+$ T-cells. This could possibly be due to recent infection in the donor, or may represent the actual baseline level present in donor 1 highlighting the potential impact of donor variability in samples.

4.3.2. Assessment of Column Format

4.3.2.1. Flow Through of T-cells

For the initial assessment of the ability to seed and remove cells into polymer A, a column format was tested. Polymer A was cast into syringes with the plunger removed. Syringes were suspended vertically and T-cell suspensions were drawn through the polymer using a syringe pump connected to the hub of the syringe, as described in **Method 2.2.2.5.1**. Flow rates were controlled using the

syringe pump and flow rates of 6; 12; 24; 36; and 48 mL/min were investigated for their effect of cell recovery and viability of T-cells passed through. These flow rates were chosen as they represented the range of the syringe pump.

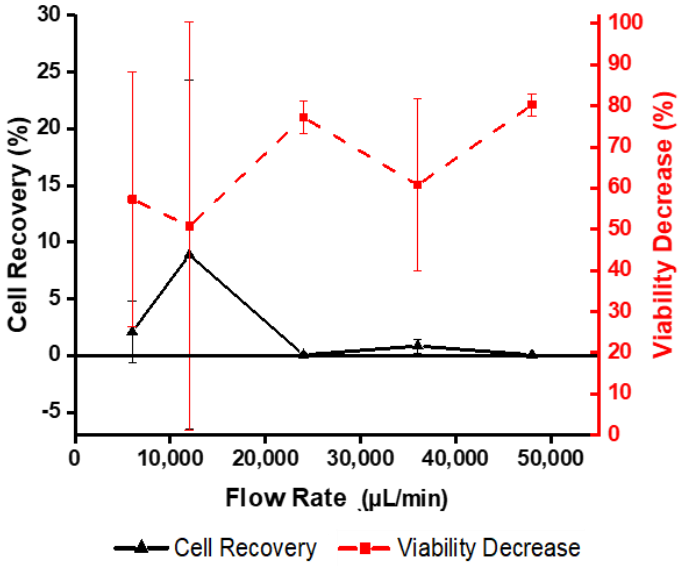

Figure 4.8. Percentage recovery and viability decrease of Jurkat T-cells passed through polymer A set within a syringe, at various flow rates. n = 3 independent experiments. Mean values are plotted. Error bars = ± 1SD. Significance was determined by a one-way ANOVA. No significant differences were found.

It was observed that the greatest cell recovery (8.9 %) and lowest decrease in viability (50.8 %) was at a flow rate of 12 mL/min (**Figure 4.8**). However, no statistically significant differences were found between results for cell recovery and viability decrease at all flow rates tested. This highlighted low confidence in the observed differences and therefore limited the conclusions which could be drawn from this study in regards to an optimal flow rate. For all flow rates, cell recovery was low, ranging from 0 – 8.8 %, and viability decrease was high, ranging from 50.8 – 80.3 %. There was no overall correlation found between the flow rates tested and cell recovery or viability of recovered T-cells.

It was anticipated that as flow rate increased, cell recovery would increase. It was also anticipated that as the flow rate increased, there would be a greater

decrease in viability due to an increase in shear forces. In this study, however, no correlation was found between either cell recovery or viability and flow rate. A possible reason for this is that as flow rate was increased, the polymer began to compress and was increasingly pulled into the hub of the syringe. This will have resulted in smaller or closed pores throughout the polymer, and consequently resulted in cells becoming trapped. Compressed pores may also have reduced the rate of flow through the polymer, and therefore the flow rate applied by the pump may not have been the true flow rate through the column. Additionally, factors such as non-specific binding of T-cells to the polymer may have reduced the amount of cells that were recovered.

The large decrease in the viability of T-cells that were recovered may also suggest that all flow rates investigated were too high and caused damage to the cells. Kumar and Srivastava (2010) describe a method in which lymphocytes were passed through a cryogel set in a 5 mL syringe, alike the set-up used here. In this method, the flow rate used was 2 mL/min. Therefore, it is suggested that for future experiments flow rates a magnitude lower should be investigated.

4.3.2.2. Non-Specific Binding – Supernatant Derived Count

Coatings of isotypes of poly-lysine, poly-L-lysine and poly-D-lysine, are commonly used to facilitate cell attachment to surfaces (Mazia *et al*., 1975; Harnett *et al*., 2007). Thus, it was conceivable that polymer A consisting of ε-PL may also promote non-specific binding. As this may be a factor contributing to the low recovery of cells from the polymer previously found, non-specific binding was investigated as per **Method 2.2.2.3**.

Jurkat T-cells were incubated with discs of polymer A for 30 minutes before supernatant removal and washing. The number of bound cells were calculated though the deduction of cells removed, from the initial pre-incubation cell count.

To account for the cells lost through sample handling, the experiment was ran without polymer present and the average cell loss was deducted from the calculated total of bound cells.

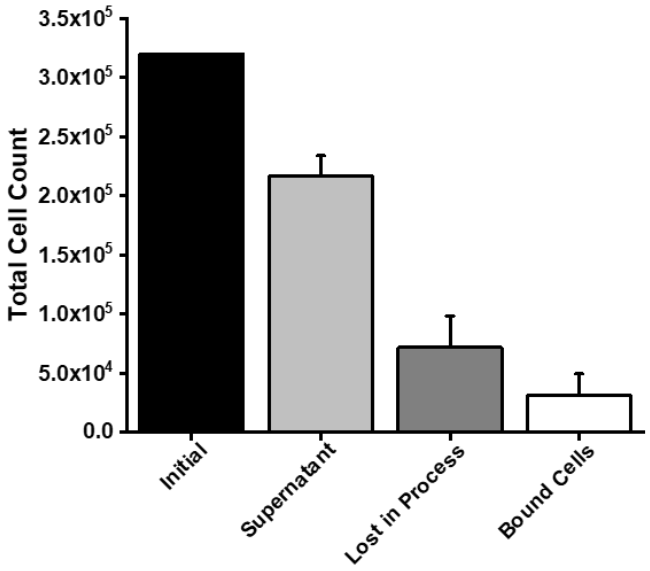

Figure 4.9. Supernatant-derived bound cell counts for Jurkat T-cells incubated with discs of polymer A. Bar chart shows initial count of cells incubated with polymer discs, the supernatant cell count from initial media removal and wash step, cells lost through processing with no polymer, and the calculated bound cells per disc. Bound cells = initial – (supernatant + lost in process). n = 1 with 5 technical repeats. Mean values are plotted. Error bars = 1SD.

The mean number of bound T-cells per disc was derived to be 3.18 x 10^4 (**Figure 4.9**). This suggests that a degree of non-specific binding between Jurkat T-cells and polymer A does occur. Furthermore, a mean value of 7.18 x 10^4 cells with standard deviation of 2.65 x 10^4 was observed to be lost through the processing of the samples. This was thought to be significant amount with a relatively high variation and therefore has implications on the reliability of the calculated value for bound cells. To mitigate the impact of this, a second method based on confocal imaging rather than supernatant cell counts was developed.

4.3.2.3. Non-Specific Binding – Confocal Imaging Derived Count

In addition to mitigating the impact of cells lost through sample handling, this second method was used to investigate the reduction of non-specific binding through suspending cells in, and washing with PBS, 1 % BSA (w/v), 0.5 M EDTA, rather than media and PBS. BSA is blocking agent commonly used to prevent electrostatic interactions, such as that between a positively charged polymer and a negatively charged cell (Buchwalow *et al*., 2011). EDTA is a chelating agent commonly used to reduce cell-cell attachment and promote a single cell suspension (Reichard and Asosingh, 2018).

Jurkat T-cells were stained with a far-red nuclear dye, before being incubated with discs of polymer A. Cell suspension was removed and polymer was washed before polymer discs were removed and fixed, as described in **Method 2.2.2.4**. 5 images per side of each disc were taken using a fluorescent confocal microscope. Images were processed to give a total T-cell count per image, program shown in **Appendix B.2.**

The experimental condition of PBS refers to cells that were originally suspended in complete RPMI media and washed with PBS, the condition “buffer” refers to cells suspended in and washed with PBS, 1 % BSA (w/v), 0.5 M EDTA. **Figure 4.10a**, highlights the large range of cells remaining bound per image for both experimental conditions. These differences in cells bound occurred not only between individual discs, but also at different positions on the same disc. A most probable explanation for this is that the surface of the polymer was not even and so cells may have become stuck in crevices across the surface. A suggested method to investigate this would be to use z-stack fluorescent imaging produce a 3D view of cells on the polymer, and observe if the majority of cells are trapped within pores.

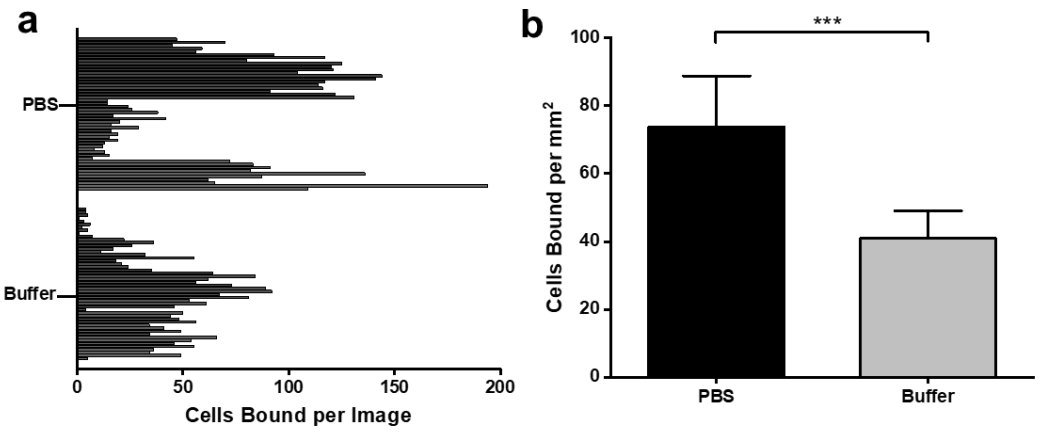

Figure 4.10. Fluorescent confocal imaging-derived bound cell counts for Jurkat T-cells incubated with discs of polymer A. Cells were pre-stained with CellTracker™ Red CMTPX Dye. PBS = cells suspended in media and washed with PBS. Buffer = cells suspended in and washed with PBS, 1 % BSA (w/v), 0.5 M EDTA. **a.** Individual values plotted per image analysed. Image dimensions = 1.1 mm x 0.8 mm. n = 5 discs per condition with 10 images analysed per disc. Error bars = 95 % confidence interval. **b.** Mean values plotted per mm^2. n = 5 discs per condition with 10 images analysed per disc. Error bars = 1SD. *p*-values were determined by a two-tailed T-test. *** = $p \leq .001$.

The mean number of cells bound was found to be 74 and 41 cell per mm^2 for PBS and buffer, respectively (**Figure 4.10b**). This difference was found to be statistically significant to with a $p \leq .001$ and therefore strongly suggests that by changing the incubation and wash media to PBS, 1 % BSA (w/v), 0.5 M EDTA, non-specific binding of T-cells to polymer A was reduced.

The calculation of cells per mm^2 was based on the assumption of a 2D surface, however as discussed above, this is not true for polymer A. The values calculated therefore are likely an overestimate. For this study an estimate was enough to provide an initial assessment of non-specific binding and compare two conditions. However, future studies may consider developing a technique to produce a flat coating of polymer A, or using polymer A beads with a smooth surface to more accurately calculate cells bound per mm^2. Additionally it may be useful to

investigate other additives, such as trypsin, to further reducing non-specific binding.

4.3.2.4. Improved Set-Up

The initial testing of flowing cells into and removing them from polymer A was performed using the set-up shown in **Figure 4.11**. 2 mL of polymer A at 0.040 g/cm^3 was set into a 5 mL syringe. Polymer A was suspended and washed through with PBS. 7.5 x 10^6 T-cells suspended in complete RPMI media were passed through and followed by a 5 mL wash of PBS. This set-up was used to investigate flow rates of between 6 – 48 mL/min (**Section 4.3.2.1**).

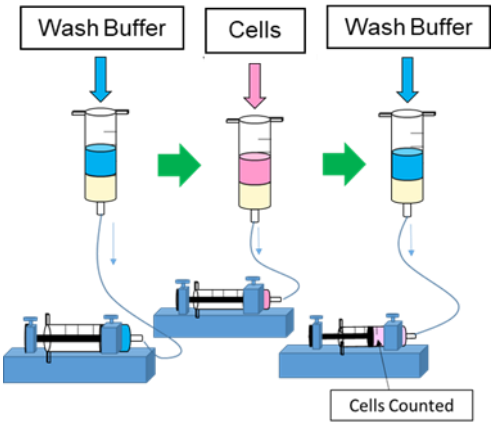

Figure 4.11. General experimental procedure for the initial and improved set-up to investigate the recovery of Jurkat T-cells passed through polymer A. Polymer A was cast into a syringe and suspended vertically. Flow rate was controlled by a syringe pump which was attached to the hub of the syringe. Polymer was initially washed with a buffer which was discarded. Cells in suspension were drawn through the polymer, followed by wash buffer. Supernatant was collected and cells were counted.

Following various observations throughout and through experimentation, numerous changes were made to improve the initial set-up:

1. The density of polymer A was decreased from 0.040 g/cm^3 to 0.033 g/cm^3 to increase porosity and reduce tortuosity.

2. The size of the syringe in which the polymer was cast was increased to 10 mL to increase the width of the polymer, thus reducing the final height and reducing the total length of which the cells have to travel.
3. PBS, 1 % BSA (w/v), 0.5 M EDTA was used to suspend T-cells in and as the wash buffer to reduce non-specific binding.
4. The volume of wash buffer was increased to 10 mL to improve the elution of cells from the polymer.
5. A support frit cut from nylon mesh was added to the base of the syringe to prevent the polymer being pulled into the hub.
6. The flow rates investigated were reduced by a magnitude to reflect the flow rate used to flow T-cells through a column by Kumar and Srivastava (2010).

These changes are summarised in **Table 4.3**. The updated set-up was used to further investigate cell recovery from polymer A.

Table 4.3. Summary of Adjustments Made to the Initial Set-up of Polymer A to Investigate the Recovery of T-cells Passed Through.

	Initial Set-Up	Improved Set-Up
Polymer	2 mL of 0.040 g/cm^3	2 mL of 0.033 g/cm^3
Syringe Size	5 mL	10 mL
Cell Buffer	Media	PBS, 1 % BSA, 0.5 M EDTA
Wash Buffer	PBS	PBS, 1 % BSA, 0.5 M EDTA
Wash Buffer Volume	5 mL	10 mL
Support Frit	None	Nylon mesh, 100 uM pores
Flow Rate Range	6,000 - 48,000 µL/min	500 - 3,000 µl/min

4.3.2.5 Flow Through of T-cells with Improved Set-Up

The improved set-up described above was used to evaluate the impact of flow rate and cell density, and the interaction between the two variables on cell

recovery and viability. Design of experiment (DoE) concepts were used to design an experiment with two factors at three levels. Flow rates of 0.5; 1.5; and 3 µL/min, and cell densities of 1, 5, and 10, x 10^6 cells/mL were investigated, as described in **Method 2.2.2.5.2**.

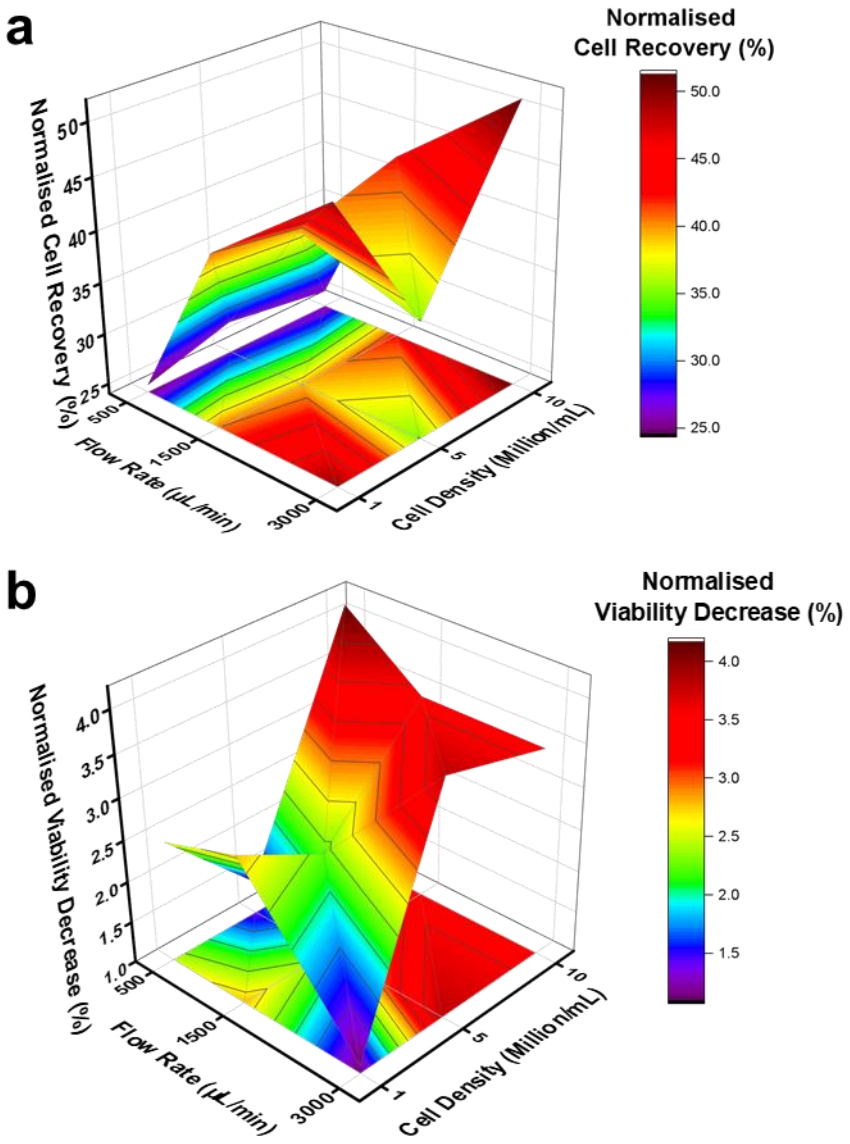

Figure 4.12. Response surface graphs showing the effect of flow rate and cell density on the recovery and viability of Jurkat T-cells passed through polymer A set in a syringe. a. The recovery of cells from the system. **b.** The decrease in viability of recovered cells from the initial viability. All values were normalised to a control of passing cells through an empty syringe. Polymer A set in a syringe was replaced for each run. n = 3 independent runs for each flow rate and cell density combination. Mean values are plotted.

Figure 4.12a shows that the highest values for cell recovery were observed when the set-up was ran at 3 mL/min with 10 x 10^6 cells/mL (51 %), and 3 mL/min with 1 x 10^6 cells/mL (49 %). **Figure 4.12b** shows that the lowest decreases in viability were found at 3 mL/min with 1 x 10^6 cells/mL (1.1 %), and 0.5 mL/min with 5 x 10^6 cells/mL. Taken together these reslults suggest that the optimal set-up in regards to maximising flow rate and minimising viability decrease was with a flow rate of 3 mL/min with a cell suspension density of 1 x 10^6 cells/mL. A two-way ANOVA was performed to further analyse the effect of each factor and the interplay between them, results are shown in **Table 4.4**.

Table 4.4. *p*-values for Between-Subject Comparisons of Flow Rate and Cell Density on Cell Recovery and Viability Decrease, and for the Comparison of Flow Rates in regards to Cell Recovery, of T-cells Passed Through Polymer A.

Between-Subject Effects of Flow Rate and Cell Density

Dependant Variable	Group	*p-value (3 d.p)*
Cell Recovery	Flow Rate	.019*
	Cell Density	.289
	Flow Rate x Cell Density	.925
Viability Reduction	Flow Rate	.996
	Cell Density	.615
	Flow Rate x Cell Density	.878

Post Hoc Tukey's Test

Dependant Variable	Group Comparisons	*p-value (3 d.p)*
Cell Recovery	500 vs 1,500 µL/min	.086
	500 vs 3,000 µL/min	.019*
	1,500 vs 3,000 µL/min	.736

Significance of between-subject effects was determined by a two-way ANOVA. Where significance was indicated a post hoc Tukey's test was performed to determine significance between groups.
* = $p \leq .050$.

No significant interaction was detected between flow rate and cell density in regards to both cell recovery and viability reduction. Analysis of each individual factor revealed that the only significant relationship observed was between the

flow rate and the resultant cell recovery. Further analysis found that increasing the flow rate from 0.5 to 3 mL/min gave a significant mean increase in cell recovery of 15.1 %.

These results suggested that there was a correlation between increases in cell recovery with an increase of flow rate, with 3 mL/min being the optimal of the flow rates tested. For the density of cell suspension, significant differences were not found in regards to cell recovery or viability, indicating that cell density was not a critical factor within the parameters tested. The viability of recovered cells was not found to be impacted by flow rate or cell density. It was anticipated that increasing the flow rate would lead to a larger viability reduction due to increased shear. However, all values for viability decrease remained low at < 4.2 % suggesting that the flow rate threshold for introducing detrimental shear was not reached within this set-up.

Although the cell recovery was increased significantly from previous studies, there still remains a large loss of ~50 % of T-cells flown into the column. The low decrease in viability of T-cells suggests that the critical flow rate was not reached within this experiment. Therefore it would be suggested that the range of the experimental design space could be expanded by increasing the high and low values for flow rate and cell density would produce a larger and more detailed picture. Additionally, further attempts to improve on cell recovery may use DoE to incorporate multiple other factors such as column height and wash volume.

4.3.2.6. Addition of a Trypsin Step

The addition of a trypsin step to the improved set-up was investigated in an attempt to further increase cell recovery. 10 x 10^6 Jurkat T-cells were flown into polymer A, followed by 2 mL of trypsin. Trypsin was held in the polymer for 2 minutes before being de-activated through the addition of complete RPMI media.

Washing was then performed with PBS, 1 % BSA (w/v), 0.5 M EDTA. This method is described in more detail in **Method 2.2.2.5.3**.

The work presented here and in **section 4.3.2.6** was performed in collaboration with Karen Trippler (University College London). Specific details of the collaboration are given in **Method 2.2.2.6**.

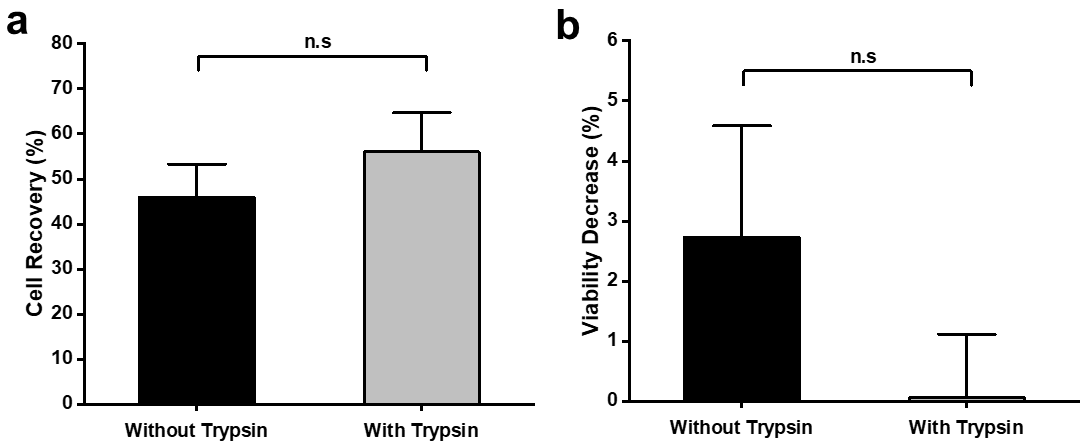

Figure 4.13. The impact of incorporating a trypsin step to Jurkat T-cells passed through polymer A on cell recovery and viability. a. The recovery of cells from the system. **b.** The decrease in viability of recovered cells from the initial viability. Polymer A set in a syringe was replaced for each run. n = 3 independent runs. Mean values are plotted. Error bars = 1SD. Significance was determined by a two-tailed T-test. No significant differences were found. n.s = not significant.

The mean cell recovery was observed to be 56 % with trypsin and 46 % without trypsin (**Figure 4.13a**). Initially this suggested that the addition of a trypsin step resulted in a 10 % increase in cell recovery, however, these differences were not found to be statistically significant. The mean viability decrease was observed to be 2.7 % with trypsin and 0.1 % without trypsin (**Figure 4.13b**). However, as with cell recovery these differences were not found to be statistically significant. This suggests that the addition of trypsin did not increase cell recovery or reduce cell viability in this case. This suggests that non-specific binding of cells by adherent

proteins is already minimal and cells are likely being retained due to being physically trapped within the polymer.

4.3.2.7. Pressure Drop within a Chromatography-Style Set-Up

Polymer A was inserted into a chromatography column and water was passed through over a range of flow rates 5 to 100 mL/min, as per **Method 2.2.2.5.4**. These flow rates were used to evaluate the behaviour of the polymer over a large range. To determine the pressure drop over the polymer, input and output pressure was measured via pressure gauges placed at either end of the column (as shown in **Method 2.2.2.5.4**). The pressure drop was also investigated with the addition of 1 x 10^7 Jurkat T-cells in suspension into the polymer, with consequent cell recovery and viability assessed.

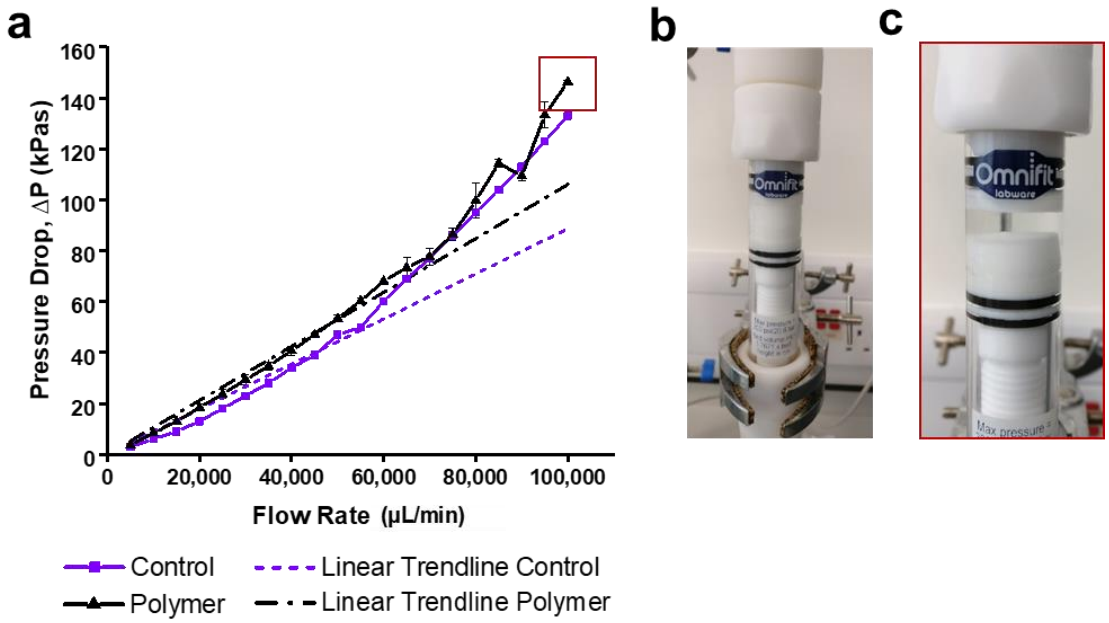

Figure 4.14. Differential pressure across polymer A at different flow rates with visible polymer compression at 100 mL/min. a. Differential pressure observed for polymer A in a chromatography column for flow rates of 5 to 100 mL/min. Control = empty column. Linear fits (dashed lines) were produced from flow rates 5 to 60 mL/min and extrapolated to 100 mL/min. **b.** Polymer in column with no flow through. **c.** Polymer in column with a flow of 100 mL/min showing compression. Image corresponds to the red box highlighted in **a.** n(polymer) = 3 independent runs. Mean values are plotted. Error bars = ± 1SD. n(control) = 1.

For flow rates between 5 and 60 mL/min a linear increase in pressure drop with an increase in flow rate was observed (**Figure 4.14a**). The trend line (R^2 = 0.99) plotted from these data points gave a slope of 0.00116 which translates to an increase of 1.16 kPas per 1 mL/min flow rate increase. The pressure drop at this interval ranged from 4 kPas to 68 kPas. As with the column with polymer A inside, the control of an empty column displayed a linear increase in pressure drop with an increase in flow rate up to 60 mL/min. The trend line (R^2 = 0.98) for the control had a slope of 0.00103, corresponding to an increase of 1.03 kPas per 1 mL/min flow rate increase. Therefore, the addition of polymer A resulted in an increase of 0.13 kPas per 1 mL/min flow rate increase over the linear section.

At flow rates greater than 60 mL/min a linear increase was no longer observed for both polymer A and the control. Furthermore, the increase in standard deviation with polymer A at these points highlighted an increase in variation in the pressure drop. Overall, the pressure drop increased from 60 to 100 mL/min to a maximum of 146 kPas with polymer A and 133 kPas without. The only decrease in pressure drop was detected at 90 mL/min with polymer A.

According to Darcy's law when laminar flow and a steady state applies, pressure is directly proportional to flow rate. However, this was found to only be the case up to a flow rate of 60 mL/min. This strongly suggests that above 60 mL/min the flow within the system was turbulent. This is a phenomenon known as post-Darcy, or Darcy-Forchheimer flow, where the non-linear increase is explained through inertial loss. Through the calculation of the Reynolds number for water travelling the 1.5 cm column length (1.08×10^5 at 100 mL/min), laminar flow (Re < 2100) was assumed for all flow rates investigated here; and so this observation was not expected, particularly with the control. A possible explanation for this is the varied

diameters of the syringe, tubing, and column. Bernoulli's principle states that as water flows from tubing of one diameter to the next, the velocity increases or decreases accordingly. Thus, the velocity used to calculate the Reynolds number may not have accurately represented the velocity at the point at which the pressure was measured. Ideally pressure gages should be connected directly at the input and output of the column to give a better depiction of pressure in the column itself, however this was not possible with this set-up.

To allow comparison, an empty column control was ran and used as a reference to which the column containing polymer A was compared. An increase in pressure drop over the control was found at all flow rates, excluding 90 mL/min which is likely an anonymous result. This increase was found to be 0.13 kPas per 1 mL/min flow rate increase below 60 mL/min, and a maximum of 13 kPas above. Particularly during linear increases, the increase in pressure drop compared to the control was found to be relatively low. Thus, this indicated a low level of flow resistance posed by polymer A. This is likely due to the polymer's highly porous nature and complements earlier reported data of low tortuosity values. Above 60 mL/min a more erratic increase in pressure drop was highlighted. A most probable explanation for this is the compressibility of the polymer resulting in an adjusted value of permeability, this could be observed at flow rates above 40 mL/min (**Figure 4.14c**). As the polymer compresses, the pores within the structure begin to collapse, which in turn results in a larger resistance to flow and an increase in back pressure. Moreover, as the polymer compresses Darcy's law is no longer applicable (as non-compressible porous media is assumed), therefore, a linear increase in pressure drop is no-longer expected even with a laminar flow. As a result flow rates below 40 mL/min where polymer compression was not visible (**Figure 4.14b**) were implemented for the following experiments.

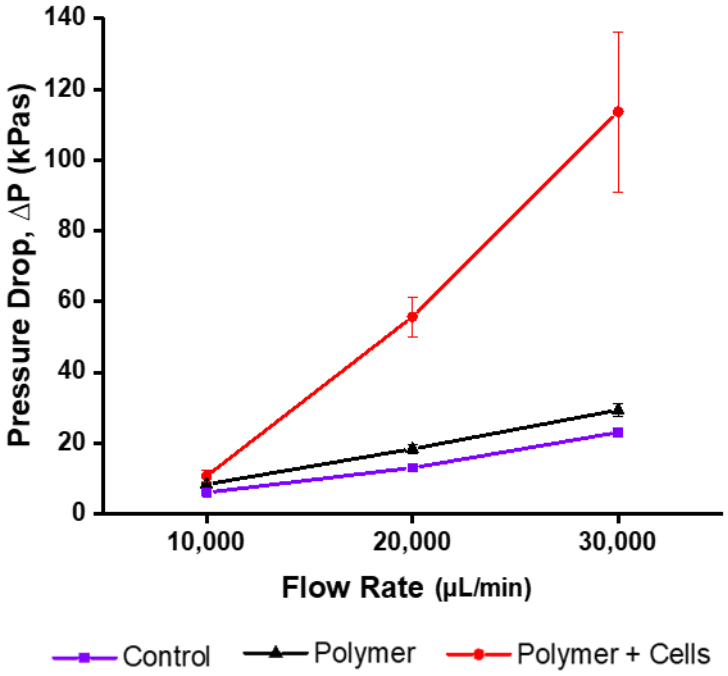

Figure 4.15. Pressure drop during elution across polymer A with Jurkat T-cells in suspension passed through at different flow rates. Differential pressure was measured during the wash step, post cell suspension. Control = cell suspension passed through an empty column. Polymer = water passed through polymer A in a column. Polymer + Cells = cell suspension passed through polymer A in a column. n = 3 independent runs. Mean values are plotted. Error bars = ± 1SD.

Table 4.5. *p*-values for the Comparison of Polymer A With and Without Cells in Regards to Pressure Drop for Different Flow Rates

	Polymer vs Polymer + Cells (*p*-value, 3 d.p)		
	Flow Rate (µL/min)		
Dependant Variable	**10,000**	**20,000**	**30,000**
Pressure Drop	.135	<.001***	.007**

Significance was determined by a two-tailed T-test.
** = $p \leq .010$. *** = $p \leq .001$

The addition of T-cells to the system considerably altered the pressure profile of polymer A. The pressure drop during elution was observed to be significantly increased with the addition of cells to the system at both 20 and 30 mL/min, compared to polymer A without cells (**Figure 4.15** and **Table 4.5**). At 10

mL/min similar pressure drops of 10.7 and 8.3 kPas for polymer A with, and without cells, respectively, were recorded. This rose dramatically to a difference of 37.6 kPas at 20 mL/min, and 84.3 kPas at 30 mL.

The increase in pressure drop over the polymer can be attributed to the addition of Jurkat T-cells which were found to have a diameter of 11.2 µm (**Section 4.3.1.1**). As this is significantly larger than a water molecule, T-cells were likely unable to pass through smaller pores within the polymer and so caused blockages. Furthermore, blocked pores would reduce the availability of flow paths, which in turn would cause an increase in flow velocity as the volume flows through a smaller number of pathways. As the polymer is compressible, this would result in the collapse of more pores, further restricting flow. The effect of this chain reaction would be amplified by an increase in flow rate, which is what was found here.

As in **Figure 4.14a**, it can be seen in **Figure 4.15** that water passed through both the control and the polymer displayed a linear increase in pressure drop as the flow rate increases, with the polymer giving a small increase over the control at all points. This linear increase can no longer be confidently established with the flow through of cells in suspension due to the increased standard deviation at 30 mL/min. Thus, Darcy's law can no longer be implemented to give predictions of the polymers behaviour with the addition of cells.

To improve this study it would be suggested that an additional control run in which the medium in which the cells were suspended in be passed through polymer A. In this study a control run with polymer A was ran with water only, whereas cells were suspended and eluted with a buffer consisting mainly of PBS. This would remove the varying factor of liquid viscosity and allow a more precise observation of the impact of the addition of cells to the system on the pressure drop.

Nevertheless, the difference in reported values for the dynamic viscosity of water (0.890 cP) and PBS (1.00 ± 0.05 cP) at 25 ºC are small and therefore the impact would likely be minimal (Kang *et al*., 2013).

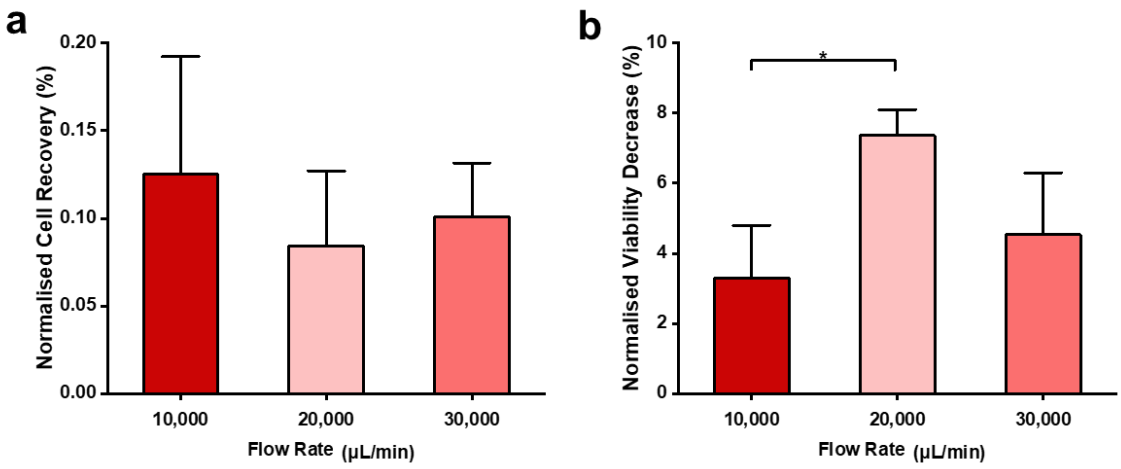

Figure 4.16. Percentage recovery and viability decrease of Jurkat T-cells passed through polymer A in a chromatography column, at various flow rates. **a.** The recovery of cells from the system. **b.** The decrease in viability of recovered cells from the initial viability. All values were normalised to a control of passing cells through an empty column. n = 3 independent runs. Mean values are plotted. Error bars = 1SD. Significance was determined by a one-way ANOVA with a post hoc Tukey's Test. * = $p \leq .050$.

Figure 4.16a shows that the normalised cell recovery was highest at a flow rate of 10 mL/min (0.13 %) and lowest at 20 mL/min (0.08 %). Cell recovery was found to be extremely low in all flow rates tested, with no significant difference between flow rates observed. A mean of 66.8 % cells were recovered when running controls of an empty column over all flow rates tested. Although this highlights that cell were being lost within the set-up itself, it also strongly suggests that the remaining cells were being lost due to the addition of the polymer.

The normalised viability decrease of recovered cells was determined to range from 3.3 % at 10 mL/min, to 7.4 % at 20 mL/min. The only difference determined

to be statistically significant was the between flow rates 10 and 20 mL/min. Viability decrease remained low at all flow rates.

Previously it was suggested that an increase in flow rate results in an increase in cell recovery, with a flow rate of 3 mL/min resulting in a 51 % cell recovery (**Section 4.3.2.5**). Although not directly comparably due to differing set-ups, taken with the results here it could be further suggested that a critical flow rate exists, where increasing beyond it becomes detrimental to cell recovery before viability. This may be because cells flown at a higher flow rate may impact the scaffold walls with additional force which may cause them to become lodged in crevices within the wall of the polymer. Cells stuck in this manner would likely require removal using a method other than flowing through buffer; such as mechanical compression, or ultra-sonic waves (Dainiak *et al.*, 2007; Kumar and Srivastava, 2010; Kurashina *et al., 2019*).

It would be recommended that future studies using this set-up be explored with flow rates lower than 10 mL/min, with a focus on increasing cell recovery and identifying the critical flow rate. Further studies may also incorporate alternative cell removal strategies such those mentioned above.

4.3.2.8. Discussion of the Suitability of Polymer A for use as a Cell Column

Initially, polymer A was found to have good flow through properties using water. This was not found to be the case with the addition of T-cells. Analysis of pores showed that the polymer would contain many pores that would be large enough to allow unstimulated T-cells through, however cells are likely still becoming stuck within the smaller pores.

One option to increase porosity would be to further decrease density. However previous data (**Section 3.3.4**) has shown that although the maximum pore size

may increase, the polymer would likely still contain a lot of smaller pores. This would result in cells still becoming trapped. Moreover, it was observed during initial testing of flow rates that polymer of lower densities are more compressible which may lead to additional issues of collapsed pores at even lower flow rates than found here.

A maximum of 51 % recovery of 10 x 10^6 T-cells passed through a section of polymer A was achieved from these studies. Although this was a vast improvement compared to the initial 8.9 % recovery, a loss of nearly half is extremely significant. Furthermore, it is critical when considering this polymer for use in a cell therapy process that maximal cell recovery be paramount; particularly where immuno-compromised patients may have low initial T-cell counts.

Taking all of this into account, it was concluded that polymer A in the current format does not meet the critical criteria of an acceptable cell recovery of T-cells flown into the column, and is therefore not suitable for use as cell column in the context of this project. Following this, it was decided that work on polymer A would cease and an alternative polymer would be investigated.

4.4. Conclusion

To begin evaluation of Polymer A for use in this project, initial studies focused on the activation of T-cells with aCD3/aCD28 polymer, and the use of polymer A as a cell column were performed in parallel. Activation studies were pre-faced by a characterisation of readouts of T-cell activation, and a comparison of primary sourced and Jurkat cell line T-cells.

Activation readouts of primary sourced human T-cells stimulated with three activation methods, Dynabeads, TransAct, and an aCD3/aCD28 coated well

plate were successfully characterised. An increase in cell count was evident from day 3 to day 5. An increase in cell diameter was detected from day 1, peaking at day 3. Activated cultures visibly changed in culture morphology from day 1, forming T-cell clusters. An increase in $CD69^+$ T-cells was detected from 3 hours post stimulation, peaking at day 1. An increase in $CD25^+$ T-cells was detected from day 1, peaking at day 5. Increased consumption of glucose and glutamine, and increased production of lactate and ammonia was identifiable from day 3. This characterisation should be considered in future studies to allow successful identification of activated T-cells.

Furthermore, activation readouts were compared between Jurkat T-cells and primary T-cells to determine the extent to which Jurkat T-cells could be used as a T-cell model in this study. When stimulated, Jurkat T-cells and primary T-cells displayed significant differences in regards to proliferation, viability, cell diameter, CD25 and CD69 expression, glucose and glutamine consumption, and lactate and ammonia production. Moreover, the extent of these differences were dependent of the method of stimulation used. This variability, coupled with a lack of major distinguishable features between unstimulated and stimulated Jurkats, deemed them unsuitable for use as a cell model for use of inferring successful T-cell activation, using the methods in this project.

Cell diameters of unstimulated Jurkat T-cells (11.2 µm) were observed to be comparable to primary T-cells from day 3 to 7 stimulated with Dynabeads (11.3 µm), TransAct (10.7 µm), and an aCD3/aCD28 coated well (11.4 µm). Thus indicating that Jurkat T-cells may be used as a model in studies for the use of representing the appropriate size of an activated primary T-cell.

Exposure of T-cells to aCD3/aCD28 polymer A for 24 hours resulted in a 16.8 % increase of early activation marker, CD69, expressing T-cells. No increase in late

activation marker, CD25, was observed. Thus suggesting that a relatively small percentage of T-cells in the culture were stimulated by aCD3/aCD28 polymer A, and that these cells were in the early stages of activation when analysed. Furthermore, this supports the hypothesis that aCD3/aCD28 polymer A is capable of activating T-cells.

T-cells were passed though sections of polymer A to assess its use as a cell column. Preliminary investigations highlighted a significantly low cell recovery (0 - 8.8 %), and high viability decrease (50.8 - 80.3 %).

Consequently, non-specific binding of binding of T-cells to polymer A was examined through supernatant- and confocal imaging- derived methods. Through a supernatant-derived count it was determined that 3.18 x 10^4 cells per 6 mm diameter polymer A disc were non-specifically bound. Image-based counts allowed for the mitigation of cells lost through processing and determined the number of bound cells to be 74 cells per mm^2. The number of bound cells was reduced to 41 cell per mm^2 through the switching of buffer to PBS, 1 % BSA (w/v), 0.5 M EDTA.

An alternative set up was developed to improve the recovery of T-cells from polymer A. This set up was used to investigate the impact of flow rate and cell suspension density on cell recovery and viability. No interaction was found between flow rate and cell density. The only significant relationship observed was between the flow rate and the resultant cell recovery, with cell recovery increasing as flow rate increases. A flow rate of 3 mL/min with a cell density of 1 x 10^6 cells/mL resulted in the greatest cell recovery (51 %) and lowest viability decrease (1.1 %). Additionally, the use of trypsin was tested but was not found to improve cell recovery.

The pressure drop over polymer A was characterised. When ran with water, a linear increase in pressure drop with an increase in flow rate was observed up to a flow rate of 60 mL/min. The addition of cells considerably increased the pressure drop up to 5-fold at 20 and 30 mL/min due to cells trapped within the polymer. Furthermore, the cell recovery was found to be extremely low (0.08 - 0.13 %).

It was decided that polymer A in its current format is not suitable for use in this project as a cell column, as cells cannot be sufficiently removed from the polymer in a 3D structure. Further studies will now investigate the use of an alternative polymer, termed polymer B.

Chapter 5. Polymer B Characterisation

5.1. Introduction

Due to the unsuccessful attempts to flow T-cells into the matrix of polymer A and efficiently remove them, the decision was made to commence studies on a second polymer, referred to in this work as polymer B. The required characteristics for a successful candidate for use in this project remain: the ability to be produced with a porous structure, the capacity to attach antibodies to its surface, and biocompatibility with T-cells in culture. As such, characterisation almost identical to that performed on polymer A was undertaken under the same broad categories of structure and porosity, antibody attachment, biocompatibility, and auto-fluorescence.

The characterisation aims and methods in this chapter duplicate those in chapter 3 applied when characterising polymer A. Hence, introductions and some discussions of method limitations here are kept brief to avoid repetition and the reader is instead referred back to chapter 3 for more detail.

5.1.1. Polymer B

Similarly to the initial polymer investigated in this thesis, polymer B is biodegradable, hydrophilic, bio-polymer scaffold (hydrogel), created through the cross-linking of ε-PL. This polymer, however, is cross-linked with an alternative bis-carboxylic acid; suberic acid, also known as octanedioic acid ($C_8H_{14}O_2$). The patent to create this polymer is owned by SpheriTech Ltd. The polymer was provided as either non-porous or porous with aCD3 and aCD28 antibodies attached by SpheriTech Ltd. This polymer was investigated due to the ability to control pore size through an additive during polymerisation and having previously

demonstrated high biocompatibility in cell culture methods (Gallager *et al*., 2016; Weil, 2016; Kennedy *et al*., 2019; Lace *et al*., 2021).

5.1.2. Structure and Porosity

The pores within the polymers structure must be of sufficient size to allow T-cells to enter into and be removed from the 3D structure. Structural characterisation was therefore undertaken to further understand the monolithic structure. The classification of pores is applied as follows: micro-porous = < 2 nm, meso-porous = 2 nm – 50 nm, macro-porous = 50 nm – 10 µm, super-macro-porous = > 10 µm (Li *et al*., 2016; Henderson *et al*., 2013).

5.1.3. Antibody Attachment

The interaction between T-cells and aCD3 and aCD28 attached to the surface of the polymer is essential for T-cell activation. As such, it is important that attachment of aCD3 and aC28 should be confirmed and evaluated.

5.1.4. Auto-fluorescence

The auto-fluorescence of polymer B was important to characterise due to the potential of interference in immunostaining and cell-polymer visualisation techniques. This auto-fluorescence has also allowed the polymer to be viewed by fluorescent microscopy without staining.

5.1.5. Biocompatibility

A successful material candidate for this project would be expected to be remain in culture with T-cells for at least 3 days. Biocompatibility was investigated using cell culture counts and viability, and an apoptosis assay to identify apoptotic and necrotic cells.

5.2. Aims and Hypotheses

5.2.1. Chapter Aims

- To evaluate the structure of polymer B, particularly the pore size of porous scaffolds.
- To confirm and evaluate the attachment of aCD3 and aCD28 to SpheriTech's polymer B.
- To evaluate the biocompatibility of polymer B with T-cells.
- To characterise the auto-fluorescent properties of polymer B.

5.2.2. Hypotheses

It is hypothesised that the structural property of pore size will be increased over that previously found with polymer A. It is expected that the non-porous polymer will not present macro-pores on the surface. It is expected that the majority of pore sizes of the porous scaffold will be super-macro-porous (> 10 µm). As the polymer chemistry is well characterised it is expected that aCD3 and aCD28 antibodies will be attached to the surface of the polymer. As this polymer has been successful in cell cultures with other cell types, it is hypothesised that polymer B will demonstrate a good level of biocompatibility with T-cells. It is also anticipated that Polymer B will fluoresce when exposed to light at certain wavelengths allowing it to be imaged via fluorescent microscopy.

5.3. Results and Discussion

5.3.1. Polymer Structure and Topology

To assess the structure and topology of polymer B, samples of both a non-porous and porous structure were imaged by SEM. This was performed in collaboration with SpheriTech Ltd, with SEM imaging being performed by Josh Greenwood of SpheriTech Ltd as detailed in **Method 2.2.1.1**. Polymer surface topology was

imaged over a variety of magnifications representing the scale at with an operator and cell would interact with the polymer.

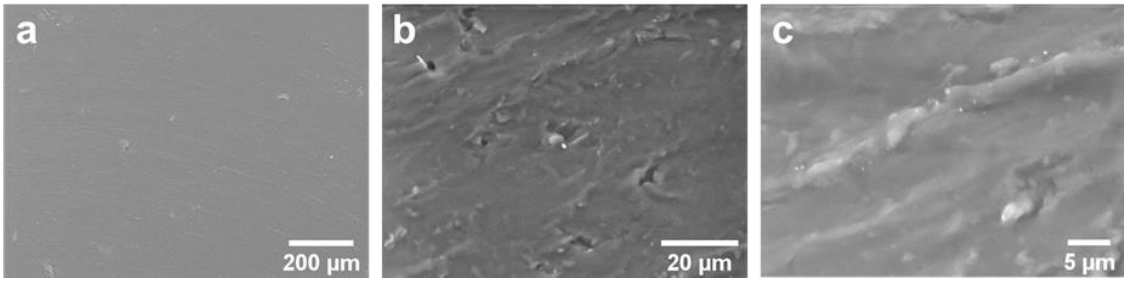

Figure 5.1. Scanning electron microscopy images of non-porous Polymer B. **a.** x150. Scale bar = 200 µm. **b.** x1,800. Scale bar = 20 µm. **c.** x4,000. Scale bar = 5 µm.

When viewed at a magnification of x150 the surface of the non-porous polymer appeared smooth (**Figure 5.1a**). At magnifications of x1,800 and x4,000 small ridges on the surface of the polymer were revealed (**Figures 5.1b** and **c**). Despite these ridges, a large proportion of the surface topology appeared even suggesting that the majority T-cells interacting with the surface of this polymer will do so in a flat planar manner.

This was in line with previous findings of this polymer reported by Lace *et al*. (2021) which found that this polymer at different cross-linking percentages resulted in a non-macroporous surface when cast into sheets.

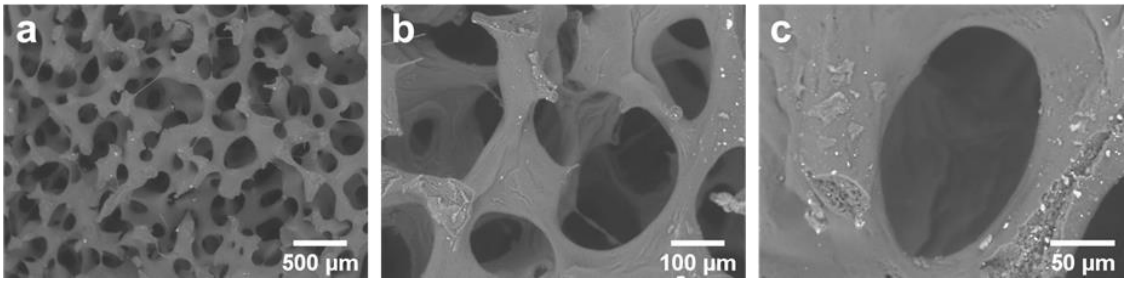

Figure 5.2. Scanning electron microscopy images of porous Polymer B. **a.** x50. Scale bar = 500 µm. **b.** x300. Scale bar = 100 µm. **c.** x600. Scale bar = 50 µm.

SEM images displayed in **Figure 5.2** show that the porous format of this polymer displayed a monolithic structure with many large and well defined pores. The surface of the polymer was observed to be generally smooth and even. **Figures 5.2b** and **c** revealed a view into the internal structure of the polymer where the polymer was cut with a scalpel. Through these small incisions an internal macro-porous structure was observed.

The structure found here suggests that T-cells will interact with either a flat polymer surface or, with interactions that occur where a pore has formed, with a slightly convex or concave surface.

Successful activation of T-cells using a flat surface is well documented, with T-cells activation protocols published by Thermo Fisher Scientific, BD Biosciences, and BioLegend detailing procedures in which antibodies are immobilised to the base of a well plate for T-cell stimulation (BD Biosciences, 2011; BioLegend, 2022; Thermo Fisher Scientific, 2022). Additionally, antibodies and other peptides attached to flat surfaces of other materials such as coated glass, PDMS, and hyrdogels have been widely utilised to explore T-cell activation parameters (Campi *et al*., 2005; O'Connor *et al* 2012; Matic *et al*., 2013; Deeg *et al* ., 2013; Guasch *et al*., 2017; Hickey *et al*., 2019; Li *et al*., 2020; Sadon *et* al., 2021).

Less reported, however, is the use of scaffolds in T-cell activation, with some of the only reported instances utilising cross-linked alginate, pre-purchased polystyrene scaffolds, 3D printed PCL lattices, electro-spun PDMS fibres, and bundled silica micro-rods (Delalat *et al*., 2017; Cheung *et al*., 2018; Dang *et al*., 2018; Pérez del Río *et al., 2018;* Majedi *et al*., 2020). Furthermore, only the latter three were used to provide both a stimulatory signal and an environment in which to grow. Of these three, the closest resembling the surface of the polymer are the

PDMS fibres and the silica micro-rods as these both provide concave and convex surfaces for T-cell interaction throughout their structure.

Given the reported success of T-cell activation through interacting with stimulus in a planar manner, it is expected the surface structure of the polymer in the non-porous format will also be equally sufficient. This would also be expected to be the case for the porous scaffold as it is anticipated that the majority of interactions between T-cell and polymer will occur in a mostly-planar manner due to the large size and wide angles within the pores. Minimal studies to date have been published investigating the use of a 3D scaffold, however, existing ones support the possibility that scaffolds can be used to activate T-cells.

5.3.2. 3D Structure

To provide a further insight into the structure of the porous polymer, 3D fluorescence imaging was performed on polymer samples through a z-stack as per **Methods 2.1.5.13** and **2.1.5.14**. Images were taken to a depth of 500 µm. Reconstruction of the z-stack produced a 3D model with additional depth information.

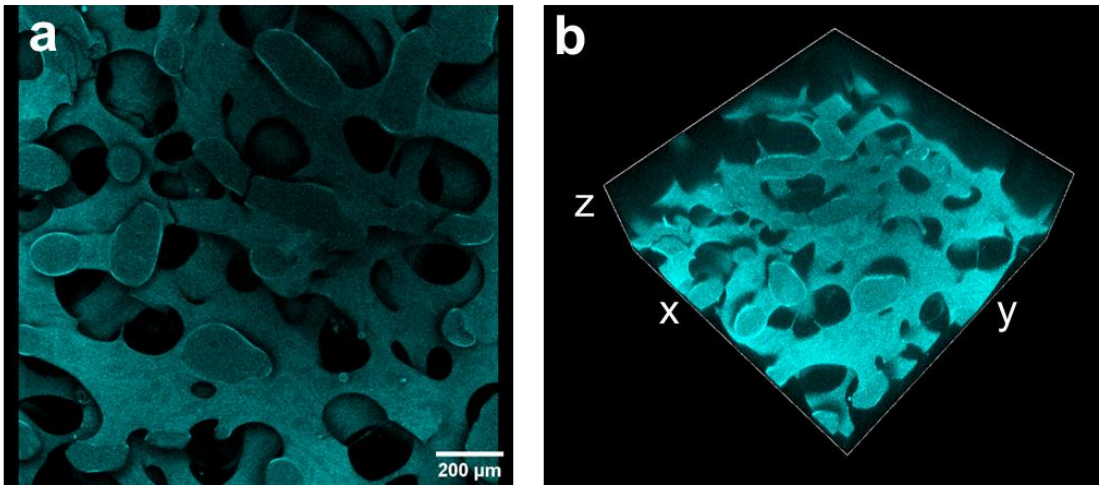

Figure 5.3. Reconstructed 3D z-stack fluorescent confocal microscopy images of porous polymer B. Polymer was visualised through the DAPI channel and pseudo-coloured cyan. **a.** Top view. Scale bar = 200 µm. **b.** Angled side view. Scale bar = 501 µm (z) x 1.42 mm (y) x 1.42 mm (x).

Super-macro-porous pores of > 10 µm were observed through the polymer section imaged (**Figure 5.3**). Viewing the 3D reconstruction from alternative angles displayed how the pores in the polymer were interconnected throughout (**Figure 5.3b**). This method of imaging confirmed the highly porous structure that found previously in section 5.3.2.

Additionally, the observed interconnectivity of the pores suggests that cavities within the polymer may in fact be larger than estimated when viewed from above. To further quantify the 3D area of pores it may be possible to use software to analyse the 3D reconstruction, such as Avizo™ which was used previously to analyse reconstructions from x-ray tomography. This would be recommended for future studies to gain a better understanding of the pore characteristics. Spherical aberration was less of a limiting factor in this sample compared to polymer A due to lower density of material. However, it is still limiting and it should be noted imaging to a depth of > 500 µm would not be recommended, thus greatly limiting the information that could be gained when further analysing pore structure using this method.

5.3.3. Pore Diameter and Area

As a means of evaluating the pores sizes in porous polymer B, SEM images were processed through Fiji image analysis software (Schindelin *et al*., 2012) to quantify pore diameter and area as described in **Method 2.2.1.1**. The pore diameter reported here is the “feret” diameter.

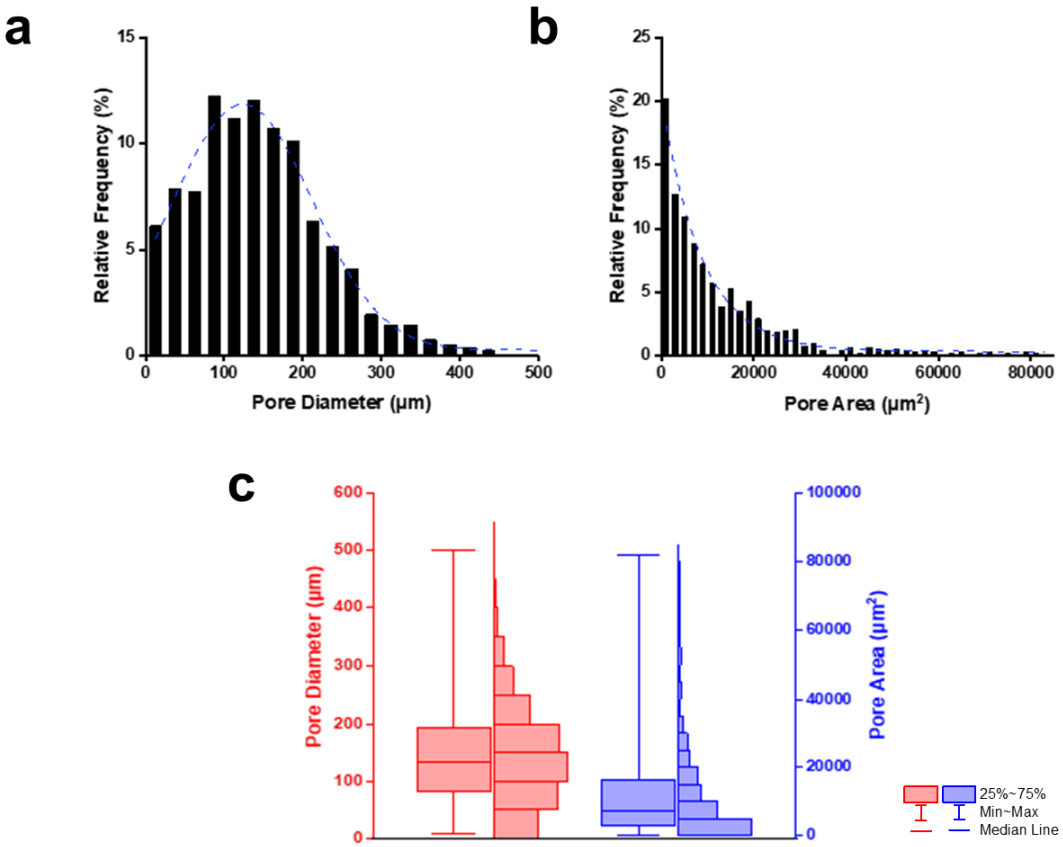

Figure 5.4. Diameter and area of pores in porous polymer B. **a.** Frequency distribution graph for pore diameter. n = 1 image, 835 pores. **b.** Frequency distribution graph for pore area. n = 1 image, 835 pores. c. Box and whisker graph for pore diameter and pore area.

Figure 5.4a revealed that the measurements of pore diameter displayed a skewed distribution, giving a median of 134 µm. 75 % of pore diameters were between 82 and 193 µm, however, a small proportion were found as small and large as 7 and 500 µm, respectively. Measurements of pore area displayed an exponential distribution (**Figure 5.4b**). The median pore area was 7,455 µm^2 with an interquartile range of 2,687 – 16,369 µm^2.

The median and interquartile range of the pore diameters and areas displayed confirm a super-macro porous structure. Furthermore, this strongly suggests that T-cells should comfortably be allowed to enter into the scaffold, with the majority

of pores being in excess of an order of magnitude larger than the diameter of a T-cell.

5.3.4. Confirmation of Antibody Attachment

Polymer B was provided by SpheriTech Ltd. with aCD3 and aCD28 antibodies pre-attached. An ELISA provided a quick semi-quantitative method to confirm successful attachment to the polymer and allowed some comparison between differing formats and batches. Details of the aCD3/aCD28 ELISA can be found in **Method 2.1.4.6.**

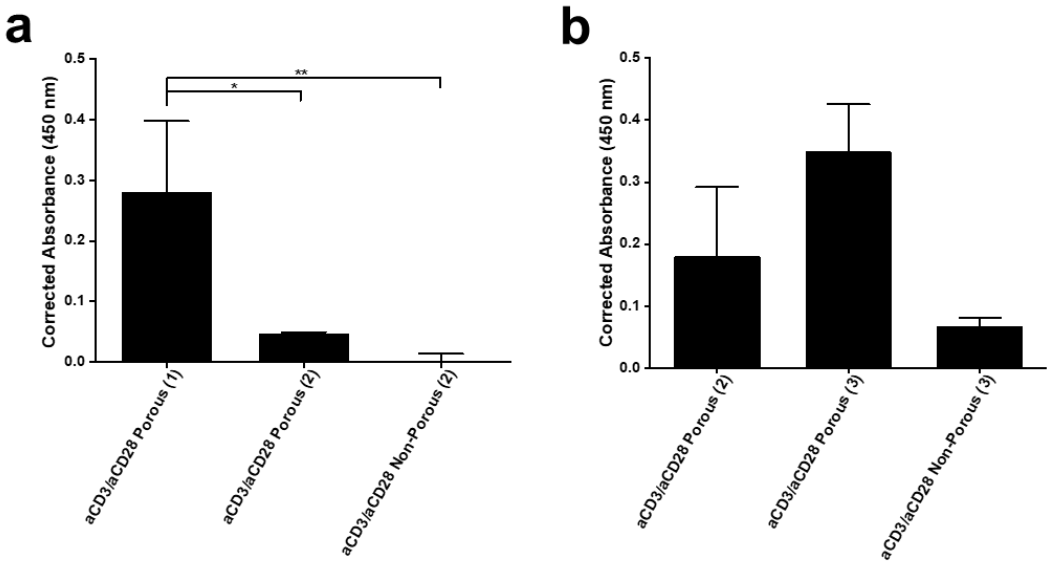

Figure 5.5. anti-CD3 and anti-CD28 ELISA with polymer B samples. The number in brackets indicates the batch supplied from SpheriTech Ltd. a. and **b**. each represent one ELISA assay performed separately. n = 1 assay with technical triplicates for all conditions. Mean values are plotted. Error bars = ± 1SD. All results have been adjusted using the negative controls to account for background.

Absorbance was detected in all samples excluding the non-porous polymer supplied in batch 2. Porous polymer supplied from batch 1 displayed a mean absorbance ~6-fold higher than that from batch 2, with significantly different means of 0.28 and 0.05, respectively (**Figure 5.5a**). These results indicated that aCD3 and aCD28 was present in both porous polymer from batch 1 and 2,

however was present in at an increased quantity in porous polymer from batch 1. The quantity of antibodies these samples were exposed to were identical, thus suggesting that antibody attachment was less efficient, or not successful in the case of non-porous polymer, in batch 2 when compared to batch 1. No absorbance was detected in the non-porous polymer batch 2, indicating that there was no antibody present on the surface of this polymer sample. This may have been due to variations in the operator and methods performed when attaching the antibodies. Consequently, this was not used in attempts to activate T-cells.

Initial antibody quantities used for the attachment protocol for batch 1 and 2 were based off calculations for total surface coverage at a 1:1 molar ratio of aCD3 and aCD28. These calculations contained a number of estimations and assumptions, such as the size of a generic antibody and the surface area of the porous polymer. Additionally, they did not take into account the efficiency of the attachment process. In an attempt to simplify the process, offset low attachment efficiency, and maximise attachment, antibody quantities at a 1:1 weight ratio were significantly increased by ~10-fold for porous samples and ~100-fold for non-porous samples for batch 3.

Figure 5.5b displays that absorbance was detected in all samples tested, indicating that antibody was present. The mean absorbance of porous polymer from batch 3 was ~2-fold higher than that from batch 2, with values of 0.35 and 0.18, respectively. This difference, however, was not found to be significantly different. It was not possible to deduce from these results if there was a true increase in antibody attached with the increase in antibody quantity. However, the observation of absorbance with non-porous polymer (3) strongly indicates that increasing the antibody quantities allowed the antibody attachment to be successful on this occasion.

An attempt to make this ELISA quantitative was undertaken through the use of a standard curve, shown in **Appendix G.1**. This was discarded due to lack of comparability between polymer samples with antibody pre-immobilised on their surface, and known concentrations of antibodies solution being adsorbed onto a well plate - leading to an overall unknown concentration. Thus, a limitation of this ELISA is that it will remain only semi-quantitative until a standard curve with a suitable comparison is developed. Furthermore, standard curves demonstrated a key consideration when running this assay as semi-quantitate. As they produced a four parameter logistic curve, “S” shaped, a proportional increase in antibody concentration with an increase in absorbance is only true where the curve is linear. Therefore, samples should preferably display absorbance values that fall within this linear section. Despite this limitation, the importance of using this ELISA to confirm antibody presence on the polymer is highlighted here and was proved to be a useful validation tool.

5.3.5. Antibody Distribution

To further characterise the attachment of antibodies to polymer B, samples of non-porous polymer with aCD3 and aCD28 attached were incubated with a secondary anti-murine antibody bound to AlexaFlour® 594, as per **Method 2.2.1.4**. Both polymer and stained aCD3 and aCD28 were visualised using a fluorescent confocal microscope. Controls are shown in **Appendix C.2**. Fluorescence intensity determined and used to infer antibody density, as per **Method 2.1.5.15.**

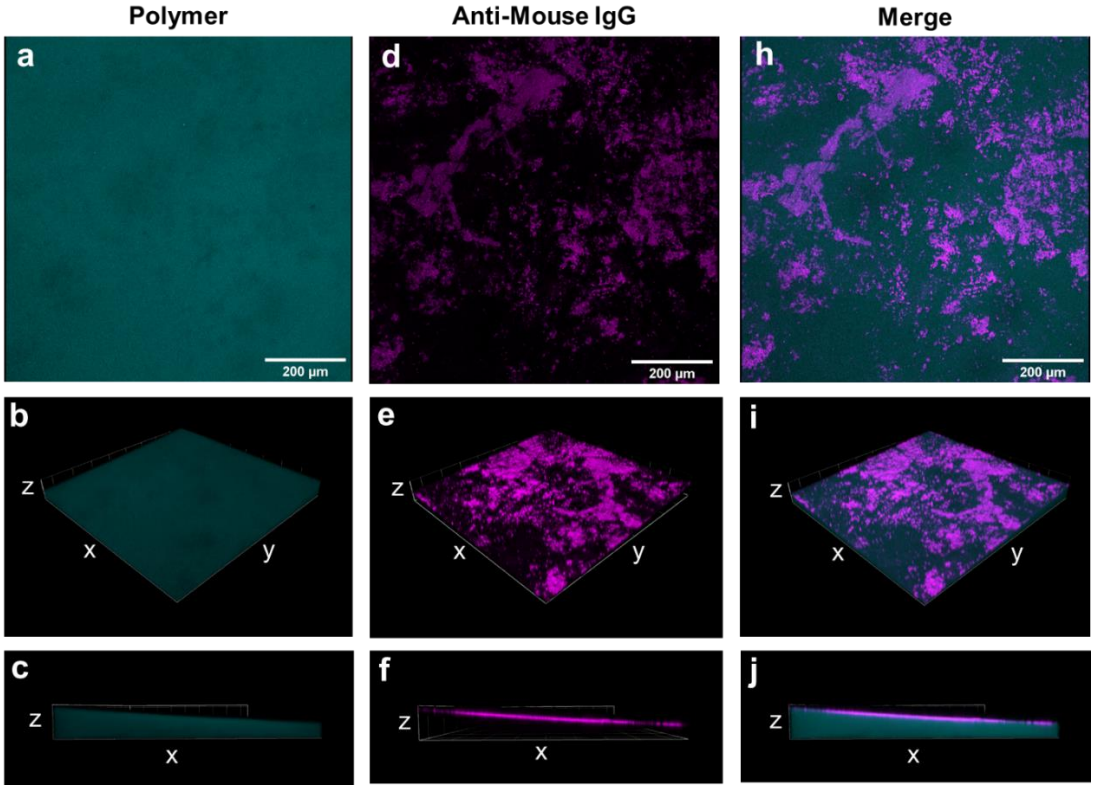

Figure 5.6. Reconstructed 3D fluorescent confocal microscopy images of non-porous polymer B showing the distribution of attached anti-CD3 and anti-CD28. **a** - **c.** Polymer A, visualised through the DAPI channel, pseudo-coloured cyan. **d** - **f.** aCD3 and aCD28, stained with anti-mouse IgG AlexaFlour® 594, pseudo-coloured magenta **h** - **j.** Merged channels. Top row images (**a, d,** and **h**) show a top view. Middle row images (**b, e,** and **i**) show an angled side view. Bottom row images (**c, f,** and **j**) show a direct side view. Scale bars = 200 µm (top row images), and 106 µm (z) x 850 µm (y) x 850 µm (x) (middle and bottom row images).

Reconstructed 3D images displayed additional confirmation that antibodies were present on and attached to the surface of polymer B in a non-porous format (**Figure 5.6**). Images further revealed a heterogeneous distribution of antibodies with patches of varied sizes over the polymer surface.

Whilst this polymer is deemed ‘non-porous’ in that is does not contain pores large enough to allow for cell migration, the possibility remains that it contains meso- or micro-pores. Whilst investigating this polymer cast into beads Weil (2016) found that SpheriTech beads contained meso-pores. Therefore diffusion of

antibody into the polymer was a possibility. To investigate this, a side view of the polymer was observed and revealed that antibody was only present on the surface suggesting minimal antibody diffusion (**Figure 5.6j**).

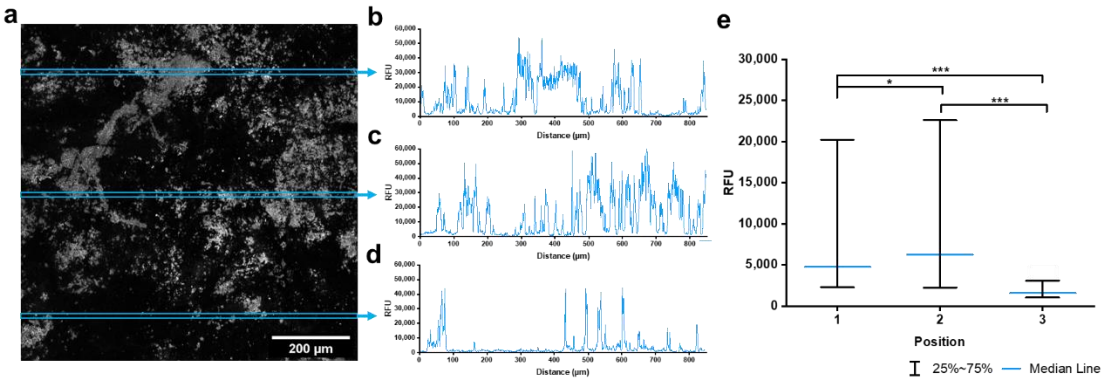

Figure 5.7. Fluorescence intensity of stained aCD3 and aCD28 on the surface of non-porous polymer B. **a.** Top view of a z-stack projection of aCD3 and aCD28, stained with anti-mouse IgG AlexaFlour® 594 displayed in grey-scale. Boxes through the image show where histograms were measured. Scale bar = 200 µm. Histograms correspond to **b.** Top position, **c.** Centre position, and **d.** Bottom position. **e.** Median fluorescence intensities for each position measured. RFU = relative fluorescence units. n = 1 image, 3 positions (top, centre, and bottom position). Statistical significance was determined by a Mann-Whitney-U test. * = $p \leq .050$. *** = $p \leq .001$.

As discussed in **Section 3.3.1** microscope settings were optimised so that fluorescence intensity could further be utilised to infer relative antibody density. **Figure 5.7** displays the fluorescence intensity of stained aCD3 and aCD28 measured at 3 points across the polymers surface. It was found that areas that appeared to show no fluorescence in fact displayed a small amount, with no measured values displaying 0 RFU with background subtraction. This suggests that antibody attached to the entire surface of the polymer. At all positions evaluated, fluorescence intensity varied massively from minimum to maximum RFU over the distance measured (**Figures 5.7b - d**). This variation was observed particularly at position 1 and 2, with interquartile ranges also displaying large

bounds (**Figure 5.7e**). It was noted that positions 1 and 2 included more patches of antibody of higher intensity, indicating that there is a large variation of antibody density in each patch of antibody attached, with some being 60,000-fold more dense than others. It was observed that the median fluorescence intensities for the top position (4757 RFU), centre position (6266 RFU), and bottom position, (1582 RFU) were all significantly different from each other with *p*-values of at least < 0.03. This further confirms the highly heterogeneous antibody distribution over the surface.

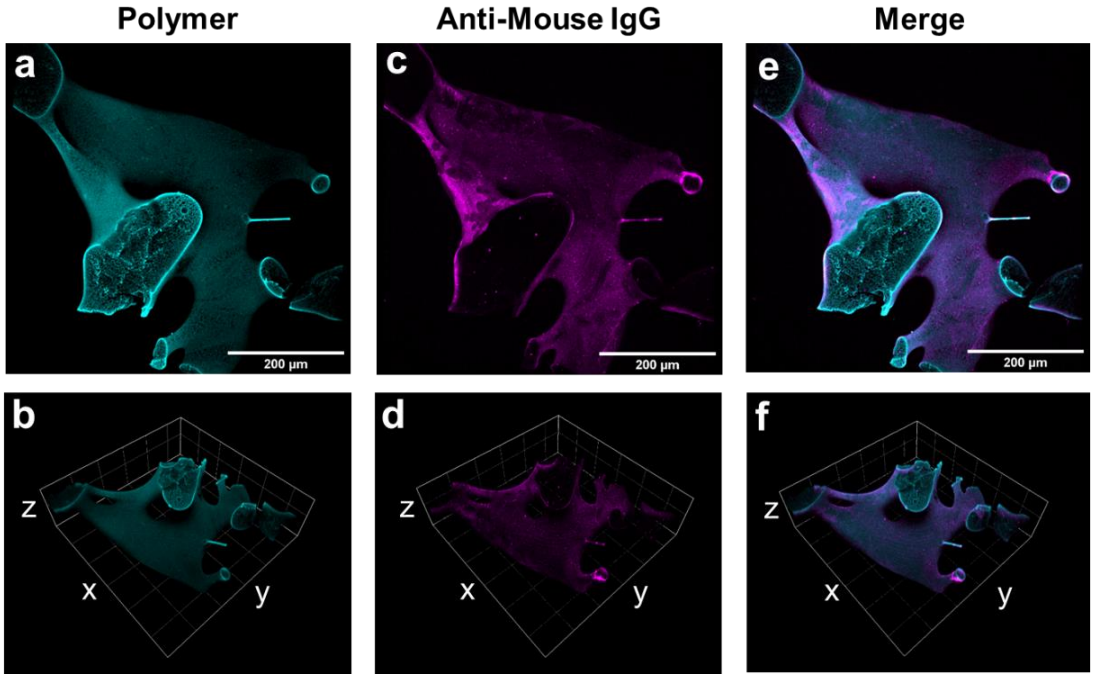

Figure 5.8. Reconstructed 3D fluorescent confocal microscopy images of porous polymer B showing the distribution of attached anti-CD3 and anti-CD28. a and **b.** Polymer A, visualised through the DAPI channel, pseudo-coloured cyan. **c** and **d.** aCD3 and aCD28, stained with anti-mouse IgG AlexaFlour® 594, pseudo-coloured magenta **e** and **f.** Merged channels. Top row images (**a, c,** and **e**) show a top view. Scale bars = 200 µm. Bottom row images (**b, d,** and **f**) show an angled side view. Scale bars = 171 µm (z) x 566 µm (y) x 566 µm (x)

Likewise, additional confirmation that antibodies were present on and attached to the surface of polymer B in a porous format (**Figure 5.8**) was observed through

3D reconstructed images. The distribution appeared to be largely homogeneous with some patches still visible. However, the low contrast between areas of lower and higher intensity suggested a more equal distribution, particularly when compared to the non-porous sample.

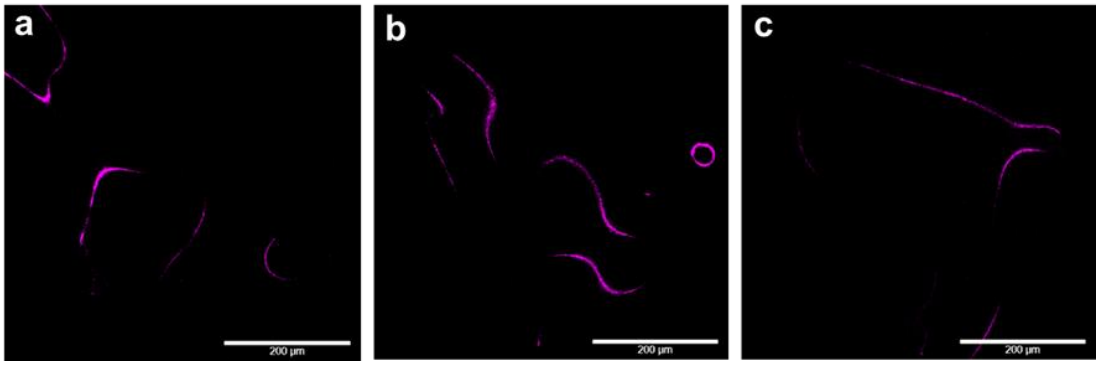

Figure 5.9. Fluorescent confocal microscopy image of stained aCD3 and aCD28 on porous Polymer B. Single slices taken from a z-stack. aCD3 and aCD28 has been stained with anti-mouse IgG AlexaFlour® 594 and pseudo-coloured magenta. **a.** A slice from the top of the z-stack. **b.** A slice from the middle of the z-stack. **c.** A slice from the bottom of the z-stack. Scale bars = 200 µm.

Images representing single slices through the z-stack at 3 positions through the polymer were investigated to assess the diffusion of antibody into the polymer itself (**Figure 5.9**). Single bands of fluorescence were observed around the perimeter of the polymer structure at the top, middle, and bottom of the structure, with no fluorescence within. This indicates that that there is no antibody diffusion below the polymer surface which is important when considering minimising waste and the cost of production.

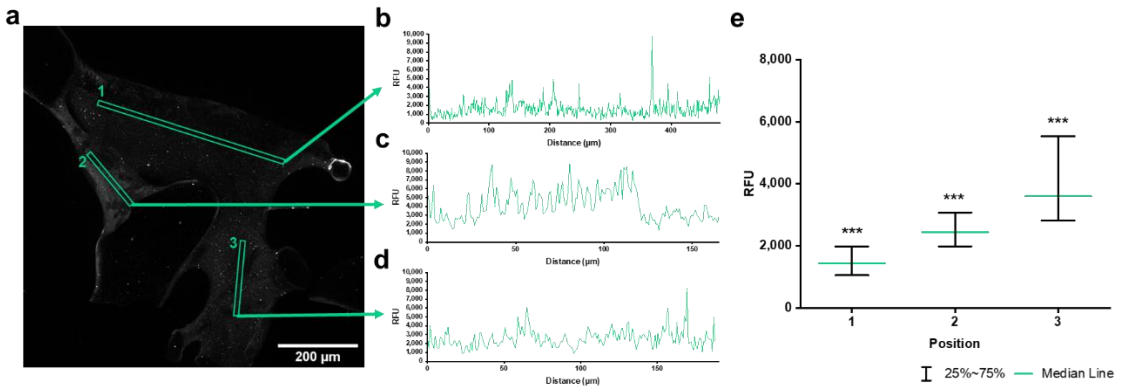

Figure 5.10. Fluorescence intensity of stained aCD3 and aCD28 on the surface of porous polymer B. a. Top view of a z-stack projection of aCD3 and aCD28, stained with anti-mouse IgG AlexaFlour® 594 displayed in grey-scale. Scale bar = 200 µm. Boxes highlighted on the image show where histograms were measured. Histograms correspond to **b.** Position 1, **c.** Position 2, and **d.** Position 3. **e.** Median fluorescence intensities for each position measured. RFU = relative fluorescence units. n = 1 image, 2 positons. Statistical significance was determined by a Mann-Whitney-U test. *** = significantly different from all at $p \leq .001$.

Histograms of fluorescence intensity at 3 positions of a z-stack projection were produced to further evaluate the antibody density over the surface of the polymer (**Figures 5.10c - e**). As with the non-porous polymer, fluorescence was detected over all measured points, implying a level of antibody had attached over the entire surface. All histograms individually displayed relatively stable pattern of fluorescence intensity, especially when compared to the non-porous polymer. This was particularly observed at position 1 and 2 which displayed small interquartile ranges. Although the intensity at each position was observed to be reasonably homogenous, the overall distribution of antibody throughout the polymer was found to be heterogeneous. **Figure 5.10e** shows the median fluorescence intensities for position 1 (1436 RFU), position 2 (2447 RFU), and position 3 (3603 RFU). These values were all found to be significantly different from each other with *p*-values of ≤ .001. Thus indicating that each position

measured displayed a different quantity of attached antibody, with position 3 displaying over a 2-fold increase compared to position 1.

A plausible explanation for the highly heterogeneous distribution of antibody of the surface of polymer B in a non-porous format may be the formation of “pools” of antibody during the attachment procedure. It is possible that the ridges observed on the surface of the polymer in **Section 5.3.1** prevented the even distribution of aCD3 and aCD28 over the polymers surface during attachment resulting in areas of lower and higher densities of antibody. For the porous format of polymer B, antibody solution was flowed through cylinders of polymer during attachment. It could be suggested that due to the structure of the polymer some surfaces within may experience a higher flow through and therefore be exposed to more antibody than others. Thus, resulting in the variation of antibody density observed across the different positions measured here.

The discussion on the significance of fully quantifying antibody ligand density from **Section 3.3.1** applies here and the optimisation of fluorescence microscopy allowed was performed to provide further semi-quantitate analysis of antibody density on the polymer surface. This was useful to infer relative quantity on the polymer surface. Future techniques such as gold-labelling antibodies to provide more precise quantities could be explored.

5.3.6. Biocompatibility

The biocompatibility of the polymer B, in both a non-porous and porous format, with T-cells was investigated through the co-culture of polymer and Jurkat T-cells over 6 days, as described in **Method 2.2.1.5**. Each day, T-cell cultures were analysed for cell number and viability, then stained with annexin V and PI to identify viable, apoptotic, and necrotic cells.

Annexin V^-PI^- cells were classified as viable. Annexin V^+PI^- were classified as early-stage apoptotic. Any cell that stained PI^+ was classified as dead, however cells which were annexin V^+PI^+ could either be late-stage apoptotic or necrotic, whereas annexin V^-PI^+ could only be identified as necrotic. Dead cells were combined into one category of late apoptotic/ necrotic.

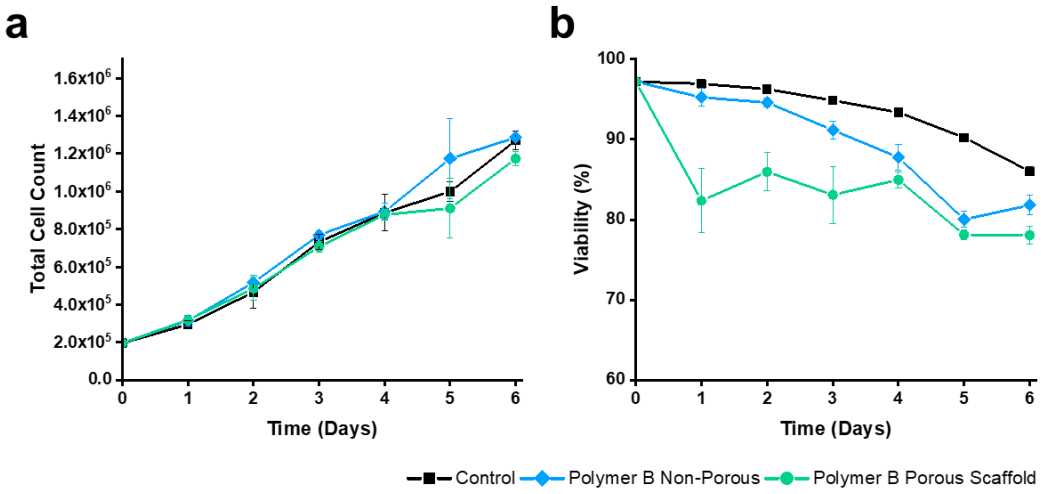

Figure 5.11. Jurkat T-cells in culture with polymer B over 6 days. a. Total culture cell count. **b.** Culture viability. n = 1 with triplicate technical repeats. Mean values are plotted. Error bars = ± 1SD

Table 5.1. *p*-values for the Comparison of T-cell Cultures with Non-Porous or Porous Polymer B, in regards to Total Cell Count and Viability.

	Control vs Polymer B Non-Porous vs Polymer B Scaffold (*p-value, 3 d.p*)						
		Day					
Dependant Variable	**Group Comparison**	**1**	**2**	**3**	**4**	**5**	**6**
Total Cell Count	Control vs Polymer B Non-Porous	.615	.778	.448	.999	.431	.971
	Control vs Polymer B Scaffold	.493	.984	.721	.997	.850	.134
	Polymer B Non-Porous vs Polymer B Scaffold	.996	.928	.113	.985	.153	.073
Viability	Control vs Polymer B Non-Porous	.995	.677	.459	.007**	*p*<.000***	.008**
	Control vs Polymer B Scaffold	.10*	*p*<.000***	.005**	.001***	*p*<.000***	*p*<.000***
	Polymer B Non-Porous vs Polymer B Scaffold	.020*	.002**	.040*	.170	.556	.016*

Significance was determined by a one-way ANOVA followed by a post hoc Tukey's test.
* = $p \leq .050$. ** = $p \leq .010$. *** = $p \leq .001$.

Significant difference was not found between the total cell count of the control and either format of polymer B over the duration of the study (**Figure 5.11a** and **Table 5.1**). This suggests that co-culturing T-cells with polymer B does not inhibit cell growth. However, significant decreases in viability from the control were

observed from day 4 onwards for non-porous polymer B and at every time point for porous polymer B (**Table 5.1**). An initial 15 % decline in viability was observed at 1 day in culture with the porous scaffold, with the following 5 days being between the range of 86 and 78 %. Non-porous polymer B did not display a decrease in viability until day 4, at which point viability declined to resemble that of the porous-format. Viability decreased for all conditions by day 6, declining from 97 to 86, 82, and 78 % for the control, non-porous, and porous polymer B, respectively.

Figure 5.12a shows representative annexin V vs PI graphs obtained from the NucleoCounter® NC-3000™. From these alone it was observed that non-porous polymer B closely resembled the population distribution of the control over the 6 days, with both displaying an increase in events in the top right quadrant by day 6. Comparatively, the porous format of polymer B displayed a decrease in events in the bottom left quadrant and an increase in events in the top right quadrant from day 1. To further classify these events, the gating strategy in **Figure 5.12b** was applied.

Figures 5.12c - e quantified and highlighted that which was viewed from the scatter graphs. Non-porous polymer B displayed significant differences from the control at day 4 and 5 only, with an increase in late apoptotic/necrotic cells of 6 and 12 %, respectively. This indicates that for the majority of this study, non-porous polymer demonstrated good biocompatibility with T-cells. No significant increase in early apoptotic cells were observed when compared to the control and so it is not possible to infer the pathway of death that resulted in the increase of dead cells displayed at day 4 and 5.

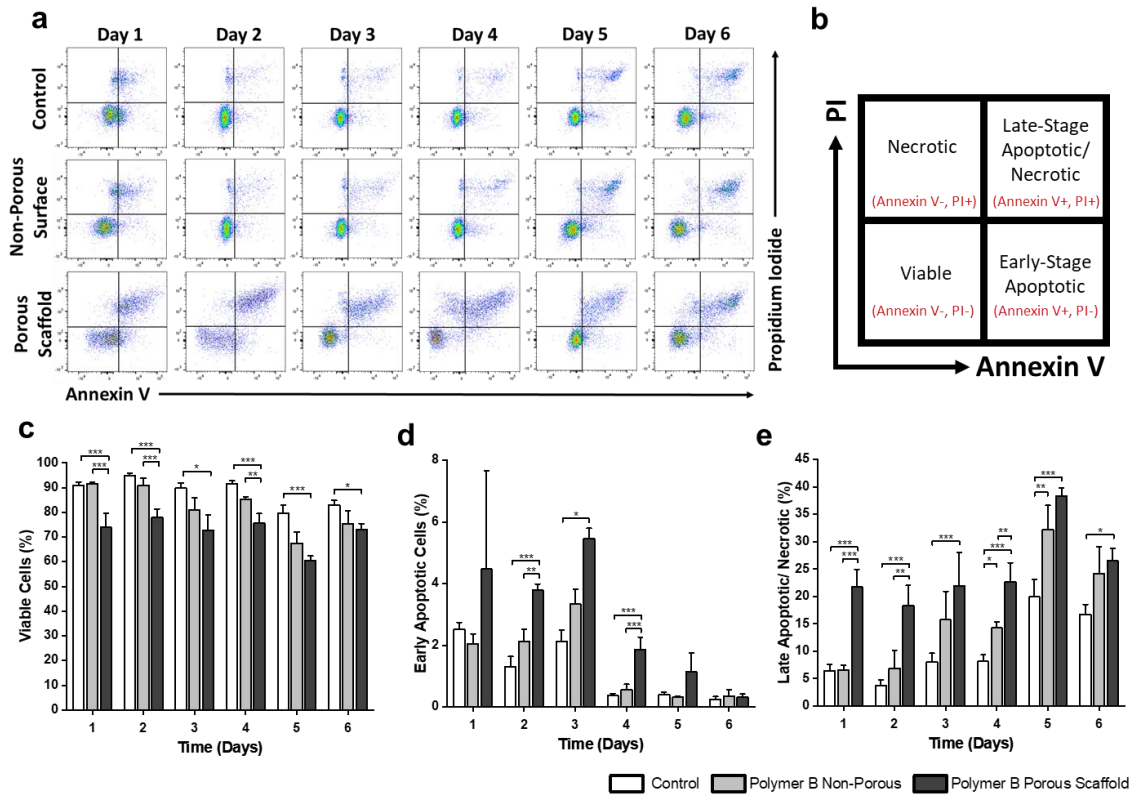

Figure 5.12. Apoptosis assay performed on Jurkat T-cells in culture with polymer B over 6 days. a. Representative scatter graphs with propidium iodide (PI) on the y-axis and annexin V on the x-axis. **b.** Gating strategy for the classification of viable (annexin V^-PI^-), early-stage apoptotic (annexin V^+PI^-), either late-stage apoptotic or necrotic (annexin V^+PI^+), and necrotic (annexin V^-PI^+) T-cells. **c.** Percentage of viable cells in the total population (annexin V^-PI^-). **d.** Percentage of early-stage apoptotic cells in the total population (annexin V^+PI^-). **e.** Percentage of either late stage apoptotic or necrotic (annexin V^+PI^+) combined with necrotic (annexin V^-PI^+) cells in the total population. n = 1 with triplicate technical repeats. Mean values are plotted. Error bars = ± 1SD. Significance was determined by a 1-way ANOVA with post-hoc Tukey's test. * = $p \leq .050$. ** = $p \leq .010$. *** = $p \leq .001$.

Porous polymer B displayed a significant decrease in the percentage of viable, and a significant decrease in the percentage of late apoptotic/ necrotic cells at every time point when compared to the control. Concurrent with the percentage viability previously reported, a sharp decline in viable cells was observed at day 1, with a decrease of 18 %. Significant increases in early apoptotic cells of 3, 2, and 5 % were observed at day 2, 3, and 4, respectively. However, these

increases were found to be relatively small when compared to the increases in late-stage apoptotic/necrotic cells observed to be between 10 and 18 % higher than the control over the 6 days. Although the increase in early-stage apoptotic cells detected suggests there was a low level of apoptosis induced during the culture, the difference between these percentages and the percentage found to be dead suggests that this was not the key pathway in which cells died. Taken together with the observation that the percentage of late apoptotic/necrotic was significantly higher from day 1, it is likely that cells underwent a rapid death, possibly as a result of cell injury from a stronger or more concentrated toxin.

At every time point throughout the 6 days, porous polymer B displayed either a significant decrease in viable cells or % viability, or an increase in apoptotic/necrotic cells when compared to the non-porous format. This strongly indicates that the porous format of polymer B was less biocompatible than the porous one. This was surprising as both consist of the same material which has also demonstrated biocompatibility in other studies (Gallagher *et al*., 2016; Weil, 2016; Kennedy *et al*., 2019; Lace *et* al., 2021). It is therefore suggested that this is either due to the addition of a potentially toxic substance to create pores, or the resultant porous structure being more difficult to wash out substances such as ethanol used during sterilisation. It is important that polymers undergo extensive washing to remove any toxic leachables and minimise impact on cell viability. An alternative wash protocol was therefore implemented for future cultures in which porous scaffolds were cut into discs before initial washing, as opposed to after which was done here, to maximise diffusion throughout the polymer.

Key limitations, such as over-simplification of cell death by the annexin/PI assay and non-optimal cell culture conditions, and suggestions to improve these are discussed in detail in **Section 3.3.8** and remain highly relevant here.

Furthermore, as was observed in **Section 4.3.1.1** Jurkat T-cells display different growth kinetics to primary human T-cells and so additionally may display differences when in culture with the polymer. For this initial early stage study, Jurkat T-cells were examined due to their ability to multiply without external stimulation simplifying the experiment. However, it would be strongly recommended that future studies aim to characterise biocompatibility of this polymer with primary derived human T-cells.

5.3.7. Auto-fluorescence

To fully characterise the auto-fluorescence spectrum of the polymer, samples were subject to an excitation/emission scan, as per **Method 2.1.5.18**. The scan was performed with an excitation wavelength range of 230 – 850 nm and an emission wavelength range of 280 – 850 nm.

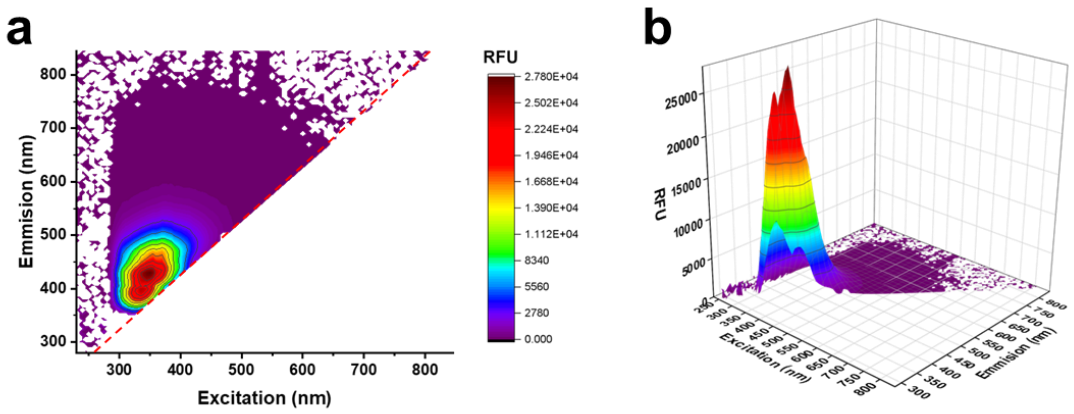

Figure 5.13. Excitation/emission spectrum of polymer B. Fluorescence intensity was measured over a range of 230 – 850 nm excitation and 280 – 850 nm emission wavelengths, with a step size of 5 nm for both. **a.** 3D surface graph of excitation/emission spectrum. Red dashed line represents the data trimming limit. **b.** 2D top-view of excitation/emission spectrum. RFU = relative fluorescence units. n = 1 scan.

Two main peaks of auto-fluorescence were highlighted through scanning (**Figure 5.13**).The most intense peak, with an RFU of 24,896 is observed at an excitation of 335 nm giving an emission of 400 nm. A second peak, with an RFU of 27,728,

is observed at an excitation of 350 nm resulting in an emission of ~430 nm. Excitation wavelengths above 500 nm resulted in lower or no emission intensity. Excitation wavelengths < 500 nm produced emissions of wavelength ≤ 600 nm. Consequently, future cell or antibody staining on polymer B will use antibodies or stains with an excitation of > 500 nm and an emission of > 600 nm.

5.4. Conclusion

The following characteristics of polymer B, in both a porous and non-porous format, were evaluated; the structure and topology, particularly the ability to form a porous structure in which T-cells could enter into; the ability to immobilise aCD3 and aCD28 antibodies on its surface; biocompatibility in culture with T-cells; and the auto-fluorescence profile.

Surface topology was analysed through the use of SEM and 3D reconstructions by fluorescent confocal microscopy. The surface of non-porous polymer B was found to be generally smooth with some visible ridges and was observed to not be macro-porous, as expected. The porous format of polymer B displayed a highly interconnected porous structure with pores within the super-macro size category of > 10 µm. The surface of the polymer was found to be smooth and did not contain macro- or miso-pores. The internal structure of the polymer was macro-porous.

Further characterisation of pores for the porous format of polymer B was undertaken through the measurement of pore diameter and area. The median pore diameter was 134 µm, with the overall majority between 82 µm to 193 µm. The median pore area was 7,455 μm^2, with the overall majority between 2,687 – 16,369 μm^2. This further confirmed the super-macro-porous structure.

An aCD3/aCD28 ELISA was performed to assess and compare the presence of aCD3 and aCD28 within polymer samples of different batches. This confirmed the presence of antibody on all samples with the exception of the non-porous polymer from batch 2. The amount of antibody detected ranged from batch to batch, with batch 2 lower than batch 1, and batch 3 higher than batch 2. Thus, successfully highlighting a reduction in antibody attachment from batch 1 to 2, and a subsequent increase from batch 2 to 3 due to the increase of aCD3 and aCD28 concentrations.

The attachment of antibodies was further confirmed, visualised, and semi-quantified through the staining and imaging of aCD3 and aCD28 on the surface of polymer B by z-stack fluorescent confocal microscopy and the analysis of relative fluorescence intensity. Antibody was observed to have attached to the entire surface of the non-porous polymer, with the distribution being highly heterogeneous. Patches of higher antibody density were found to be up to 60,000 times denser than patches of low concentration. Porous polymer B was also observed to have antibody attached to the entire surface. The distribution of the antibody was found to be more heterogeneous than with the non-porous polymer, with the highest densities being up 10 times denser than the lowest densities. Overall, the antibody distribution was deemed as heterogeneous throughout the structure due to median RFU's being significantly different at each position evaluated.

Non-porous polymer B displayed good biocompatibility when co-cultured with T-cells, with no observed impact on cell growth, or the percentage of viable cells as determined by an annexin V/ PI assay, compared to the control. Significant increases in the percentage of late apoptotic/necrotic were found on days 4 and 5, displaying an increase of 6 and 12 %, respectively.

Porous polymer B displayed worse biocompatibility in comparison to the non-porous format. No impact was observed on cell growth, however, a sharp decline in viability (-15 %) and percentage of viable cells (-18 %) was evident from day 1 and remained for the duration of the study. Porous polymer B was observed to convey a minor increase in apoptotic cells. However, the significant increase in late/apoptotic cells from day 1 indicate rapid cell death rather than the induction of apoptosis as the foremost pathway of death. This is suggested to be due to insufficient washing as a result of the structure. Future porous polymers will be pre-sectioned before washing to optimise diffusion and allow a more thorough wash.

Auto-fluorescence was characterised to minimise interference in future immunostaining techniques. Auto-fluorescence was found to be most intense at excitation wavelengths of < 500 nm producing emission wavelengths of ≤ 600 nm. Therefore, fluorescent imaging techniques should use stains or fluorophore conjugated antibodies which are visualised though excitation wavelengths higher than 500 nm and emission wavelengths higher than 600 nm to minimise background fluorescence.

Chapter 6. T-cell Interaction with Polymer B

6.1. Introduction

The characterisation of the super-macro-porous structure polymer B in **Chapter 5** suggest that porous polymer B will be a more suitable material for use as a 3D structure in which T-cells can enter into and be removed. Additionally, a significant advantage of non-porous polymer B is that it is transparent, allowing live cell imaging and analysis of T-cells cultured on polymer B.

In this chapter, initial studies on the interaction of T-cells with polymer B are presented. These focused on: the use of polymer B as a 3D scaffold – specifically the capacity in which T-cells can be seeded into the polymer structure and then subsequently removed; the mobility of T-cells on polymer B; and the ability of polymer B to be used as a material on which primary T-cells can expand.

6.1.1. T-cell Recovery

The recovery of T-cells from polymer in a porous 3D format is essential for use in this project. The relevance of this has previously been discussed in **Chapter 4** whilst assessing polymer A, with low cell recovery resulting in the determination of polymer A as unsuitable for this project. Thus, it was crucial to demonstrate the practicality of porous polymer B in allowing T-cells to be removed from its structure.

6.1.1. T-cell Mobility

T-cell mobility is essential for T-cells to search for antigen and target cells. This mobility is governed by an ‘exploitation–exploration trade-off ’, in which T-cells must balance the requirement for rapid scanning of APCs with engaging for a sufficient enough time to initiate activation (Krummel *et al*., 2016). As shown in **Figure 6.1**, three definitions of random walks have been used to model T-cell

mobility: Sub-diffusive, diffusive (Brownian-type), and super-diffusive (Lévy-type) (Krummel *et al*., 2016). Naïve T-cells have been found to display a diffusive or sub-diffusive random walks within lymph nodes, displaying no directional persistence and with fluctuations in velocity (Beauchemin *et al*., 2007; Cahalan and Parker, 2008). T-cells exposed to *Toxoplasma gondii* within the brain have been observed to display a super-diffusive random walk, characterised by short random movements interjected with longer trajectories (Harris *et al*., 2012). Reynolds (2021) proposed that T-cells migrating via Lévy walk can be attributed to the lack of mechanical stiffness in T-cells as a result of activation. As T-cell culture with polymer B is novel it was important to characterise the mobility of T-cells on polymer B. Additionally, migratory patterns could be useful to infer the activation status of T-cells.

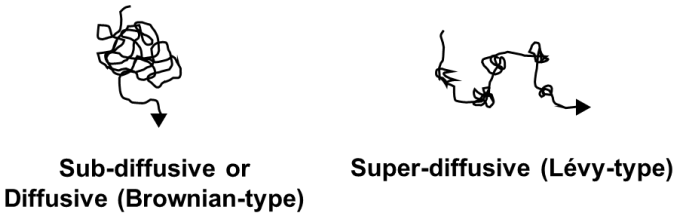

Figure 6.1. Characteristic tracks of sub-diffusive, diffusive, and super-diffusive migratory modes of T-cells. Adapted from Krummel *et al*., 2016.

6.1.2. T-cell Expansion

Previously, initial studies demonstrated the ability of polymer B to be cultured with T-cell line Jurkat (**Section 5.3.6.**). In line with the intended use of polymer B as a platform for the expansion of primary-sourced human T-cells, it was important to validate this with primary human T-cells. T-cells were cultured with polymer B and assessed non-invasively through automated intervals of confocal imaging to investigate culture confluency.

6.2. Aims and Hypotheses

6.2.1. Chapter Aims

- To demonstrate the successful seeding and removal of T-cells into porous polymer B
- To evaluate and characterise the migration of T-cells on polymer B
- To validate polymer B as a suitable material on which primary T-cells can expand
- To investigate the impact of expanding T-cells on polymer B on T-cell growth

6.2.2. Hypotheses

As porous polymer B has a super-macro-porous structure, it is expected that a high cell recovery of T-cells passed through polymer B will be observed. It is also expected that cell recovery will comparatively decrease with the attachment of aCD3 and aCD28 to polymer B, as T-cells will bind as they flow through. In regards to mobility, it is anticipated that T-cells exposed to polymer B will decrease in velocity due to the hydrogel being softer than a polystyrene well plate; that migratory patterns of T-cells exposed to aCD3/aCD28 polymer B will differ from exposure to polymer B alone; and that there will be an increase in the percentage of non-mobile T-cells on aCD3/aCD28 polymer B, as T-cells interact with and attach to aCD3 and aCD28. Furthermore, due to the good biocompatibility demonstrated with non-porous polymer B with Jurkat T-cells, expansion with primary T-cells is not expected to be negatively impacted when cultured together.

6.3. Results and Discussion

6.3.1. Cell Recovery from a Polymer B Column

As low cell recovery of T-cells from polymer A was a substantial factor in the determination of the material as unsuitable for the project, it was of great significance to commence further characterisation of polymer B - by first assessing the ability to seed and remove T-cells into porous polymer B. Porous polymer B, either with aCD3 and aCD28 attached or without, housed within plastic casing (as shown in **Method 2.1.4.7**, **Figure 2.6**) was suspended vertically with a syringe without the plunger connected to the top (as shown in **Method 2.2.3.1**, **Figure 2.12**). T-cell suspensions containing 10 x 10^6 Jurkat T-cells were deposited into the syringe and passed through polymer B via gravity. Output cell suspensions were collected and passed back through polymer B for a total of 10 passes. Cell suspensions were counted and analysed for viability after each pass.

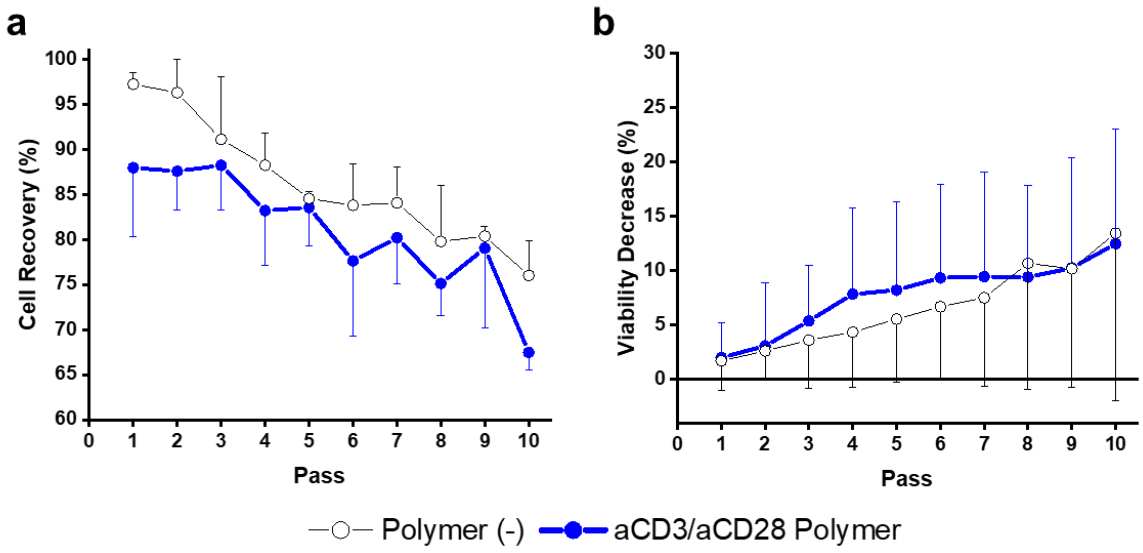

Figure 6.2. Cell recovery and viability decrease of Jurkat T-cells passed through porous polymer B. T-cells were passed through polymer B 10 times via gravity. **a.** Cell recovery. **b.** Viability decrease. n = 3 independent runs. Mean values are plotted. Error bars = ± 1SD.

Table 6.1. *p*-values for the Comparison of Polymer B With and Without aCD3/aCD28 attached, in Regards to Cell Recovery and Viability Decrease of T-cells passed through polymer B

	Polymer (-) vs aCD3/aCD28 Polymer (*p-value, 3 d.p*)									
	Pass									
Dependant Variable	**1**	**2**	**3**	**4**	**5**	**6**	**7**	**8**	**9**	**10**
Cell Recovery	.142	.054	.167	.201	.370	.230	.116	.027*	.461	.031*
Viability Decrease	.909	.905	.673	.556	.669	.692	.804	.886	.994	.933

Significance was determined by a two-tailed T-test.
* = $p \leq .050$.

Figure 6.2a displays that for both polymer (-) and aCD3/aCD28 polymer, a steady decline in cell recovery was observed from pass 1. With polymer (-), cell recovery ranged from 97.3 % at pass 1 to 76.0 % at pass 10. With a CD3/aCD28 polymer, cell recovery ranged from 88.0 % at pass 1 to 67.5 % at pass 10. aCD3/aCD28 polymer consistently resulted at in a lower cell recovery than polymer (-) at each pass. These differences were found to be statistically significant at pass 8 and 10 (**Table 6.1**).

The viability decrease of both polymer (-) and aCD3/aCD28 polymer (**Figure 6.2b**) both displayed a gradual increase from pass 1 to pass 10. The viability decrease with polymer (-) ranged from 1.7 to 13.5 %, and with aCD3/aCD28 polymer ranged from 2.0 % to 12.5 %. Increasing values of standard deviation for viability decrease were noted as the pass number increased for both conditions. Furthermore, no significant differences were found between polymer (-) and aCD3/aCD28 polymer at all passes.

Due to the characterisation of porous polymer B's super-macro-porous structure, it was anticipated that a high cell recovery of T-cells that were passed through polymer B would be observed. Here it was observed that after 1 pass through polymer B the recovery of cells was 97.3 %. This high level of recovery was

achieved without optimisation of the set up and represents a significant increase when compared to the maximum of 51 % cell recovery observed with polymer A. This strongly indicated that porous polymer B is a good candidate for a 3D cell scaffold as T-cells can enter into and be removed easily.

It was further predicted that passing T-cells through polymer B with aCD3/aCD28 attached would result in a lower cell recovery due to T-cells binding to the antibodies. At the majority of passes, no significant difference was found between the cell recovery of polymer (-) and aCD3/aCD28 polymer. This may indicate that T-cells did not interact with and bind to aCD3/aCD28 attached to polymer B. A potential reason for this may be that cells require a slower and controlled flow rate to allow them to be held in suspension and increase contact when within polymer B. As discussed previously, a flow rate of 2 mL/min would be recommended (Kumar and Srivastava, 2010). It is also possible, however, that T-cells did interact but did not bind, possibly due to shear forces or low affinity or avidity of antibodies.

It was not expected that cell recovery would decrease after each pass regardless of antibody attachment. It is likely that this occurred due to cells lost through the process of sample collection and transferring between passes, perhaps in combination with a small level of non-specific binding. Furthermore, a small decrease in viability of T-cells over the course of the experiment was also not expected and was likely influenced by the study being performed at room temperature. Initially cells were suspended in buffer at 4 ºC, however with each pass and analysis taking ~10 minutes each, this will have gradually increased potentially damaging cells.

6.3.2. Migration of Primary T-cells on a Polymer B Surface

To investigate the initial interaction of primary T-cells with polymer B, non-porous polymer B discs both with and without aCD3 and aCD28 attached, were placed at the bottom of a well plate and T-cells were seeded on top. Cultures were then imaged via time lapse confocal imaging at intervals of 10 seconds for a total of 4 hours. Time lapse videos were divided into 30 minute intervals and analysed using the TrackMate plugin (Tinevez *et al.* 2017) on Fiji image analysis software to determine cell tracks, percentage of mobile cells, and the velocity of mobile cells. Control wells contained no polymer and so were effectively cultured on a polystyrene surface. More details can be found in **Method 2.2.3.3**.

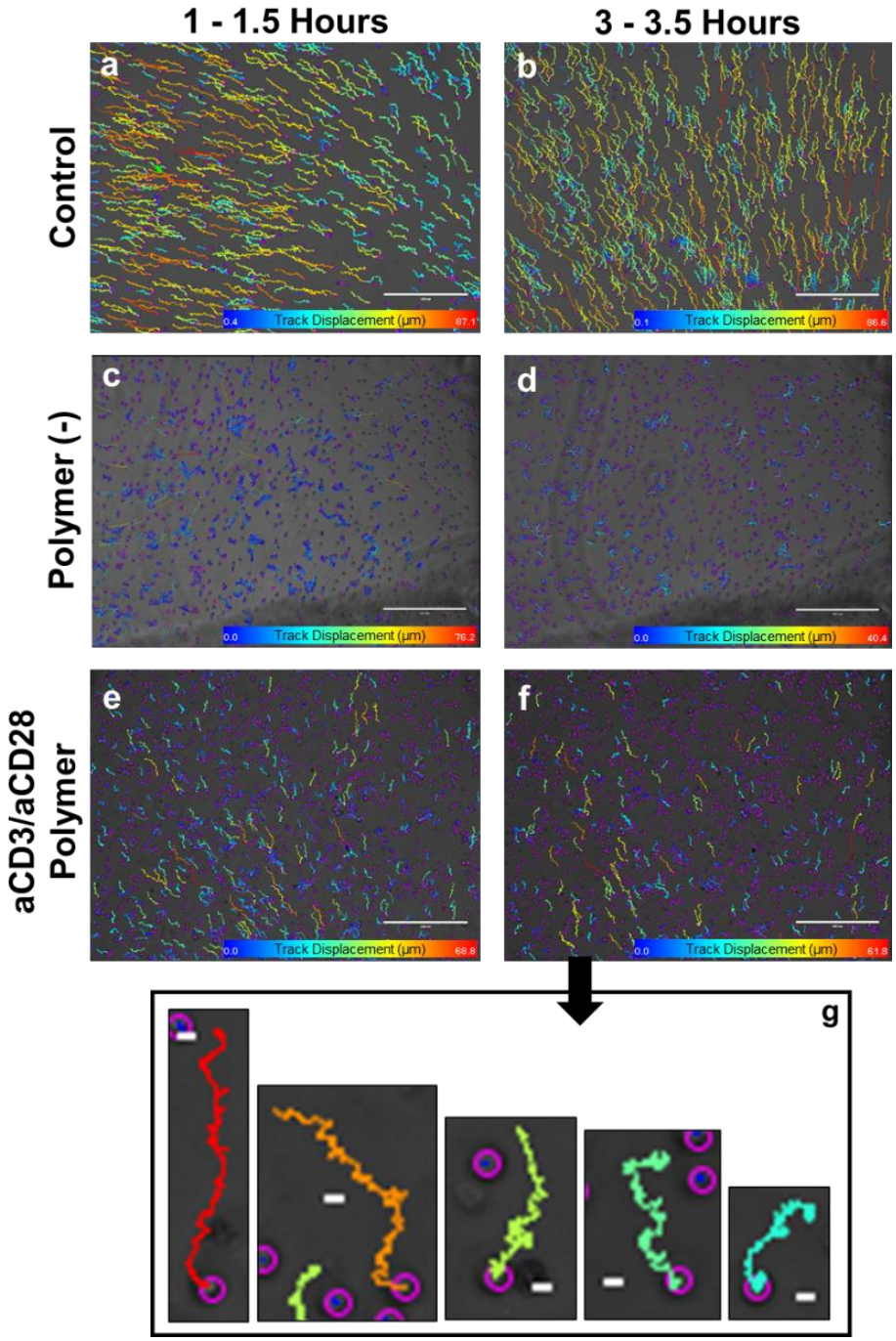

Figure 6.3. Visualisation of T-cell tracks on Polymer B. Tracks were visualised using time-lapse confocal imaging followed by TrackMate analysis. Track colour represents increasing total displacement from blue to red with minimum and maximums shown on each figure. Top row (**a** and **b**) T-cells on the base of a polystyrene well plate (Control). Centre row (**c** and **b**) T-cells on polymer B (Polymer (-)). Bottom row (**e** and **f**) T-cells on aCD3/aCD28 polymer B (aCD3/aCD28 Polymer). Left column (**a, c,** and **e**) = 1 - 1.5 hours. Right column (**b, d,** and **f**) = 3 - 3.5 hours. Images are representative of n = 3 independent experiments per donor, for a total of 3 donors. Scale bar = 200 µm. **g.** Magnified view of 5 individual T-cell tracks from T-cells on aCD3/aCD28 polymer B at 3 - 3.5 hours. Scale bar = 5 µm.

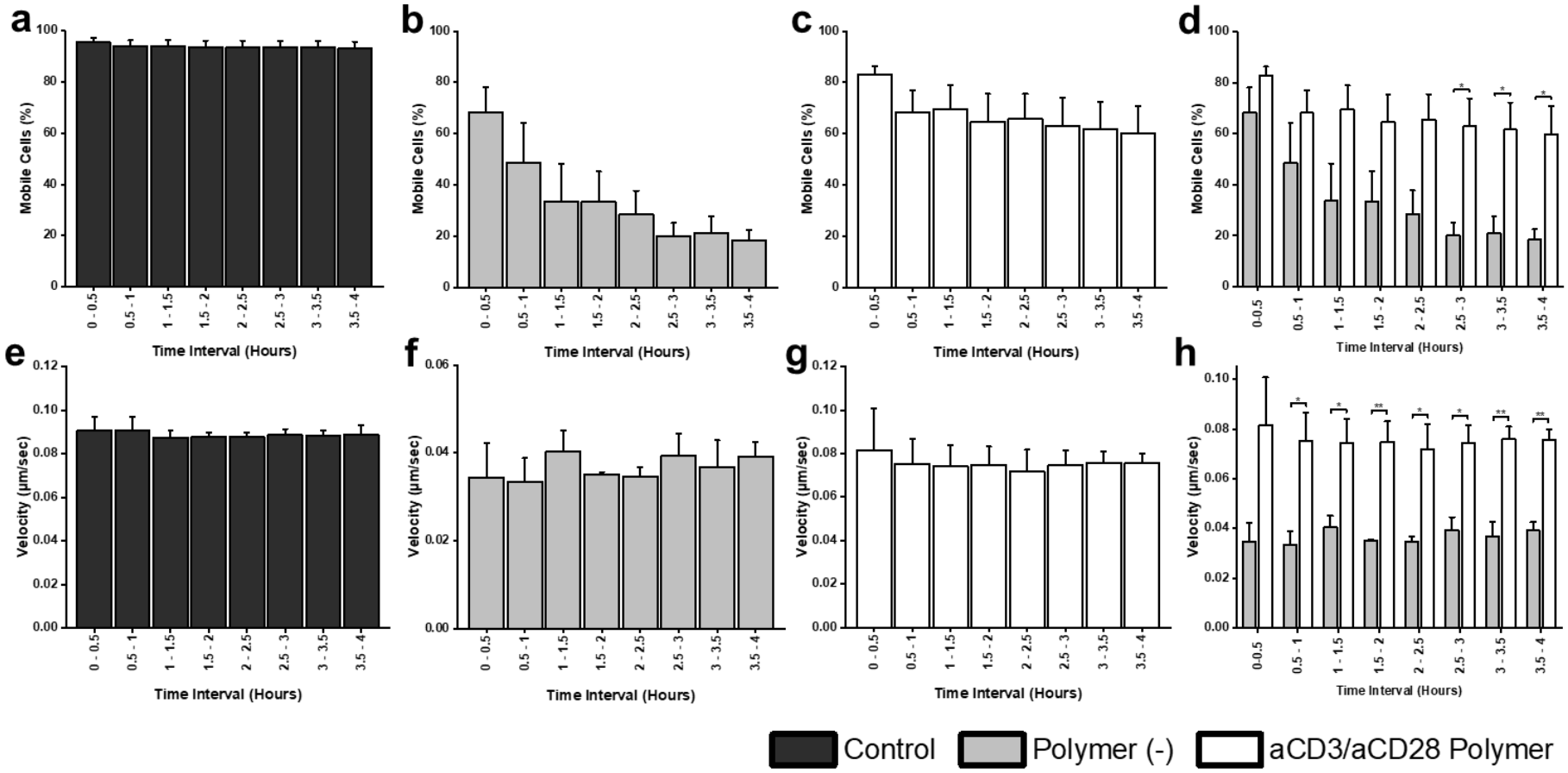

Figure 6.4. Percentage and velocity of mobile T-cells on Polymer B over 4 hours. Tow row (**a** - **d**) = Percentage of mobile cells. Bottom row (**e - h**) = Velocity of mobile cells. **a** and **e.** T-cells on the base of a polystyrene well plate (Control). **b.** T-cells on polymer B (Polymer (-)). **c.** T-cells on aCD3/aCD28 polymer B (aCD3/aCD28 Polymer) **d.** A comparison between Polymer (-) and aCD3/aCD28 Polymer. n = 3 per donor, for a total of 3 donors. Mean values are plotted. Error bars = ± 1SD. Significance was determined by a two-tailed T-test for **d** and **h.** * = $p \leq .050$. ** = $p \leq .010$.

Through the use of TrackMate, individual T-cells were tracked over each 30 minute interval. A representative visualisation of the resultant tracks are shown in **Figure 6.3**. T-cells cultured on polymer B displayed a decrease in the number and length of tracks compared to when cultured on a polystyrene base (control). Polymer (-) displayed the most small length displacement tracks at both time points, with many cells appearing stationary by 3 – 3.5 hours (**Figures 6.3c** and **d**). T-cells cultured on aCD3/aCD28 polymer B also appeared to reduce in mobility from 1 – 1.5 hours to 3 – 3.5 hours (**Figures 6.3e** and **f**). However, tracks remained comparatively greater in length and appeared to show directionality when compared to those on polymer (-).

T-cell displacement tracks were further analysed to give the percentage and velocity of mobile cells (**Figure 6.4**). The greatest percentage of mobile cells was found with the control, ranging from 95.6 to 93.2 % and remaining stable over the 4 hours (**Figure 6.4a**). As was inferred from the track displacement images, T-cells cultured on polymer (-) displayed a comparative decrease of 27.3 % at 0 – 0.5 hours. The percentage of mobile cells on polymer (-) decreased as time progressed, from 68.3 % at 0 – 0.5 hours to 7.9 % at 3.5 – 4 hours (**Figure 6.4b**). T-cells cultured on aCD3/aCD28 polymer B displayed a smaller decrease (12.6 %) of mobile cells compared to the control. The percentage of mobile cells slowly declined over the 4 hours from 83.0 to 60.0 % (**Figure 6.4c**).

Similarly as with the percentage of mobile cells, control T-cells displayed the greatest velocity which remained stable over 4 hours, ranging from 0.091 to 0.088 µm/sec (**Figure 6.4e**). Comparatively, mobile T-cells on polymer (-) were observed to have a lower velocity ranging from 0.040 – 0.033 µm/sec (**Figure 6.4f**). Mobile T-cells on aCD3/aCD28 polymer B displayed a range in velocity of 0.082 – 0.072 µm/sec (**Figure 6.4g**).

To assess the impact of aCD3 and aCD28 on polymer B on the migration of T-cells, direct comparisons between polymer (-) and aCD3/aCD28 polymer were made in **Figures 6.4d** and **h**. From **Figure 6.4d** it can be seen that in regards to mobile cells, a decline was observed with both conditions, however, the percentage of mobile cells decreased at a faster rate with polymer (-). T-cells on aCD3/aCD28 polymer displayed a consistently higher percentage of mobile cells, with the difference increasing as time progressed and becoming significant from 2.5 – 3 hours onwards. By 3.5 – 4 hours, T-cells on aCD3/aCD28 polymer were 41.4 % more mobile than on polymer (-). **Figure 6.4h** showed that not only were T-cells on aCD3/aCD28 polymer more mobile, but that these mobile cells migrated at a higher velocity. Velocity was found to be significantly increased by 0.042 - 0.033 µm/sec from 0.5 – 1 hours onwards with aCD3/aCD28 polymer.

It has previously been reported that surface stiffness impacts the velocity of migrating T-cells, with an increase in velocity observed on a stiffer substrate (Saitakis *et al*., 2017; Majedi *et al*., 2020). Although stiffness was not quantified here it is apparent that the polystyrene surface used as the control was stiffer than the polymer B hydrogel, and therefore the findings here are concurrent with those studies. It was anticipated that T-cells that interacted with polymer B without aCD3/aCD28 would display a migration pattern of T-cells in search of antigen, maintaining a high level of movement in a sub-diffusive or diffusive pattern, with speed fluctuations (Krummel *et al*., 2016). Fluctuations in velocity were observed, however these were much smaller than the fluctuations of ~0.03 to 0.3 µm/sec of T-cells migrating within a lymph node reported by Miller *et al.* (2002). Furthermore, T-cells on polymer (-) displayed a large quantity of migratory arrest, with the percentage of mobile T-cells dropping to 7.9 %. Due to this and the low

level of movement of mobile cells within each 30 minute segment, it was not possible to infer the type of T-cell migration occurring.

Though it was expected that interacting with polymer (-) would result in a decrease in velocity, it was not expected that the majority of cells would cease migration completely. One possible explanation for this may lie in the chemistry of the polymer itself. Research into functionalised self-assembled monolayers (SAMs) has demonstrated that surfaces with –COOH terminal groups promote adhesion in numerous mammalian cells (Lee *et al*., 1994; Arima and Iwata, 2007; Li *et al*., 2015). As polymer B pre-antibody attachment contains many free –COOH, this will likely have influenced the adhesion of T-cells. This is further supported through the comparative increase in mobility and velocity of T-cells observed on aCD3/aCD28 polymer B, where the only difference between materials is that -COOH groups have been utilised to attach antibodies via NH3. Moreover, Arima and Iwata (2015) found that –COOH SAMs adsorbed attachment promoting proteins, fibronectin and vitronectin, from culture media additive FBS. As fibronectin has been demonstrated to increase T-cell binding (Krivacic and Levine., 2003) and T-cell integrin chain αV is able to bind to vitronectin (Kim., 2014) , it is plausible that these interactions also impeded T-cell mobility on polymer (-) due to the addition of FBS to culture medium.

As T-cell activation is known to induce migratory arrest (Dustin *et al.,* 1997), T-cells on aCD3/aCD28 polymer B were anticipated to display a large number of non-mobile cells. A decrease of ~30 % mobile T-cells over 4 hours compared to the control was indeed observed. However, it was not possible to confidently deduce whether the reduction in mobile T-cells was due to interaction and activation by aCD3 and aCD28, or if other factors, such as those discussed with polymer (-), may be responsible.

Whilst investigating the interaction of T-cells and dendritic cells (DCs) within a 3D scaffold, Steponavicius-Cruz *et al*. (2013) demonstrated that T-cells that were in contact with activated DCs displayed an increase in velocity. In this present study, T-cells on aCD3/aCD28 polymer displayed a consistent increase in the velocity of mobile cells compared to polymer (-), suggesting that T-cells may in fact have been stimulated by the attached aCD3/aCD28. Additionally, T-cells tracks (**Figure 6.3g**) were found to be most characteristic of Lévy type super-diffusion on aCD3/aCD28 polymer, indicating antigen search. The serial encounter model of T-cell activation proposes that multiple transient and dynamic interactions with antigen, known as kinapses, can eventually results in T-cell activation (Friedl and Gunzer, 2001), particularly in environments of low ligand density (Henrickson *et al*., 2008). Moreover, upon suboptimal stimulation, T-cells continue to migrate, adopting a local scanning behaviour (Moreau *et al*., 2015).

6.3.3. Expansion of Primary T-cells on a Polymer B Surface

Previously it was demonstrated that it was possible for cell line Jurkat T-cells to proliferate on a polymer B surface (**Section 5.3.6**). To further validate this for primary T-cells and explore the impact polymer B may have on their expansion, primary sourced human T-cells were stimulated to proliferate and cultured on polymer B. Stimulation was achieved through either the addition of Dynabeads or TransAct prior to exposure to polymer B. Cultures in 96-well plates were set up within an Incucyte live cell imager and imaged at 2 hour intervals for 7.5 days. Resultant images were then processed and analysed for confluency using the Incucyte analysis software, as described in **Method 2.2.3.2**. Control cultures contained unstimulated T-cells without polymer (Control), unstimulated T-cells with polymer (Polymer (-)), Dynabead stimulated T-cells without polymer (Dynabeads), or TransAct stimulated T-cells without polymer (TransAct).

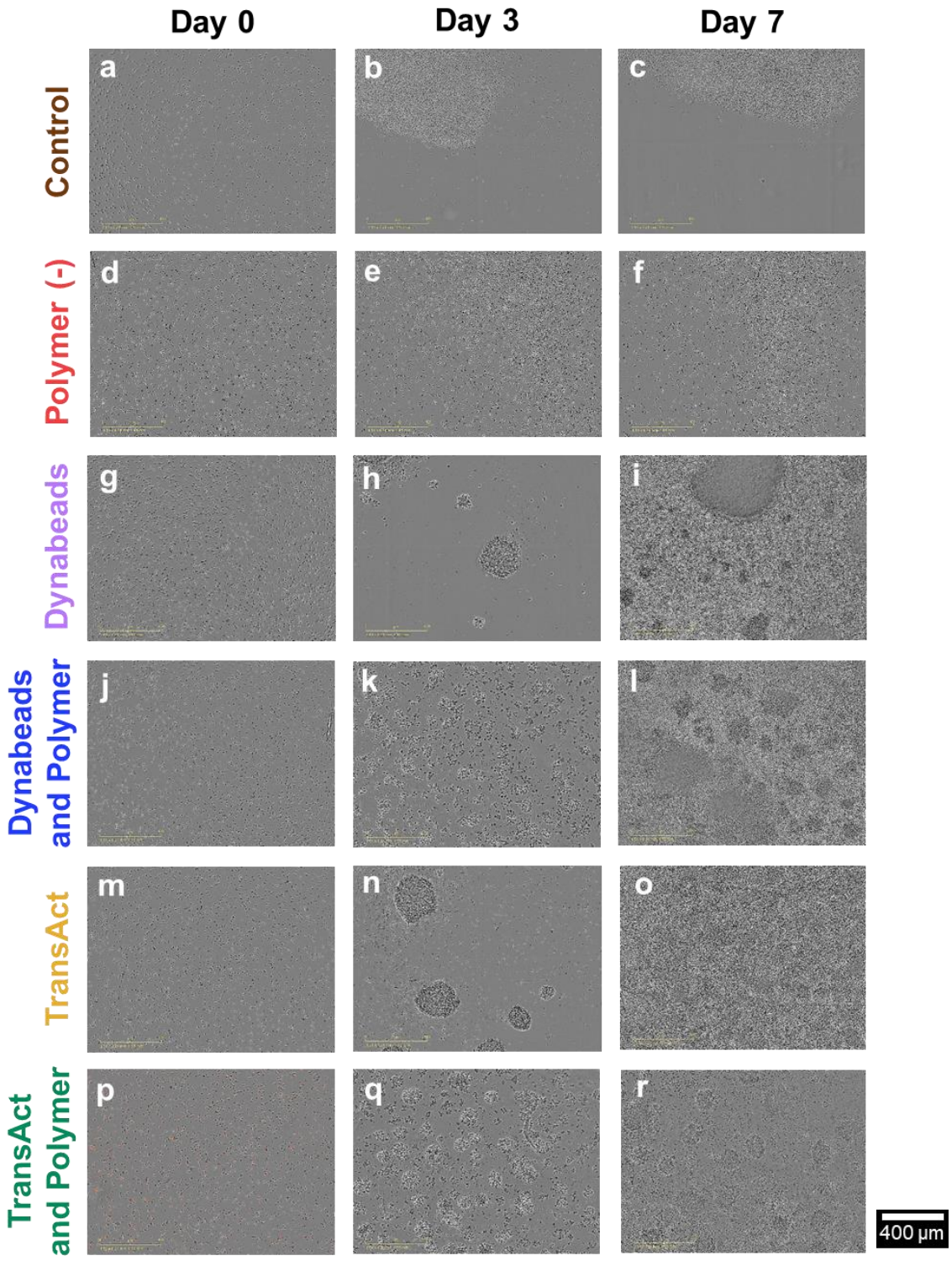

Figure 6.5. Confocal images of T-cells expanding on a polymer B surface taken via an Incucyte® live cell imaging system over 7.5 days. a. b. and **c.** Unstimulated T-cells cultured with no addition (Control). **d. e.** and **f.** Unstimulated T-cells cultured on polymer B (Polymer (-)). **g. h.** and **i.** Dynabead® stimulated T-cells (Dynabeads). **j. k.** and **l.** Dynabead® stimulated T-cells cultured on polymer B (Dynabeads and Polymer). **m. n.** and **o.** TransAct™ stimulated T-cells (TransAct). **p. q.** and **r.** TransAct™ stimulated T-cells cultured on polymer B (TransAct and Polymer). Left column (**a. d. g. j. m.** and **p.**) = Day 0. Centre column (**b. e. h. k. n.** and **q.**) = Day 3. Right column (**c. f. i. l. o.** and **r.**) = Day 7. Images are representative of a minimum of 2 donors with a minimum of 2 replicates each. Scale bar = 400 µm.

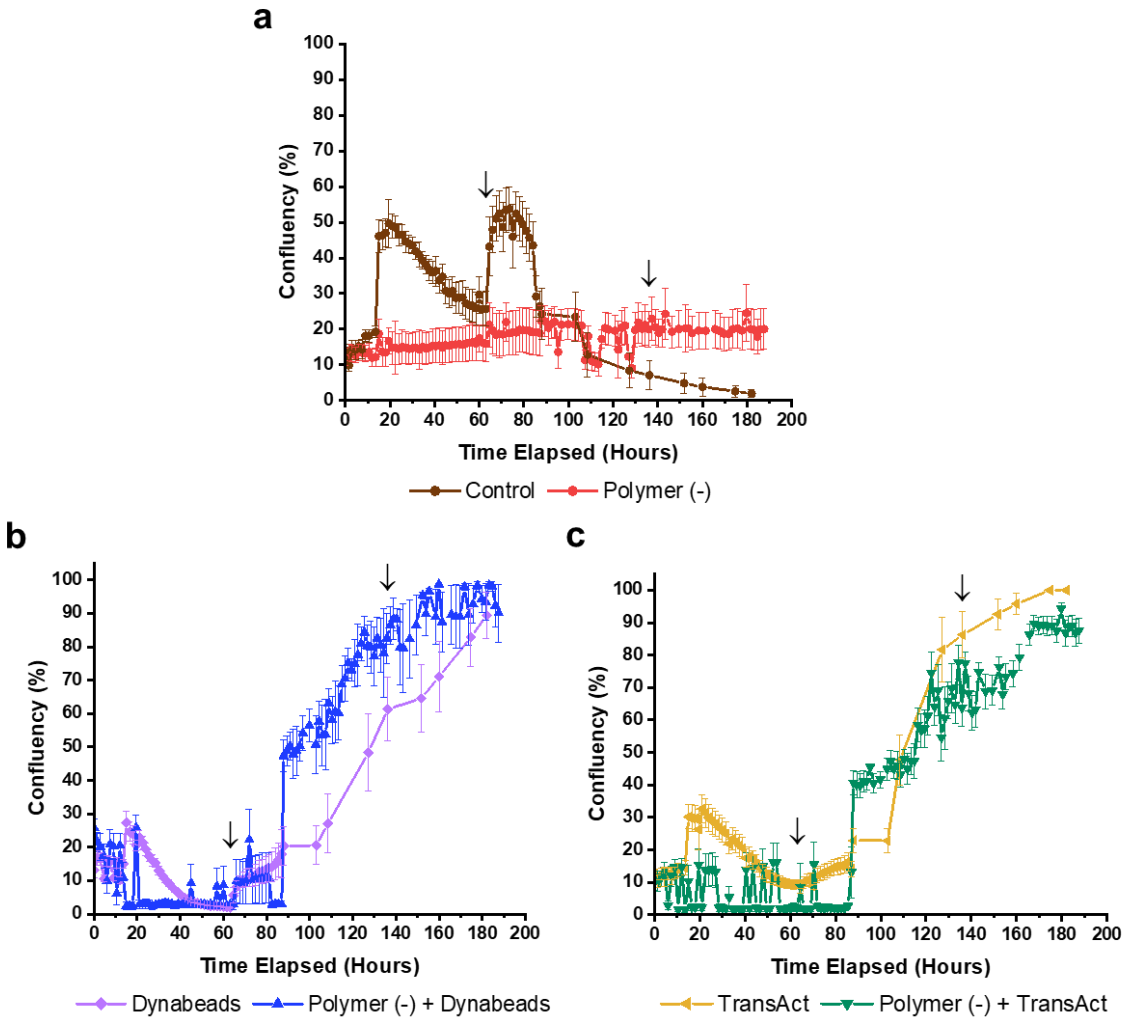

Figure 6.6. Confluency analysis of T-cells cultured on polymer B measured using an IncuCyte live cell imaging system. a. Unstimulated T-cells cultured with no addition (Control) or on polymer B (Polymer (-)). **b.** T-cells stimulated with Dynabeads®, cultured with polymer B (Polymer (-) + Dynabeads), and without (Dynabeads). **c.** T-cells stimulated with TransAct™, cultured with polymer B (Polymer (-) + TransAct) and without (TransAct). ↓ indicates media addition. n = minimum of 2 donors with a minimum of 2 replicates each. Mean values are plotted. Error bars = ± 1SE.

Figure 6.5 displays representative images of T-cells in culture over the experimental time course. T-cells in control and polymer (-) cultures (**Figures 6.5a** - **f**) are observed as single cell suspensions over the 7.5 days. The main difference was that T-cells on polymer (-) remained more evenly distributed over images, whereas T-cells in the control appeared to gather together over time – notably towards the edges of the well plate. All stimulated T-cell cultures (**Figures 6.5g** - **r**) displayed characteristic activated T-cell culture morphology, with single

cells at day 0 and the formation of clusters from day 3 onwards. As with control and polymer (-), stimulated T-cell cultures cultured on polymer B displayed a more even distribution of cells, this was most clearly observed on day 3.

Subsequent confluency analysis of images are displayed in **Figure 6.6**. Confluency in control cultures (**Figure 6.6a**) increased from 13.9 % at 0 hours to 49.6 % at 20 hours, followed by a decline until 63 hours (25.7 %) and then another increase to the maximum confluency of 63.7 % at 74 hours. Post 74 hours, confluency declined, reaching a minimum of 1.9 % at 182 hours. In contrast, the confluency of polymer (-) cultures (**Figure 6.6a**) remained largely stable, increasing marginally from 12.3 % at 0 hours to 20.0 % at 188 hours.

Both Dynabeads and TransAct displayed similar patterns of confluency (**Figures 6.6b** and **c**); an increase in confluency from 0 hours to ~20 hours followed by a decline until ~65 hours and a subsequent continuous increase until the end of the study. Dynabeads reached a final maximum culture confluency of 89.4 % and TransAct reached 100 %. Both polymer (-) + Dynabeads, and polymer (-) + TransAct also displayed similar patterns of confluency (**Figures 6.6b** and **c**). Pre-88 hours, an erratic low level of confluency varying from ~1.5 to ~20 % was observed. Post- 88 hours a sharp increase of 44.4 and 38.0 % with polymer with Dynabeads and TransAct, respectively, was displayed. Following this, both cultures continued to increase in confluency until the end of the study, with a maximum of 90.0 % for polymer (-) + Dynabeads, and 87.6 % for polymer (-) + TransAct.

It was expected that the confluency of control and polymer (-) would remain stable over the experiment, as T-cells were not stimulated and therefore would not be expected to be proliferating. Although polymer (-) displayed a comparatively small increase of 7.7 % confluency, the standard deviation of data points indicate that

it is likely not a true increase. Control cultures displayed the most surprising results, with confluency fluctuations throughout the experiment. This however, is highly likely due to the observation, previously mentioned and highlighted in **Figures 6.5a - c**, that T-cells gathered towards the edges of well plates over time. Confluency was measured as the percentage of well plate covered by cells in images, and only images taken from the centre of wells were analysed. Thus, the movement of cells out of the imaging frame skewed subsequent confluency analysis. This is further supported by the jump in confluency observed at 74 hours, post media addition (**Figure 6.6a**) which likely disturbed cells from the sides of wells and into the image frame. Moreover, it was observed in **Section 6.3.2** that culture of T-cells on polymer (-) drastically reduced their mobility which is why the same effect was not visible with T-cells in culture with polymer (-).

Stimulated T-cells in culture with polymer B reached high levels of confluency, and in the case of Dynabead stimulation, culture with polymer B resulted in an increased percentage confluency than without. These results confirm that the proliferation of primary human T-cells is supported on polymer B. However, due to limitations discussed below, it was not possible to confidently conclude whether the presence of polymer B in T-cell cultures truly impacted cell growth, positively in the case of Dynabeads or negatively with TransAct.

Here culture confluency was inferred through the coverage of the base of wells or polymer with T-cells. This however does not account for the reality that T-cells are non-adherent and can grow in suspension not only in the X- and Y- plane but also in the Z-plane - meaning that cultures defined by this method to be fully confluent may actually still be proliferating. Therefore, confluency measurements are limited and likely an overestimate of true culture confluency, particularly when the formation of 3D cell clusters occurs.

Another major limitation of this study was that the Incucyte live cell analyser was not optimised to take images in wells that contained an additional layer such as polymer B. This resulted in many images focusing on the base of the polymer where no cells were present. A significant improvement was found when wells with polymer were scheduled to be imaged separately from wells without polymer. However, two separate scans for the same well plate were unable to be scheduled. As a compromise, scans for wells without polymer were implemented manually post ~90 hours resulting in less detailed confluency curves. Additionally, images taken at the edges of the polymer skewed confluency measurements and had to be removed from analysis which reduced the size of the final data set.

6.4. Conclusion

Both porous and non-porous polymer B were investigated to characterise the interaction of T-cells with both. The following characteristics were evaluated: the ability of T-cells to be seeded into and removed from porous polymer B, the mobility of T-cells interacting with non-porous polymer B, and the ability of polymer B to be used as surface on which to expand primary human T-cells. Here the use of (-) denotes unaltered polymer, whereas aCD3/aCD28 polymer B refers to polymer B with aCD3 and aCD28 attached.

A high recovery of T-cells (97.3 %), passed once through porous polymer B (-), was demonstrated. Additionally, T-cells displayed a small decrease in viability of 1.7%. aCD3/aCD28 polymer B displayed similar results with 88 % cell recovery and a decrease in viability of 2 % following one pass through. With both formats of polymer, typically a continual decrease in cell recovery and viability was observed over 10 passes. This, however, was believed to have been impacted by the loss of cells through processing. The attachment of aCD3 and aCD28 to

polymer B was deemed overall to have no significant impact on either cell recovery or viability in this set up.

The mobility of T-cells on non-porous polymer B was evaluated through time-lapse confocal imaging of T-cells in culture with polymer B. Analysis of time-lapses revealed that T-cells on polymer B (-) reduced significantly in mobility from 68.3 to 7.9 % over 4 hours. Additionally, cells that were still mobile exhibited a decrease in velocity ranging from 0.040 – 0.033 µm/sec. Due to a lack of assessable tracks, classification of migration mode for polymer B (-) was not possible. Comparatively, aCD3/aCD28 polymer B cultures displayed significantly higher numbers of mobile T-cells (83.0 – 60.0 %) migrating at a significantly increased velocity (0.082 – 0.072 µm/sec). Furthermore, patterns of movement exhibited by T-cells suggested that cells migration could be characterised as Lévy type super-diffusion. This is of significance as it demonstrates that T-cell migratory patterns are consistent with those expected of an activated T-cell and indicates T-cell interaction with stimulating antibodies has occurred.

The validation of polymer B as a material on which primary human T-cells can expand was undertaken through the external activation of T-cells, using Dynabeads or TranAct, and culture on polymer B (-). Cultures were assessed using an Incucyte live cell imaging system to assess the growth of T-cells by evaluating culture confluency. High confluency was achieved with both Dynabeads (90.0 %) and TransAct (87.6 %) stimulated T-cells expanded on polymer B (-). This strongly supports that polymer B is a suitable surface on which primary T-cells can expand. It was also anticipated that this study would allow the determination of the impact of culture on polymer B on T-cell growth, if any. However, limitations in both equipment calibration and methodology rendered any conclusions in this regard unreliable.

Chapter 7. T-cell Activation and Expansion with Polymer B

7.1. Introduction

Confirmation of antibody attachment, demonstration of seeding and removal of T-cells, and the ability of primary T-cells to expand when cultured on polymer B, strongly suggest that polymer B is a suitable material for use as a T-cell activating scaffold.

In this chapter the ability of both non-porous and porous polymer B with aCD3 and aCD28 attached to activate and expand T-cells is investigated; focusing on a characterisation of expansion and an analysis of the resultant T-cell populations.

7.1.1. T-cell Activation and Expansion

Previously, T-cell activation was introduced in **Section 5.1.1**. As a key aim of this project is to establish a material that is capable of activating T-cells, it was fundamentally important to demonstrate the activation of T-cells with polymer B with aCD3 and aCD28 attached. T-cell activation was assessed through the following outputs: cell proliferation, cell diameter, culture morphology, expression of activation markers CD69 and CD25, and metabolic profile. In these studies, particular emphasis is placed on expansion as an important output of activation as this is a crucial step in the production of T-cell therapies.

7.1.2. Expansion Characterisation

Further to assessing the activation status of T-cells, it was also important to begin initial characterisation of the expansion process using polymer B. T-cell cultures stimulated with non-porous polymer B were evaluated in regards to: fold

expansion, viability, phenotypic composition, expression of exhaustion markers LAG-3 and PD-1, cell cycle status, and early-stage proliferation of $CD4^+$ and $CD8^+$ T-cells. T-cell cultures stimulated with porous polymer B were evaluated in regards to: fold expansion, viability, phenotypic composition, cell cycle status, apoptosis, IFNγ production, and metabolite consumption and production. Additionally, T-cell expansions with polymer B were directly compared to cultures stimulated with the current industrial gold standard, Dynabeads. Cultures were expanded for 14 days to best observe the expansion effect and to most closely mimic the expansion timeline of clinical manufacture.

7.1.2. T-cell Populations

The two main populations of T-cells are classified through the expression of CD4 and CD8. $CD4^+$ T-cells are known as helper T-cells, with their main roles being the recognition of MHC class-II peptide and the secretion of cytokines which are instrumental in a number of outputs - such as cell recruitment, inflammation, and immune response suppression (Luckheeram *et al*., 2012). $CD8^+$ T-cells are known as cytotoxic T-cells, with their main role being the direct targeting and killing of infected cells (Pennock *et* al., 2013). Prior to activation, both $CD4^+$ and $CD8^+$ T-cells exist in a non-dividing resting state, however, when T-cells are activated and commence proliferation, they begin a process of maturation and differentiation to a further multitude of different subsets. Ex-vivo, the resultant composition of phenotypes of expanded T-cells has been demonstrated to be impacted by multiple environmental factors, including substrate stiffness (Harrison *et al*., 2019).

In this study, a simplified version of these subsets is identified: T_N, T_{CM}, T_{EM}, T_{EMRA}. These were classified through the absence and presence of markers CCR7 and CD45RO. Previously, T_N and T_{CM} have been found to play an essential

role in the persistence of CAR T-cells in vivo (Gattinoni *et al*., 2012; Busch *et al*., 2016); thereby highlighting the importance of characterising the phenotypic composition of T-cells expanded with polymer B when considering use in T-cell therapy processes.

7.2. Aims and hypotheses

7.2.1. Chapter Aims

- To demonstrate the ability of aCD3/aCD28 polymer B, in both a non-porous and porous format, to activate and expand primary human T-cells,
- To characterise T-cell expansion with aCD3/aCD28 polymer B.
- To investigate the impact of expansion with aCD3/aCD28 polymer B on the resultant populations of T-cells.
- To compare expansion with aCD3/aCD28 polymer B with expansion via Dynabeads.
- To visualise T-cell growth on aCD3/aCD28 polymer B.

7.2.2. Hypotheses

It is hypothesised that T-cells will be activated by polymer B with aCD3 and aCD28 attached, in both a non-porous and porous (scaffold) format. It is expected that this successful activation will result in the expansion of T-cells. Due to material differences in methods, it is anticipated that activation with polymer B will result in a change in the final phenotypic composition of T-cells when compared to cultures activated with Dynabeads. It is also hypothesised that T-cells expanded with aCD3/aCD28 polymer may display a less exhausted phenotype than with Dynabeads, possibly due to reduced TCR stimulation with antibodies presented on the polymer in comparison to multiple beads interacting with a single cell. Further, it is expected that z-stack fluorescent confocal microscopy

can be used effectively to visualise, in 3D, the interaction and growth of T-cells activated with porous polymer B.

7.3. Results

7.3.1. Activation and Expansion with Non-porous Polymer B

Primary human T-cells isolated from whole blood were suspended in complete RPMI media supplemented with 1 % Antibiotic-Antimycotic (v/v) and 30 IU/mL rIL-2, seeded into wells, and stimulated with either non-porous polymer B with aCD3/aCD28 attached (aCD3/aCD28 polymer), or Dynabeads (Dynabeads) and cultured for 14 days. Unstimulated T-cell cultures with (polymer (-)) and without (control (-)) the presence of non-porous polymer B without antibodies attached were used as negative controls. Dynabead stimulated cultures served as both a positive control and a comparison. Cultures were imaged via confocal microscope over the course the culture. T-cells were harvested at time points of 0 days, 3 days, 5 days, 7, days, 10 days, and 14 days, and assessed for cell count, viability, and cell diameter. At time points of 0 days, 3 days, 7 days, and 14 days, T-cells were also subject to the analysis of activation marker expression. At day 14, end point analysis also included phenotype characterisation, exhaustion marker expression, and cell cycle analysis. Further details of this method can be found in **Method 2.2.4.1**.

Additionally, a semi-quantitative ELISA was developed to allow a comparison between the amount of aCD3 and aCD28 antibodies presented by aCD3/aCD28 polymer and Dynabeads in cultures.

7.3.1.1. Culture morphology

Figures 7.1a - **h** show confocal images of T-cells stimulated with non-porous aCD3/aCD28 polymer B over 14 days. Negative control cultures are shown in

Appendix H.1. From day 3, the formation of small T-cell aggregates was observed over the surface of the polymer. Both the number and size of observable clusters continued to increase over the remainder of the culture, with aggregates also forming at the edges of the polymer disc. Comparatively, T-cell cultures stimulated with aCD3/aCD28 polymer displayed the formation of clusters at a later time point than Dynabeads (**Figures 7.1i** - **p**). Additionally, they appeared to be smaller in size and more evenly dispersed throughout the well.

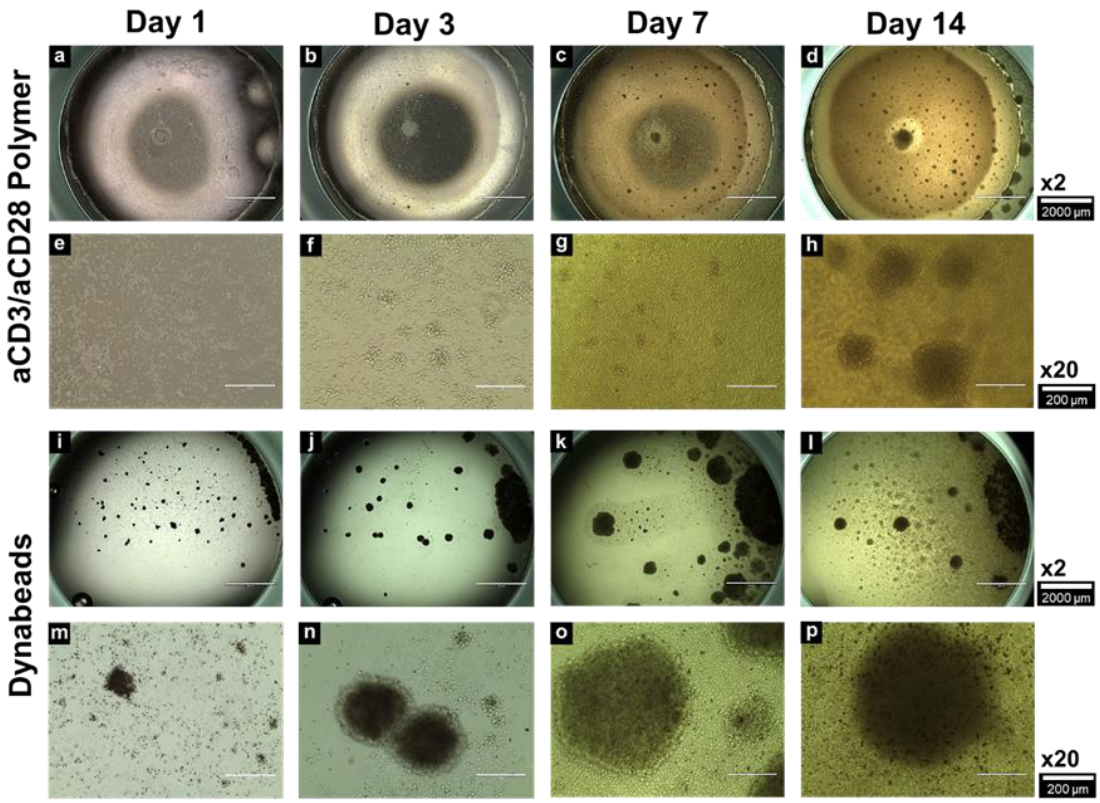

Figure 7.1. Confocal images showing the culture morphology of T-cells stimulated with non-porous aCD3/aCD28 polymer B over 14 days. Cultures stimulated with non-porous polymer B with aCD3 and aCD28 attached (aCD3/aCD28 polymer) imaged at x2 (**a - d.** Scale bars = 2,000 µm), and x20 (**e - h.** Scale bars = 200 µm). Cultures stimulated with Dynabeads® (Dynabeads) imaged at x2 (**j - l.** Scale bars = 2,000 µm), and x20 (**m - p.** Scale bars = 200 µm). Images are representative of n = 3 independent experiments for 3 donors, with 3 replicates each.

7.3.1.2. Expansion, Culture Viability, and Cell Diameter

Figure 7.2a and **b** display the growth dynamics and overall fold expansion of T-cell cultures. The total T-cell count in cultures stimulated with aCD3/aCD28 polymer increased from 5.2 x 10^5 to 4.3 x 10^6, representing an 8.3-fold expansion. This was a small increase when compared to the fold expansion displayed by cultures stimulated with Dynabeads (7.8-fold). With both negative controls, control (-) and polymer (-), an expansion of 2.9 and 2.2 –fold respectively, was observed, with an increase in cell number visible from day 7 – 14. Fold expansion was found to be significantly increased with aCD3/aCD28 polymer when compared to both negative controls, and not significantly different when compared to Dynabeads.

Growth dynamics were found to be comparable between aCD3/aCD28 polymer B and Dynabeads, with both displaying growth from day 0. However, some minor differences were noted. Dynabead stimulation resulted in a significantly higher cell count on day 5. **Figure 7.2a** shows that this growth remains linear by day 14 with aCD3/aCD28 polymer, whereas with Dynabeads growth appeared to slow. Error bars, however, indicate that this may in fact not be the case.

Figure 7.2c displays that from day 0 to 5, the viability of T-cell cultures stimulated with aCD3/aCD28 polymer decreased by 6 %, from 97.7 to 91.7 %, before gradually increasing again to 93.0 % by day 14. The greatest decrease in viability was observed with Dynabeads, with a reduction of 18.7 %, from 97.7 to 79.0 % viability from day 0 to 7. This was followed by an increase, resulting in a viability of 88.9 % on day 14.

The cell diameter (**Figure 7.2d**) of T-cells stimulated with aCD3/aCD28 polymer was observed to fluctuate slightly over the course of the study; increasing from

8.7 µm (day 0) to 10.7 µm (day 5), decreasing to 10.0 µm (day 7), increasing back to the peak level of 10.9 µm on day 10. T-cells from Dynabeads cultures displayed the largest cell diameter of 12.5 µm on day 3, which gradually reduced to 11.4 µm on day 10 to 14. Overall, the cell diameter of T-cells stimulated by aCD3/aCD28 polymer remained larger than both negative controls, and smaller than T-cells stimulated by Dynabeads, at every point.

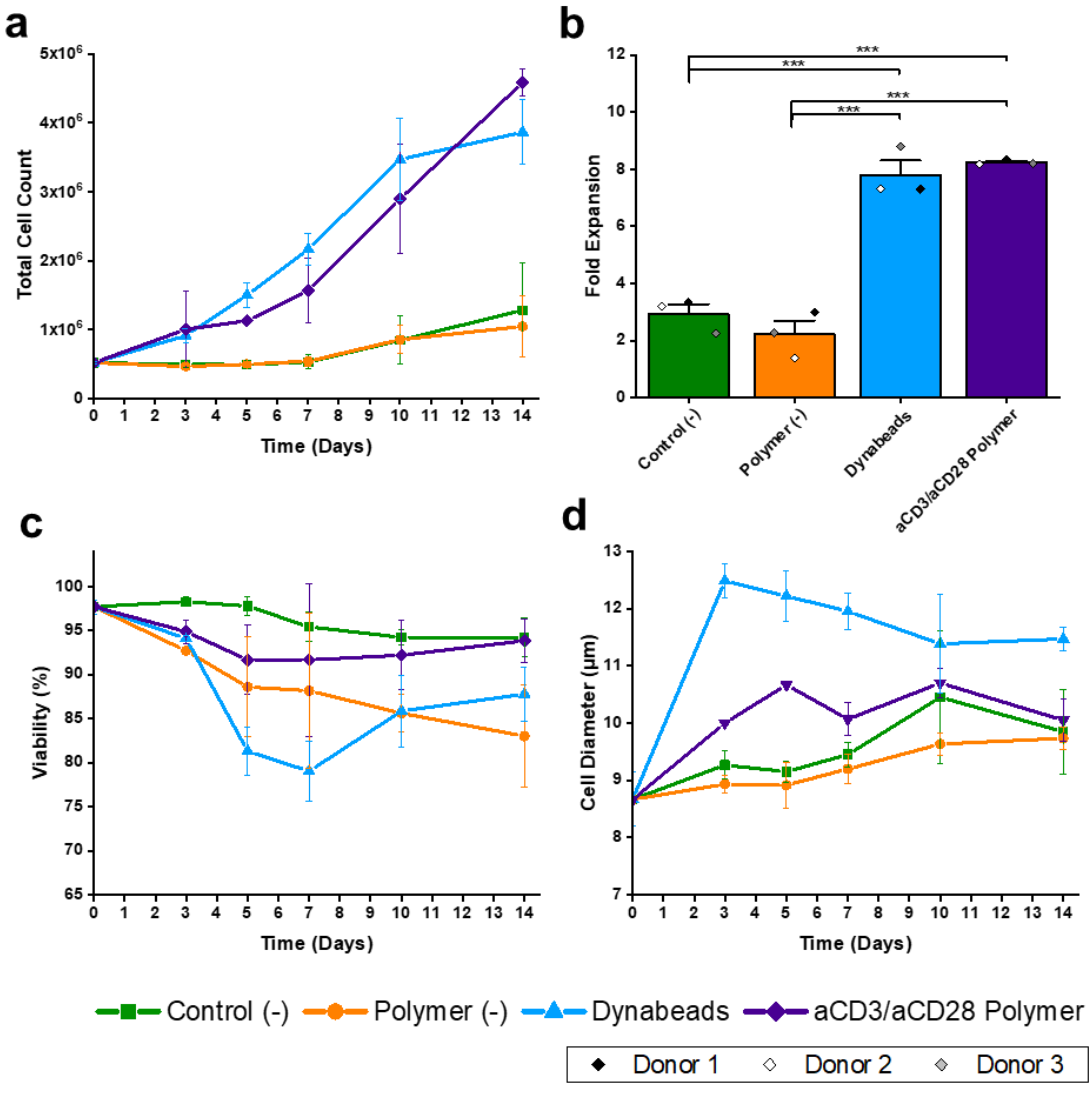

Figure 7.2. Culture dynamics of T-cells stimulated with aCD3/aCD28 non-porous polymer B over 14 days. **a.** Total cell count. **b.** Fold expansion on day 14. **c.** Viability. **d.** Cell diameter. Mean values are plotted; error bars = ± 1SD for all graphs. **a, c,** and **d.** n = 3 independent experiments with 3 donors; days 0 – 10 = 2 replicates each; day 14 = 5 replicates. **b.** n = 3 donors, with 5 replicates each. *p*-values were determined by a one-way ANOVA with a post hoc Tukey's test. *** = $p \leq .001$.

7.3.1.3. Activation Marker Expression

Through the application of the gating strategy shown in **Figure 7.3a**, percentages of CD69 and CD25 expressing T-cells were identified and quantified over the 14 day culture. Representative scatter graphs, and unstained and isotype controls are shown in **Appendices F.4** and **E.3**. **Figures 7.3b - e** shows the expression profiles of CD69 and CD25 obtained from cultures. At day 0 the majority of T-cells (86.8 %) were $CD69^{-}CD25^{-}$, negligible T-cells were $CD69^{+}CD25^{-}$ (0.9 %) or $CD69^{+}CD25^{+}$ (0.2 %), and 12.1 % of T-cells were $CD69^{-}CD25^{+}$. T-cells stimulated with aCD3/aCD28 polymer (**Figure 7.3e**) displayed an increase in $CD69^{+}CD25^{-}$ (8.2 %), $CD69^{+}CD25^{+}$ (19.0 %), and $CD69^{-}CD25^{+}$ (25.0 %) T-cells on day 3. The percentage of $CD69^{+}CD25^{-}$ T-cells reduced to 3.4 % at day 7 and increased again a peak of 10.0 % at day 14. Double positive $CD69^{+}CD25^{+}$ T-cells decreased from day 3, to 4.9 % on day 7, followed by a marginal increase to 6.4 % on day 14. The percentage of $CD69^{-}CD25^{+}$ T-cells peaked at 31.5 % on day 7, and reduced to 20.1% on day 14.

Cultures stimulated with Dynabeads (**Figure 7.3d**) displayed a high expression of both $CD69^{+}CD25^{+}$ and $CD69^{-}CD25^{+}$ from day 1, with their combined total accounting for 97.0 % and 97.1 % of T-cells on day 3 and day 7, respectively. By day 14 this percentage had dropped considerably, with double negative $CD69^{-}CD25^{-}$ observed as the dominant expression type (56.9 %).

When both activation markers were examined separately (**Figures 7.3f** and **g**), it was observed that stimulation with aCD3/aCD28 polymer resulted in a significant increase in the percentage of CD69 expressing T-cells on day 3 (27.4 %), and of CD25 expressing T-cells on day 3 (44.0 %) and 7 (36.4 %), when compared to both negative controls. At day 3 and 7 the percentage of both CD69 and CD25

expressing T-cells was found to be significantly lower than when stimulated with Dynabeads. On day 14, no significant differences were observed.

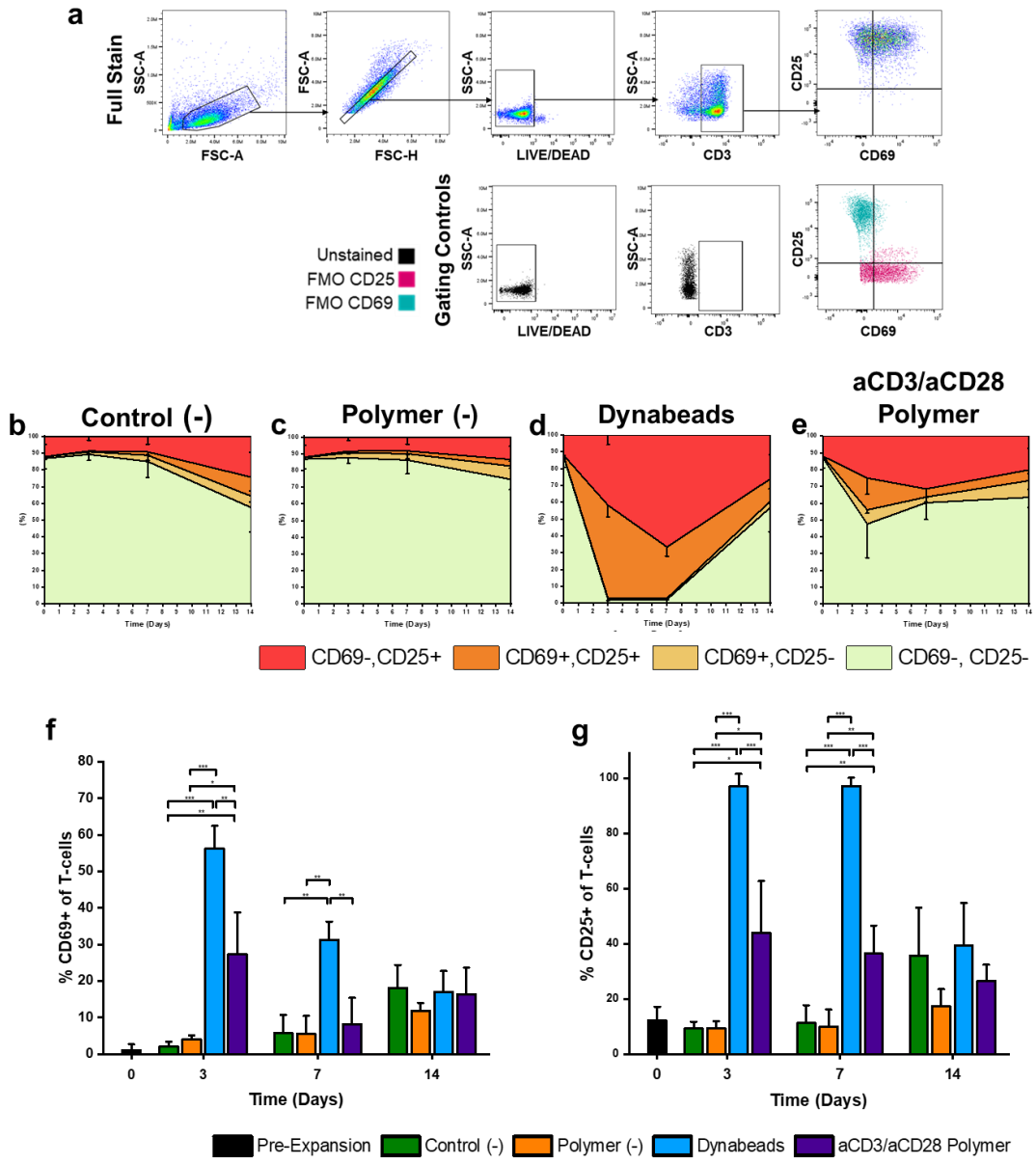

Figure 7.3. Expression of activation markers CD69 and CD25 by T-cells stimulated with aCD3/aCD28 non-porous polymer B over 14 days. a. Flow cytometry gating strategy applied to identify CD69 and CD25 expressing T-cells. **b – e.** CD69 and CD25 expression profiles of **b.** unstimulated T-cells (Control (-)), **c.** T-cells cultured on polymer B without antibody (Polymer (-), **d.** T-cells stimulated with Dynabeads®, or **e.** T-cells stimulated with polymer B with aCD3 and aCD28 attached (aCD3/aCD28 Polymer). Separated expression of **h.** CD69, and **g.** CD25. n = 3 independent experiments with 3 donors, with 2 replicates each. Mean values are plotted. Error bars = ± 1SD. *p*-values were determined by a one-way ANOVA with a post hoc Tukey's test. * = $p \leq .050$. ** = $p \leq .010$. *** = $p \leq .001$.

7.3.1.4. Phenotypic Characterisation

To identify and classify the phenotypic composition of T-cell cultures, the flow cytometry gating strategy shown in **Figure 7.4** was applied. The first classification of T-cells analysed was the percentage of $CD4^+$ and $CD8^+$ T-cells, this is displayed as the ratio of CD4:CD8 in **Figure 7.5**. Secondly, $CD4^+$ and $CD8^+$ T-cells were separately classified into naïve (N) ($CCR7^+$, $CD45RO^-$), central memory (CM) ($CCR7^+$, $CD4RO^+$), effector memory (EM) ($CCR7^-$, $CD45RO^+$), or effector memory terminally differentiated (EMRA) ($CCR7^-$,$CD45RO^-$), these are displayed in **Figures 7.6** and **7.7**. Representative scatter graphs, and unstained and isotype controls are shown in **Appendices F.5** and **E.4**.

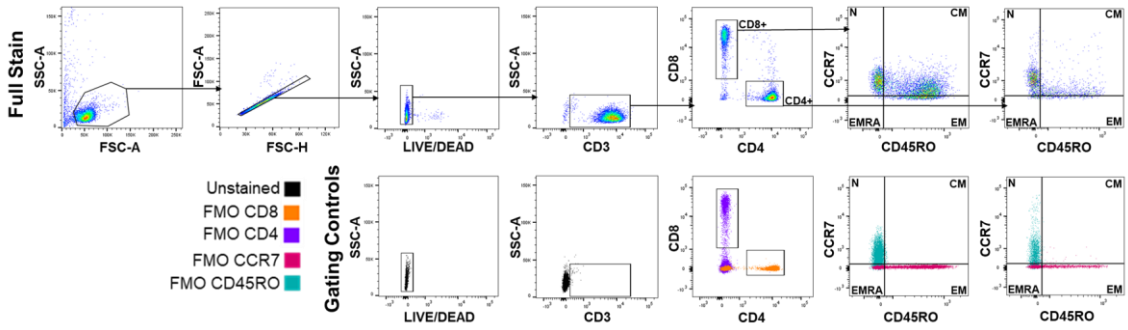

Figure 7.4. Flow cytometry gating strategy applied to identify subsets of T-cells. The first classification of T-cells was $CD4^+$ or $CD8^+$. These were then further classified into naïve (N) ($CCR7^+CD45RO^-$), central memory (CM) ($CCR7^+CD4RO^-$), effector memory (EM) ($CCR7^-$, $CD45RO^+$), or effector memory terminally differentiated (EMRA) ($CCR7^-CD45RO^-$).

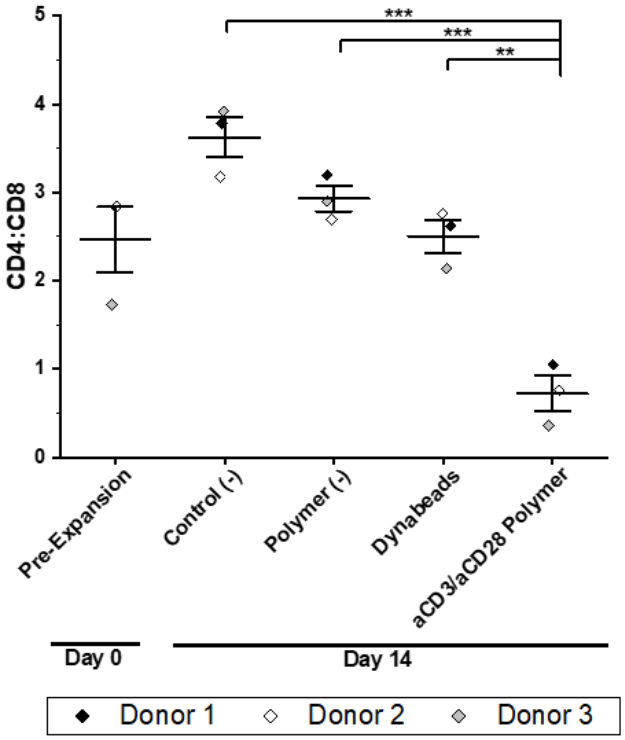

Figure 7.5. Ratio of CD4⁺ to CD8⁺ T-cells expanded with aCD3/aCD28 non-porous polymer B. T-cells were cultured for 14 days. Pre-Expansion = T-cells on day 0. Control (-) = unstimulated T-cells. Polymer (-) = T-cells cultured on polymer B without antibody. Dynabeads = T-cells stimulated with Dynabeads®. aCD3/aCD28 Polymer = T-cells stimulated with polymer B with aCD3 and aCD28 attached. n = 3 independent experiments for 3 donors, with 3 replicates each. Mean values are plotted. Error bars = ± 1SD. *p*-values of day 14 data were determined by a one-way ANOVA with a post hoc Tukey's test. * = $p \leq .050$. ** = $p \leq .010$. *** = $p \leq .001$.

On day 14, for T-cell cultures expanded with aCD3/aCD28 polymer, a mean CD4:CD8 ratio of 0.72 was observed (**Figure 7.5**). T-cells expanded with Dynabeads exhibited a CD4:CD8 ratio of 2.5. These ratios were found to be significantly different ($p \leq .010$).

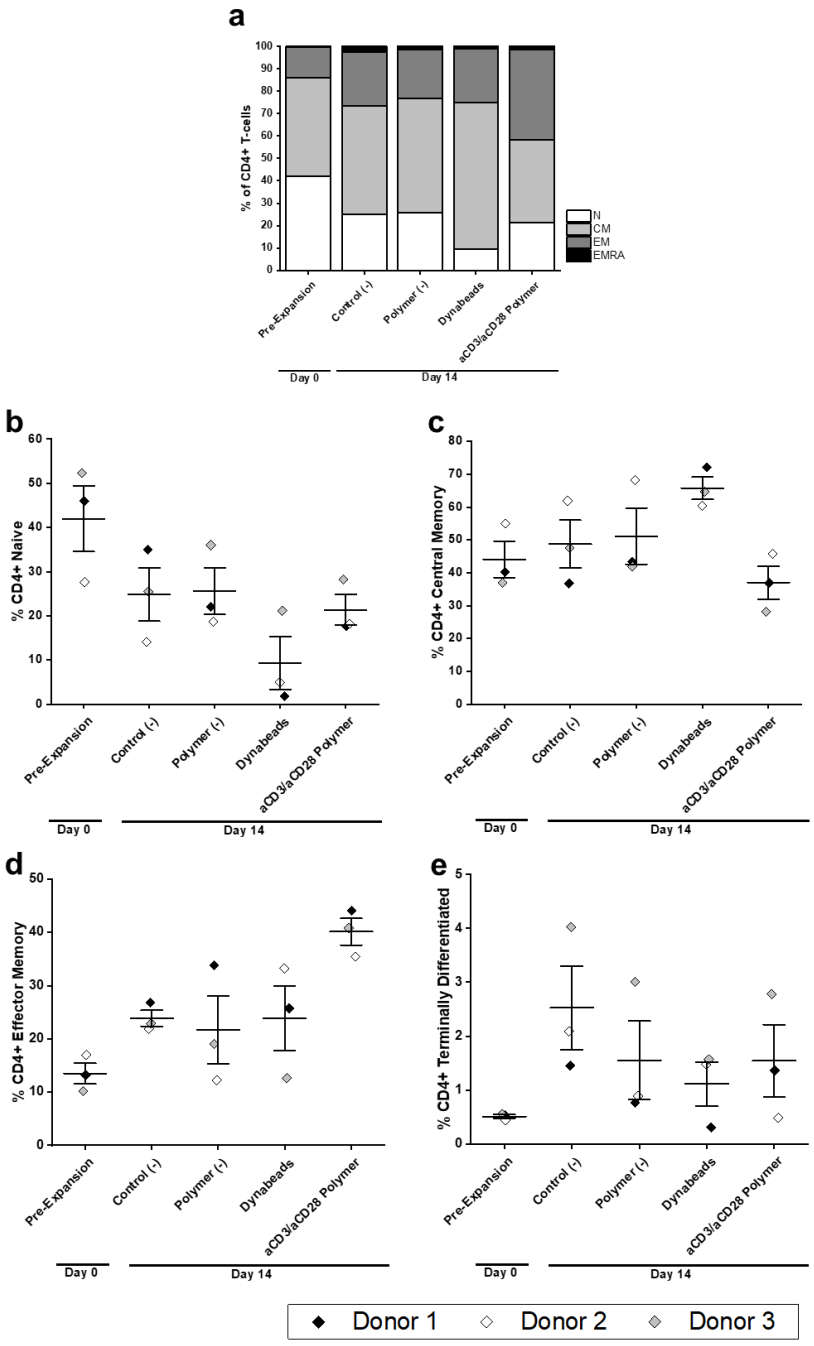

Figure 7.6. Phenotypic analysis of CD4⁺ T-cells expanded with non-porous aCD3/aCD28 polymer B. T-cells were cultured for 14 days. **a.** Whole population breakdown of CD4⁺ T-cells. N = naïve; CM = central memory; EM = effector memory; EMRA = effector memory terminally differentiated. Individual comparisons of **b.** naïve, **c.** central memory, **d.** effector memory, and **e.** effector memory terminally differentiated. Pre-Expansion = T-cells on day 0. Control (-) = unstimulated T-cells. Polymer (-) = T-cells cultured on polymer B without antibody. Dynabeads = T-cells stimulated with Dynabeads®. aCD3/aCD28 Polymer = T-cells stimulated with polymer B with aCD3 and aCD28 attached. n = 3 independent experiments for 3 donors, with 3 replicates each. Mean values are plotted. Error bars = ± 1SD. Day 14 data were assessed by a one-way ANOVA, no significant ($p \leq .050$) *p*-values were obtained.

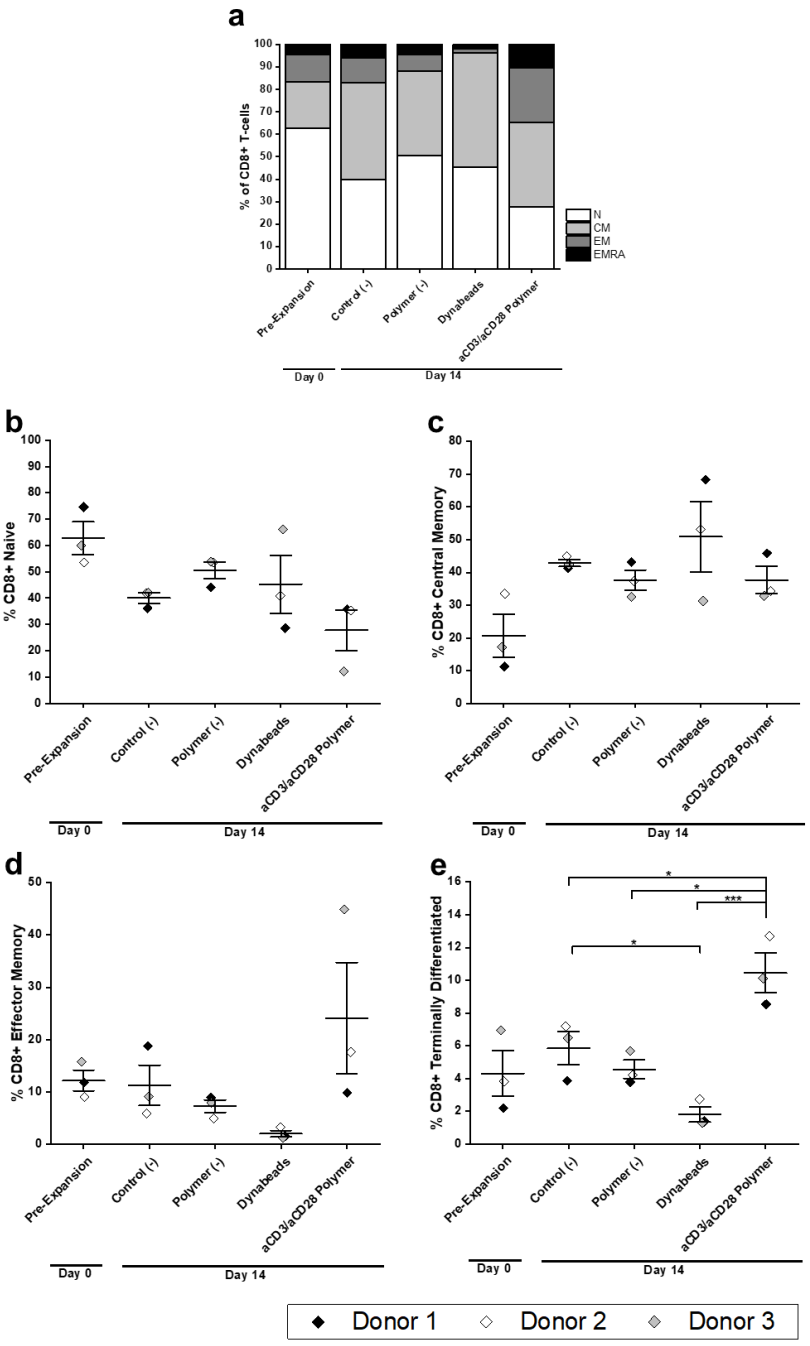

Figure 7.7. Phenotypic analysis of CD8⁺ T-cells expanded with non-porous aCD3/aCD28 polymer B. T-cells were cultured for 14 days. **a.** Whole population breakdown of CD8⁺ T-cells. N = naïve; CM = central memory; EM = effector memory; EMRA = effector memory terminally differentiated. Individual comparisons of **b.** naïve, **c.** central memory, **d.** effector memory, and **e.** effector memory terminally differentiated. Pre-Expansion = T-cells on day 0. Control (-) = unstimulated T-cells. Polymer (-) = T-cells cultured on polymer B without antibody. Dynabeads = T-cells stimulated with Dynabeads®. aCD3/aCD28 Polymer = T-cells stimulated with polymer B with aCD3 and aCD28 attached. n = 3 independent experiments for 3 donors, with 3 replicates each. Mean values are plotted. Error bars = ± 1SD. *p*-values of day 14 data were determined by a one-way ANOVA with a post hoc Tukey's test. * = $p \leq .050$. *** = $p \leq .001$.

Figure 7.6 shows that within the $CD4^+$ subset of T-cells, T_{EM} (40.1 %) was the dominant phenotype of T-cells stimulated with aCD3/aCD28 polymer, followed closely by T_{CM} (37.0 %). Dynabead stimulated cultured displayed a more evident dominance of T_{CM} (65.7 %), seconded by T_{EM} (23.9 %). Both negative controls displayed similar phenotypic distributions with a decrease of ~17.0 % T_N, and a shift towards T_{CM} and T_{EM} with increases of 4.7 – 10.4 %, resulting in a majority of T_{CM} at day 14. aCD3/aCD28 polymer maintained an increased percentage of T_N (21.4 %) compared to Dynabeads (9.3 %). Differences between $CD4^+$ subsets were not found to be statistically significant.

Figure 7.7 shows that within the $CD8^+$ subset of T-cells, T_{CM} (37.7 %) was observed to be the dominant phenotype of aCD3/aCD28 polymer expanded cultures. This was seconded by T_N (27.7 %), and then T_{EM} (24.1 %). Dynabeads cultures displayed a similar composition, where T_{CM} (50.9 %) was also the dominant phenotype, followed by T_N (45.2 %). Both negative controls displayed a reduction in T_N from day 0 to 14, decreasing from 62.7 % to 40.0 % (Control (-)), and 50.5 % (Polymer (-)). T_N remained the dominant phenotype with polymer (-), whereas with Control (-) this became T_{CM} at 42.9%.

Comparatively, within the $CD4^+$ subset of T-cells, cultures stimulated with aCD3/aCD28 Polymer resulted in a 12.1 % increase of T_N, 28.7 % decrease of T_{CM}, 16.3 % increase of T_{EM}, and a 0.4 % increase of T_{EMRA}, than when simulated with Dynabeads. Within the $CD8^+$ subset of T-cells, aCD3/aCD28 polymer expanded cultures were observed to compose of 17.5 % less T_N, 13.2 % less T_{CM}, 22.1 % more T_{EM}, and 8.6 % more T_{EMRA}. The only difference found to be significant was in regards to $CD8^+$ T_{EMRA}.

7.3.1.5. Exhaustion Marker Expression

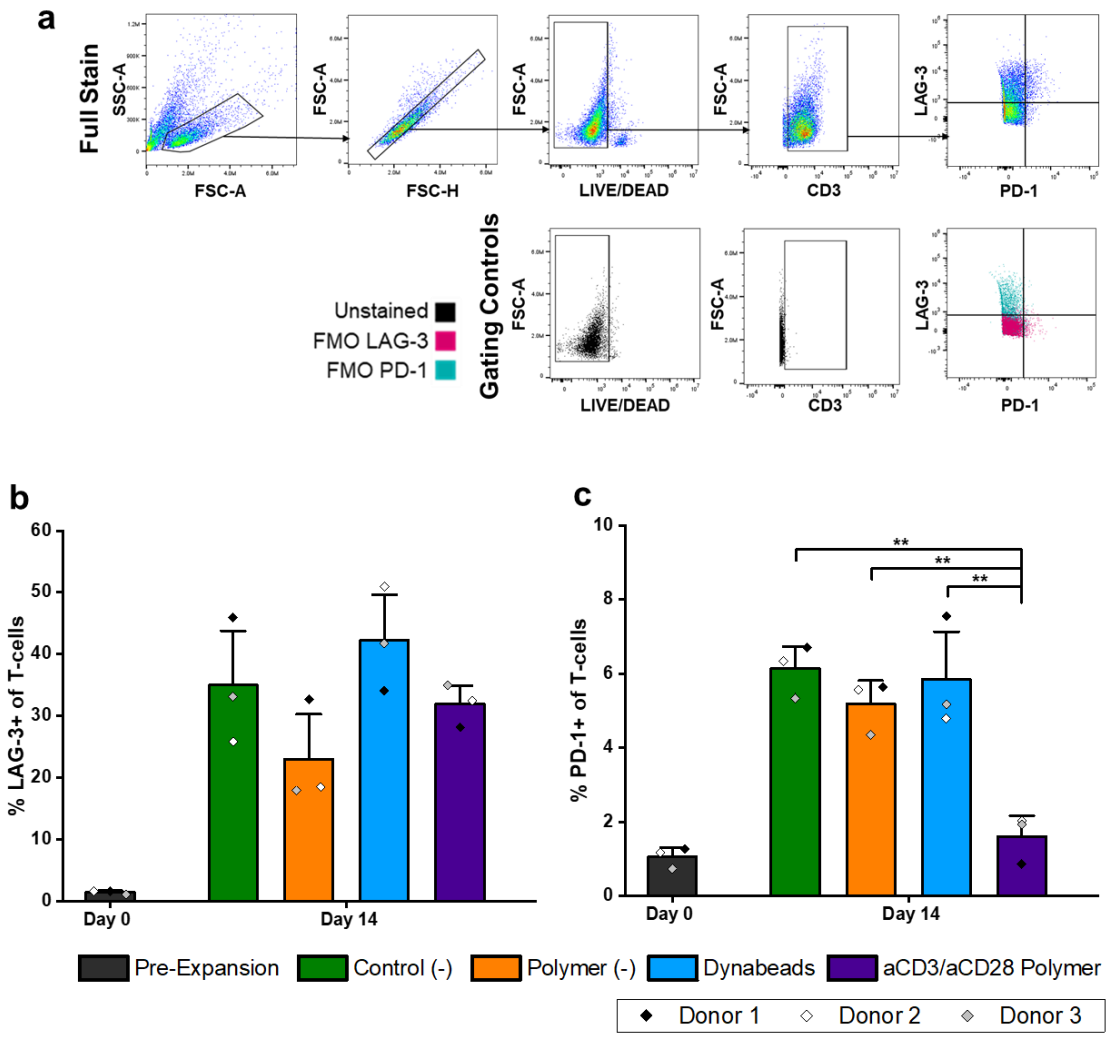

Figure 7.8. Expression of exhaustion markers LAG-3 and PD-1 by T-cells stimulated with aCD3/aCD28 non-porous polymer B for 14 days. T-cells were cultured for 14 days. **a.** Flow cytometry gating strategy applied to identify LAG-3 and PD-1 expressing T-cells. Quantified expression of **b.** LAG-3 and **c.** PD-1. Pre-Expansion = T-cells on day 0. Control (-) = unstimulated T-cells. Polymer (-) = T-cells cultured on polymer B without antibody. Dynabeads = T-cells stimulated with Dynabeads®. aCD3/aCD28 Polymer = T-cells stimulated with polymer B with aCD3 and aCD28 attached. n = 3 independent experiments for 3 donors, with 3 replicates each. Mean values are plotted. Error bars = ± 1SD. *p*-values of day 14 data were determined by a one-way ANOVA with a post hoc Tukey's test. ** = $p \leq .010$. *** = $p \leq .001$.

The flow cytometry gating strategy in **Figure 7.8a** was applied to identify and quantify the percentages of LAG-3 and PD-1 expressing T-cells in cultures on day 14. Representative scatter graphs, and unstained and isotype controls are

shown in **Appendices F.6** and **E.5**. It was observed that the mean percentage of LAG-3$^+$ T-cells (**Figure 7.8b**) in cultures stimulated with aCD3/aCD28 Polymer was 31.9 %, representing an increase of 30.5 % from day 0. This was lower than both Dynabeads (42.3 %), and control (-) (35.0 %). Differences however, were not found to be statistically significant.

The mean percentage of PD-1$^+$ T-cells (**Figure 7.8c**) was observed to be 1.6 % in cultures expanded with aCD3/aCD28 Polymer, representing a small increase from day 0 of 0.6 %. Cultures stimulated with aCD3/aCD28 polymer displayed a statistically significant decrease in the percentage of PD-1$^+$ T-cells when comparted to all other culture conditions. When compared to cultures expanded with Dynabeads this was a difference of 3.6 %

7.3.1.6. Cell Cycle Analysis

Representative graphs for each culture condition were produced using data obtained from a NucleoCounter® NC-3000™ and are displayed in **Figure 7.9a**. From these graphs it can be seen that cells classified as being in the G0/G1 phase displayed the largest peak in all conditions.

Percentages of T-cells in each phase were quantified using FlowJo software and the quantities are displayed in **Figure 7.9b** as a percentage of the total T-cell population. On day 14 of T-cells expansion with aCD3/aCD28 polymer, the majority (63.6 %) were observed in G0/G1 phase. The second largest population was T-cells in sub-G1 phase (24.8 %), followed by T-cells in S phase (11.9 %). Cultures stimulated with Dynabeads also displayed a majority population of T-cells in G0/G1 phase (57.4 %), and the second largest population was S phase T-cells (24.0 %).

Through the exclusion of cells in sub-G1 phase, the amount of dividing T-cells expressed as a percentage of the live cell population was calculated (**Figure 7.9c**). aCD3/aCD28 polymer stimulated cultures displayed a mean of 16.9 % diving cells. This was observed to be 15.0 % lower than that of cultures stimulated with Dynabeads, and 6.9 % lower than control (-). Polymer (-) displayed the lowest percentage of diving cells at day 14 (14.1 %). The only significant difference was observed between polymer (-) and Dynabeads.

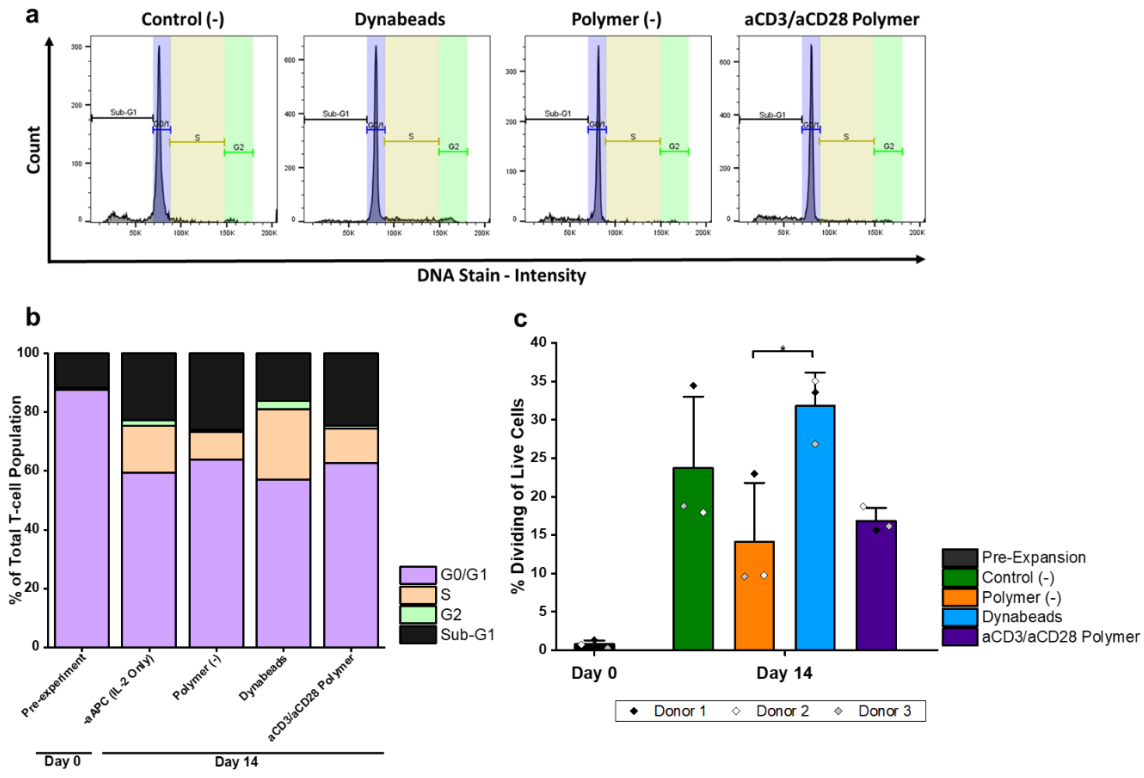

Figure 7.9. Cell cycle analysis of T-cells stimulated with aCD3/aCD28 non-porous polymer B for 14 days. a. Representative cell cycle analysis' – representative of 3 donors, with 3 replicates each. **b.** Total population breakdown of cell cycle phases. **c.** Quantification of dividing cells with non-viable cells excluded. Pre-Expansion = T-cells on day 0. Control (-) = unstimulated T-cells. Polymer (-) = T-cells cultured on polymer B without antibody. Dynabeads = T-cells stimulated with Dynabeads®. aCD3/aCD28 Polymer = T-cells stimulated with polymer B with aCD3 and aCD28 attached. n = 3 independent experiments for 3 donors, with 3 replicates each. Mean values are plotted. Error bars = ± 1SD. *p*-values of day 14 data were determined by a one-way ANOVA with a post hoc Tukey's test. * = $p \leq .050$.

7.3.1.7. Early-stage Proliferation

To investigate the early-stage proliferation of T-cells, cultures containing T-cells pre-stained with CFSE were set up in an identical manner to the above study. CFSE is an intracellular dye which fluorescently labelled cells. When labelled cells divide the fluorescence of the cell halves in intensity. This allows the identification of proliferating cells for up to ~8 generations of division by flow cytometry. Cultures were harvested on day 4 and further stained for CD8 and CD4 expression before being analysed for proliferation, as described in **Method 2.2.4.3**. Representative scatter graphs, and unstained and isotype controls are shown in **Appendices F.7** and **E.6**.

Proliferation data was used to generate descriptive indices using FlowJo software. Percentage divided refers to the percentage of cells that have undergone 1 or more divisions. The expansion index refers to the fold expansion of the entire cell culture. The replication index refers to the fold expansion of replicating cells only. The proliferation index refers to the average number of divisions of dividing cells only.

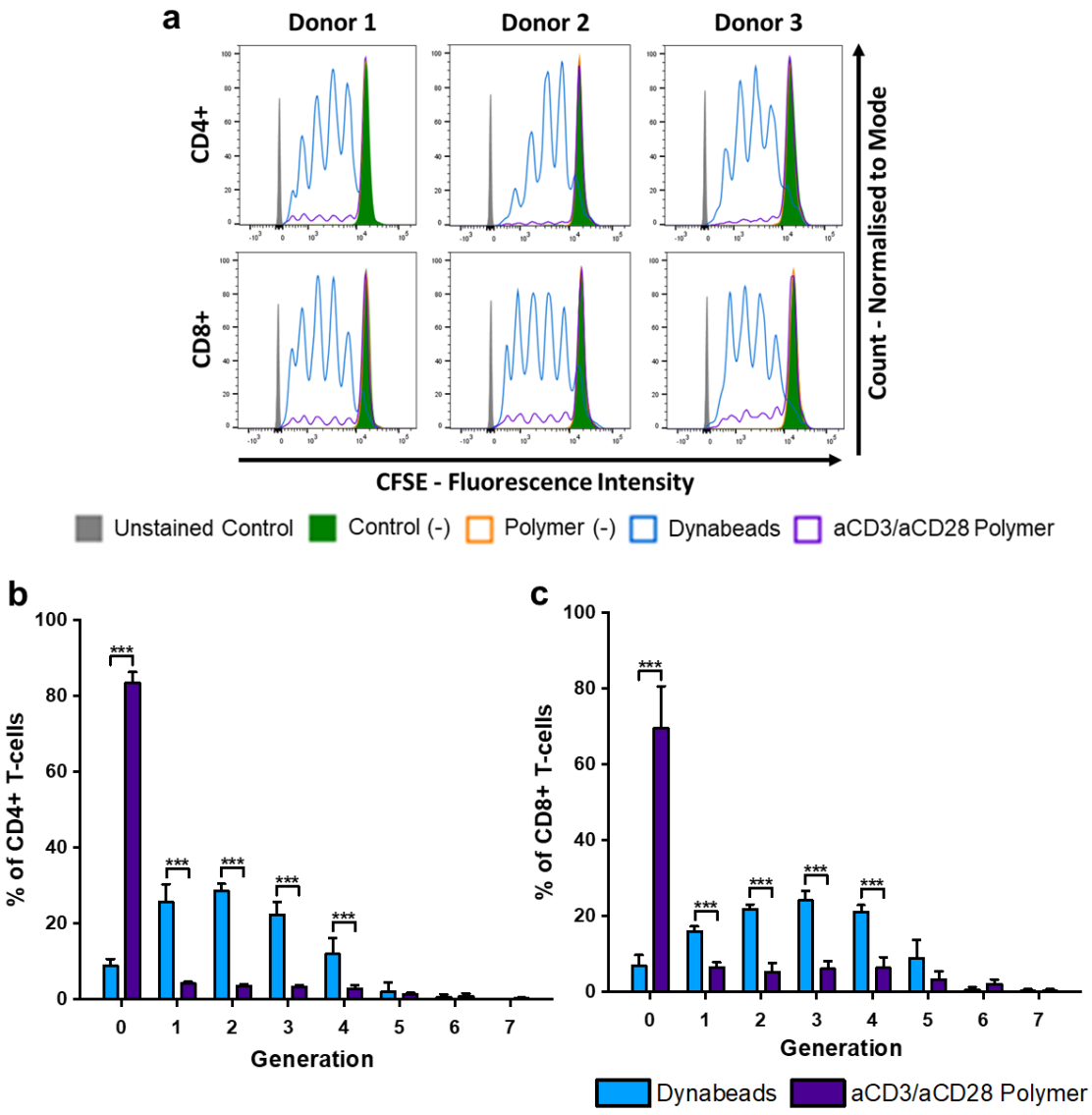

Figure 7.10. Early-stage proliferation analysis of CD4⁺ and CD8⁺ T-cells stimulated with aCD3/aCD28 non-porous polymer B for 4 days. a. Representative graphs showing the fluorescence intensity of T-cells stained with carboxyfluorescein succinimidyl ester (CFSE) for 3 donors. Top row = CD4⁺ T-cells. Bottom row = CD8⁺ T-cells. Graphs are representative of 3 replicates. Quantified comparison of **b.** CD4⁺ and **c.** CD8⁺ T-cells from Dynabeads or aCD3/aCD28 Polymer cultures. Control (-) = unstimulated T-cells. Polymer (-) = T-cells cultured on polymer B without antibody. Dynabeads = T-cells stimulated with Dynabeads®. aCD3/aCD28 Polymer = T-cells stimulated with polymer B with aCD3 and aCD28 attached. n = 3 independent experiments for 3 donors, with 3 replicates each. Mean values are plotted. Error bars = ± 1SD. *p*-values were determined by a two-tailed T-test. *** = $p \leq .001$.

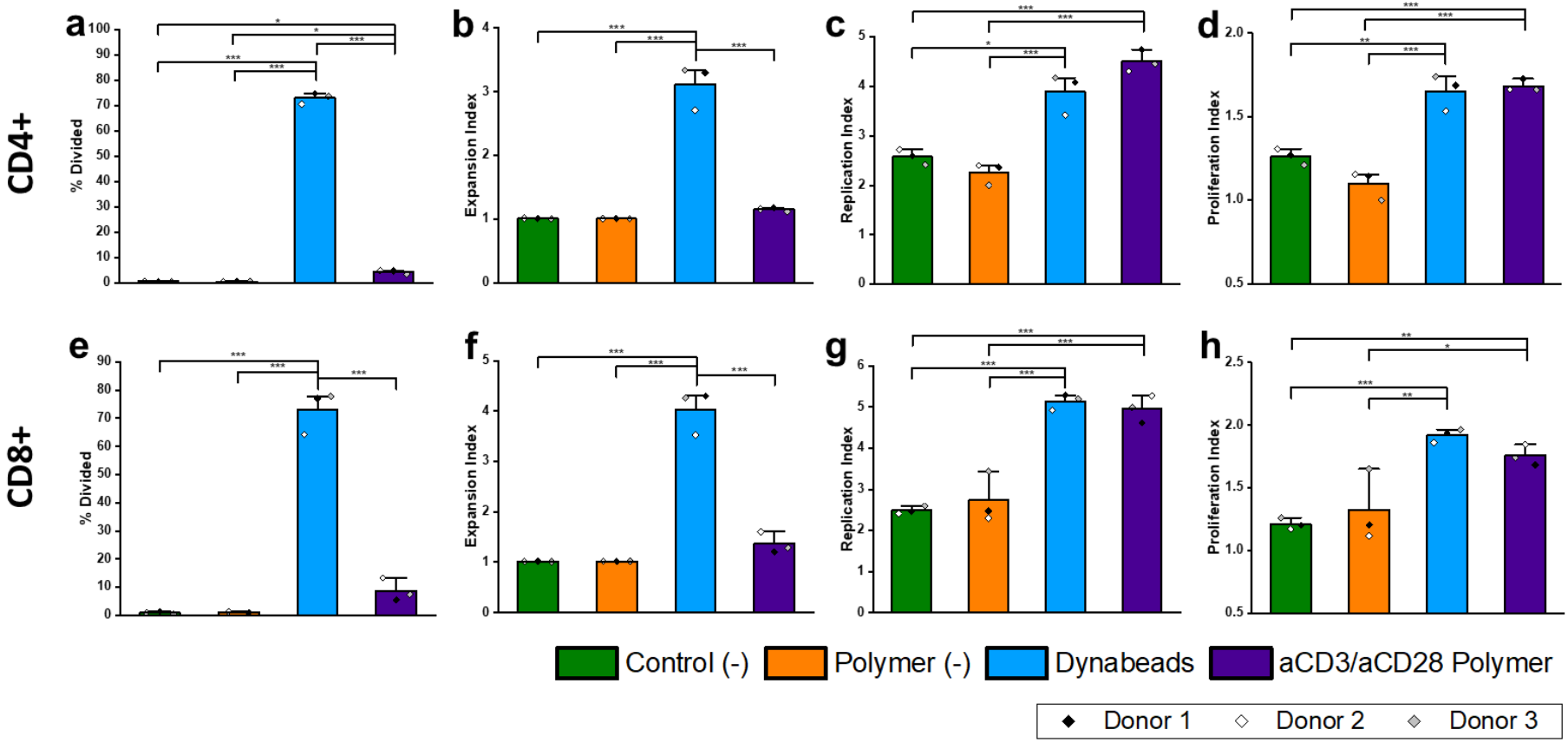

Figure 7.11. Percentage of divided cells, and expansion, proliferation, and replication indexes of CD4+ and CD8+ T-cells stimulated with aCD3/aCD28 non-porous polymer B for 4 days. Values were derived from CFSE analysis. Top row = $CD4^+$ T-cells. Bottom row = $CD8^+$ T-cells. Control (-) = unstimulated T-cells. Polymer (-) = T-cells cultured on polymer B without antibody. Dynabeads = T-cells stimulated with Dynabeads®. aCD3/aCD28 Polymer = T-cells stimulated with polymer B with aCD3 and aCD28 attached. n = 3 independent experiments for 3 donors, with 3 replicates each. Mean values are plotted. Error bars = ± 1SD. *p*-values were determined by a one-way ANOVA with a post hoc Tukey's test. * = $p \leq .050$. ** = $p \leq .010$. *** = $p \leq .001$.

$CD4^+$ and $CD8^+$ T-cells were identified using the same flow cytometry gating strategy displayed in **Figure 7.4**. CFSE fluorescence was used to analyse the proliferation of both populations 4 days post-activation (**Figure 7.10a**) which was then quantified using FlowJo software. From **Figure 7.10b** it can be seen that the majority (83.5 %) of $CD4^+$ T-cells stimulated by aCD3/aCD28 polymer were in generation 0 (Gen 0) (undivided). The percentage of T-cells in a generation > 0 was low and continually decreased as the generation number increased, from 4.2 % (Gen 1) to 0.3 % (Gen 7). Similar was observed for $CD8^+$ T-cells (**Figure 7.10c**), where the percentage of undivided T-cells was observed to be slightly lower than with $CD4^+$ T-cells (69.6 %) but was still the clear majority. Moreover, low values for T-cells in a generation > 0 were displayed and ranged from 0.2 to 6.5 %. A significant increase in the percentage of both $CD4^+$ and $CD8^+$ T-cells in Gen 1, 2, 3, and 4 was found when T-cells were stimulated with Dynabeads®.

Additional descriptive indices were extracted from the data using FlowJo software to further assess proliferation (**Figure 7.11**). $CD4^+$ T-cells stimulated with aCD3/aCD28 polymer were determined to be 4.3 % divided (**Figure 7.11a**), with an expansion index of 1.15 (**Figure 7.11b**), replication index of 4.5 (**Figure 7.11c**), and proliferation index of 1.68 (**Figure 7.11d**). $CD8^+$ T-cells stimulated with aCD3/aCD28 polymer were determined to be 8.4 % divided (**Figure 7.11e**), with an expansion index of 1.37 (**Figure 7.11f**), replication index of 4.96 (**Figure 7.11g**), and a proliferation index of 1.76 (**Figure 7.11h**).

With $CD4^+$ T-cells, a significant decrease of 68.7 % dividing cells and a significant decrease in expansion index value (2.7) was observed when compared to Dynabeads. Increases of 0.6 and 0.03 were also found with both the replication and proliferation indices respectively, however, these were not found to be statistically significant. With $CD8^+$ T-cells compared to Dynabeads, a significant

decrease of 64.3 % dividing cells, and a significant decrease in the expansion index (2.66) was highlighted. Comparative decreases of 0.2 were also noted in the replication and proliferation indices which were not determined to be statistically significant.

7.3.2.8. Comparison of Antibody Content

To allow a comparison between the antibody content of aCD3/aCD28 polymer and Dynabeads, an aCD3 and aCD28 ELISA was developed. Polymer discs equivalent to those in culture with T-cells were assayed alongside 5 x 10^5 or 5 x 10^4 Dynabeads. 5 x 10^5 was equivalent to the amount added to T-cell cultures to give a 1:1 bead to cell ratio. Further details on the method of the ELISA can be found in **Method 2.1.5.5**.

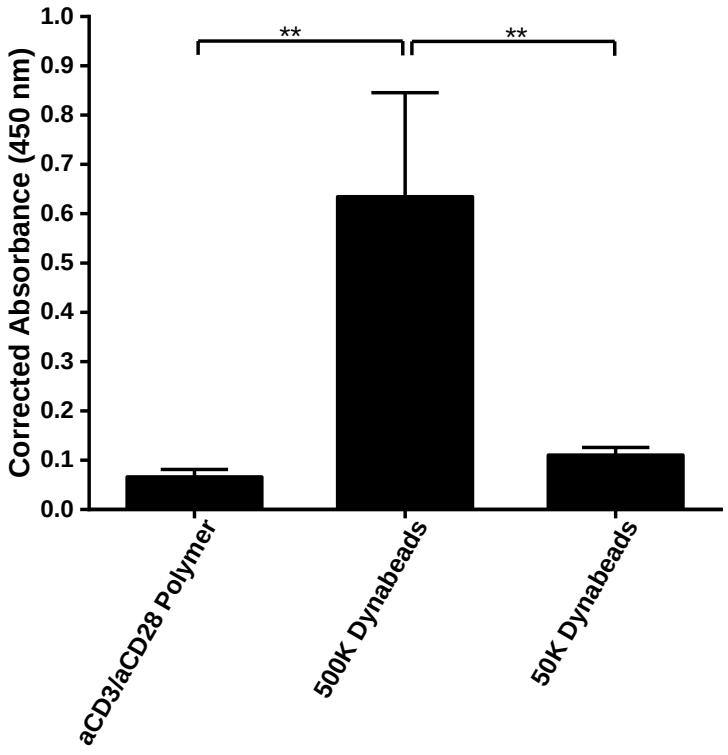

Figure 7.12. anti-CD3 and anti-CD28 ELISA with non-porous polymer B samples and Dynabeads. aCD3/aCD28 Polymer = non-porous polymer B with aCD3 and aCD28 attached. 500K Dynabeads = 5 x 10^5 Dynabeads®. 50K Dynabeads = 5 x 10^4 Dynabeads®. All results have been adjusted using the negative controls to account for background. n = 1 with triplicates. Error bars = ± 1SD. *p*-values were determined by a 1-way ANOVA with post-hoc Tukey's test. ** = $p \leq .010$.

It was observed that aCD3/aCD28 polymer displayed a significantly lower absorbance than 5 x 10^5 Dynabeads, 0.07 compared to 0.63. 5 x 10^4 Dynabeads displayed a mean absorbance of 0.11 which was not found to be significantly different to aCD3/aCD28 polymer.

7.3.2. Activation and Expansion with Porous Polymer B Scaffold

To demonstrate the feasibility of also using polymer B in a scaffold format to active and expand T-cells, 5 x 10^5 primary human T-cells were cultured with porous polymer B with aCD3 and aCD28 attached (aCD3/aCD28 scaffold) within a well plate insert for 14 days. Unstimulated T-cell cultures without polymer were used as the negative control (control (-)). Dynabead stimulated cultures (Dynabeads) served as both a positive control and a comparison. Additionally, T-cells were stimulated with Dynabeads® and cultured with porous polymer B without antibody attached (Dynabeads + scaffold) to investigate the impact of the presence of the scaffold alone. Over the course of the study, spent media was collected on days 0, 3, 5, 7, 9, 11, and 13 and was assessed for glucose, glutamine, lactate, and ammonia production. Additionally, media samples taken over all days was pooled and subject to an IFNγ ELISA to determine IFNγ production. T-cells on day 0 or harvested on day 14 were subject to: cell count, culture viability, cell diameter, phenotypic characterisation, cell cycle analysis, and an apoptosis assay. Further details can be found in **Method 2.2.4.3**.

7.3.2.1. Expansion, Culture Viability, and Cell Diameter

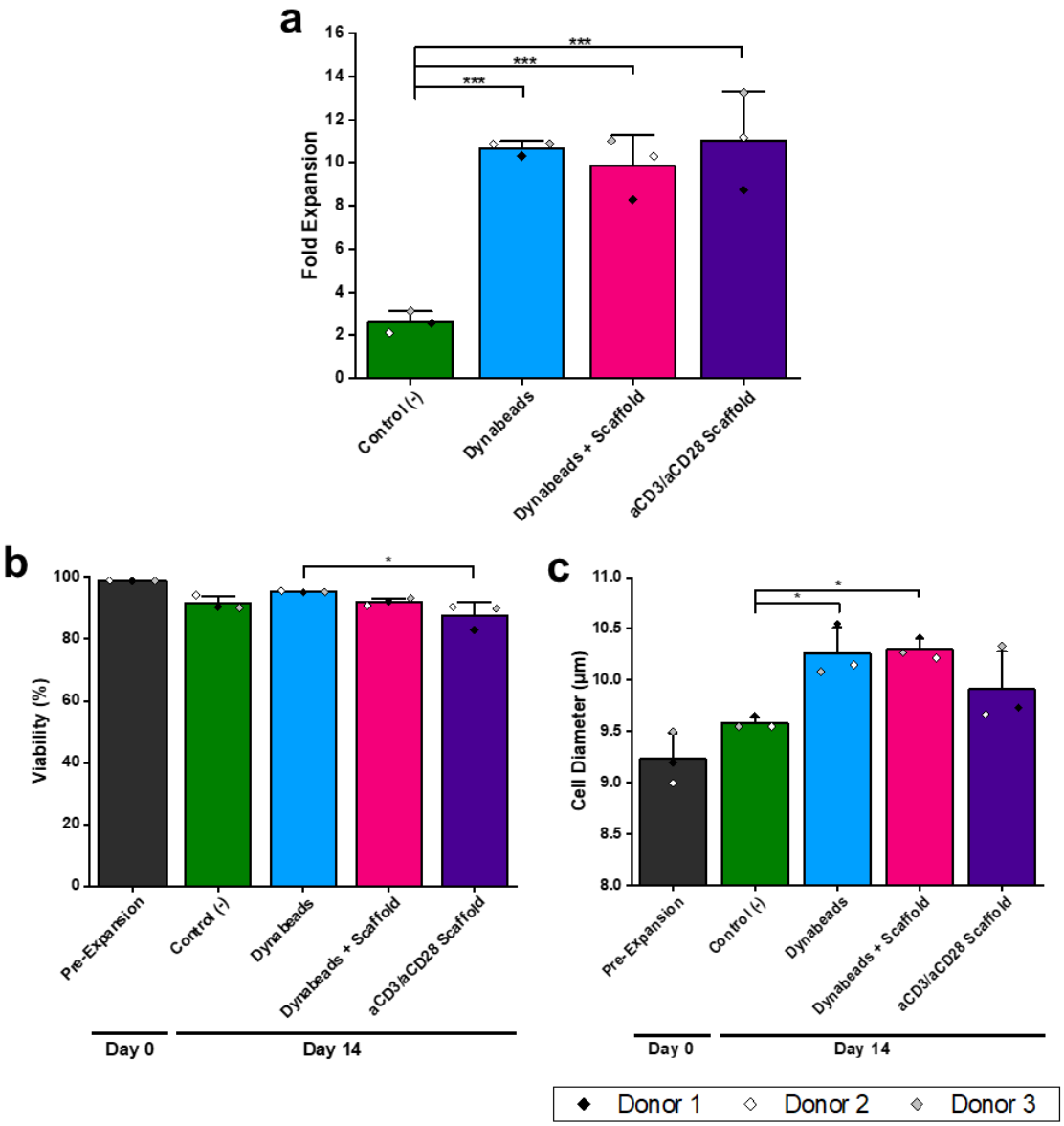

Figure 7.13. Fold expansion, viability, and cell diameter of T-cells stimulated with aCD3/aCD28 porous polymer B for 14 days. a. Fold expansion. **b.** Viability. **c.** Cell diameter. Pre-Expansion = T-cells on day 0. Control (-) = unstimulated T-cells. Dynabeads = T-cells stimulated with Dynabeads®. Dynabeads + Scaffold = T-cells stimulated with Dynabeads® and cultured on porous polymer B without antibody. aCD3/aCD28 Scaffold = T-cells stimulated with porous polymer B with aCD3 and aCD28 attached. n = 3 independent experiments for 3 donors, with 6 replicates each. Mean values are plotted. Error bars = ± 1SD. *p*-values of day 14 data were determined by a one-way ANOVA with a post hoc Tukey's test. * = $p \leq .050$. ** = $p \leq .010$. *** = $p \leq .001$.

T-cell stimulation and culture for 14 days with an aCD3/aCD28 scaffold resulted in a mean 11.0-fold increase of T-cells (**Figure 7.13a**). This represents a small increase (0.3 %) compared to Dynabeads. Dynabeads + scaffold cultures displayed a 9.9-fold increase, a reduction of 0.8 % compared to Dynabeads alone.

Figure 7.13b shows that all cultures displayed a decrease in viability from day 0 (99 %), however all remained above 87.8 %. With aCD3/aCD28 scaffold cultures a decrease of 3.8 % viability was observed compared to the control (-), also representing a significant 7.5 % decrease over Dynabeads. Dynabeads + scaffold cultures had a viability of 92.1 %, 3.2 % lower than with Dynabeads alone.

On day 14, T-cells from aCD3/aCD28 scaffold cultures displayed an increase in cell diameter of 0.3 µm compared to the control (-), with a mean diameter of 9.9 µm (**Figure 7.13c**). This was 0.4 µm lower than both Dynabeads and Dynabeads + scaffold which both had a mean diameter of 10.3 µm.

7.3.2.2. Phenotypic Characterisation

T-cell phenotypes were classified and identified using the same classifications and method described previously in **Section 7.3.1.4**, with the flow cytometry gating strategy in **Figure 7.4**. Representative scatter graphs, and unstained and isotype controls are shown in **Appendices F.8** and **E.7**. It was observed that aCD3/aCD28 scaffold cultures resulted in a CD4:CD8 ratio of 1.2 (**Figure 7.14**). This was equal to Dynabeads cultures, and slightly lower than Dynabeads + scaffold cultures (1.3). It was noted that aCD3/aCD28 Scaffold and Dynabeads + scaffold displayed greater variation of ratios between donors than Dynabeads.

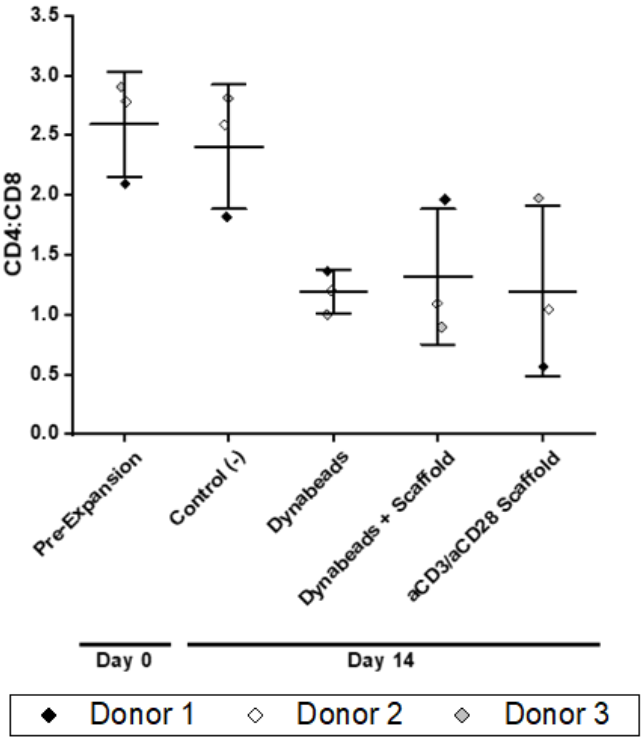

Figure 7.14. Ratio of $CD4^+$ to $CD8^+$ T-cells expanded with aCD3/aCD28 porous polymer B. Pre-Expansion = T-cells on day 0. Control (-) = unstimulated T-cells. Dynabeads = T-cells stimulated with Dynabeads®. Dynabeads + Scaffold = T-cells stimulated with Dynabeads® and cultured on porous polymer B without antibody. aCD3/aCD28 Scaffold = T-cells stimulated with porous polymer B with aCD3 and aCD28 attached. n = 3 independent experiments for 3 donors, with 6 replicates each. Mean values are plotted. Error bars = ± 1SD. Day 14 data were assessed by a one-way ANOVA, no significant ($p \leq .050$) *p*-values were obtained.

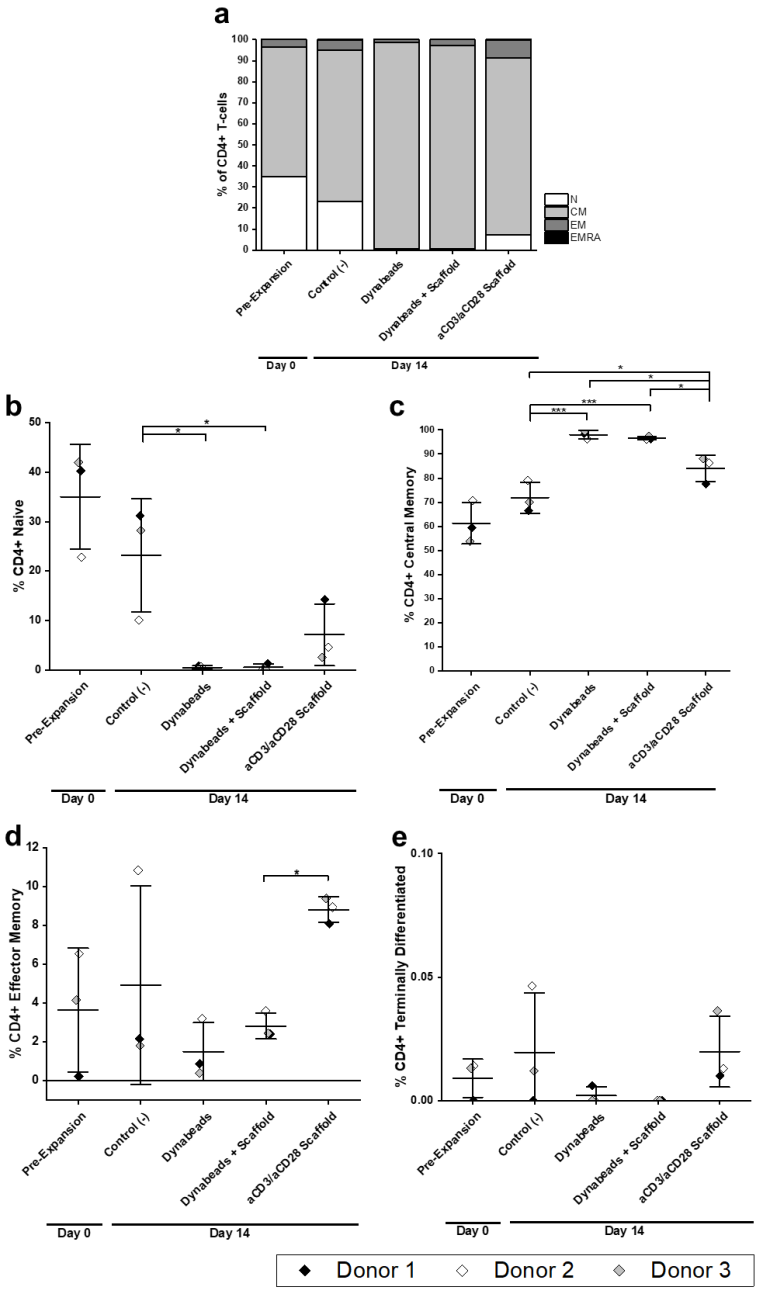

Figure 7.15. Phenotypic analysis of CD4⁺ T-cells expanded with aCD3/aCD28 porous polymer B. T-cells were cultured for 14 days. **a.** Whole population breakdown of CD4⁺ T-cells. N = naïve; CM = central memory; EM = effector memory; EMRA = effector memory terminally differentiated. Individual comparisons of **b.** naïve, **c.** central memory, **d.** effector memory, and **e.** effector memory terminally differentiated. Pre-Expansion = T-cells on day 0. Control (-) = unstimulated T-cells. Dynabeads = T-cells stimulated with Dynabeads®. Dynabeads + Scaffold = T-cells stimulated with Dynabeads® and cultured on porous polymer B without antibody. aCD3/aCD28 Scaffold = T-cells stimulated with porous polymer B with aCD3 and aCD28 attached. n = 3 independent experiments for 3 donors, with 3 replicates each. Mean values are plotted. Error bars = ± 1SD. *p*-values of day 14 data were determined by a one-way ANOVA with a post hoc Tukey's test. * = $p \leq .050$. *** = $p \leq .001$.

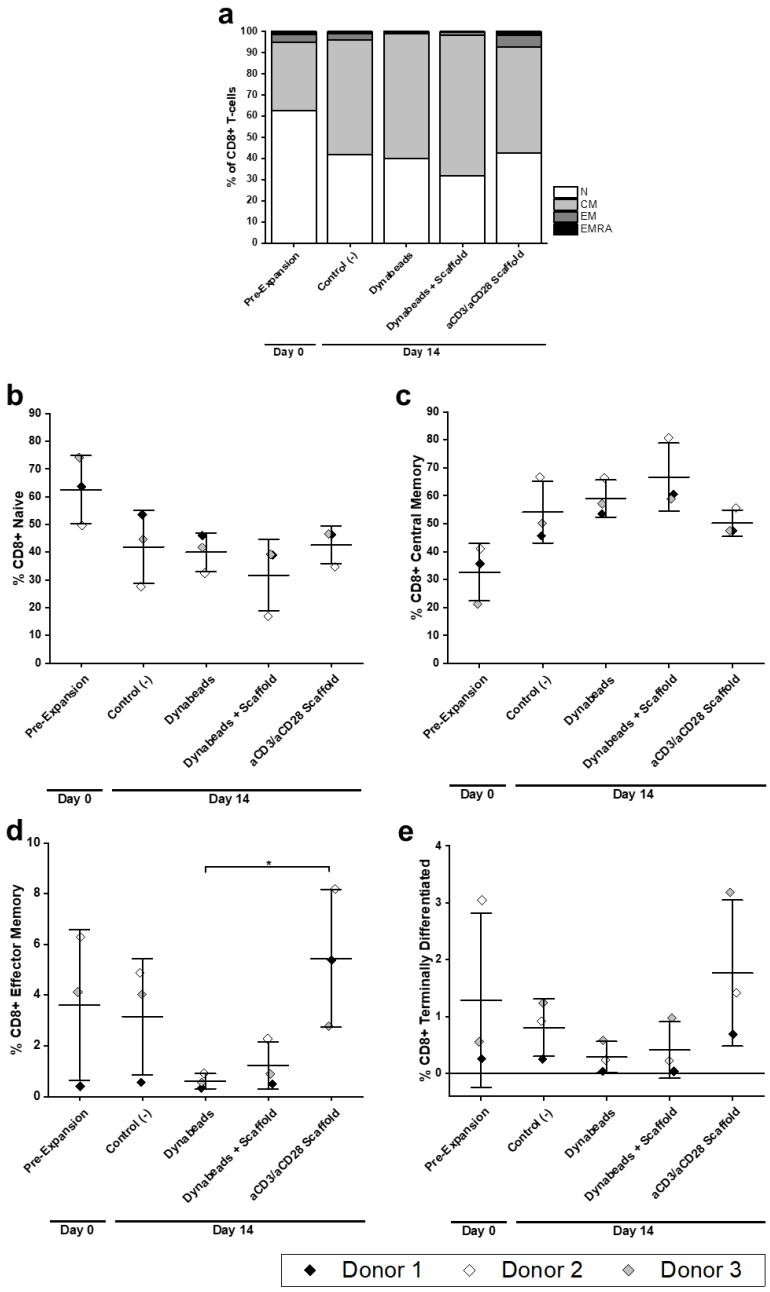

Figure 7.16. Phenotypic analysis of CD8⁺ T-cells expanded with porous aCD3/aCD28 porous polymer B. T-cells were cultured for 14 days. a. Whole population breakdown of CD8⁺ T-cells. N = naïve; CM = central memory; EM = effector memory; EMRA = effector memory terminally differentiated. Individual comparisons of **b.** naïve, **c.** central memory, **d.** effector memory, and **e.** effector memory terminally differentiated. Pre-Expansion = T-cells on day 0. Control (-) = unstimulated T-cells. Dynabeads = T-cells stimulated with Dynabeads®. Dynabeads + Scaffold = T-cells stimulated with Dynabeads® and cultured on porous polymer B without antibody. aCD3/aCD28 Scaffold = T-cells stimulated with porous polymer B with aCD3 and aCD28 attached. n = 3 independent experiments for 3 donors, with 3 replicates each. Mean values are plotted. Error bars = ± 1SD. *p*-values of day 14 data were determined by a one-way ANOVA with a post hoc Tukey's test. * = $p \leq .050$.

Figure 7.15 shows that within the $CD4^+$ subset of T-cells, T_{CM} (84.0 %) was the clear dominant phenotype of T-cells stimulated with aCD3/aCD28 scaffold. A T_{CM} majority was echoed in results of cultures stimulated with Dynabeads (98.0 %) and Dynabeads + scaffold (96.6 %), which were both significantly higher than aCD3/aCD28 scaffold. aCD3/aCD28 scaffold displayed a small percentage of T_{EM} (8.8 %). All stimulated cultures resulted in negligible percentages of T_{EMRA}.

Similar results were demonstrated within the $CD8^+$ subset of T-cells (**Figure 7.16**), with T_{CM} being the dominant phenotype for aCD3/aCD28 scaffold (50.2 %), Dynabeads (59.0 %), and Dynabeads + scaffold (66.7 %). Additionally, aCD3/aCD28 scaffold cultures displayed a small significant increase (4.8 %) in T_{EM} compared to Dynabeads. T_N was observed to be the second largest phenotype for all stimulated conditions, and T_{EMRA} the lowest ranging from 0.3 to 1.8 %.

7.3.2.3. Cell Cycle Analysis

Figure 7.17a shows representative graphs for each culture condition. From these it was observed that the largest peak in all conditions appeared to be that of G0/G1. Quantified values for each cell cycle phase are displayed in **Figure 7.17b** as a percentage of the total T-cell population. With aCD3/aCD28 scaffold T-cell cultures, 66.5 % of T-cells were determined as being in the G0/G1 phase which represented the majority. 14.8 % were in the S phase, 1.6 % in the G2 phase, and 17 % in the sub-G1 phase. Similarly, cells in the G0/G1 phase represented the greatest proportion of T-cells in Dynabeads (70.0 %) and Dynabeads + scaffold (65.8 %) cultures.

Sub-G1 phase cells were excluded to allow the calculation of dividing cells presented as a percentage of live cells (**Figure 7.17c**). aCD3/aCD28 scaffold stimulated cultures displayed a mean of 19.7 % dividing cells. This was observed to be a 0.9 % decrease compared to Dynabeads. Dynabeads + scaffold cultures displayed the greatest percentage of dividing cells (24.6 %). No significant differences were observed between all culture conditions.

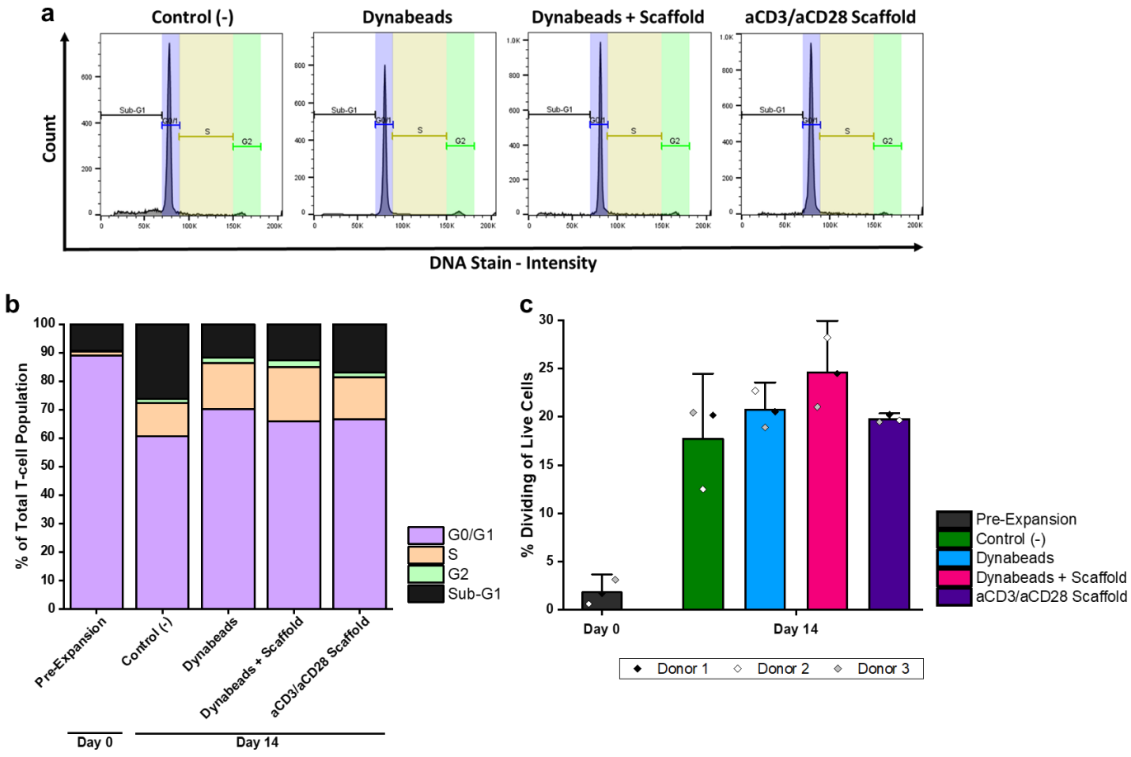

Figure 7.17. Cell cycle analysis of T-cells stimulated with aCD3/aCD28 porous polymer B for 14 days. a. Representative cell cycle analysis' – representative of 3 donors, with 3 replicates each. **b.** Total population breakdown of cell cycle phases. **c.** Quantification of dividing cells with non-viable cells excluded. Pre-Expansion = T-cells on day 0. Pre-Expansion = T-cells on day 0. Control (-) = unstimulated T-cells. Dynabeads = T-cells stimulated with Dynabeads®. Dynabeads + Scaffold = T-cells stimulated with Dynabeads® and cultured on porous polymer B without antibody. aCD3/aCD28 Scaffold = T-cells stimulated with porous polymer B with aCD3 and aCD28 attached. n = 3 independent experiments for 3 donors, with 3 replicates each. Mean values are plotted. Error bars = ± 1SD. Day 14 data were assessed by a one-way ANOVA, no significant ($p \leq .050$) *p*-values were obtained.

7.3.2.4. Apoptosis Assay

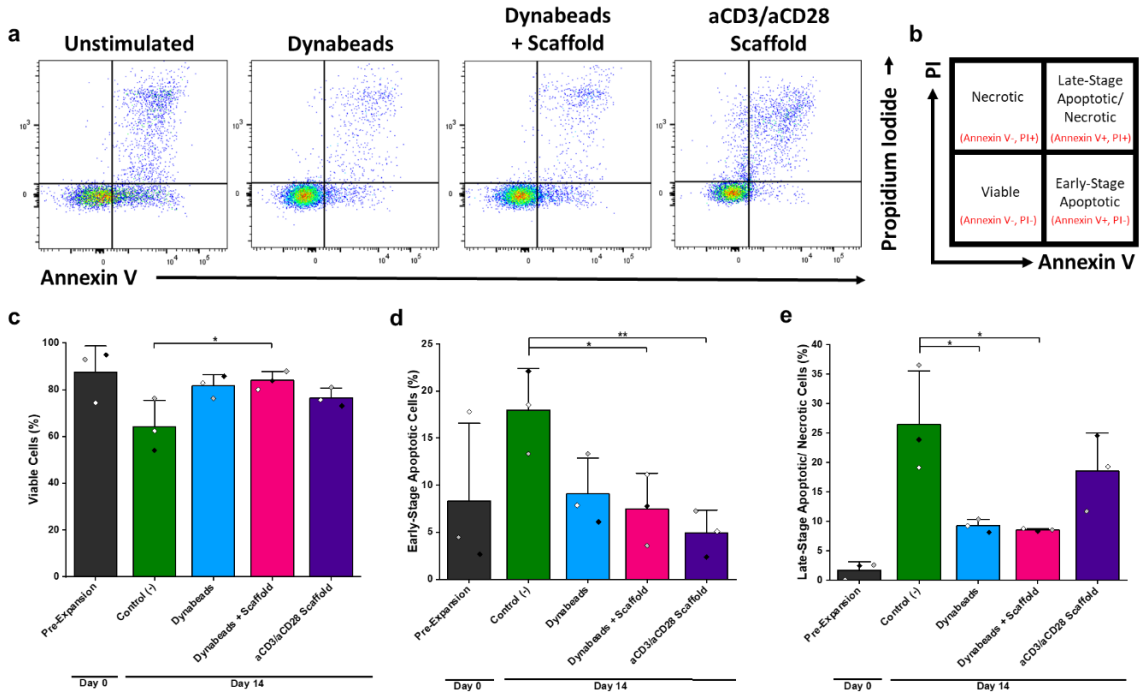

Figure 7.18. Apoptosis assay performed on T-cells cultured on aCD3/aCD28 porous polymer B for 14 days. a. Representative scatter graphs with propidium iodide (PI) on the y-axis and annexin V on the x-axis. **b.** Gating strategy for the classification of viable (annexin V^-PI^-), early-stage apoptotic (annexin V^+,PI^-), either late-stage apoptotic or necrotic (annexin V^+, PI^+), and necrotic (annexin V^-PI^+) T-cells. **c.** Percentage of viable cells in the total population (annexin V^-, PI^-). **d.** Percentage of early-stage apoptotic cells in the total population (annexin V^+PI^-). **e.** Percentage of either late stage apoptotic or necrotic (annexin V^+PI^+) combined with necrotic (annexin V^-PI^+) cells in the total population. Pre-Expansion = T-cells on day 0. Control (-) = unstimulated T-cells. Dynabeads = T-cells stimulated with Dynabeads®. Dynabeads + Scaffold = T-cells stimulated with Dynabeads® and cultured on porous polymer B without antibody. aCD3/aCD28 Scaffold = T-cells stimulated with porous polymer B with aCD3 and aCD28 attached. n = 3 independent experiments for 3 donors, with 3 replicates each. Mean values are plotted. Error bars = ± 1SD. *p*-values of day 14 data were determined by a 1-way ANOVA with post-hoc Tukey's test. * = $p \leq .050$. ** = $p \leq .010$.

Figure 7.18a displays representative annexin V vs PI graphs obtained from the NucleoCounter® NC-3000™. Scatter graphs were classified and quantified as per **Figure 7.18b**. From **Figure 7.18c** it can be viewed that cultured stimulated with aCD3/aCD28 Scaffold for 14 days consisted of a mean of 76.6 % viable T-

cells and displayed the lowest percentage of early-stage apoptotic cells (4.9 %), which was 4.2 % lower than Dynabeads and 2.6 % lower than Dynabeads + scaffold. Additionally, aCD3/aCD28 Scaffold cultures displayed a mean of 18.5 % late-stage apoptotic/necrotic cells. Both Dynabeads and Dynabeads + scaffold cultures resulted in similar levels of late-stage apoptotic/necrotic cells, 9.2, and 8.6 %, respectively. Control (-) cultures produced both the highest level of early-stage apoptotic (16.7 %) and late-stage apoptotic/necrotic (26.5 %) cells. Significant differences were highlighted with the control (-), with none found between stimulated cultures of any classification

7.3.2.5. IFNγ Production

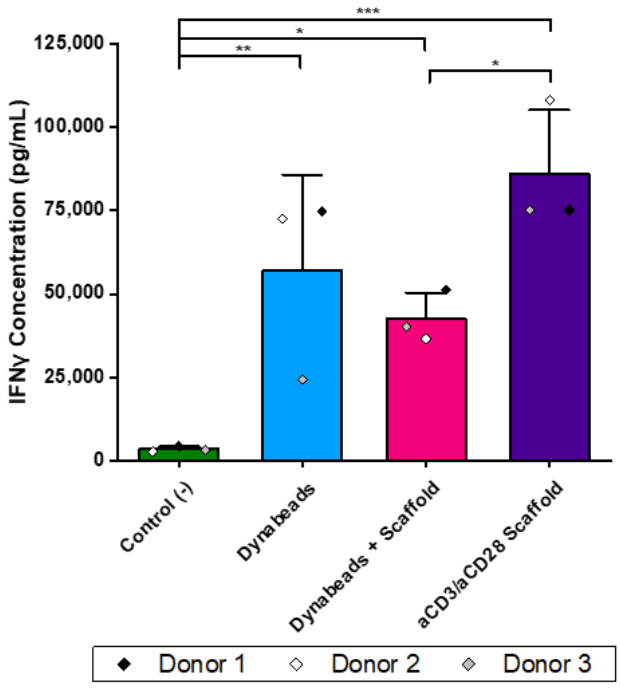

Figure 7.19. Interferon-γ production of T-cells stimulated with aCD3/aCD28 porous polymer B. Concentrations were determined by ELISA assay using pooled media from over 13 days in culture. Control (-) = unstimulated T-cells. Dynabeads = T-cells stimulated with Dynabeads®. Dynabeads + Scaffold = T-cells stimulated with Dynabeads® and cultured on porous polymer B without antibody. aCD3/aCD28 Scaffold = T-cells stimulated with porous polymer B with aCD3 and aCD28 attached. n = 1 assay for 3 donors, with 3 replicates each. Mean values are plotted**.** Error bars = ± 1SD. *p*-values were determined by a 1-way ANOVA with post-hoc Tukey's test. * = $p \leq .050$. ** = $p \leq .010$. *** = $p \leq .001$

T-cell cultures expanded with an aCD3/aCD28 scaffold displayed the greatest IFNγ concentration (86,073 pg/mL). Dynabeads cultures produced 57,197 pg/mL, and Dynabeads + scaffold 42,704 pg/mL. All stimulated cultures contained significantly greater concentrations of IFNγ than the Control (-).

7.3.2.6. Metabolic Profile

The metabolic profiles of glucose, glutamine, lactate, and ammonia concentrations from T-cell cultures over 13 days is displayed in **Figures 7.20a** - **e**, and differences quantified in **Figures 7.20e** - **h**. From 3-5 days onwards, cultures stimulated with aCD3/aCD28 scaffold demonstrated a significant increase in glucose consumption and lactate production compared to Control (-). Glucose consumption was consistently lower, and lactate production was consistently higher when compared to Dynabeads stimulated cultures. Similarly, glutamine consumption of aCD3/aCD28 scaffold cultures increased from 3-5 days onwards, with significant increases at time intervals of 3-5, 5-7, and 9-11 days compared to control (-), and consistently lower consumption than Dynabeads throughout. Dynabeads + scaffold cultures did not display any significant differences to Dynabeads alone with any metabolite.

Figure 7.21 shows that in total, over 13 days, culture with aCD3/aCD28 scaffold was observed to result in significant increases in glucose and glutamine consumption of 17.3 µmol and 1.0 µmol respectively compared to control (-), and significant decreases of 8.3 µmol and 1.4 µmol respectively, compared to Dynabeads. Furthermore, a significant decrease in the total lactate production of 15.8 µmol was demonstrated when compared to Dynabeads. Ammonia production remained low throughout and no significant differences between culture conditions were found.

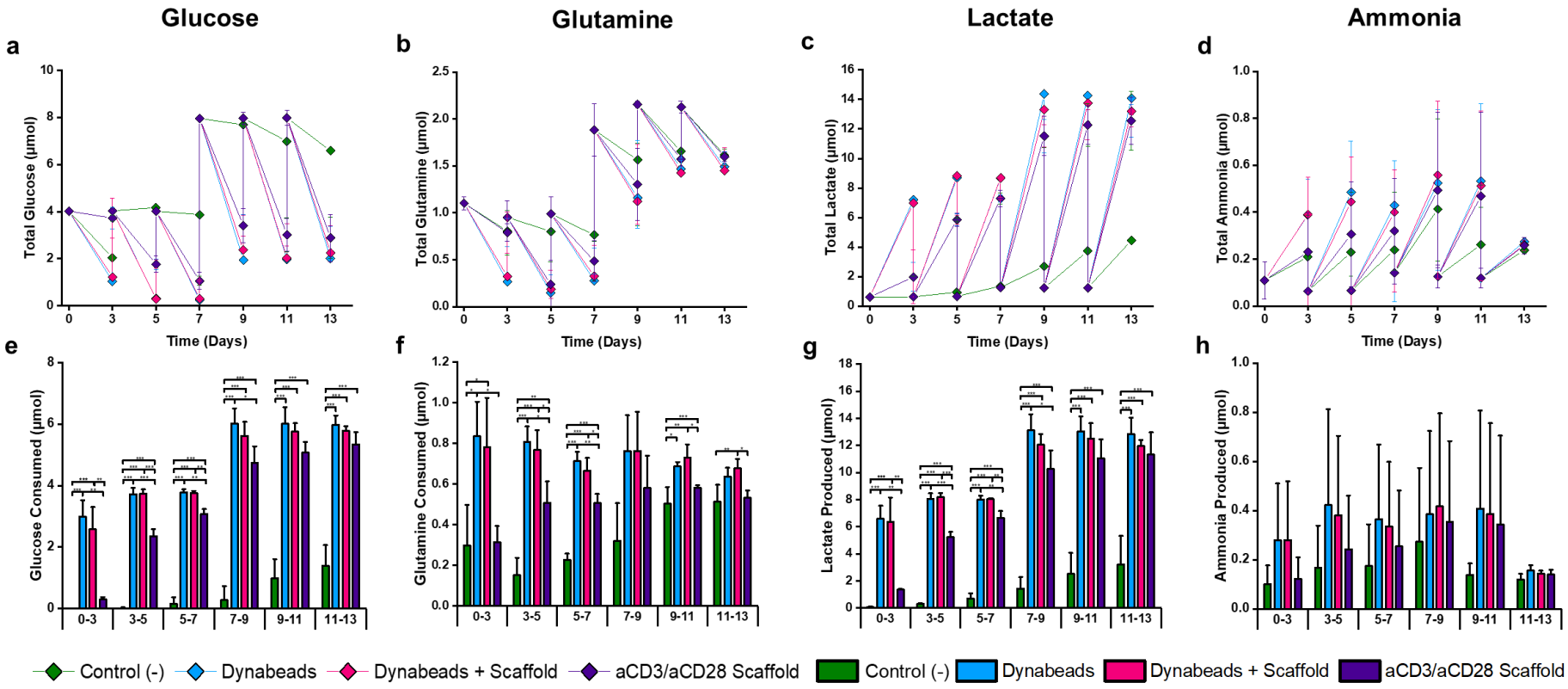

Figure 7.20. Metabolic profiles of cultures of T-cells stimulated with aCD3/aCD28 porous polymer B over 13 days. Culture concentration of **a.** glucose, **b.** glutamine, **c.** lactate, and **d.** ammonia. Quantified consumption of **e.** glucose and **f.** glutamine. Quantified production of **g.** lactate and **h.** ammonia. Control (-) = unstimulated T-cells. Dynabeads = T-cells stimulated with Dynabeads®. Dynabeads + Scaffold = T-cells stimulated with Dynabeads® and cultured on porous polymer B without antibody. aCD3/aCD28 Scaffold = T-cells stimulated with porous polymer B with aCD3 and aCD28 attached. n = 3 independent experiments for 3 donors, with 3 replicates each. Mean values are plotted**.** Error bars = ± 1SD. *p*-values were determined by a 1-way ANOVA with post-hoc Tukey's test. * = $p \leq .050$. ** = $p \leq .010$. *** = $p \leq .001$

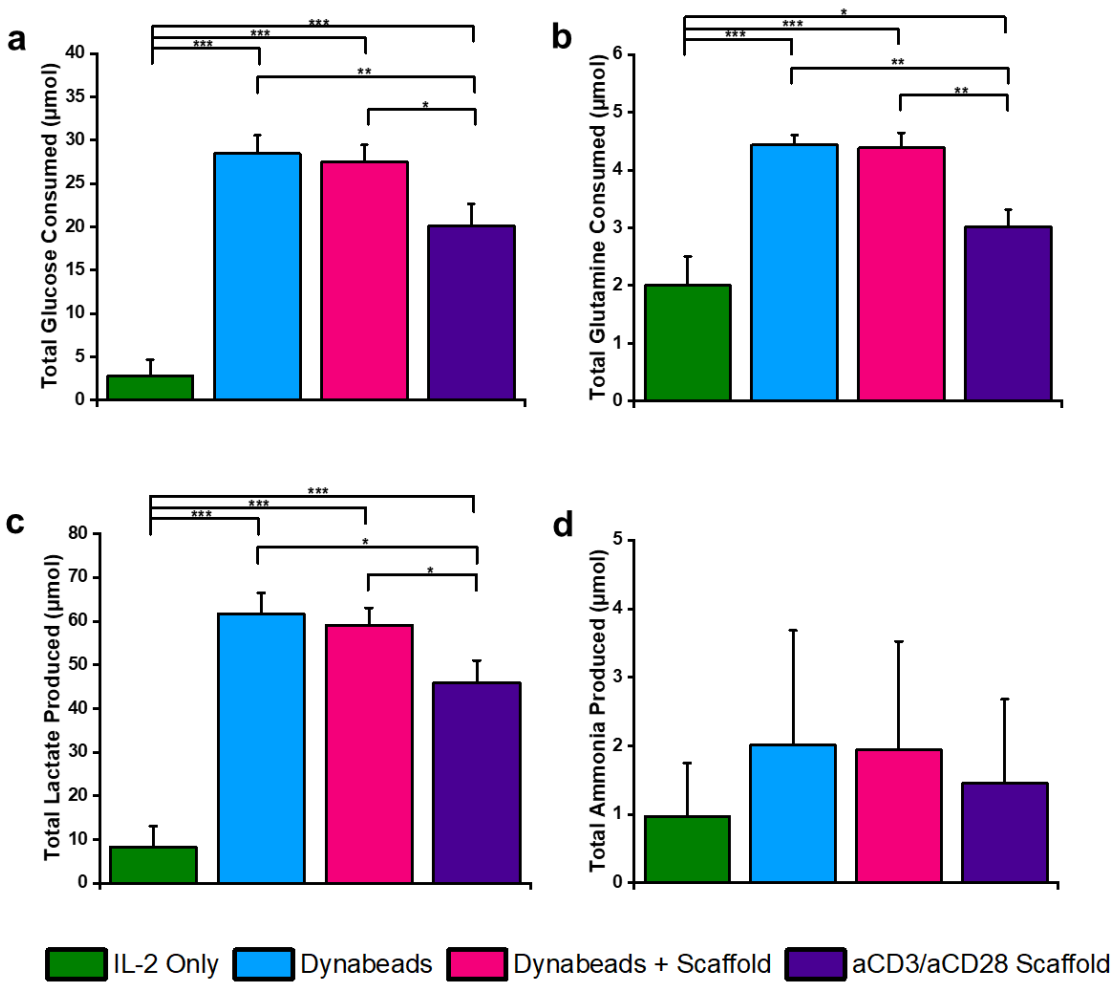

Figure 7.21. Total metabolite consumption and production for T-cells stimulated with aCD3/aCD28 porous polymer B. a. Total glucose consumed. **b.** Total glutamine consumed. **c.** Total lactate produced. **d.** Total ammonia produced. Mean values are plotted. Error bars = ± 1SD. n = 3 independent experiments for 3 donors, with 3 replicates each. All totals are a culture of 14 days *p*-values were determined by a 1-way ANOVA with post-hoc Tukey's test. * = $p \leq .050$. ** = $p \leq .010$. *** = $p \leq .001$.

7.3.2.7. Culture Visualisation

To visualise T-cell expansion with a polymer B scaffold, z-stack fluorescent confocal imaging was employed which allowed the reconstruction of a 3D image, as described in **Method 2.2.4.4**. T-cells were pre-stained with a red fluorescent membrane dye and cultured with porous polymer B before being stained with a deep red nuclear dye and imaged. Cultures were imaged on days 1, 3, 5, and 7. Controls are shown in **Appendix C.4**.

Unfortunately, the polymer scaffold appeared to absorb low levels of residual dye and resulted in the polymer displaying fluorescence in all channels (**Appendix C.4)**. T-cells, however, were still able to be identified through bright spots in the red fluorescence channels accompanied by the absence of fluorescence in the DAPI channel.

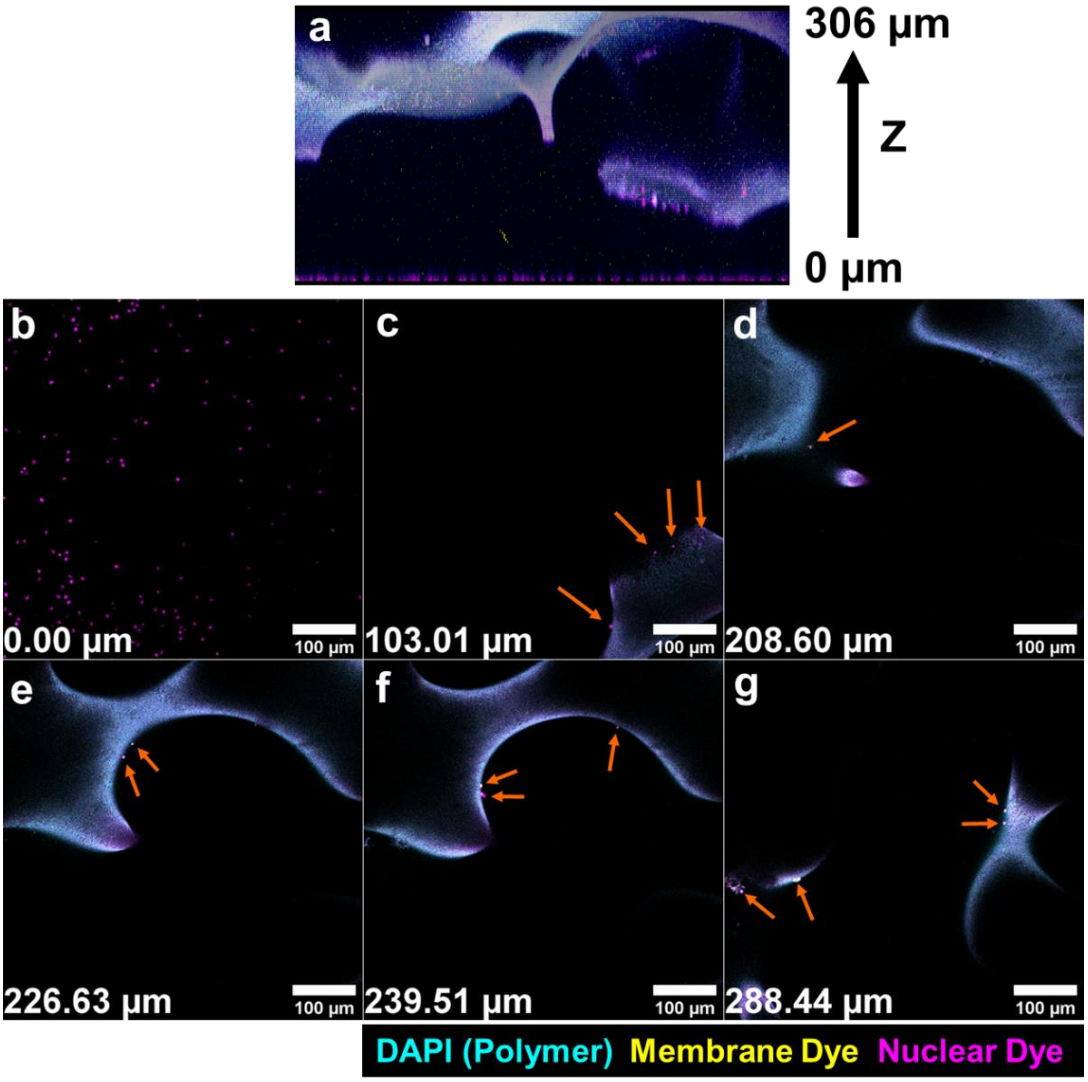

Figure 7.22. T-cells on an aCD3/aCD28 porous polymer B scaffold at day 1. a. Side view of a reconstructed 3D projection of fluorescent confocal microscopy images. Imaging was initiated from the base (z = 0 µm) to a maximum depth of 306 µm. **b** - **g.** Individual images extracted from the z-stack. Identified cells are indicated by arrows. Z position is displayed in the lower left of each image. Scale bars = 100 µm. Polymer was visualised through the DAPI channel, pseudo-coloured cyan. Cells were pre-stained with a red membrane dye prior to seeding into the scaffold, pseudo-coloured yellow. A deep red nuclear dye was added to cultures prior to imaging, pseudo-coloured magenta. All images display merged fluorescence channels.

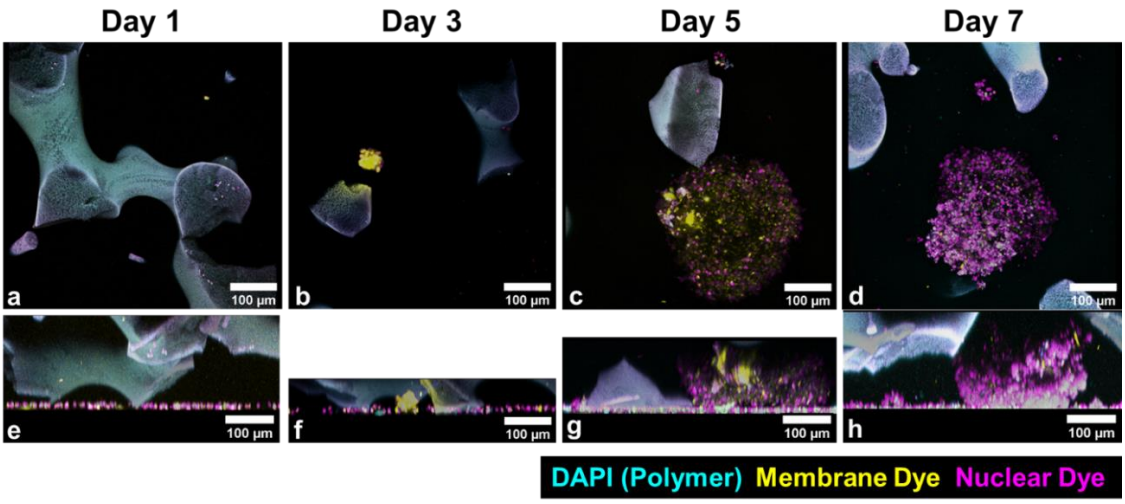

Figure 7.23. T-cell expansion with an aCD3/aCD28 porous polymer B scaffold over 7 days. 3D reconstructions of fluorescent confocal microscopy images: **a - d.** view from the bottom of the culture with settled cells removed, and **e - h.** side view. Images were taken on day 1 (**a** and **e**), day 3 (**b** and **f**), day 5 (**c** and **g**), and day 7 (**d** and **h**). Scale bars = 100 µm. Polymer, visualised through the DAPI channel, is pseudo-coloured cyan. Membranes, stained red, are pseudo-coloured yellow. Nuclei, stained deep red, are pseudo-coloured magenta. All images display merged fluorescence channels.

Figure 7.22a shows a 3D reconstruction of a z-stack of images taken from a T-cell culture containing an aCD3/aCD28 polymer scaffold 1 day post seeding. A large number of cells were observed to have settled to the base of the culture dish, with a section of scaffold ~100 µm above. Cells appeared attached to the base of the scaffold. Images extracted from throughout the z-stack (**Figures 7.22b** - **g**) displayed a small number of T-cells bound to the polymer throughout the section.

Clusters of proliferating T-cells were observed and increased in size from day 3 onwards (**Figure 7.23**). The majority of clusters appeared to be in contact with the base of the culture dish (**Figures 7.23e** - **h**). This is further visualised in **Figure 7.24 c**, which shows extracted images from a z-stack of a cluster on day 7. These images display that clusters are also in contact with the scaffold as they grow. An exception was observed in which a T-cell cluster was attached to the

scaffold only, with no contact with the base of the culture dish (**Figure 7.24d**). Visualisation using this technique was limited to an approximate 300 µm depth into the polymer before imaging became distorted by spherical aberration.

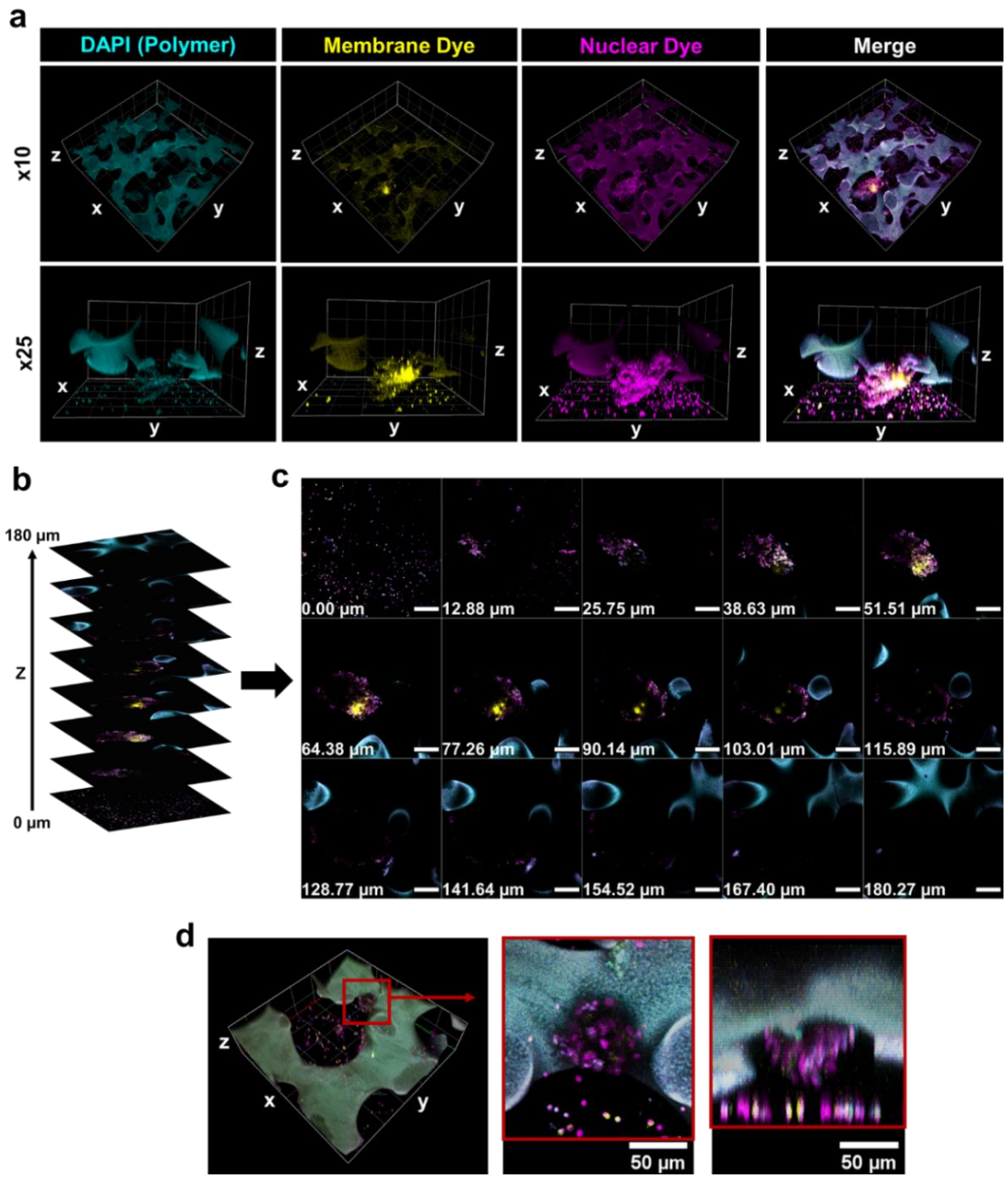

Figure 7.24. T-cells growing an aCD3/aCD28 polymer B scaffold at day 7. a. 3D reconstructions of fluorescent confocal microscopy images. Top row = x10 magnification; scale bars = 402 µm (z) x 1.4 mm (y) x 1.4 mm (x). Bottom row = x25 magnification; scale bars = 402 µm (z) x 567 µm (y) x 567µm (x). **b.** Z-stack formation of slices taken from **a.** (x25) to a z depth of 180 µm. **c.** Extracted images displaying cell-scaffold contact. Scale bars = 50 µm. **d.** A T-cell cluster anchored on polymer. Scale bars of first image = 155 µm (z) x 567 µm (y) x 567 µm (x). Scale bars of magnified region = 50 µm.

7.4. Discussion

7.4.1. T-cell Activation and Expansion with aCD3/aCD28 Polymer B

The activation and expansion of T-cells is a crucial step within the production of T-cell therapies. It was hypothesised that T-cells in contact with polymer B with aCD3/aCD28 attached (aCD3/aCD28 polymer B) would result in activation and consequent expansion of T-cells. This was investigated through the stimulation of T-cell cultures with both non-porous and porous aCD3/aCD28 polymer B.

T-cell cultures stimulated with non-porous aCD3/aCD28 polymer B resulted in significant increases in the percentage of T-cells expressing activation markers CD69 and CD25, and increases in cell diameter (a known indicator of activation) and total cell count over 14 days – equating to a 8.3-fold expansion (**Figures 7.2a - d and 7.3**). Additionally, CFSE staining and analysis of cultures highlighted small percentages of T-cells that were proliferating at day 4 (**Figures 7.10** and **7.11**). Collectively these results demonstrate the ability of non-porous aCD3/aCD28 polymer B to activate and expand T-cells.

T-cell cultures stimulated with a porous aCD3/aCD28 polymer B scaffold resulted in: an 11-fold expansion (**Figure 7.13a**); increases in lFNγ production (**Figure 7.19**); an increase in glucose and glutamine consumption, and an increase in lactate production (**Figures 7.20** and **7.21**). lFNγ is a cytokine secreted by activated lymphocytes, particularly cytotoxic $CD8^+$ T-cells and $CD4^+$ helper type 1 T-cells (Castro *et al*., 2018) and therefore indicates T-cell activation and cytotoxic activity. Furthermore, the metabolic profiles of cultures demonstrate that T-cells were in a metabolically active state. Therefore, these results strongly suggest that T-cells stimulated by an aCD3/aCD28 scaffold were successfully activated, cytotoxic, and confirm the expansion of T-cells via scaffold exposure.

Unexpectedly, T-cells stimulated by porous aCD3/aCD28 polymer B scaffold did not display a significant increase in cell diameter (**Figure 7.13c**). However, the equivalent was found on day 14 of stimulation by polymer in a non-porous format, with the most apparent increases in diameter being displayed between day 3 to 10, and a reduction on day 14 (**Figure 7.2d**). This indicates that significant increases in cell diameter were likely missed with aCD3/aCD28 scaffold cultures, as only end-point measurements were taken.

Although stimulation with aCD3/aCD28 polymer B in a porous format resulted in an additional 2.7-fold expansion when compared to a non-porous format, it is not possible to determine whether this was due to polymer format or differing culture conditions and feeding strategies. T-cells stimulated with a scaffold were within well plate inserts and were subject to almost total spent media removal and replacement from the outer well every 2 days from day 3. With non-porous polymer, polymer was placed at the base of wells and only half of spend media was removed and replaced following the same time frame. This resulted in cultures stimulated with scaffolds receiving additional nutrients overall and it is highly likely that this considerably impacted cell expansions.

Expansions found in literature can be found ranging from 7 to 1,300 -fold in 7 – 21 days (Delalat *et al*., 2017; Hickey *et al*., 2019; Arcangali *et al*., 2020). Such a wide range is due to many varying process factors such as: scale, technologies and reagents used, cytokine addition, starting patient material, expansion parameters (seeding density, feeding regime, etc.). Often the achieved expansion reflects the state at which processes are in development, with more novel and less optimised technologies displaying lower fold-expansions. The fold expansions achieved here would be considered to be within the lower range of T-cell expansion technology, but are consistent with the expectations of a small

scale, unoptimised, proof-of-concept study. It would be expected that the overall expansion would improve as the culture conditions are optimised. Nonetheless, this proof-of-concept study has demonstrated that aCD3/aCD28 polymer B can be used as platform to activate and expand T-cells which may possess advantageous cytotoxic activity.

7.4.2. Culture/ Expansion Characterisation

In order to begin characterisation of these novel activation and expansion processes, cultures were assessed for various different outputs.

7.4.2.1. Non-porous aCD3/aCD28 Polymer

T-cells cultures stimulated with non-porous aCD3/aCD28 polymer displayed an increase in cell number consistently from the first time point day 3, with linear growth apparent from day 5 - 7 (**Figure 7.2a**). This suggests that that cultures were in lag phase until day 5 - 7, and that cells were still in exponential growth at day 14 when the study was terminated. Data points at day 7 and 10 are within the linear section, however, display relatively larger values of standard deviation and so it is possible that this section may be more curved than it first appears. Variation likely arose from inconsistencies in the concentration of antibody across the surface of the polymers (highlighted in **Section 5.3.5**) surface resulting in variations in the amount of antibody T-cells were exposed to. Additional variation was also introduced through the natural variation of the proliferative capabilities of different donors T-cells.

To further investigate and characterise the culture in the early stages of the expansion, the proliferation of T-cells was assessed 4 days post exposure to non-porous aCD3/aCD28 polymer using CFSE. Both $CD4^+$ and $CD8^+$ T-cells displayed high percentages (> ~70 %) of T-cells in Gen 0, with low percentages

progressing to a maximum of Gen 7 (**Figures 7.10b** and **c**). This indicated that the majority of cells were not proliferating 4 days post exposure. Using the descriptive indices, further details of the expansion were able to be extracted. Overall, $CD4^+$ T-cells in culture expanded by a total of 1.15-fold, this was achieved by a small percentage of T-cells that expanded 4.5-fold and averaged 1.68 divisions (**Figures 7.11b** - **d**). Similarly, $CD8^+$ T-cells expanded by a total of 1.37-fold, achieved by a small percentage of T-cells that expanded 4.96-fold and averaged 1.76 divisions (**Figures 7.11f** - **h**).

Furthermore, through the assessment of the cell cycle it was observed that only ~17 % of T-cells were dividing at day 14 (**Figure 7.9c**). This may suggest that only a small number of T-cells were proliferating throughout. However, the length of the expansion must also be taken into consideration here as it would also be expected that less T-cells would be dividing as the culture time progresses, with some activation methods recommending re-stimulation to maintain proliferation (Thermo Fisher Scientific, 2011). To test these hypotheses it would be suggested that additional time-points be assessed.

Small increases were observed in the fold expansions (both overall and responding cells only) and the number of average divisions by $CD8^+$ T-cells compared to $CD4^+$ (**Figure 7.11b** - **d** and **f** - **h**). This, in addition to the observation of an increase (~10 %) of $CD8^+$ T-cells above Gen 0 (**Figures 7.10b** and **c**), suggested an initial preferential expansion of $CD8^+$ T-cells with aCD3/aCD28 polymer. This was most evident with donor 2 and 3 (**Figure 7.10a**), further indicating that donor variability also influences the extent of this preference. Descriptive indices extracted from analysis on FlowJo software also calculated the percentage of dividing cells and displayed a smaller increase of ~4 % in the percentage of $CD8^+$ T-cells dividing compared to $CD4^+$ (**Figures 7.11a** and **e**). It

is worth noting that differences observed in the percentage of dividing cells compared to the percentage of cells > Gen 0 is likely due to minor differences in the analysis applied by the semi-automated calculation of descriptive indices.

Previous work (**Section 6.3.2**) demonstrated that T-cells exposed to aCD3/aCD28 polymer remained mobile and increased in velocity, resulting in the consideration of activation as per the serial encounter model: multiple transient and dynamic interactions (kinapses). Activation through kinapses require additional time to reach the activation threshold and consequently to initiate proliferation. Therefore, this hypothesis is further supported here through the low number of dividing T-cells found here 4 days post-exposure, in addition to the indications of activation and eventual proliferation. Moreover, activation through this mode is thought to occur in situations of low ligand density (Henrickson *et al*., 2008), which was highlighted to be the case in areas over the surface of the polymer due to uneven antibody distribution. Thus it is hypothesised that T-cell activation with aCD3/aCD28 polymer occurs through multiple interactions with the presented antibodies.

The viability of T-cell cultured with non-porous aCD3/aCD28 polymer was monitored and was found to remain high (> 91.7 %) throughout the expansion (**Figure 7.2c**), indicating a healthy culture. In addition to overall culture viability, the health of an expanded T-cell culture can be assessed through the exhaustion of the cells. Exhausted T-cells are cells that are towards the end of their life cycle and as such possess low proliferative and functional capabilities (Catakovic *et al.,*2017). Commonly, T-cells are assessed for exhaustion through the identification of “exhaustion markers”. However, it is not just the expression of one which indicates exhaustion, but rather the chronic expression of multiple markers (ie. the more markers expressed, the more exhausted the T-cell). In

cultures stimulated with non-porous polymer were assessed for two such markers and ~30 % T-cells were found to be LAG-3^{+}, and ~1.5 % were PD-1^{+} on day 14 (**Figures 7.8b** and **c**). As noteworthy expression of only one of the markers was identified, and negligible proportions of cells were found to be double positive, it would be suggested that it is unlikely that T-cells were exhausted. Furthermore, LAG-3 is a marker that is transiently upregulated during activation which may be the case here (Grosso *et al.,* 2009). This assessment could be greatly improved through the incorporation of additional exhaustion markers such as TIM-3 into the flow cytometry panel.

T-cells stimulated with non-porous aCD3/aCD28 polymer detectably increased 2 µm in diameter from day 0 to 5 (**Figure 7.2d**), suggesting that cell diameter could be used as an indicator of activation in cultures. However, it would be suggested that this only be used early in the culture, as it became difficult to distinguish between the diameters of T-cells in negative control cultures post day 7.

7.4.2.2. Porous aCD3/aCD28 Polymer Scaffold

Due to limitations in cells numbers available from donors and material limitations of polymer produced from the same batch, it was not possible to investigate cells throughout the culture and provide as much detail as with non-porous polymer. Culture characterisation was maximised using the available cells at the end of the expansion and through assessing metabolites and cytokines from spent media culture.

As T-cells are activated the rate of glycolosis and glutaminolysis is increased which results in an increased uptake of glucose and glutamine from culture medium. A significant increase in both was observed in cultures stimulated with aCD3/aCD28 scaffold between days 3 - 5 and then onwards (**Figures 7.20e** and

f). Only a small increase of both was highlighted between 0 - 3 days. This suggests that T-cells were not activated to the threshold necessary to initiate the metabolic switch associated with proliferation until between days 3 - 5. Additionally, cultures increased in glucose and glutamine consumption throughout, indicating that T-cells were in a continued state of growth for the remainder of the culture. It should, however, be highlighted that on day 7 for glucose, and day 5 for glutamine, concentrations declined to close to 0 µmol (**Figures 7.20a** and **b**) and likely resulted in a limiting effect on the growth of cells. Consequent increases in the waste products of glycolysis and glutaminolysis: lactate and ammonia, were also anticipated and observed correspondingly. Ammonia production was low overall (**Figures 7.20d** and **h**, and **Figure 7.21d**) which indicated favourable growth conditions as the build-up of ammonia is known to inhibit the growth in mammalian cell cultures (Schneider and U von Stockar, 1996).

The percentage of dividing cells in a state of division was found to be 20 % (**Figure 7.17c**). As discussed above in **Section 7.4.2.1** it is not possible to distinguish whether this is the result of a low percentage of cells dividing throughout the expansion, or the result of a longer culture time. To investigate this would require the harvest and analysis of additional time points.

The health of cultures was assessed through the viability at day 14. Cultures stimulated with aCD3/aCD28 scaffolds demonstrated high culture viability (88 %) (**Figure 7.13b**), indicating that cells were healthy. A second assessment of cell viability was performed through an apoptosis assay which presented a slightly lower value of viable cells of 77 % (**Figure 7.18c**). The disparity between these two measurements is likely largely due to the differences in methods. Culture viabilities were obtained from a method in which cells that are stained with DAPI

are identified as non-viable. With the apoptosis assay, early-stage apoptotic cells retain in-tact membrane and thus are not stained by DAPI and classified as viable. Furthermore, ~19 % of T-cells were identified as late-stage apoptotic/necrotic (**Figure 7.18e**). Although it is not possible to identify the root cause of necrosis, the small increase in early-stage apoptotic cells also observed suggests that a low level of apoptosis was induced. General limitations of using a PI and annexin based apoptosis assay have been discussed previously in **Section 3.3.8.**

It was anticipated that an increase in cell diameter would be observed, as activated T-cells increase in size when activated as they synthesise DNA required for cell division (Teague *et al*., 1993). T-cells stimulated with an aCD3/aCD28 scaffold displayed only a small increase in cell diameter at day 14 which was not found to be statistically significant from the control (**Figure 7.13c**). Previously it was discussed that only a small percentage of T-cells were found to be dividing at the same time point. This offers the most plausible explanation that as the cell diameter is an average of the total population and the majority were not actively dividing, that a smaller mean cell diameter would in fact be expected. Additionally it was found with non-porous aCD3/aCD28 polymer that the cell diameter was notably increased only until day 7, after which the decrease in stimulated T-cells and increase in the control resulted in indistinguishable diameters by day 14 (**Figure 7.2d**). This would suggest that the time point at which the difference was detectable was missed in this study and perhaps analysing at ~day 5 would be more suitable to allow cell diameter to be used as an indicator of activation.

T-cell cultures were also assessed for the production of the cytokine IFNγ. IFNγ is a cytokine secreted by activated T-cells and is an indicator of functionality and cytotoxicity (Tau and Rothman, 1999; Bhat *et al*., 2017). Cultures of T-cells

expanded with an aCD3/aCD28 scaffold were found to have a significantly increased concentration compared to the control (**Figure 7.19**). This indicated that activated T-cells were both functional and possessed cytotoxic capabilities.

7.4.3. Impact on T-cell Populations

Previous studies have suggested that the production of CAR T-cell products with a defined CD4:CD8 ratio can improve product consistency and further suggest that this desired ratio is 1:1 (Sommermeyer *et al*., 2016). Here is was demonstrated that activation with non-porous aCD3/aCD28 polymer and porous aCD3/aCD28 polymer scaffold resulted in CD4:CD8 ratios of 0.72 and 1.2, respectively (**Figures 7.5** and **7.14**). Generally, ratios between 1.5 and 2.5 are considered normal for healthy donors which was demonstrated here with pre-expansion populations (Amadori *et al*., 1995). Expansions with both non-porous and porous aCD3/aCD28 polymer demonstrated notable reductions in CD4:CD8 ratios, with the former resulting in a significant shift towards a cytotoxic $CD8^+$ T-cell population. Previous studies have demonstrated that not only do T-cells possess the ability to interact with their physical environment, but that the sensing of mechanical forces also influences recognition, activation, differentiation, and function. A possible explanation for the increase in $CD8^+$ T-cells demonstrated with the non-porous polymer may be that it is the result of mechanosensing of the polymer by the expanding T-cells.

The sub-population composition of T-cells has emerged as a critical parameter to increase potency and persistence (Liu *et al*., 2020; Ren *et al*., 2021). To this end, it is desirable to produce T-cell products that consist of T-cells in less differentiated states, such as stem cell memory T-cells (T_{SCM}), T_{CM}, and T_N (Crompton *et al*., 2014; Arcangeli *et al*., 2020; Tantalo *et al*., 2021). The resultant phenotypes were assessed within both $CD4^+$ and $CD8^+$ T-cells to further identify

sub-populations of T_N, T_{CM}, T_{EM}, and T_{EMRA}. Within $CD4^+$ T-cells, cultures expanded with non-porous aCD3/aCD28 polymer were dominated in almost equivalent populations by T_{EM} and T_{CM} (**Figure 7.6**). Within $CD8^+$ T-cells, the dominant population was T_{CM} (**Figure 7.7**). When expanded with porous aCD3/aCD28 polymer scaffold, the dominant sub-population within both $CD4^+$ and $CD8^+$ was T_{CM} (**Figure 7.15** and **7.16**). Furthermore, a high population of ~40 % $CD8^+$ T_N was observed when stimulated with aCD3/aCD28 scaffold (**Figure 7.16b**). This indicates that T-cells activated with this technology result in overall favourable T-cell populations for cell therapy. Furthermore, these results highlight that aCD3/aCD28 scaffolds can be used to influence the resultant phenotype of T-cells.

7.4.4. Culturing Dynabead Stimulated T-cells in the Presence of a Scaffold

In addition to T-cell cultures stimulated with Dynabeads and aCD3/aCD28 scaffolds alone, parallel cultures were ran that contained T-cells stimulated with Dynabeads that had been seeded onto a polymer scaffold without antibody attached. This was performed to gain a greater understanding into the impact that the scaffold alone had on proliferating T-cell cultures.

Although some minor differences were observed between Dynabeads and Dynabeads + scaffold, not one of these differences was demonstrated to be statistically significant. This indicates that the presence of the scaffold alone did not notably impact the cells cultures in regards to the outputs measured. Furthermore, this suggests that differences observed between Dynabeads and aCD3/aCD28 scaffold cultures were due to activation by the scaffold and not just the presence of, and interaction with, the scaffold alone.

It was interesting, however, to note that in some instances the addition of the scaffold resulted in an increase in variability between donors (fold expansion, CD4:CD8 ratio, all phenotypes within $CD8^+$, and percentage dividing), whereas in others it resulted in a decrease in variability (cell diameter, $CD4^+$ T_{EM}, and IFNγ concentration). Though it is not fully understood why this may be the case, it strongly highlights the variation in responses that can be produced by different donors T-cells to the same stimuli.

7.4.5. Comparison to Activation with Dynabeads

Throughout expansion studies, cultures stimulated with Dynabeads were performed with a dual purpose; as a positive control and to compare the outputs of polymer stimulation to the current industry gold standard.

Additionally, previous studies have demonstrated that not only do T-cells possess the ability to interact with their physical environment, but that the sensing of mechanical forces also influences recognition, activation, differentiation, and function – these can be found reviewed elsewhere (Harrison *et al*., 2019). While the exact impact of substrate stiffness us yet to be fully understood, there is some evidence that decreasing the stiffness of the material that T-cells are activated and cultured on can increase proliferation and enhance differentiation of specific populations compared to their more rigid counterparts (O'Connor *et al*., 2012). Although the stiffness of the polymer used here was not quantified, it was apparent that the hydrogel material was softer than the polystyrene beads, polystyrene well plate surface, and polyethylene cell culture inserts that T-cells activated were Dynabeads® were exposed to. It was therefore anticipated that differences in culture outputs between the two activation technologies would be observed.

7.4.5.1. Non-porous aCD3/aCD28 Polymer

In comparison to Dynabeads, T-cell cultures stimulated with non-porous aCD3/aCD28 polymer resulted in a comparatively slower growth within the early stages of expansion (**Figure 7.2a**), significantly less CD69 and CD25 expressing T-cells (**Figures 7.3f** and **e**), and a consistently lower average cell diameter (**Figure 7.2d**). Moreover, through proliferation analysis using CFSE it was demonstrated that aCD3/aCD28 Polymer cultures at day 4 contained considerably less dividing cells (**Figure 7.11**), and that Dynabead cultures contained significantly more T-cells in Gen 1 - 4, with both $CD4^+$ and $CD8^+$ T-cells (**Figures 7.10b** and **c**). Taken together, these results strongly suggest that the initial activation with aCD3/aCD28 polymer requires additional time and results in a lower percentage of the overall population being activated compared to Dynabeads. Nevertheless, the proliferation rate increased dramatically from day 7 - 14 (**Figure 7.2a**) and overall fold-expansions between the two were not found to be significantly different (**Figure 7.2b**). Descriptive indices further revealed that the small percentages of T-cells that were dividing, had responded equally to Dynabeads stimulation as they presented comparable values for replication and proliferation indices (**Figure 7.11**). By day 14, both cultures stimulated with aCD3/aCD28 polymer and Dynabeads contained low numbers of cells dividing (**Figure 7.9c**). As mentioned previously, that was as expected due to the length of the culture time.

Dynabeads cultures displayed a large drop in viability from day 3 that was not observed with aCD3/aCD28 polymer cultures (**Figure 7.2c**), and displayed a significant increase in the expression of the exhaustion marker PD-1 (**Figure 7.8c**). This would suggest that T-cell health was improved through expansion with non-porous aCD3/aCD28 polymer. Though, it is important to note that the

increase in PD-1$^+$ T-cells was only found to be 3.6 % and that, as discussed previously, this assessment could be improved through the identification of additional markers.

The most significant difference demonstrated through the expansion of T-cells with aCD3/aCD28 polymer compared to Dynabeads was observed with the CD4:CD8 ratio (**Figure 7.5**). Not only did expansion with aCD3/aCD28 polymer significantly lower the ratio, but the dominant population was reversed – from CD4 with Dynabeads to CD8 with aCD3/aCD28 Polymer. Culture with aCD3/aCD28 polymer resulted in a ratio (0.72) that was closer to the desired 1:1, Dynabeads resulted in a ratio of 2.5 displaying a strong preference for CD4 expansion. aCD3/aCD28 polymer expansion resulted in an increase in CD4$^+$ T_N, CD4$^+$ T_{EFF}, CD4$^+$ T_{EMRA}, CD8$^+$ T_{EM}, and CD8$^+$ T_{EMRA} and a decrease in CD4$^+$ T_{CM}, CD8$^+$ T_N, CD8$^+$ T_{CM} (**Figures 7.6** and **7.7**) compared to Dynabeads. However, the only difference found to be statistically significant, however, was the increase of 8.6 % CD8$^+$ T_{EMRA} (**Figure 7.7e**).

Significant differences were also observed between the absorbance values of aCD3/aCD28 polymer and 5 x 10^5 Dynabeads when assessed for antibody content via ELISA (**Figure 7.12**). This strongly suggests that the amount of Dynabeads used to stimulated T-cell cultures contained significantly more aCD3 and aC28 than aCD3/aCD28 polymer. Antibody content of aCD3/aCD28 polymer was found to be similar to 5 x 10^4 Dynabeads, which is a 10-fold decrease in the minimum recommended amount (1:1 bead to cell ratio for 5 x 10^5 T-cells). This is interesting as cultures stimulated with both methods were found to produce comparable results in regards to expansion. Previously it has been suggested that the majority of Dynabeads are underutilised due to bead aggregation and lack of cell contact (Chin *et al*., 2020). The results found here would indicate the

same. Antibodies present a significant cost in T-cell activation technologies and it is desirable that antibody usage be as minimal and efficient as possible in order to drive down costs. The use of alternative technologies such as the one presented here may have a role to play in achieving this.

7.4.5.2. Porous aCD3/aCD28 Polymer Scaffold

T-cells stimulated with aCD3/aCD28 scaffold resulted in a slightly higher fold expansion than with Dynabeads. This difference, however was not found to be statistically significant. Additionally, the percentage of T-cells observed to still be dividing at day 14 was found to be similar (~20 %) in both cultures (**Figure 7.17c**).

Overall T-cell cultures stimulated with aCD3/aCD28 scaffold consumed significantly less glucose and glutamine, and produced less lactate (**Figures 7.21a** - **c**). This was thought to be an effect predominantly of the substantially lower consumption of glucose and glutamine, and production of lactate, observed at day 0 - 3 and 3 - 5 (**Figures 7.20e** and **f**). Glucose and glutamine consumption, and lactate production was also found to be moderately lower than with Dynabeads throughout. Ammonia production was displayed to be slightly lower throughout, however, no statistically significant differences were observed (**Figure 7.20h**). This was anticipated due to the previous demonstration that cultures expanded with non-porous aCD3/aCD28 polymer had an increased lag phase and potentially resulted in less T-cells being activated throughout the culture. Although glucose and glutamine consumption was reduced, final fold-expansions were comparable (**Figure 7.13a**). Thus, activation with aCD3/aCD28 scaffold could result less culture additives compared to Dynabeads which may help to reduce costs. It is important to note that the available glucose and glutamine in aCD3/aCD28 scaffold and Dynabeads and approached or reached 0 µmol early within the culture (**Figures 7.20a** and **b**), suggesting that the usage

reported here is not as high as it could potentially be if supply was not limited. Furthermore, with the optimisation of the feeding regime, fold-expansions would be expected to increase further.

Expansion with aCD3/aCD28 scaffold resulted in a slightly diminished culture viability of 7.5 % on day 14 compared to Dynabeads (**Figure 7.13a**). Additionally, an increase in the percentage of late-stage apoptotic/ necrotic T-cells was observed (**Figure 7.18e**) – however, this was not found to be statistically significant.

T-cell cultures stimulated with aCD3/aCD28 scaffold resulted in an equal mean CD4:CD8 ratio to Dynabeads of 1.2 (**Figure 7.14**). Furthermore, T-cell cultures stimulated with aCD3/aCD28 scaffold resulted in an increase in the percentage of both $CD4^+$ and $CD8^+$ T_N, T_{EM}, and T_{EMRA}, and decreases in T_{CM} (**Figures 7.15** and **7.16**). Of these, only small increases in the percentage of $CD4^+$ and $CD8^+$ T_{EM} were found to be statistically significant. This suggests that the overall, cultures stimulated with both aCD3/aCD28 scaffold and Dynabeads resulted in comparable populations of T-cells. This was surprising, particularly with the CD4:CD8 ratio, as studies with non-porous aCD3/aCD28 polymer resulted in a lowered CD4:CD8 ratio that favoured CD8 T-cells (**Figure 7.5**). It is most likely that the lack of difference between aCD3/aCD28 scaffold and Dynabeads was due to minimal contact between T-cells and the scaffold highlighted through imaging (discussed further in **Section 7.4.7**).

Additionally, the CD4:CD8 ratio for Dynabead cultures was displayed to have reduced from 2.5 in the previous study to 1.2 here. This was thought to have occurred due to changes in the experimental set-up, chiefly the culture of T-cells within a cell culture insert rather than directly into a well. This meant that T-cells

were suspended in ~250 µL media within the insert resulting in a higher cell density and also allowed additional media to be added to cultures with minimal cell disturbance. Furthermore, it has been reported that stiff substances with pores can promote the differentiation of other cell types to phenotypes observed on softer substrates (Cheung *et al*., 2018). This would indicate that the porous cell culture insert membrane may have presented itself to T-cells as more alike to a softer surface, thus impacting the resultant phenotype. Nevertheless, here it is reported a method of culturing T-cells, with both aCD3/aCD28 scaffold and Dynabeads, that resulted in a favourable, more even, CD4:CD8 ratio, and comprised predominantly of T_{CM}.

Finally, it was observed that T-cells activated with aCD3/aCD28 scaffold produced more IFNγ than when stimulated with Dynabeads. This difference was not found to be statistically significant, however, this was likely due to donor variation which is common within T-cell cultures.

It was interesting to note that, generally, the variation in results appeared to increase with aCD3/aCD28 scaffold cultures compared to Dynabeads, with the exceptions of $CD4^+$ T_{EM}, percentage dividing, and IFNγ production. This was likely due to the variation in physical contact with individual scaffold sections that proliferating T-cells were found to have, which introduced differences between individual aCD3/aCD28 scaffold cultures (further discussed below in **Section 7.4.7**).

7.4.6. Comparison to other 2D and 3D Hydrogels and Scaffolds

The use of hydrogels for biomedical applications has proved useful in many areas including contact lenses, hygiene products, wound dressings, tissue engineering scaffolds, and drug delivery systems. These can be found reviewed elsewhere

(Caló and Khutoryanskiy, 2015). More specifically in the field of T-cell immunotherapy, hydrogels have most often been employed either as a delivery vector or to study the impact of mechanical properties, such as stiffness, on T-cell functionality and immune synapse formation (Judokusumo *et al*., 2012; Singh and Peppas, 2014; Basu *et al.,* 2016; Weiden *et al*., 2018; Wahl *et al*., 2019; Majedi *et al*., 2020).

Most commonly T-cell activation and expansion studies employing a 2D or 3D hydrogel focus either on activation alone, or expansion where activation is provided externally (Stephan *at al.,* 2015; Smith *et al*., 2017; Pérez del Río *et al*.; 2018; Weiden *et al*., 2018; Chin *et al*., 2020; Majedi *et al*., 2020; Zhang *et al.,* 2021). Furthermore reported expansion studies tend to last a maximum of 7 days. To the best of my knowledge at the time of writing, the literature available on the activation and expansion of primary human T-cells both with and on a 2D or 3D hydrogel is limited and it is therefore difficult to directly compare this T-cell activation technology.

In regards to the use of a 2D hydrogel for both T-cell activation and expansion, Li *et al.* (2020) describe a hydrogel synthesised from tufsin (a naturally occurring terapeptide) and Nap-GDFDFDY (a vaccine adjuvant) which was successfully used to stimulate murine $CD8^+$ T-cells. Alike to the results presented here, the group reported that the hydrogel resulted in a preferential stimulation of $CD8^+$ T-cells after a 5 day culture. Differences in studies, however, must be highlighted and include T-cell origins, sample time point, stimulating ligands, and hydrogel material.

More closely resembling the aCD3/aCD28 polymer, Hickey *et al*. (2019) reported a hydrogel comprised of cross-linked hyaluronic acid and polyethylene glycol

diacrylate with aCD3 and aCD28 attached that successfully activated and expanded murine $CD8^+$ T-cells. Expansion over 7 days was found to be 7 to 20 –fold, dependant on ligand density. As expansion here was demonstrated to be around the lower value (~8-fold, **Figure 7.2b**) it would suggest that further antibody optimisation may be required in order to increase fold expansion. Most interestingly it was found by Hickey *et al*. that T-cells required at least 5 days in contact with the hydrogel for successful activation and that T-cells removed on days 1 and 3 were sub-optimally activated. This strongly coincides with results that were observed here – that only a very low percentage of T-cells were proliferating 4 days post aCD3/aCD28 polymer exposure (**Figures 7.10** and **7.11a** and **e**) and that T-cells appeared to be in lag phase until day 5 – 7 (**Figure 7.2a**). Furthermore, Hickey *et al*. also assessed the resultant T-cell phenotype, and found that the dominant population for hydrogels with a stiffness ≤ 1 kPa was T_{CM}, and ≥ 1.7 kPa was T_{EM}. Comparatively, within the $CD8^+$ T-cell population here it was demonstrated that T_{CM} was the dominant population (**Figure 7.7**) which most closely corresponds to the results reported for ≤ 1 kPa. Moreover, future studies may consider altering the stiffness of aCD3/aCD28 polymer through varying the ε-PL to cross-linker ratio as a tool to modulate the resultant T-cell populations.

Similarly, Saitakis *et al*. (2017) used a PA hydrogel with aCD3 and aCD28 attached to investigate the impact of stiffness on human $CD4^+$ T-cell responses. It was found that stimulation with their hydrogel resulted in increased CD25 expression, progression through the cell cycle, number of proliferating cells, and IFNγ concentration. This was alike to the results presented here. However, it is important to note that cultures with the PA hydrogel were only ran for 1 day and cell numbers were not reported.

The use of scaffolds with aCD3 and aCD28 attached to activate and expand T-cells has been reported and include electrospun PDMS (Dang *et al*., 2018), 3D printed PCL lattices (Delalat *et al*., 2017), and silica micro-rods which settle in culture to form a "scaffold" (Cheung *et al.,*2018; Zhang *et al.,* 2020). Additionally, other studies describe the use of a scaffold where T-cells were pre-activated and transferred into scaffolds for expansion. These include a polystyrene scaffold (purchased from 3D Biotek), Matrigel™ (Pérez del Río *et al*., 2018), a PEG-Hep hydrogel (Pérez del Río *et al*., 2020), and alginate scaffolds (Majedi *et al*., 2020). Of these, the latter two are considered the most comparable to the aCD3/aCD28 polymer scaffold presented here, due to their hydrogel materials and similar pore sizes.

Pérez del Río *et al*. (2020) demonstrated that human $CD4^+$ T-cells activated with Dynabeads displayed an increase in replication, proliferation, and expansion indices when cultured on a PEG-Hep scaffold on day 6. Proliferation indices were not assessed with aCD3/aCD28 scaffold, however the non-significant difference in overall-fold expansion (**Figure 7.13a**) suggests that there were no significant increases in proliferation; however differences in the timings of the assessment and stimulation method must be noted. Additionally, Pérez del Río *et al*. assessed cultures for T_N, T_{CM}, and T_{EM} on day 5 and found a decrease in T_{CM} and an increase in T_N and T_{EM} with cultures on PEG-Hep compared to in suspension. This mirrored what was found here within the $CD4^+$ population (**Figure 7.15**), with the main difference being a slightly smaller decrease in the percentage of T_{CM} (~20 % with PEG-Hep, ~15 % with aCD3/aCD28 polymer scaffold). Unfortunately, values for cell numbers themselves were not reported and so comparisons of expansion are not possible.

Alginate scaffolds have been used as both a T-cell delivery method via implantation (Stephan *et al*., 2015; Smith *et al*., 2017) and more recently, as a tool to study the effect of stiffness on T-cell activation in a 3D microenvironment (Majedi *et al*., 2020). Majedi *et al.* (2020) stimulated murine $CD4^+$ T-cells with either peptide loaded APCs or aCD3/aCD28 micro-particles that were seeded into scaffolds of varied stiffness's, and reported enhanced activation with stiffer scaffolds (40 kPa). Similarly as mentioned above with non-porous aCD3/aCD28 polymer, this highlights the potential that future studies involving the variation of stiffness of porous aCD3/aCD28 scaffolds may further improve and modulate the T-cell activation process.

One final study worth mentioning here is one in which the hydrogel format does not strictly fall into the category of 2D or 3D as those already discussed. Jesuraj *et al*. (2016) describe a T-cell activating technology in which an alginate-based hydrogel is coated onto micro-particles and aDC3/aD28 is bound. It was reported that expansion for 13 days via this method promoted the expansion of $CD8^+$, T_N and T_{CM} cells. This was in concurrence with the results that were found here; that activation with non-porous aCD3/aCD28 polymer displayed a preferential expansion of $CD8^+$ T-cells in which the majority were T_{CM} or T_N, and that expansion with aCD3/aCD28 scaffold resulted in a dominant population of T_{CM}, closely seconded by T_N, within $CD8^+$ T-cells.

7.4.7. Culture Visualisation

The transparent nature of non-porous aCD3/aCD28 polymer B enabled cultures to be imaged via confocal microscopy. Though this, clusters of proliferating T-cells in contact with the scaffold were able to be visualised (**Figure 7.1**). Interestingly, cultures stimulated with aCD3/aCD28 polymer appeared to display smaller T-cell colonies when compared to Dynabeads cultures which appeared

to display larger clusters from day 3. It is possible that this is due to the activated T-cells on the polymer attaching to the polymer surface thereby restricting movement. If this is indeed the case it would be plausible that an increased number of smaller proliferating clusters may lead to an increase in the diversity of TCR receptors and it would be of interest to assess this through methods such as TCR spectratyping (Ciupe *et al*., 2013).

Porous aCD3/aCD28 scaffold cultures were imaged via z-stack fluorescence confocal imaging to produce 3D reconstructions and assess cell-scaffold interactions. Although T-cells were found to be attached throughout aCD3/aCD28 Scaffolds at day 1, it was revealed that the majority of T-cells were at the base of the culture dish with no contact with the scaffold (**Figure 7.22** and **7.23**). By day 7, T-cell clusters were predominantly identified growing at the base of the scaffold (**Figures 7.23d** and **h**). With proliferating T-cell clusters, single points of contact with the scaffold could be identified (**Figure 7.24c**). However, the majority of cells within the cluster were not observed to be in contact with the scaffold, and cells at the base of clusters were, in most cases, in contact with the bottom of the culture dish (**Figures 7.24a** and **d**). This was not expected as it was anticipated that the majority of T-cells would be attached throughout - through the interaction with aCD3/aCD28 antibodies bound to the polymer.

Previously it was demonstrated that T-cells in contact with aCD3/aCD28 polymer remained mobile which lead to the postulation that this was due to a low antibody density and that T-cell activation ultimately occurred through kinapses. It likely that, also due to low antibody density, gravitational forces in this case were stronger than cell-scaffold interactions resulting in cells settling to the bottom of the culture. Additionally, given the small height of scaffold sections (30 mm) it is also likely that migrating T-cells will have fallen through pores to the base of the

dish relatively quickly instead of to another section of scaffold, as would occur with a scaffold of increased height. Furthermore, cultures were transported from one building to another for imaging. Whilst the best of care was taken to ensure minimal disruption to cultures it is unlikely they were not subject significant movement, particularly as scaffolds were much smaller than the imaging dishes. This agitation may have caused T-cells to physically be removed from scaffolds.

In order to increase T-cell attachment to the scaffold modifications may be made, including the attachment of additional ligands. Arg-Gly-Asp (RGD) is a peptide known to promote cell adhesion and its use to promote T-cell binding to an alginate scaffold has previously been reported; moreover the addition of RGD to alginate scaffolds increased both the percentage of T-cells proliferating and the percentage of and MFI of CD25 expressing T-cells (Majedi *et al*., 2020). Additionally, lymphocyte function associated antigen-3 (LFA-3) and intercellular adhesion molecule 1 (ICAM-1) are ligands which bind to CD2 and lymphocyte function associated antigen-1 (LFA-1) on T-cells, respectively, promoting both adhesion and proliferation (Wingren *et al*., 1995). Moreover, RGD, LFA-3, and ICAM-1 all possess a NH_2 terminal group which would allow them to be attached to COOH functionalised polymer B in the same manner as aCD3 and aCD28 (Wallner *et al.,*1987; Suh and Tirrel, 2011; Yang, 2012).

Another potential option would be to load gels with chemokines such as chemokine (C-C motif) ligand 19 (CCL19) and CCL21, as was implemented by Pérez del Río *et al*. (2020). Both CCL19 and CCL21 bind to CCR7 on expressing T-cells and induce chemotaxis which may encourage migration of T-cells into scaffolds (Hipkin, 2007). Furthermore, it may be worth investigating the impact of seeding cells onto dry scaffolds vs wet scaffolds as studies by Agarwalla *et al*. (li

e) demonstrated increased contact with alginate scaffolds when they were dried before T-cell seeding.

It was not expected that the polymer would fluoresce in channels used to observe the membrane and nuclear dye (**Figure 7.24a**). The fact that this did not occur during imaging of unstained controls (**Appendix C.4**) suggests that this was due to non-specific absorption of excess dyes by the polymer. It is likely that this was further exacerbated by the exclusion of washing steps, which was implemented to maintain culture integrity and cell-scaffold interactions. Fortunately, T-cells were still able to be identified through their lack of fluorescence in the DAPI channel, however it would be suggested that the staining process should be further optimised. Possibly though the use of fluorescent antibodies, which were not found to be non-specifically absorbed by the polymer previously (**Appendices C.2** and **C.3**). Nonetheless, z-stack fluorescence confocal microscopy was successfully implemented to visualise proliferating T-cells stimulated by porous aCD3/aCD28 polymer scaffolds. Though, as with previous imaging using this technique (**Sections 5.3.2** and **5.3.5**), image depth was limited by spherical aberration, resulting in an approximate maximum of 300 µm depth into the polymer before imaging became distorted by spherical aberration.

7.5. Conclusion

Both porous and non-porous polymer B with aCD3 and aCD28 attached were investigated for their ability to activate and expand primary human T-cells. Here, the non-porous format is referred to as non-porous aCD3/aCD28 polymer, and the porous format is referred to as aCD3/aCD28 scaffold. In these proof-of-concept studies, both non-porous aCD3/aCD28 polymer and aCD3/aCD28

scaffold demonstrated successful activation and expansion of T-cells over a 14 day period, with final expansions of 8.3 and 11 –fold, respectively.

The expansion of T-cells with non-porous aCD3/aCD28 polymer was characterised through the evaluation of the following over the culture duration: growth, viability, cell diameter, and activation marker expression (CD69 and CD25). End-point analysis was preformed to determine exhaustion marker expression (LAG-3 and PD-1), and cell cycle. Additionally, early-stage proliferation was assessed at day 4 through the use of CFSE. The expansion of T-cells with aCD3/aCD28 scaffold was characterised through metabolic profile over the course of the culture, and end-point analysis of the following: viability, cell diameter, apoptosis, cell cycle, and IFNγ concentration.

Overall it was found that the viability of cultures stimulated with non-porous aCD3/aCD28 polymer demonstrated remained high (> 91.7 %) throughout the culture. Additionally, analysis of the expression of exhaustion markers indicated after a 14 days, T-cells were not exhausted. Thus, expansion with non-porous aCD3/aCD28 polymer resulted a viable and healthy T-cell culture. Cultures stimulated with Dynabeads demonstrated both a decrease in viability for the majority of time points, and an increase in exhaustion marker PD-1 in comparison.

An increase in the average cell diameter was observed from day 1 with a maximum increase of 2 µm on day 5. The percentage of T-cells expressing one or both activation markers peaked at 53 % on day 3 and declined to 37 % by day 14. Low numbers of cells (~17 %) were determined to be in an active state of division by day 14. Analysis of total cell numbers over time and the low percentages of T-cells found dividing at day 4 through proliferation analysis,

indicated a lag-time in growth of approximately 5 days. This is believed to be due to the serial encounter mode in which it is hypothesised that T-cells interacting with aCD3/aCD28 polymer become activated by.

Stimulation of T-cells with aCD3/aCD28 scaffold was found to induce IFNγ secretion, indicating the expansion of T-cells with cytotoxic function. The percentage of cells dividing at day 14 was determined to be 20 %. The average cell diameter of T-cells was not found to be significantly different to the negative control on day 14. This was unexpected, however, it is believed to be due to the gradual increase in diameter of the control and it is suggested that future studies investigate earlier time points. Culture health when stimulated with aCD3/aCD28 scaffolds was assessed by two methods, non-viable cell exclusion via DAPI staining and an apoptosis assay via annexin V and PI staining. These methods determined good percentages of viable T-cells of 88 % and 77 %, respectively.

Glucose, glutamine, lactate, and ammonia concentrations in spent media were analysed in aCD3/aCD28 scaffold cultures over 13 days. Glucose and glutamine consumption rates at days 0 – 3 were not significantly different to the control, indicating that cells were not metabolically active before this point. As with non-porous aCD3/aCD28 polymer it is thought that this is due to activation by the serial encounter method which requires additional stimulation time. Overall, cultures stimulated with aCD3/aCD28 scaffold consumed less glucose and glutamine, and produced less lactate than cultures stimulated with Dynabeads. Additionally, ammonia concentrations were low which indicates favourable culture conditions.

Multi-parameter flow cytometry was employed to assess the population composition of expanded T-cells for $CD8^+$ and $CD4^+$, and sub-populations within

of T_N, T_{CM}, T_{EM}, T_{EMRA}. Phenotypic analysis of T-cells expanded with non-porous aCD3/aCD28 polymer revealed a CD4:CD8 ratio of 0.72, indicating a preferential expansion of $CD8^+$ T-cells. This was significantly lower than the CD4:CD8 ratio of 2.5 observed with Dynabeads. Furthermore, proliferation analysis at day 4 of the culture also indicated a slight preference for $CD8^+$ T-cell stimulation. When expanded with aCD3/aCD28 scaffold the CD4:CD8 ratio was 1.2.

For expansion with non-porous aCD3/aCD28 polymer, within $CD4^+$ T-cells, T_{EM} (40 %) and T_{CM} (37 %) were the dominant sub-populations. Within $CD8^+$ T-cells this was found to be T_{CM} (38 %). When compared to expansion via Dynabeads the only significant difference highlighted was an increase of 9 % $CD8^+$ T_{EMRA}. For expansion with aCD3/aCD28 scaffold, T_{CM} was demonstrated to be the dominant sub-population within both $CD4^+$ (84 %) and $CD8^+$ (50 %) T-cells. Small increases in both $CD4^+$ and $CD8^+$ T_{EM} were found to be the only significant differences compared to Dynabeads.

Thus it was demonstrated that expansion with both non-porous and porous aCD3/aCD28 polymer B resulted in the generation of clinically relevant sub-populations of T-cells. Furthermore these were found to be comparable to stimulation with the current industry gold standard, Dynabeads.

Visualisation of cultures with non-porous aCD3/acD28 polymer was successfully achieved through the use of confocal microscopy. It was observed that T-cells formed small clusters on the surface of the polymer which expanded as T-cells proliferated.

The more challenging visualisation of cultures with aCD3/aCD28 scaffold was successfully achieved through the use of z-stack fluorescence confocal microscopy and the re-construction of 3D images. Through these images it was

observed that although T-cells were attached throughout the scaffold, the majority had settled to the base of the culture dish by day 1. T-cell colonies were observed growing both suspended on the scaffold, and, most commonly, at the base of the culture with a single contact point on the scaffold.

Chapter 8. Summary, Conclusion, and Future Work

8.1. Summary of Key Findings

The aim of this thesis was to demonstrate and characterise the activation and expansion of primary human T-cells using SpheriTech's biopolymer technologies as a platform. Additionally, it was sought that this technology would operate as a 3D cell scaffold to maximise the surface area presenting stimulating ligands to cells, and to allow the mitigation of the bead removal process step currently required when activating T-cells with antibody coated beads; ultimately with the aim of reducing processing costs in T-cell therapies.

The work presented in this thesis describes initial characterisation and studies to provide proof-of-concept of two novel biopolymer based T-cell activation platforms, performed in line with the thesis aim. The key findings of each results chapter are summarised below.

Initially, a first polymer termed polymer A was investigated. Characterisation of polymer A was performed in **Chapter 3**. It was found that the polymer was highly porous and consisted of a vastly interconnected pore network, with pores within the macro-porous (50 nm - 10 µm) range. Furthermore, it was found that as the polymer density decreased, porosity increased and a small proportion of the pores increased to a larger maximum size. An ELISA assay was developed and confirmed the attachment of T-cell stimulating antibodies aCD3 and aCD28 to polymer A. Attached antibodies were visualised and found to be distributed throughout the polymers 3D surface, with minimal diffusion into the polymer structure itself. Values for tortuosity indicated good flow through properties of polymer A. Minor toxicity to T-cells in culture with polymer A was found and believed to be due to poor polymer washing. Finally, auto-fluorescence of

polymer A was found to be lowest towards the higher (red) end of the excitation/ emission spectrum.

Polymer A was then evaluated for its suitability as a T-cell activating cell scaffold in **Chapter 4**. Initial studies focused on T-cell activation. It was found that exposure of primary human T-cells to aCD3/aCD28 polymer A resulted in an increased expression of the activation marker CD69, which indicated T-cell activation. Parallel studies investigated the ability to seed and remove T-cells from polymer A through the application of flow. Initial studies found an extremely low recovery of cells from polymer A. The initial experimental set up was adjusted to include various improvements and was used to investigate the impact of cell suspension density and flow rate on cell recovery. No interaction between the two variables was found, with the only significant factor found to be flow rate. Cell recovery was found to have increased dramatically from the initial study, to a maximum of 51 %. The pressure drop over polymer A in a chromatography style set up was characterised with water and found to increase linearly up to a maximum flow rate. The pressure within the system increased significantly with the addition of T-cells and indicated that cells were trapped within the polymer. It was decided that polymer A in its current format was not suitable for use in this project, as cells could not be sufficiently removed from the polymers 3D structure.

A second polymer termed polymer B was investigated. Characterisation of polymer B was performed in **Chapter 5**. The surface of the non-porous format of polymer B was found not to be macro-porous, as expected. The porous format of polymer B was found to possess a highly interconnected porous structure with pores in the super-macro-porous category (> 10 µm). The surface of porous polymer B was found to be smooth and devoid of macro- or miso- pores, and the internal structure of the polymer was found to be macro-porous. The attachment

of aCD3 and aCD28 was confirmed via ELISA on all polymer samples with the exception of non-porous polymer from batch 2. Attached antibodies were visualised and semi-quantified. Antibody was found attached to the entire surface of both non-porous and porous polymer B, with the distribution observed to be heterogeneous – particularly with the non-porous format. Non-porous polymer B was found to have good biocompatibility with T-cells. Porous polymer B was found to convey minor toxicity to T-cells, believed to be due to difficulties washing larger sections of polymer. Finally, auto-fluorescence of polymer B was found to be lowest towards the higher (red) end of the excitation/ emission spectrum.

Initial investigations into the interaction of T-cells and polymer B were performed in **Chapter 6**. Crucially, it was found that there was a high recovery of T-cells that were seeded into porous polymer B. The mobility of T-cells was found to be significantly reduced on polymer B, with comparatively high numbers of mobile cells found when aCD3 and aCD28 was attached. Patterns of movement exhibited by T-cells in contact with aCD3/aCD28 polymer B was characterised as Lévy type super-diffusion. Additionally, polymer B was validated as a material on which primary human T-cells can expand.

The ability of both non-porous and porous polymer B to activate and expand primary human T-cells, and the impact this had on the culture was investigated in **Chapter 7**. It was successfully demonstrated that polymer B in both a non-porous and a porous 3D scaffold format was able to activate and instigate T-cell expansion. Furthermore, expansions were characterised in regards to multiple outputs, such as culture health, growth dynamics, and metabolic profile, and were found to be largely comparable to the current most commonly used technology, aCD3/aCD28 magnetic beads (Dynabeads). With non-porous polymer B a preferential expansion of $CD8^+$ T-cells over $CD4^+$ was indicated, with the opposite

found for bead based expansion. This preference was not exhibited with the porous scaffold format and was hypothesised to be due to the lack of cell-polymer contact of growing T-cells; this was highlighted through the visualisation of live cultures which was achieved via 3D reconstructions of z-stack fluorescence confocal microscopy images. T-cells expanded with both non-porous and porous polymer B were found to comprise of clinically desirable sub-populations, with high percentages of T_{CM}. Moreover, T-cells demonstrated increased cytotoxic capabilities, such as increases in $CD8^+$ T-cells and IFNγ production, in addition to decreased expression of the exhaustion marker PD-1 compared to Dynabeads.

8.2. Final Thesis Conclusion

The work presented in this thesis has successfully demonstrated the ability of an aCD3/aCD28 coated biopolymer, in both a non-porous and a porous 3D scaffold format, to activate and expand primary human T-cells. Expansion using this novel platform was found to be comparable to expansion with the current industry gold standard, antibody coated magnetic beads (Dynabeads). Furthermore, T-cells expanded with aCD3/aCD28 polymers consisted of clinically desirable populations with advantageous functional characteristics and reduced exhaustion.

8.3. Recommendations for Future Work

8.3.1. Increase T-cell Interaction with Scaffolds

Although contact with porous aCD3/aCD28 polymer B scaffolds resulted in the activation and expansion of T-cells, microscopy images in **Chapter 7** highlighted a low level of cell-scaffold contact throughout the scaffolds structure. It would be recommended that future studies investigate methods of increasing cell-scaffold

contact in order to utilise the full surface area of the 3D structure for antibody presentation. This may be achieved through the attachment of adhesion promoting molecules to the scaffolds surface, such the peptide RGD (Majedi *et al*., 2020), or ligands LFA-3 and ICAM-1 (Saitakis *et al*., 2017). Aspects of the culture set-up may also be considered, such as an introduction of flow into the polymer scaffold to counteract the settling of T-cells to the base of the scaffold/culture, or re-circulating T-cells that have fallen through back into the scaffold. Additionally, the orientation of antibodies bound to the polymers surface may be considered with the aim of optimising the presentation of attached antibodies to increase their interaction with T-cells (Shen *et al*., 2017).

If the attachment of T-cells to the scaffold was considerably improved, biopolymer scaffolds may also have the capacity be used as a cell separation/enrichment technology. Perhaps even with the potential to consolidate the selection and activation steps of T-cell therapy into a single processing step.

8.3.2. Attachment of Alternative Stimulatory Molecules

For the purpose of this work aCD3 was immobilised to stimulate the CD3 domain of the TCR to generate a primary stimulation signal to T-cells. aCD28 was immobilised to provide a second co-stimulatory signal through the stimulation of the CD28 receptor. This combination of stimulatory molecules is commonly used in T-cell activation and was successful in this project. There are, however, many additional co-stimulatory receptors that exist and their stimulation is understood to play roles in modulating T-cell survival, proliferation, and memory generation (Croft, 2003; Cheng and Flies, 2013). Receptors include: CD2, inducible co-stimulatory molecule (ICOS), OX40 (CD134), 4-1BB (CD137), and CD27. It is envisaged that future work would involve the attachment of corresponding ligands or targeted antibodies to polymer scaffolds to investigate whether T-cell

expansion could be enhanced, and to further control the resultant T-cell populations.

Furthermore, CD3 and CD28 stimulation of T-cells is used for the polyclonal expansion of T-cells which is required in the production of CAR T-cell therapies, however, there is also demand within ACT for the selection and expansion of antigen-specific T-cells (Yee *et al.,* 2002; Chruściel *et al*., 2020). This may be achieved in the future through the modification of polymer scaffolds to present tumour-related antigens.

8.3.3. Viral Transduction

To produce CAR T-cells, T-cells must be transduced with a CAR containing gene before expansion. Within the field, this has been achieved predominantly through the use DNA electroporation, plasmid-based transposon/transposase systems, and viral vectors. It would be strongly recommended that future work explore: 1) the compatibility of gene delivery methods with scaffold mediated activation and expansion, and 2) the best practices to optimise gene transduction. This would be an important avenue to validate the use of this novel technology in T-cell therapy.

Interestingly, Agarwalla *et al.* (2020) recently demonstrated scaffold-mediated static CAR gene transduction of T-cells using a porous alginate scaffold and gamma retrovirus. It is promising that the reported scaffold exhibits similar properties to the polymer scaffold in this thesis. It is therefore envisaged that CAR gene transduction using SpheriTech's biopolymer scaffolds may occur by the same method – addition of concentrated T-cells and retrovirus to a dry scaffold to facilitate interaction. It is also possible that this would allow activation and gene delivery to occur in a single step, whilst simultaneously providing an environment for subsequent expansion.

8.3.4. Scale-up and Process Intensification

The proof-of-concept studies presented in this thesis have demonstrated successful expansion of T-cells, however, during the production of T-cell therapies it is necessary to expand T-cells to clinically relevant quantities. Hence, it would be important for future studies to show that this is possible - to validate the potential use of this technology for clinical ACT production.

Three key approaches exist to increase the output quantity of T-cells: scale-out, scale-up, and process intensification. Scale-out would seek to increase cell numbers through multiple duplications of the current set-up; scale-up, by increasing the hardware capacity/ total culture volume; and process intensification, by optimising the set-up to give the most efficient output of cells. Given the labour intensity of the small scale expansion studies undertaken in this thesis, scale-out would be highly impracticable in a clinical setting. It would therefore be recommended that future studies explore both scale-up and process intensification to demonstrate a clinically significant expansion of T-cells.

Scale-up could be achieved by simply making polymer scaffolds in larger moulds, and the recommendations previously discussed in **Section 8.3.1** and **8.3.2** are examples of how the process could be optimised and thereby intensified. Additionally, the porous nature of the polymer scaffolds suggest that T-cells may be cultured to a high density within the scaffold via perfusion culture. Not only would this present another opportunity for process intensification, but also a method to overcome potential oxygen transfer issues which are commonly incurred when scaling up (Müller *et al*., 2022).

During this thesis, a preliminary effort to incorporate both a polymer scale-up and perfusion culture was undertaken and showed some promise (**Appendix I.1)**. Unfortunately, due to time constraints this was unable to be fully explored.

8.3.5. Alternative Applications

This thesis presents studies centred on the application of SpheriTech's biopolymer to activate and expand T-cells. These porous biopolymer scaffolds, however, may also be considered for use in alternative applications within the T-cell and general cell therapy field in the future.

Briefly, one such area of application may be within a scaled-down microfluidic device, such as the device developed by Chin *et al*. (2020) to investigate the physiochemical modulation of T-cell activation. This could also be used to investigate the activation conditions of other cells, such as B-cells and DCs. Another application may be within the area of therapy delivery, whereby scaffolds containing activated/modified cells are implanted within patients to facilitate the localised delivery of active cells to target areas (Shields IV *et al*., 2019). Furthermore, the notion of implantable scaffolds could be taken a step further with scaffolds placed to locally stimulate cells *in vivo* (Schluck *et al*., 2019).

References

Agarwalla, P., Ogunnaike, E., Ahn, S., Ligler, F., Dotti, G. and Brudno, Y. (2020). Scaffold-Mediated Static Transduction of T Cells for CAR-T Cell Therapy. *Advanced Healthcare Materials*, 9(14), p.2000275.

Ahmad, Z., Yeap, S., Ali, A., Ho, W., Alitheen, N. and Hamid, M. (2012). scFv Antibody: Principles and Clinical Application. *Clinical and Developmental Immunology*, 2012, pp.1-15.

Ahmed E. M. (2015). Hydrogel: Preparation, characterization, and applications: A review. *Journal of advanced research*, 6(2), pp. 105–121.

Ahn, Y., Ren, L., Kim, S., Seo, S., Jung, C., Kim, D., Noh, J., Lee, S., Lee, H., Cho, M., Jung, H., Yoon, S., Kim, J., Lee, S., Kim, S., Shin, I., Shin, H., Hong, K., Lim, Y., Choi, I. and Kim, T. (2020). A three-dimensional hyaluronic acid-based niche enhances the therapeutic efficacy of human natural killer cell-based cancer immunotherapy. *Biomaterials*, 247, p.e119960.

Akbar, A., Henson, S. and Lanna, A. (2016). Senescence of T Lymphocytes: Implications for Enhancing Human Immunity. *Trends in Immunology*, 37(12), pp.866-876.

Ali, O., Huebsch, N., Cao, L., Dranoff, G. and Mooney, D. (2009). Infection-mimicking materials to program dendritic cells in situ. *Nature Materials*, 8(2), pp.151-158.

Amadori, A., Zamarchi, R., De Silvestro, G., Forza, G., Cavatton, G., Danieli, G., Clementi, M. and Chieco-Bianchi, L. (1995). Genetic control of the CD4/CD8 T-cell ratio in humans. *Nature Medicine*, 1(12), pp.1279-1283.

Arcangeli, S., Falcone, L., Camisa, B., De Girardi, F., Biondi, M., Giglio, F., Ciceri, F., Bonini, C., Bondanza, A. and Casucci, M. (2020). Next-Generation Manufacturing Protocols Enriching TSCM CAR T Cells Can Overcome Disease-Specific T Cell Defects in Cancer Patients. *Frontiers in Immunology*, 11.

Arima, Y. and Iwata, H. (2015). Preferential adsorption of cell adhesive proteins from complex media on self-assembled monolayers and its effect on subsequent cell adhesion. *Acta Biomaterialia*, 26, pp. 72-81.

Asfour, H., Otridge, J., Thomasian, R., Larson, C. and Sarvazyan, N. (2020). Autofluorescence properties of balloon polymers used in medical applications. *Journal of Biomedical Optics*, 25(10).

Bajaj, I. and Singhal, R. (2011). Poly (glutamic acid) – An emerging biopolymer of commercial interest. *Bioresource Technology*, 102(10), pp.5551-5561.

Balvan, J., Krizova, A., Gumulec, J., Raudenska, M., Sladek, Z., Sedlackova, M., Babula, P., Sztalmachova, M., Kizek, R., Chmelik, R. and Masarik, M. (2015). Multimodal Holographic Microscopy: Distinction between Apoptosis and Oncosis. *PLOS ONE*, 10(3), p.e0121674.

Basu, R., Whitlock, B., Husson, J., Le Floc'h, A., Jin, W., Oyler-Yaniv, A., Dotiwala, F., Giannone, G., Hivroz, C., Biais, N., Lieberman, J., Kam, L. and Huse, M. (2016). Cytotoxic T Cells Use Mechanical Force to Potentiate Target Cell Killing. *Cell*, 165(1), pp. 100-110.

Batchu, R., Gruzdyn, O., Mahmud, E., Chukr, F., Dachepalli, R., Manmari, S., Mostafa, G., Weaver, D. and Gruber, S. (2018). Inhibition of Interleukin-10 in the tumor microenvironment can restore mesothelin chimeric antigen receptor T cell activity in pancreatic cancer in vitro. *Surgery*, 163(3), pp.627-632.

BD Biosciences. (2011). Technical Resources: Protocol for CD3 Stimulation of Human T cells for the Detection of Activation Markers. BD Biosciences.

Beauchemin, C., Dixit, N. and Perelson, A. (2007). Characterizing T Cell Movement within Lymph Nodes in the Absence of Antigen. *The Journal of Immunology*, 178(9), pp. 5505-5512.

Bencherif, S., Warren Sands, R., Ali, O., Li, W., Lewin, S., Braschler, T., Shih, T., Verbeke, C., Bhatta, D., Dranoff, G. and Mooney, D. (2015). Injectable cryogel-based whole-cell cancer vaccines. *Nature Communications*, 6(1).

Bhat, P., Leggatt, G., Waterhouse, N. and Frazer, I. (2017). Interferon-γ derived from cytotoxic lymphocytes directly enhances their motility and cytotoxicity. *Cell Death & Disease*, 8(6), pp. e2836-e2836.

BioLegend. (2022). Technical Protocols: T cell activation with anti-CD3 Antibodies Protocol - Human. [online]. Available at: https://www.biolegend.com/en-us/protocols/t-cell-activation-with-anti-cd3-antibodies-protocol-human [Accessed 04 May 2022].

Bio-Techne. (2022). GMP Cloudz Human T Cell Activation Kit. [online]. Available at: https://www.bio-techne.com/p/cell-culture/gmp-cloudz-human-t-cell-activation-kit_cld001-gmp [Accessed 21 April 2022].

Blaese, R., Culver, K., Miller, A., Carter, C., Fleisher, T., Clerici, M., Shearer, G., Chang, L., Chiang, Y., Tolstoshev, P., Greenblatt, J., Rosenberg, S., Klein, H., Berger, M., Mullen, C., Ramsey, W., Muul, L., Morgan, R. and Anderson, W. (1995). T Lymphocyte-Directed Gene Therapy for ADA- SCID: Initial Trial Results After 4 Years. *Science,* 270(5235), pp.475-480.

Böhmer, R., Bandala-Sanchez, E. and Harrison, L. (2011). Forward light scatter is a simple measure of T-cell activation and proliferation but is not universally suited for doublet discrimination. *Cytometry Part A,* 79A(8), pp.646-652.

Borgert, R. (2021). Improving outcomes and mitigating costs associated with CAR T-cell therapy. *American Journal of Managed Care*, 27(Suppl 13), pp.S253-S261.

Bryn, T., Yaqub, S., Mahic, M., Henjum, K., Aandahl, E. and Tasken, K. (2007). LPS-activated monocytes suppress T-cell immune responses and induce FOXP3+ T cells through a COX-2-PGE2-dependent mechanism. *International Immunology*, 20(2), pp.235-245.

Buchwalow, I., Samoilova, V., Boecker, W. and Tiemann, M. (2011). Non-specific binding of antibodies in immunohistochemistry: fallacies and facts. *Scientific Reports*. 1 (1).

Buhl, T., Legler, T. J., Rosenberger, A., Schardt, A., Schön, M. P., & Haenssle, H. A. (2012). Controlled-rate freezer cryopreservation of highly concentrated peripheral blood mononuclear cells results in higher cell yields and superior autologous T-cell stimulation for dendritic cell-based immunotherapy. *Cancer immunology, immunotherapy : CII*, 61(11), pp.2021–2031.

Busch, D., Fräßle, S., Sommermeyer, D., Buchholz, V. and Riddell, S. (2016). Role of memory T cell subsets for adoptive immunotherapy. *Seminars in Immunology*, 28(1), pp. 28-34.

Butler, M. and Hirano, N. (2013). Human cell-based artificial antigen-presenting cells for cancer immunotherapy. *Immunological Reviews*, 257(1), pp.191-209.

Cahalan, M. and Parker, I. (2008). Choreography of Cell Motility and Interaction Dynamics Imaged by Two-Photon Microscopy in Lymphoid Organs. *Annual Review of Immunology*, 26(1), pp. 585-626.

Caló, E. and Khutoryanskiy, V. (2015). Biomedical applications of hydrogels: A review of patents and commercial products. *European Polymer Journal*, 65, pp.252-267.

Campi, G., Varma, R. and Dustin, M. (2005). Actin and agonist MHC–peptide complex–dependent T cell receptor microclusters as scaffolds for signaling. *Journal of Experimental Medicine*, 202(8), pp. 1031-1036.

Castella, M., Caballero-Baños, M., Ortiz-Maldonado, V., González-Navarro, E., Suñé, G., Antoñana-Vidósola, A., Boronat, A., Marzal, B., Millán, L., Martín-Antonio, B., Cid, J., Lozano, M., García, E., Tabera, J., Trias, E., Perpiña, U., Canals, J., Baumann, T., Benítez-Ribas, D., Campo, E., Yagüe, J., Urbano-Ispizua, Á., Rives, S., Delgado, J. and Juan, M. (2020). Point-Of-Care CAR T-Cell Production (ARI-0001) Using a Closed Semi-

automatic Bioreactor: Experience From an Academic Phase I Clinical Trial. *Frontiers in Immunology*, 11.

Castro, F., Cardoso, A., Gonçalves, R., Serre, K. and Oliveira, M. (2018). Interferon-Gamma at the Crossroads of Tumor Immune Surveillance or Evasion. *Frontiers in Immunology*, 9.

Catakovic, K., Klieser, E., Neureiter, D. and Geisberger, R. (2017). T cell exhaustion: from pathophysiological basics to tumor immunotherapy. *Cell Communication and Signaling*, 15(1).

Chen, L. and Flies, D. (2013). Molecular mechanisms of T cell co-stimulation and co-inhibition. *Nature Reviews Immunology*, 13(4), pp. 227-242.

Cheung, A., Zhang, D., Koshy, S. and Mooney, D. (2018). Scaffolds that mimic antigen-presenting cells enable *ex vivo* expansion of primary T cells. *Nature Biotechnology*, 36(2), pp.160-169.

Chin, M., Norman, M., Gentleman, E., Coppens, M. and Day, R. (2020). A Hydrogel-Integrated Culture Device to Interrogate T Cell Activation with Physicochemical Cues. *ACS Applied Materials & Interfaces*, 12(42), pp.e47355-47367.

Chmielewski, M. and Abken, H. (2020). TRUCKS, the fourth-generation CAR T cells: Current developments and clinical translation. *Advances in Cell and Gene Therapy*, 3(3).

Chow, C., Rincón, M. and Davis, R. (1999). Requirement for Transcription Factor NFAT in Interleukin-2 Expression. *Molecular and Cellular Biology*, 19(3), pp.2300-2307.

Chruściel, E., Urban-Wójciuk, Z., Arcimowicz, Ł., Kurkowiak, M., Kowalski, J., Gliwiński, M., Marjański, T., Rzyman, W., Biernat, W., Dziadziuszko, R., Montesano, C., Bernardini, R. and Marek-Trzonkowska, N. (2020). Adoptive Cell Therapy—Harnessing Antigen-Specific T Cells to Target Solid Tumours. *Cancers*, 12(3), p. 683.

Cibrián, D. and Sánchez-Madrid, F. (2017). CD69: from activation marker to metabolic gatekeeper. *European Journal of Immunology*, 47(6), pp. 946-953.

Ciupe, S., Devlin, B., Markert, M. and Kepler, T. (2013). Quantification of total T-cell receptor diversity by flow cytometry and spectratyping. *BMC Immunology*, 14(1),

Coley, W. (1891). Contribution To The Knowledge of Sarcoma. *Annals of Surgery*, 14, pp.199-220.

Committee for Medicinal Products for Human Use. (2018). Assessment Report: Kymriah. European Medicines Agency, p. 33.

Costariol, E., Rotondi, M., Amini, A., Hewitt, C., Nienow, A., Heathman, T. and Rafiq, Q. (2020). Demonstrating the Manufacture of Human CAR-T Cells in an Automated Stirred-Tank Bioreactor. *Biotechnology Journal*, 15(9), p.e2000177.

Croft, M. (2003). Costimulation of T cells by OX40, 4-1BB, and CD27. *Cytokine & Growth Factor Reviews*, 14(3-4), pp. 265-273.

Crompton, J., Sukumar, M. and Restifo, N. (2013). Uncoupling T-cell expansion from effector differentiation in cell-based immunotherapy. *Immunological Reviews*, 257(1), pp. 264-276.

d'Ambrosio, D., Cantrell, D., Frati, L., Santoni, A. and Testi, R. (1994). Involvement of p21ras activation in T cell CD69 expression. *European Journal of Immunology*, 24(3), pp.616-620.

Dainiak, M., Kumar, A., Galaev, I. and Mattiasson, B. (2007). Methods in Cell Separations. *Cell Separation*, pp. 1-18.

Dang, A., De Leo, S., Bogdanowicz, D., Yuan, D., Fernandes, S., Brown, J., Lu, H. and Kam, L. (2018). Enhanced Activation and Expansion of T Cells Using Mechanically Soft Elastomer Fibers. *Advanced Biosystems*, 2(2), p.e1700167.

Darzynkiewicz, Z., Sharpless, T., Staiano-Coico, L., Melamed, M. R. Subcompartments of the G1 phase of cell cycle detected by flow cytometry. (1980) *Proceedings of the National Academy of Sciences of the United States of America*. 77(11), pp.6696-6699.

Deeg, J., Axmann, M., Matic, J., Liapis, A., Depoil, D., Afrose, J., Curado, S., Dustin, M. and Spatz, J. (2013). T Cell Activation is Determined by the Number of Presented Antigens. *Nano Letters*, 13(11), pp.5619-5626.

Delalat, B., Harding, F., Gundsambuu, B., De-Juan-Pardo, E., Wunner, F., Wille, M., Jasieniak, M., Malatesta, K., Griesser, H., Simula, A., Hutmacher, D., Voelcker, N. and Barry, S. (2017). 3D printed lattices as an activation and expansion platform for T cell therapy. *Biomaterials*, 140, pp.58-68.

Dudley, M., Wunderlich, J., Shelton, T., Even, J. and Rosenberg, S. (2003). Generation of Tumor-Infiltrating Lymphocyte Cultures for Use in Adoptive Transfer Therapy for Melanoma Patients. *Journal of Immunotherapy*, 26(4), pp.332-342.

Dustin, M., Bromley, S., Kan, Z., Peterson, D. and Unanue, E. (1997). Antigen receptor engagement delivers a stop signal to migrating T lymphocytes. *Proceedings of the National Academy of Sciences*, 94(8), pp. 3909-3913.

Eggermont, L., Paulis, L., Tel, J. and Figdor, C. (2014). Towards efficient cancer immunotherapy: advances in developing artificial antigen-presenting cells. *Trends in Biotechnology*, 32(9), pp.456-465.

Fadel, T., Sharp, F., Vudattu, N., Ragheb, R., Garyu, J., Kim, D., Hong, E., Li, N., Haller, G., Pfefferle, L., Justesen, S., Herold, K. and Fahmy, T. (2014). Erratum: Corrigendum: A carbon nanotube–polymer composite for T-cell therapy. *Nature Nanotechnology*, 9(9), pp.723-723.

Fernández-Riejos, P., Goberna, R. and Sánchez-Margalet, V. (2008). Leptin promotes cell survival and activates Jurkat T lymphocytes by stimulation of mitogen-activated protein kinase. *Clinical and Experimental Immunology*, 151(3), pp.505-518.

Ferreira, C., Barros, L., Baptista, M., Blankenhaus, B., Barros, A., Figueiredo-Campos, P., Konjar, Š., Lainé, A., Kamenjarin, N., Stojanovic, A., Cerwenka, A., Probst, H., Marie, J. and Veldhoen, M. (2020). Type 1 Treg cells promote the generation of CD8+ tissue-resident memory T cells. *Nature Immunology*, 21(7), pp. 766-776.

Finney, H., Lawson, A., Bebbington, C., Neil, A. and Weir, C. (1998). Chimeric Receptors Providing Both Primary and Costimulatory Signaling in T Cells from a Single Gene Product. *Journal of Immunology*, 161(6), pp.2791-2797.

Freed, E. and Martin, M. (1994). HIV-1 infection of non-dividing cells. *Nature*, 369(6476), pp.107-108.

Friedl, P. and Gunzer, M. (2001). Interaction of T cells with APCs: the serial encounter model. *Trends in Immunology*, 22 (4), pp. 187-191.

Gallagher, A. G. (2017). A Novel Peptide Hydrogel for an Antimicrobial Bandage Contact Lens. PhD thesis, University of Liverpool, Liverpool.

Gallagher, A., Alorabi, J., Wellings, D., Lace, R., Horsburgh, M. and Williams, R. (2016). A Novel Peptide Hydrogel for an Antimicrobial Bandage Contact Lens. *Advanced Healthcare Materials*, 5(16), pp.2013-2018.

Ganeeva, I., Zmievskaya, E., Valiullina, A., Kudriaeva, A., Miftakhova, R., Rybalov, A., Bulatov, E. Recent Advances in the Development of Bioreactors for Manufacturing of Adoptive Cell Immunotherapies. (2022). *Bioengineering*. 9(12). pp. 808.

Gattinoni, L., Klebanoff, C. and Restifo, N. (2012). Paths to stemness: building the ultimate antitumour T cell. *Nature Reviews Cancer*, 12 (10), pp. 671-684.

Gattinoni, N., Lugli, E., Ji, Y., Pos, Z., Paulos, C., Quigely, M., Ameida, J., Gostick, E., Yu, Z., Carpenito, C., Wang, E., Douek, D., Price, D., June, C., Marincola, F., Roederer,

M. and Restifo, N. (2011). A human memory T-cell subset with stem cell-like properties. *Nature Medicine*, 17(10), pp.1290-1297.

Germain, R. (2002). T-cell development and the CD4–CD8 lineage decision. *Nature Reviews Immunology*, 2(5), pp.309-322.

Gershon, R., Cohen, P., Hencin, R. and Liebhaber, S. (1972). Suppressor T cells. *Journal of Immunology*, 108, pp.586-550.

Golubovskaya, V. and Wu, L. (2016). Different Subsets of T Cells, Memory, Effector Functions, and CAR-T Immunotherapy. *Cancers,* 8(3), p.36.

Goronzy, J. and Weyand, C. (2017). Successful and Maladaptive T Cell Aging. *Immunity*, 46(3), pp.364-378.

Gowthaman, N., Lim, H., Sreeraj, T., Amalraj, A. and Gopi, S. (2021). Advantages of biopolymers over synthetic polymers. *Biopolymers and their Industrial Applications*, pp.351-372.

Grosso, J., Goldberg, M., Getnet, D., Bruno, T., Yen, H., Pyle, K., Hipkiss, E., Vignali, D., Pardoll, D. and Drake, C. (2009). Functionally Distinct LAG-3 and PD-1 Subsets on Activated and Chronically Stimulated CD8 T Cells. *The Journal of Immunology*. 182 (11). pp. 6659-6669.

Guasch, J., Muth, C., Diemer, J., Riahinezhad, H. and Spatz, J. (2017). Integrin-Assisted T-Cell Activation on Nanostructured Hydrogels. *Nano Letters*. 17 (10). pp. 6110-6116.

Hammarlund, E., Lewis, M., Hansen, S., Strelow, L., Nelson, J., Sexton, G., Hanifin, J. and Slifka, M. (2003). Duration of antiviral immunity after smallpox vaccination. *Nature Medicine,* 9(9), pp.1131-1137.

Han, S. and Wu, J. (2022). Three-dimensional (3D) scaffolds as powerful weapons for tumor immunotherapy. *Bioactive Materials*, 17, pp.300-319.

Harnett, E., Alderman, J. and Wood, T. (2007). The surface energy of various biomaterials coated with adhesion molecules used in cell culture. *Colloids and Surfaces B: Biointerfaces*, 55(1), pp. 90-97.

Harris, T., Banigan, E., Christian, D., Konradt, C., Tait Wojno, E., Norose, K., Wilson, E., John, B., Weninger, W., Luster, A., Liu, A. and Hunter, C. (2012). Generalized Lévy walks and the role of chemokines in migration of effector CD8+ T cells. *Nature*, 486(7404), pp. 545-548.

Harrison, D., Fang, Y. and Huang, J. (2019). T-Cell Mechanobiology: Force Sensation, Potentiation, and Translation. *Frontiers in Physics*, 7.

Henderson, T., Ladewig, K., Haylock, D., McLean, K. and O'Connor, A. (2013). Cryogels for biomedical applications. *Journal of Materials Chemistry B*, 1(21). p. 2682.

Henrickson, S., Mempel, T., Mazo, I., Liu, B., Artyomov, M., Zheng, H., Peixoto, A., Flynn, M., Senman, B., Junt, T., Wong, H., Chakraborty, A. and von Andrian, U. (2008). T cell sensing of antigen dose governs interactive behavior with dendritic cells and sets a threshold for T cell activation. *Nature Immunology*. 9(3), pp. 282-291.

Hewitt, E. (2003). The MHC class I antigen presentation pathway: strategies for viral immune evasion. *Immunology*, 110(2), pp.163-169.

Hickey, J., Dong, Y., Chung, J., Salathe, S., Pruitt, H., Li, X., Chang, C., Fraser, A., Bessell, C., Ewald, A., Gerecht, S., Mao, H. and Schneck, J. (2019). Engineering an Artificial T-Cell Stimulating Matrix for Immunotherapy. *Advanced Materials*, 31(23), p.e1807359.

Hicklin, D., Marincola, F. and Ferrone, S. (1999). HLA class I antigen downregulation in human cancers: T-cell immunotherapy revives an old story. *Molecular Medicine Today*, 5(4), pp.178-186.

Hipkin, W. (2007). CCR7 Chemokine Receptor. *xPharm: The Comprehensive Pharmacology Reference*. pp. 1-10.

Hiraki, J. (2000). ε-Polylysine, its development and utilization. Fine Chemicals 29: pp.18–25.

Hollyman, D., Stefanski, J., Przybylowski, M., Bartido, S., Borquez-Ojeda, O., Taylor, C., Yeh, R., Capacio, V., Olszewska, M., Hosey, J., Sadelain, M., Brentjens, R. and Rivière, I. (2009). Manufacturing Validation of Biologically Functional T Cells Targeted to CD19 Antigen for Autologous Adoptive Cell Therapy. *Journal of Immunotherapy*, 32(2), pp.169-180.

Hosseinzadeh, S., Lindsay, S., Gallagher, A., Wellings, D., Riehle, M., Riddell, J. and Barnett, S. (2020). A novel poly-ε-lysine based implant, Proliferate®, for promotion of CNS repair following spinal cord injury. *Biomaterials Science*, 8(13), pp.3611-3627.

Hu, Q., Li, H., Archibong, E., Chen, Q., Ruan, H., Ahn, S., Dukhovlinova, E., Kang, Y., Wen, D., Dotti, G. and Gu, Z. (2021). Inhibition of post-surgery tumour recurrence via a hydrogel releasing CAR-T cells and anti-PDL1-conjugated platelets. *Nature Biomedical Engineering*, 5(9), pp.1038-1047.

Hua, J., Li, Z., Xia, W., Yang, N., Gong, J., Zhang, J. and Qiao, C. (2016). Preparation and properties of EDC/NHS mediated crosslinking poly (gamma-glutamic acid)/epsilon-polylysine hydrogels. *Materials Science and Engineering: C*, 61, pp.879-892.

Imai, C., Mihara, K., Andreansky, M., Nicholson, I., Pui, C., Geiger, T. and Campana, D. (2004). Chimeric receptors with 4-1BB signaling capacity provoke potent cytotoxicity against acute lymphoblastic leukemia. *Leukemia*, 18(4), pp.676-684.

Ivica, N. and Young, C. (2021). Tracking the CAR-T Revolution: Analysis of Clinical Trials of CAR-T and TCR-T Therapies for the Treatment of Cancer (1997–2020). *Healthcare*, 9(8), p.1062.

Izsvák, Z., Hackett, P., Cooper, L. and Ivics, Z. (2010). Translating Sleeping Beauty transposition into cellular therapies: Victories and challenges. *BioEssays*, 32(9), pp.756-767.

Iyer, R. K., Bowles, P. A., Kim, H., & Dulgar-Tulloch, A. (2018). Industrializing Autologous Adoptive Immunotherapies: Manufacturing Advances and Challenges. *Frontiers in medicine*, 5, p.150.

Jackson, Z., Roe, A., Sharma, A. A., Lopes, F. B. T. P., Talla, A., Kleinsorge-Block, S., Zamborsky, K., Schiavone, J., Manjappa, S., Schauner, R., Lee, G., Liu, R., Caimi, P. F., Xiong, Y., Krueger, W., Worden, A., Kadan, M., Schneider, D., Orentas, R., Dropulic, B., … Reese, J. S. (2020). Automated Manufacture of Autologous CD19 CAR-T Cells for Treatment of Non-hodgkin Lymphoma. *Frontiers in immunology*, 11, pp.1941.

Janssen, W., Ribickas, A., Meyer, L. and Smilee, R. (2010). Large-scale Ficoll gradient separations using a commercially available, effectively closed, system. *Cytotherapy*, 12(3), pp.418-424.

Jesuraj, N., Cole, J., Bedoya, F., Wells, S., Qin, G., Kevlahan, S., Maus, M. and Ball, A. (2016). A Novel Phase-Change Hydrogel Substrate for T Cell Activation Promotes Increased Expansion of CD8+ Cells Expressing Central Memory and Naive Phenotype Markers. *Blood*, 128(22), pp.3368-3368.

Judokusumo, E., Tabdanov, E., Kumari, S., Dustin, M. and Kam, L. (2012). Mechanosensing in T Lymphocyte Activation. *Biophysical Journal*. 102 (2). pp.L5-L7.

Kagoya, Y., Tanaka, S., Guo, T., Anczurowski, M., Wang, C., Saso, K., Butler, M., Minden, M. and Hirano, N. (2018). A novel chimeric antigen receptor containing a JAK–STAT signaling domain mediates superior antitumor effects. *Nature Medicine*, 24(3), pp.352-359.

Kamiya, T., Wong, D., Png, Y. and Campana, D. (2018). A novel method to generate T-cell receptor–deficient chimeric antigen receptor T cells. *Blood Advances*, 2(5), pp.517-528.

Kang, J. Y., Yeom, E. and Lee, S. (2013). A microfluidic device for simultaneous measurement of viscosity and flow rate of blood in a complex fluidic network. *Biomicrofluidics*, 7 (5), p.e054111.

Kantoff, P., Kohn, D., Mitsuya, H., Armentano, D., Sieberg, M., Zwiebel, J., Eglitis, M., McLachlin, J., Wiginton, D. and Hutton, J. (1986). Correction of adenosine deaminase deficiency in cultured human T and B cells by retrovirus-mediated gene transfer. *Proceedings of the National Academy of Sciences*, 83(17), pp.6563-6567.

Kärger, J., Ruthven, D. and Theodorou, D. (2012). *Diffusion in Nanoporous Materials*. Wiley.

Kennedy, S., Lace, R., Carserides, C., Gallagher, A., Wellings, D., Williams, R. and Levis, H. (2019). Poly-ε-lysine based hydrogels as synthetic substrates for the expansion of corneal endothelial cells for transplantation. *Journal of Materials Science: Materials in Medicine*, 30(9).

Kim, C. (2014). Crawling of effector T cells on extracellular matrix: role of integrins in interstitial migration in inflamed tissues. *Cellular & Molecular Immunology*. 11(1). pp.1-4.

Koch, S., Larbi, A., Derhovanessian, E., Özcelik, D., Naumova, E. and Pawelec, G. (2008). Multiparameter flow cytometric analysis of CD4 and CD8 T cell subsets in young and old people. *Immunity & Ageing*, 5(1).

Korin, Y. and Zack, J. (1998). Progression to the G1b Phase of the Cell Cycle Is Required for Completion of Human Immunodeficiency Virus Type 1 Reverse Transcription in T Cells. *American Society for Microbiology*, 71(4), pp.3161-3168.

Korngold, B. and Sprent, J. (1978). Lethal graft-versus-host disease after bone marrow transplantation across minor histocompatibility barriers in mice. Prevention by removing mature T cells from marrow. Journal of Experimental Medicine, 148(6), pp.1687-1698.

Krivacic, K. and Levine, A. (2003). Extracellular Matrix Conditions T Cells for Adhesion to Tissue Interstitium. *The Journal of Immunology*, 170(10), pp.5034-5044.

Krummel, M., Bartumeus, F. and Gérard, A. (2016). T cell migration, search strategies and mechanisms. *Nature Reviews Immunology*, 16(3), pp.193-201.

Kumar, A. and Srivastava, A. (2010). Cell separation using cryogel-based affinity chromatography. *Nature Protocols*, 5(11), pp.1737-1747.

Kurashina, Y., Imashiro, C., Hirano, M., Kuribara, T., Totani, K., Ohnuma, K., Friend, J. and Takemura, K. (2019). Enzyme-free release of adhered cells from standard culture dishes using intermittent ultrasonic traveling waves. *Communications Biology*, 2(1).

Kuse, R., Schuster, S., Schübbe, H., Dix, S. and Hausmann, K. (1985). Blood lymphocyte volumes and diameters in patients with chronic lymphocytic leukemia and normal controls. *Blut*, 50(4), pp.243-248.

Lace, R., Duffy, G., Gallagher, A., Doherty, K., Maklad, O., Wellings, D. and Williams, R. (2021). Characterization of Tunable Poly-ε-Lysine-Based Hydrogels for Corneal Tissue Engineering. *Macromolecular Bioscience*, 21(7), p.2100036.

Lambert, L., Goebrecht, G., De Leo, S., O'Connor, R., Nunez-Cruz, S., Li, T., Yuan, J., Milone, M. and Kam, L. (2017). Improving T Cell Expansion with a Soft Touch. *Nano Letters*, 17(2), pp.821-826.

Lämmermann, T., Bader, B., Monkley, S., Worbs, T., Wedlich-Söldner, R., Hirsch, K., Keller, M., Förster, R., Critchley, D., Fässler, R. and Sixt, M. (2008). Rapid leukocyte migration by integrin-independent flowing and squeezing. *Nature*, 453(7191), pp.51-55.

Lecoeur, H., Prévost, M. and Gougeon, M. (2001). Oncosis is associated with exposure of phosphatidylserine residues on the outside layer of the plasma membrane: A reconsideration of the specificity of the annexin V/propidium iodide assay. *Cytometry*, 44(1), pp.65-72.

Lee, G. and Arepally, G. (2012). Anticoagulation techniques in apheresis: From heparin to citrate and beyond. *Journal of Clinical Apheresis*, 27(3), pp.117-125.

Lee, J., Jung, H., Kang, I. and Lee, H. (1994). Cell behaviour on polymer surfaces with different functional groups. *Biomaterials*. 15 (9). pp. 705-711.

Levine, B. (2015). Performance-enhancing drugs: design and production of redirected chimeric antigen receptor (CAR) T cells. *Cancer Gene Therapy*, 22(2), pp.79-84.

Li, A., Sobral, M., Badrinath, S., Choi, Y., Graveline, A., Stafford, A., Weaver, J., Dellacherie, M., Shih, T., Ali, O., Kim, J., Wucherpfennig, K. and Mooney, D. (2018). A facile approach to enhance antigen response for personalized cancer vaccination. *Nature Materials*, 17(6), pp.528-534.

Li, J., Guan, T., Hao, C., Li, L. and Zhang, Y. (2015). Effects of Self-Assembled Monolayers with Different Chemical Groups on Ovarian Cancer Cell Line Behavior In Vitro. *Journal of Chemistry*, 2015, pp.1-10.

Li, X., Wang, Y., Wang, S., Liang, C., Pu, G., Chen, Y., Wang, L., Xu, H., Shi, Y. and Yang, Z. (2020). A strong CD8+ T cell-stimulating supramolecular hydrogel. *Nanoscale*. 12(3), pp.2111-2117.

Lin, H., Wang, W., Huang, Y., Liao, W., Lin, T., Lin, S. and Liu, D. (2019). Decellularized Lymph Node Scaffolding as a Carrier for Dendritic Cells to Induce Anti-Tumor Immunity. *Pharmaceutics*, 11(11), p.553.

Liu, Q., Sun, Z. and Chen, L. (2020). Memory T cells: strategies for optimizing tumor immunotherapy. *Protein & Cell*, 11(8), pp. 549-564.

Liu, Y. (1994). *The costimulatory pathway for T cell response*. 1st ed. Austin: R.G. Landes.

Locke, F., Miklos, D., Jacobson, C., Perales, M., Kersten, M., Oluwole, O., Ghobadi, A., Rapoport, A., McGuirk, J., Pagel, J., Muñoz, J., Farooq, U., van Meerten, T., Reagan, P., Sureda, A., Flinn, I., Vandenberghe, P., Song, K., Dickinson, M., Minnema, M., Riedell, P., Leslie, L., Chaganti, S., Yang, Y., Filosto, S., Shah, J., Schupp, M., To, C., Cheng, P., Gordon, L. and Westin, J. (2022). Axicabtagene Ciloleucel as Second-Line Therapy for Large B-Cell Lymphoma. *New England Journal of Medicine*, 386(7), pp.640-654.

Lonza. (2021). Lonza and Sheba Medical Center Use Cocoon® Platform and Show Successful Clinical Outcomes in Patients Treated with CAR-T Cell Immunotherapy. [online]. Available at: https://www.lonza.com/news/2021-08-12-15-00 [Accessed 03 May 2022]

Luckheeram, R., Zhou, R., Verma, A. and Xia, B. (2012). CD4+ T Cells: Differentiation and Functions. *Clinical and Developmental Immunology*, 2012, pp.1-12.

Lydyard, P., Whelan, A. and Fanger, M. (2011). Immunology. 3rd ed. Garland Science, pp.4-28.

MacDonald, H. and Zaech, P. (1982). Light scatter analysis and sorting of cells activated in mixed leukocyte culture. *Cytometry*, 3(1), pp.55-58.

MacDonald, K., Ivison, S., Hippen, K., Hoeppli, R., Hall, M., Zheng, G., Dijke, I., Aklabi, M., Freed, D., Rebeyka, I., Gandhi, S., West, L., Piret, J., Blazar, B. and Levings, M. (2019). Cryopreservation timing is a critical process parameter in a thymic regulatory T-cell therapy manufacturing protocol. *Cytotherapy*, 21(12), pp.1216-1233.

Maher, J., Brentjens, R., Gunset, G., Rivière, I. and Sadelain, M. (2002). Human T-lymphocyte cytotoxicity and proliferation directed by a single chimeric TCRζ /CD28 receptor. *Nature Biotechnology*, 20(1), pp.70-75.

Majedi, F., Hasani-Sadrabadi, M., Thauland, T., Li, S., Bouchard, L. and Butte, M. (2020). T-cell activation is modulated by the 3D mechanical microenvironment. *Biomaterials*, 252, p.e120058.

Majno G, Joris I. (1995). Apoptosis, oncosis, and necrosis. An overview of cell death. *American Journal of Pathology*, 146(1), pp.3-15.

Malek, T. (2008). The Biology of Interleukin-2. *Annual Review of Immunology*, 26(1), pp.453-479.

Maruhashi, T., Sugiura, D., Okazaki, I. and Okazaki, T. (2020). LAG-3: from molecular functions to clinical applications. *Journal for ImmunoTherapy of Cancer*, 8(2), p.e001014.

Matic, J., Deeg, J., Scheffold, A., Goldstein, I. and Spatz, J. (2013). Fine Tuning and Efficient T Cell Activation with Stimulatory aCD3 Nanoarrays. *Nano Letters*, 13(11), pp.5090-5097.

Maude, S., Laetsch, T., Buechner, J., Rives, S., Boyer, M., Bittencourt, H., Bader, P., Verneris, M., Stefanski, H., Myers, G., Qayed, M., De Moerloose, B., Hiramatsu, H., Schlis, K., Davis, K., Martin, P., Nemecek, E., Yanik, G., Peters, C., Baruchel, A., Boissel, N., Mechinaud, F., Balduzzi, A., Krueger, J., June, C., Levine, B., Wood, P., Taran, T., Leung, M., Mueller, K., Zhang, Y., Sen, K., Lebwohl, D., Pulsipher, M. and Grupp, S., 2018. Tisagenlecleucel in Children and Young Adults with B-Cell Lymphoblastic Leukemia. *New England Journal of Medicine*, 378(5), pp.439-448.

Mauer, D., Mockel-Tenbrinck, N., Drechsel, K., Lehmann, C., Johnston, I., Bohnenkamp, H., Assenmacher, M. and Kaiser, A. (2014). Potent polyclonal T cell activation and expansion through GMP-grade transact nano-matrices. *Cytotherapy*, 16(4), p.S36.

Maus, M., Fraietta, J., Levine, B., Kalos, M., Zhao, Y. and June, C. (2014). Adoptive Immunotherapy for Cancer or Viruses. *Annual Review of Immunology*, 32(1), pp.189-225.

Mazia, D., Schatten, G. and Sale, W. (1975). Adhesion of cells to surfaces coated with polylysine. Applications to electron microscopy. *Journal of Cell Biology*, 66(1), pp.198-200.

Mehrabadi, A., Ranjbar, R., Farzanehpour, M., Shahriary, A., Dorostkar, R., Hamidinejad, M. and Ghaleh, H. (2022). Therapeutic potential of CAR T cell in malignancies: A scoping review. *Biomedicine & Pharmacotherapy*, 146, p.e112512.

Meng, Y., Sun, J., Hu, T., Ma, Y., Du, T., Kong, C., Zhang, G., Yu, T., Piao, H. Rapid expansion in the WAVE bioreactor of clinical scale cells for tumor immunotherapy. (2018). *Human Vaccines & Immunotherapeutics*.14(10), pp, 2516-2526.

Mescher, M. (1992). Surface contact requirements for activation of cytotoxic T lymphocytes. *Jouornal of Immunology*, 149(7), pp.2402-2405.

Miller, D., Adam, M. and Miller, A. (1990). Gene transfer by retrovirus vectors occurs only in cells that are actively replicating at the time of infection. *Molecular and Cellular Biology*, 10(8), pp.4239-4242.

Miller, M., Wei, S., Parker, I. and Cahalan, M. (2002). Two-Photon Imaging of Lymphocyte Motility and Antigen Response in Intact Lymph Node. *Science*, 296(5574). pp.1869-1873.

Moffett, H., Coon, M., Radtke, S., Stephan, S., McKnight, L., Lambert, A., Stoddard, B., Kiem, H. and Stephan, M. (2017). Hit-and-run programming of therapeutic cytoreagents using mRNA nanocarriers. *Nature Communications*, 8(1).

Montano, M. (2014). Model systems. *Translational Biology in Medicine*, pp.9-33.

Moreau, H., Lemaître, F., Garrod, K., Garcia, Z., Lennon-Duménil, A. and Bousso, P. (2015). Signal strength regulates antigen-mediated T-cell deceleration by distinct mechanisms to promote local exploration or arrest. *Proceedings of the National Academy of Sciences*, 112(39), pp.e12151-12156.

Morgan, R. and Boyerinas, B. (2016). Genetic Modification of T Cells. Biomedicines, 4(2), p.9.

Mtibe, A., Motloung, M., Bandyopadhyay, J. and Ray, S. (2021). Synthetic Biopolymers and Their Composites: Advantages and Limitations—An Overview. *Macromolecular Rapid Communications*, 42(15), p.2100130.

Mueller, K. P., Piscopo, N. J., Forsberg, M. H., Saraspe, L. A., Das, A., Russell, B., Smerchansky, M., Cappabianca, D., Shi, L., Shankar, K., Sarko, L., Khajanchi, N., La Vonne Denne, N., Ramamurthy, A., Ali, A., Lazzarotto, C. R., Tsai, S. Q., Capitini, C. M., & Saha, K. (2022). Production and characterization of virus-free, CRISPR-CAR T cells capable of inducing solid tumor regression. *Journal for immunotherapy of cancer*, 10(9), e004446.

Müller, D., Klein, L., Lemke, J., Schulze, M., Kruse, T., Saballus, M., Matuszczyk, J., Kampmann, M. and Zijlstra, G. (2022). Process intensification in the biopharma industry: Improving efficiency of protein manufacturing processes from development to production scale using synergistic approaches. *Chemical Engineering and Processing - Process Intensification*, 171, p.e108727.

Najarro, K., Nguyen, H., Chen, G., Xu, M., Alcorta, S., Yao, X., Zukley, L., Metter, E., Truong, T., Lin, Y., Li, H., Oelke, M., Xu, X., Ling, S., Longo, D., Schneck, J., Leng, S., Ferrucci, L. and Weng, N. (2015). Telomere Length as an Indicator of the Robustness of

B- and T-Cell Response to Influenza in Older Adults. *Journal of Infectious Diseases*, 212(8), pp.1261-1269.

Newell, E., Sigal, N., Bendall, S., Nolan, G. and Davis, M. (2012). Cytometry by Time-of-Flight Shows Combinatorial Cytokine Expression and Virus-Specific Cell Niches within a Continuum of CD8+ T Cell Phenotypes. *Immunity*, 36(1), pp.142-152.

North, A. (2006). Seeing is believing? A beginners' guide to practical pitfalls in image acquisition. *Journal of Cell Biology*, 172(1), pp.9-18.

O'Connor, R., Hao, X., Shen, K., Bashour, K., Akimova, T., Hancock, W., Kam, L. and Milone, M. (2012). Substrate Rigidity Regulates Human T Cell Activation and Proliferation. *The Journal of Immunology*, 189(3), pp.1330-1339.

Ohteki, T., Parsons, M., Zakarian, A., Jones, R., Nguyen, L., Woodgett, J. and Ohashi, P. (2000). Negative Regulation of T Cell Proliferation and Interleukin 2 Production by the Serine Threonine Kinase Gsk-3. *The Journal of Experimental Medicine,* 192(1), pp.99-104.

Ortiz-Maldonado, V., Frigola, G., Español-Rego, M., Balagué, O., Martínez-Cibrián, N., Magnano, L., Giné, E., Pascal, M., Correa, J., Martínez-Roca, A., Cid, J., Lozano, M., Villamor, N., Benítez-Ribas, D., Esteve, J., López-Guillermo, A., Campo, E., Urbano-Ispizua, Á., Juan, M. and Delgado, J. (2022). Results of ARI-0001 CART19 Cells in Patients With Chronic Lymphocytic Leukemia and Richter's Transformation. *Frontiers in Oncology*, 12.

Park, J., Geyer, M. and Brentjens, R. (2016). CD19-targeted CAR T-cell therapeutics for hematologic malignancies: interpreting clinical outcomes to date. *Blood*, 127(26), pp.3312-3320.

Pellerin, L., Jenks, J., Bégin, P., Bacchetta, R. and Nadeau, K. (2014). Regulatory T cells and their roles in immune dysregulation and allergy. *Immunologic Research*, 58(2-3), pp.358-368.

Pennock, N., White, J., Cross, E., Cheney, E., Tamburini, B. and Kedl, R. (2013). T cell responses: naive to memory and everything in between. *AJP: Advances in Physiology Education*, 37(4), pp.273-283.

Pérez del Río, E., Martinez Miguel, M., Veciana, J., Ratera, I. and Guasch, J. (2018). Artificial 3D Culture Systems for T Cell Expansion. *ACS Omega*, 3(5), pp.5273-5280.

Pérez del Río, E., Santos, F., Rodriguez Rodriguez, X., Martínez-Miguel, M., Roca-Pinilla, R., Arís, A., Garcia-Fruitós, E., Veciana, J., Spatz, J., Ratera, I. and Guasch, J.

(2020). CCL21-loaded 3D hydrogels for T cell expansion and differentiation. *Biomaterials*, 259, p.120313.

Plunkett, F., Franzese, O., Finney, H., Fletcher, J., Belaramani, L., Salmon, M., Dokal, I., Webster, D., Lawson, A. and Akbar, A. (2007). The Loss of Telomerase Activity in Highly Differentiated CD8 T Cells Is Associated with Decreased Akt Phosphorylation. *The Journal of Immunology*, 178(12), pp.7710-7719.

Poltorak, M., Graef, P., Tschulik, C., Wagner, M., Cletiu, V., Dreher, S., Borjan, B., Fraessle, S., Effenberger, M., Turk, M., Busch, D., Plitzko, J., Kugler, D., Ragan, S., Schmidt, T., Stemberger, C. and Germeroth, L. (2020). Expamers: a new technology to control T cell activation. *Scientific Reports*, 10(1).

Reddy, M., Eirikis, E., Davis, C., Davis, H. and Prabhakar, U. (2004). Comparative analysis of lymphocyte activation marker expression and cytokine secretion profile in stimulated human peripheral blood mononuclear cell cultures: an in vitro model to monitor cellular immune function. *Journal of Immunological Methods*, 293 (1-2), pp.127-142.

Reddy, M., Ponnamma, D., Choudhary, R. and Sadasivuni, K. (2021). A Comparative Review of Natural and Synthetic Biopolymer Composite Scaffolds. *Polymers*, 13(7), p.1105.

Reichard, A. and Asosingh, K. (2018). Best Practices for Preparing a Single Cell Suspension from Solid Tissues for Flow Cytometry. *Cytometry Part A*, 95(2), pp.219-226.

Ren, H., Cao, K. and Wang, M. (2021). A Correlation Between Differentiation Phenotypes of Infused T Cells and Anti-Cancer Immunotherapy. *Frontiers in Immunology*, 12.

Renner, K., Bruss, C., and Färber, S. (2020). *Monitoring Human T Cell Activation in the Context of Immunotherapeutic Approaches.* Bremen, Germany: OLS OMNI Life Science GmbH & Co KG. Available online at: https://www.bulldog-bio.com/wp-content/uploads/2020/06/T-cell-activation-CASY-AppNote_OLS.pdf

Reynolds, A. (2021). Loss of mechanical stiffness and the emergence of Lévy walks in active T cells. *Physics Letters A*, 408, p.e127507.

Robinson, J. and Delvig, A. (2002). Diversity in MHC class II antigen presentation. *Immunology*, 105(3), pp.252-262.

Roose, J. and Weiss, a. (2000). T cells: getting a GRP on Ras. *Nature Immunology*, 1, pp.275-276.

Rosenberg, S., Aebersold, P., Cornetta, K., Kasid, A., Morgan, R., Moen, R., Karson, E., Lotze, M., Yang, J., Topalian, S., Merino, M., Culver, K., Miller, A., Blaese, R. and Anderson, W. (1990). Gene Transfer into Humans — Immunotherapy of Patients with Advanced Melanoma, Using Tumor-Infiltrating Lymphocytes Modified by Retroviral Gene Transduction. *New England Journal of Medicine*, 323(9), pp.570-578.

Rossoff, J., Baggott, C., Prabhu, S., Pacenta, H., Phillips, C., Stefanski, H., Talano, J., Moskop, A., Margossian, S., Verneris, M., Myers, G., Karras, N., Brown, P., Qayed, M., Hermiston, M., Satwani, P., Krupski, C., Keating, A., Wilcox, R., Rabik, C., Fabrizio, V., Kunicki, M., Chinnabhandar, V., Goksenin, A., Curran, K., Mackall, C., Laetsch, T. and Schultz, L. (2021). Out-of-specification tisagenlecleucel does not compromise safety or efficacy in pediatric acute lymphoblastic leukemia. *Blood*, 138(21), pp.2138-2142.

Rozenbaum, M., Meir, A., Aharony, Y., Itzhaki, O., Schachter, J., Bank, I., Jacoby, E., Besser, M. J. (2013). Gamma-Delta CAR-T Cells Show CAR-Directed and Independent Activity Against Leukemia. *Frontiers in Immunology*. 11. pp. 1347.

Sadelain, M., Brentjens, R. and Rivière, I. (2013). The Basic Principles of Chimeric Antigen Receptor Design. *Cancer Discovery*, 3(4), pp.388-398.

Sadelain, M., Rivière, I. and Brentjens, R. (2003). Targeting tumours with genetically enhanced T lymphocytes. *Nature Reviews Cancer*, 3(1), pp.35-45.

Sadoun, A., Biarnes-Pelicot, M., Ghesquiere-Dierickx, L., Wu, A., Théodoly, O., Limozin, L., Hamon, Y. and Puech, P. (2021). Controlling T cells spreading, mechanics and activation by micropatterning. *Scientific Reports*, 11(1).

Saitakis, M., Dogniaux, S., Goudot, C., Bufi, N., Asnacios, S., Maurin, M., Randriamampita, C., Asnacios, A. and Hivroz, C. (2017). Different TCR-induced T lymphocyte responses are potentiated by stiffness with variable sensitivity. *eLife*, 6.

Saito, T. and Germain, R. (1987). Predictable acquisition of a new MHC recognition specificity following expression of a transfected T-cell receptor β-chain gene. *Nature*, 329(6136), pp.256-259.

Sallusto, F., Lenig, D., Förster, R., Lipp, M. and Lanzavecchia, A. (1999). Two subsets of memory T lymphocytes with distinct homing potentials and effector functions. *Nature*, 401(6754), pp.708-712.

Schindelin, J., Arganda-Carreras, I., Frise, E., Kaynig, V., Longair, M., Pietzsch, T., Cardona, A. (2012). Fiji: an open-source platform for biological-image analysis. *Nature Methods*, *9*(7), 676–682.

Schluck, M., Hammink, R., Figdor, C., Verdoes, M. and Weiden, J. (2019). Biomaterial-Based Activation and Expansion of Tumor-Specific T Cells. *Frontiers in Immunology*. 10.

Schneider, M. (1996). The importance of ammonia in mammalian cell culture. *Journal of Biotechnology*. 46 (3). pp. 161-185.

Schuster, S., Bishop, M., Tam, C., Waller, E., Borchmann, P., McGuirk, J., Jäger, U., Jaglowski, S., Andreadis, C., Westin, J., Fleury, I., Bachanova, V., Foley, S., Ho, P., Mielke, S., Magenau, J., Holte, H., Pantano, S., Pacaud, L., Awasthi, R., Chu, J., Anak, Ö., Salles, G. and Maziarz, R. (2019). Tisagenlecleucel in Adult Relapsed or Refractory Diffuse Large B-Cell Lymphoma. *New England Journal of Medicine*, 380(1), pp.45-56.

Shen, M., Rusling, J. and Dixit, C. (2017). Site-selective orientated immobilization of antibodies and conjugates for immunodiagnostics development. *Methods*, 116, pp.95-111.

Shi, C., Zhong, S., Sun, Y., Xu, L., He, S., Dou, Y., Zhao, S., Gao, Y. and Cui, X. (2020). Sonochemical preparation of folic acid-decorated reductive-responsive ε-poly-L-lysine-based microcapsules for targeted drug delivery and reductive-triggered release. *Materials Science and Engineering: C*, 106, p.e110251.

Shields IV, C., Wang, L., Evans, M. and Mitragotri, S. (2019). Materials for Immunotherapy. *Advanced Materials*. 32(13), p.e1901633.

Shipkova, M. and Wieland, E. (2012). Surface markers of lymphocyte activation and markers of cell proliferation. Clinica Chimica Acta, 413(17-18), pp.1338-1349.

Shirasu, N. and Kuroki, M. (2012). Functional Design of Chimeric T-Cell Antigen Receptors for Adoptive Immunotherapy of Cancer: Architecture and Outcomes. *Anticancer Research*, 32(6), pp.2377-2383.

Singh, A. and Peppas, N. (2014). Hydrogels and Scaffolds for Immunomodulation. *Advanced Materials*. 26 (38). pp. 6530-6541.

Smith, J. (1997). Apheresis Techniques and Cellular Immunomodulation. *Therapeutic Apheresis*, 1(3), pp.203-206.

Smith, T., Moffett, H., Stephan, S., Opel, C., Dumigan, A., Jiang, X., Pillarisetty, V., Pillai, S., Wittrup, K. and Stephan, M. (2017). Biopolymers codelivering engineered T cells and STING agonists can eliminate heterogeneous tumors. *Journal of Clinical Investigation*, 127(6), pp.2176-2191.

Smith-Garvin, J., Koretzky, G. and Jordan, M. (2009). T Cell Activation. *Annual Review of Immunology*, 27, pp.591-619.

Somerville, R. and Dudley, M. (2012). Bioreactors get personal. *OncoImmunology*, 1(8), pp.1435-1437.

Sommermeyer, D., Hudecek, M., Kosasih, P., Gogishvili, T., Maloney, D., Turtle, C. and Riddell, S. (2015). Chimeric antigen receptor-modified T cells derived from defined CD8+ and CD4+ subsets confer superior antitumor reactivity in vivo. *Leukemia*, 30(2), pp.492-500.

Steenblock, E. and Fahmy, T. (2008). A Comprehensive Platform for *Ex Vivo* T-cell Expansion Based on Biodegradable Polymeric Artificial Antigen-presenting Cells. *Molecular Therapy*, 16(4), pp.765-772.

Steenblock, E., Fadel, T., Labowsky, M., Pober, J. and Fahmy, T. (2011). An Artificial Antigen-presenting Cell with Paracrine Delivery of IL-2 Impacts the Magnitude and Direction of the T Cell Response. *Journal of Biological Chemistry*, 286(40), pp.e34883-34892.

Stephan, S., Taber, A., Jileaeva, I., Pegues, E., Sentman, C. and Stephan, M. (2014). Biopolymer implants enhance the efficacy of adoptive T-cell therapy. *Nature Biotechnology*, 33(1), pp.97-101.

Steponavicius-Cruz, K., Freitas, V. and Barbuto, J. (2013). Dendritic Cells and T Lymphocytes Interactions in a Novel 3D System. *Procedia Engineering*, 59, pp.166-173.

Suh, W. and Tirrell, M. (2011). Surface Engineering Using Peptide Amphiphiles. *Comprehensive Biomaterials*, pp.219-245.

Suhoski, M., Golovina, T., Aqui, N., Tai, V., Varela-Rohena, A., Milone, M., Carroll, R., Riley, J. and June, C. (2007). Engineering Artificial Antigen-presenting Cells to Express a Diverse Array of Co-stimulatory Molecules. *Molecular Therapy*, 15(5), pp.981-988.

Sunshine, J. and Green, J. (2013). Nanoengineering approaches to the design of artificial antigen-presenting cells. *Nanomedicine*, 8(7), pp.1173-1189.

Tantalo, D., Oliver, A., von Scheidt, B., Harrison, A., Mueller, S., Kershaw, M. and Slaney, C. (2021). Understanding T cell phenotype for the design of effective chimeric antigen receptor T cell therapies. *Journal for ImmunoTherapy of Cancer*, 9(5), p.e002555.

Tau, G. and Rothman, P. (1999). Biologic functions of the IFN-gamma receptors. *Allergy*, 54(12), pp.1233-1251.

Teague, T., Munn, L., Zygourakis, K. and McIntyre, B. (1993). Analysis of lymphocyte activation and proliferation by video microscopy and digital imaging. *Cytometry*, 14(7), pp.772-782.

Tecan. (2010). Application Note: Improved Fluorescence Top Measurements. Tecan.

Tecan. (2022). Technical Note: Optimizing the acquisition of 3D fluorescence spectra. Tecan.

Teixeira, L., Fonseca, B., Barboza, B. and Viola, J. (2005). The role of interferon-gamma on immune and allergic responses. *Memórias do Instituto Oswaldo Cruz*, 100, pp.137-144.

Thermo Fisher Scientific. (2011). Product Protocol: Dynabeads® Human T-Activator CD3/CD28. Gibco: Life Technologies: Thermo Fisher Scientific.

Thermo Fisher Scientific. (2022). Dynabeads™ [online]. Available at: https://www.thermofisher.com/order/catalog/product/11137D [Accessed 15 April 2022]

Thermo Fisher Scientific. (2022). Protocols for Immunology: T Cell Activation with Anti-CD3 and Anti-CD28. [online]. Available at: https://www.thermofisher.com/uk/en/home/life-science/cell-analysis/cell-analysis-learning-center/immunology-at-work/immunology-protocols/t-cell-activation-anti-cd3-anti-cd28.html [Accessed 04 May 2022].

Thong, Y., Currell, J. and Rodwell, R. (1983). The rapid one-step gradient centrifugation procedure for simultaneous isolation of granulocytic and mononuclear leukocytes from human blood: Biological, physical and chemical bases. *Medical Hypotheses*, 12(2), pp.103-111.

Thornton, A. and Shevach, E. (2000). Suppressor Effector Function of CD4+CD25+ Immunoregulatory T Cells Is Antigen Nonspecific. *The Journal of Immunology*, 164(1), pp.183-190.

Tian, Y., Babor, M., Lane, J., Schulten, V., Patil, V., Seumois, G., Rosales, S., Fu, Z., Picarda, G., Burel, J., Zapardiel-Gonzalo, J., Tennekoon, R., De Silva, A., Premawansa, S., Premawansa, G., Wijewickrama, A., Greenbaum, J., Vijayanand, P., Weiskopf, D., Sette, A. and Peters, B. (2017). Unique phenotypes and clonal expansions of human CD4 effector memory T cells re-expressing CD45RA. *Nature Communications*, 8(1).

Tian, Y., Sette, A. and Weiskopf, D. (2016). Cytotoxic CD4 T Cells: Differentiation, Function, and Application to Dengue Virus Infection. *Frontiers in Immunology*, 7.

Tinevez, J.-Y., Perry, N., Schindelin, J., Hoopes, G. M., Reynolds, G. D., Laplantine, E., Eliceiri, K. W. (2017). TrackMate: An open and extensible platform for single-particle tracking. *Methods*, *115*, pp.80–90.

Tokarew, N., Ogonek, J., Endres, S., von Bergwelt-Baildon, M. and Kobold, S. (2019). Teaching an old dog new tricks: next-generation CAR T cells. *British Journal of Cancer*, 120(1), pp.26-37.

Tsao, C., Kievit, F., Ravanpay, A., Erickson, A., Jensen, M., Ellenbogen, R. and Zhang, M. (2014). Thermoreversible Poly(ethylene glycol)-g-Chitosan Hydrogel as a Therapeutic T Lymphocyte Depot for Localized Glioblastoma Immunotherapy. *Biomacromolecules*, 15(7), pp.2656-2662.

Tumaini, B., Lee, D., Lin, T., Castiello, L., Stroncek, D., Mackall, C., Wayne, A. and Sabatino, M. (2013). Simplified process for the production of anti–CD19-CAR–engineered T cells. *Cytotherapy*, 15(11), pp.1406-1415.

Tumeh, P., Koya, R., Chodon, T., Graham, N., Graeber, T., Comin-Anduix, B. and Ribas, A. (2010). The Impact of *Ex Vivo* Clinical Grade Activation Protocols on Human T-cell Phenotype and Function for the Generation of Genetically Modified Cells for Adoptive Cell Transfer Therapy. *Journal of Immunotherapy*, 33(8), pp.759-768.

Turtle, C. and Riddell, S. (2010). Artificial Antigen-Presenting Cells for Use in Adoptive Immunotherapy. *The Cancer Journal*, 16(4), pp.374-381.

Unnikrishnan, K., Thomas, L. and Ram Kumar, R. (2021). Advancement of Scaffold-Based 3D Cellular Models in Cancer Tissue Engineering: An Update. *Frontiers in Oncology*, 11.

van der Stegen, S., Hamieh, M. and Sadelain, M. (2015). The pharmacology of second-generation chimeric antigen receptors. *Nature Reviews Drug Discovery*, 14(7), pp.499-509.

van der Walle, C., Godbert, S., Saito, G. and Azhari, Z. (2021). Formulation Considerations for Autologous T Cell Drug Products. *Pharmaceutics*, 13(8), p.1317.

Vannucci, L., Lai, M., Chiuppesi, F., Ceccherini-Nelli, L. and Pistello, M. (2013). Viral vectors: a look back and ahead on gene transfer technology. *New Microbiologica*, 36, pp.1-22.

Vignali, D., Collison, L. and Workman, C. (2008). How regulatory T cells work. Nature Reviews Immunology, 8(7), pp.523-532.

Vinay, D. S., Ryan, E. P., Pawelec, G., Talib, W. H., Stagg, J., Elkord, E., Kwon, B. S. (2015). Immune evasion in cancer: Mechanistic basis and therapeutic strategies. *Seminars in Cancer Biology*, 35, pp.185-198.

Vormittag, P., Gunn, R., Ghorashian, S. and Veraitch, F. (2018). A guide to manufacturing CAR T cell therapies. *Current Opinion in Biotechnology*, 53, pp.164-181.

Vossenkamper, A. and Warnes, G. (2019). Flow Cytometry Reveals the Nature of Oncotic Cells. *International Journal of Molecular Sciences*, 20(18), pp.4379.

Wagner, D. L., Koehl, U., Chmielewski, M., Scheid, C., & Stripecke, R. (2022). Review: Sustainable Clinical Development of CAR-T Cells - Switching From Viral Transduction Towards CRISPR-Cas Gene Editing. *Frontiers in immunology*, 13, pp.865424.

Wahl, A., Dinet, C., Dillard, P., Nassereddine, A., Puech, P., Limozin, L. and Sengupta, K. (2019). Biphasic mechanosensitivity of T cell receptor-mediated spreading of lymphocytes. *Proceedings of the National Academy of Sciences*. 116 (13). pp. 5908-5913.

Walker, A. and Johnson, R. (2016). Commercialization of cellular immunotherapies for cancer. *Biochemical Society Transactions*, 44(2), pp.329-332.

Wallner, B., Frey, A., Tizard, R., Mattaliano, R., Hession, C., Sanders, M., Dustin, M. and Springer, T. (1987). Primary structure of lymphocyte function-associated antigen 3 (LFA-3). The ligand of the T lymphocyte CD2 glycoprotein. *Journal of Experimental Medicine*, 166(4), pp.923-932.

Walsh, A., Mueller, K., Tweed, K., Jones, I., Walsh, C., Piscopo, N., Niemi, N., Pagliarini, D., Saha, K. and Skala, M. (2020). Classification of T-cell activation via autofluorescence lifetime imaging. *Nature Biomedical Engineering*, 5(1), pp.77-88.

Wang, C., Wang, J., Zhang, X., Yu, S., Wen, D., Hu, Q., Ye, Y., Bomba, H., Hu, X., Liu, Z., Dotti, G. and Gu, Z. (2018). In situ formed reactive oxygen species–responsive scaffold with gemcitabine and checkpoint inhibitor for combination therapy. *Science Translational Medicine*, 10(429).

Wang, R., Zhou, B., Xu, D., Xu, H., Liang, L., Feng, X., Ouyang, P. and Chi, B. (2016). Antimicrobial and biocompatible ε-polylysine–γ-poly(glutamic acid)–based hydrogel system for wound healing. *Journal of Bioactive and Compatible Polymers*, 31(3), pp.242-259.

Wang, X. and Rivière, I. (2016). Clinical manufacturing of CAR T cells: foundation of a promising therapy. *Molecular Therapy - Oncolytics*, 3, p.16015.

Wang, X., Qu, J., Stefanski, J., Borquez-Ojeda, O., Hack, A., He, Q., Wasielewska, T., Du, F., Sadelain, M. and Rivière, I. (2016). Evaluation of Miltenyi ExpAct and TransAct CD3/28 Beads for CAR-T Cell Manufacturing. *Molecular Therapy*, 24, p.S182.

Wardenburg, J., Fu, C., Jackman, J., Flotow, H., Wilkinson, S., Williams, D., Johnson, R., Kong, G., Chan, A. and Findell, P. (1996). Phosphorylation of SLP-76 by the ZAP-70

Protein-tyrosine Kinase Is Required for T-cell Receptor Function. *Journal of Biological Chemistry*, 271(33), pp.19641-19644.

Wei, S., Duffy, C. and Allison, J. (2018). Fundamental Mechanisms of Immune Checkpoint Blockade Therapy. *Cancer Discovery*, 8(9), pp.1069-1086.

Weiden, J., Voerman, D., Dölen, Y., Das, R., van Duffelen, A., Hammink, R., Eggermont, L., Rowan, A., Tel, J. and Figdor, C. (2018). Injectable Biomimetic Hydrogels as Tools for Efficient T Cell Expansion and Delivery. *Frontiers in Immunology*, 9.

Weiden, P., Flournoy, N., Thomas, E., Prentice, R., Fefer, A., Buckner, C. and Storb, R. (1979). Antileukemic Effect of Graft-versus-Host Disease in Human Recipients of Allogeneic-Marrow Grafts. *New England Journal of Medicine*, 300(19), pp.1068-1073.

Weil, B. D. (2016). Purification of Progenitor Photoreceptors Derived From The Directed Differentiation of Human Pluripotent Stem Cells. PhD thesis, University College London, London.

Weninger, W., Biro, M. and Jain, R. (2014). Leukocyte migration in the interstitial space of non-lymphoid organs. *Nature Reviews Immunology*, 14(4), pp.232-246.

Wherry, E. and Kurachi, M. (2015). Molecular and cellular insights into T cell exhaustion. *Nature Reviews Immunology*, 15(8), pp.486-499.

Wingren, A., Parra, E., Varga, M., Kalland, T., Sjogren, H., Hedlund, G. and Dohlsten, M. (1995). T Cell Activation Pathways: B7, LFA-3, and ICAM-1 Shape Unique T Cell Profiles. *Critical Reviews in Immunology*, 15(3-4), pp.235-253.

Wolf, K., Müller, R., Borgmann, S., Bröcker, E. and Friedl, P. (2003). Amoeboid shape change and contact guidance: T-lymphocyte crawling through fibrillar collagen is independent of matrix remodeling by MMPs and other proteases. *Blood*, 102(9), pp.3262-3269.

Wolf, Y., Anderson, A. and Kuchroo, V. (2019). TIM3 comes of age as an inhibitory receptor. *Nature Reviews Immunology*, 20(3), pp.173-185.

Yang, H. (2012). Structure, Expression, and Function of ICAM-5. *International Journal of Genomics*, 2012, pp.1-11.

Yang, K. and Kallies, A. (2021). Tissue-specific differentiation of CD8+ resident memory T cells. *Trends in Immunology*, 42(10), pp.876-890.

Yee, C., Thompson, J., Byrd, D., Riddell, S., Roche, P., Celis, E. and Greenberg, P. (2002). Adoptive T cell therapy using antigen-specific CD8+ T cell clones for the treatment of patients with metastatic melanoma: In vivo persistence, migration, and

antitumor effect of transferred T cells. *Proceedings of the National Academy of Sciences*, 99(25), pp.e16168-16173.

Yoshida, T. and Nagasawa, T. (2003). ε-Poly-l-lysine: microbial production, biodegradation and application potential. *Applied Microbiology and Biotechnology*, 62(1), pp.21-26.

Zhang, D., Cheung, A. and Mooney, D. (2020). Activation and expansion of human T cells using artificial antigen-presenting cell scaffolds. *Nature Protocols*, 15(3), pp.773-798.

Zhang, W., Sloan-Lancaster, J., Kitchen, J., Trible, R. and Samelson, L. (1998). the ZAP-70 tyrosine kinase substrate that links T cell receptor to cellular activation. *Cell*, 92(1), pp.83-92.

Zheng, M. and Wakim, L. (2021). Tissue resident memory T cells in the respiratory tract. *Mucosal Immunology,* 15(3), pp.379-388.

Zhou, D., Eid, R., Boucher, E., Miller, K., Mandato, C. and Greenwood, M. (2019). Stress is an agonist for the induction of programmed cell death: A review. *Biochimica et Biophysica Acta - Molecular Cell Research*, 1866(4), pp.699-712.

Appendix

A. Industrial Implementation and Validation

A.1. Introduction

As per the requirements for a Doctorate in Engineering (EngD), the following section details future studies and considerations for the conceptual translation of the technology outlined in this thesis into a commercial manufacturing setting. Here the focus will be on the implementation of such technology into the manufacturing process of CAR T-cell therapies, as this was a key focal point of this project.

A.2. Moving Towards Commercialisation

The work in this thesis presented initial proof-of-concept studies of a novel T-cell activation and expansion platform. Consequently, the technology is currently in the very early stages of development, and the road to commercialisation would likely be a long one. With this in mind, recommendations for future work in **Section 8.3** outline some of the first steps towards developing a commercially viable product. These include studies based on the optimisation of activation achieved by the technology through increasing cell contact, and optimising ligand selection and density bound to the polymer. Ultimately, the aim would to be to scale up the technology so that it would be suitable for use with the required input, and able to produce the required output, of a clinically relevant volume of T-cells. In order to achieve this, a definition of the overall process and methodology would be required. This would require decisions to be made on the final format of the technology, i.e. final size, culture type (batch, fed-batch, or perfusion), and level of automation. It should be considered whether the polymer would be most effective as an activation technology alone, or additionally as an expansion

platform. These should be decided on through further rigorous investigations into the optimal set-up, and process parameters, such as perfusion rate and media volume; and should take into account material properties such as pore size and porosity which may impact the efficacy of the process. Furthermore, in regards to automation, it is desirable to automate the seeding, feeding, and removal of T-cells from the polymer as this would result in the reduction of open-handling, thereby reducing the risk of product contamination.

A.3. Quality by Design Considerations

The Quality by Design (QbD) approach is described by the European Medicines Agency (EMA) in The International Council for Harmonisation of Technical Requirements for Pharmaceuticals for Human Use (ICH) guideline Q8 (2004) as: “A systematic approach to development that begins with predefined objectives and emphasizes product and process understanding and process control, based on sound science and quality risk management.”. The proposed benefits of the successful implementation of QbD include: improved product design, risk mitigation, more flexible manufacturing changes in technology, less waste, continuous improvement, and a reduction in overall manufacturing cost (Zhang *et al*., 2013).

A QbD approach is often applied to the process development and validation of cell and gene therapies, and is important to gain a comprehensive understanding of the manufacturing process. The QbD process begins with identifying the target product profile during the process and analytical development. This may include factors such as treatment target, dose, and efficacy. A quality target product profile (QTPP) is then identified. The QTPP is a summary of quality characteristics which ensure the quality, safety and efficacy of the product, such as shelf-life, dose strength, and purity. Following this, critical quality attributes

(CQAs) can be defined; these are properties of the final product that should be within an appropriate range to ensure the fulfilment of the QTPP.

Table A.1 shows examples of CQAs of in existing CAR T-cell manufacturing processes. It will be important when developing new manufacturing technologies, such as that proposed in this thesis, to consider such CQAs in the early stages - to assure built-in quality of the final product. This top-down approach will allow the development of technologies that are custom-made and fit-for-purpose, as opposed to retrofitting existing technology which may not be optimal. QbD should also be considered in the selection of technology for the same reasons.

The implementation of QbD introduced by ICH Q8 (EMA, 2004), should also be considered in parallel with ICH Q9 (EMA, 2006), and ICH Q10 (EMA, 2007) which give guidelines on quality risk management and pharmaceutical quality system. Guidance includes topics such as the life cycle assessment of a product, which will be an essential safety and economical consideration.

Table A.1. Examples of Existing Critical Quality Attributes of CAR T-cell Therapies and their Testing Methods.

Quality Target Product Profile	Critical Quality Attribute	Testing Method
Safety	Sterility	Gram stain
	Mycoplasma	Mycoplasma detection kit
	Endotoxin level	Chromogenic LAL assay
Purity	% CD3+ T-cells	Flow cytometry
	% CAR T-cells	Flow cytometry
	Residual beads	Microscopy
Identity	% CAR T-cells	Flow cytometry
Potency	IFNγ secretion in response to target cells	ELISA

LAL = limulus amebocyte lysate. CAR = chimeric antigen receptor. IFNγ = interferon-γ. Adapted from Hollyman *et al*. (2009) and Wang and Rivière (2016).

A.4. Integration into Manufacturing

The integration pathway of the activation technology described in this thesis into the manufacturing process of CAR T-cell therapies depends largely on the final format. If the goal was to integrate into a fully-closed automated system it is likely that a novel bespoke system would have to be designed; as current developed systems, such as the CliniMACS Prodigy®, are not compatible with alternative activation technologies. The economic impact of undertaking such a project should be evaluated thoroughly and compared to the potential revenue the finished product could generate - if selling the product, or the potential costs saved - if planning to both develop and implement in-house. This should take into consideration the savings made through reduced operator handling and improved safety, as well as costs incurred for installation and training new operators.

An alternative integration route may be followed if this technology was to be integrated as a single operating unit to simply replace an existing one, as this would not require the additional development and so would be faster to implement. It's compatibility with the existing units should be assessed before installation. Again, dependant on the final format, this may also give the opportunity to create a semi-automated manufacturing system.

Regardless of the route, integration of this technology into an industrial setting will require it to be subject to further validation to ensure its suitability for safe-use in a cell and gene therapy process. These may include tests on the polymer of sterility, human toxicity, leachables, and stability. Once validated, installation of equipment should be preceded with a risk assessment to highlight associated current and potential hazards. Furthermore, installation itself will require an appropriate lab-space with the necessary connections i.e. electrical sockets, and operators should be given appropriate training on how to operate the system.

A.5. Process Validation and Monitoring

Once installed, the whole manufacturing process will have to be validated to confirm the ability of the process to produce a high quality product that meets safety requirements. Critical process parameters (CPPs) are parameters which should be monitored and controlled during runs to ensure the desired quality. CPPs are identified through establishing a “design space”, to understand the impact of variations in process parameters on the CQAs of the product, this subsequently allows the definition of a “control space” in which CPPs are implemented; this is often defined though investigations using a DoE approach. CQAs of output material from batches should also be monitored to ensure that they fall within the acceptable ranges outlined. Examples of testing methods for CQAs are highlighted in **Table A.1.** Additionally, if the technology is implemented as a process change in an existing manufacturing process, outputs should be compared to the original process.

A.6. References

Elliott, P., Billingham, S., Bi, J. and Zhang, H. (2013). Quality by design for biopharmaceuticals: a historical review and guide for implementation. *Pharmaceutical Bioprocessing*, 1(1), pp.105-122.

EMA. (2004). ICH guideline Q8 (R2) on pharmaceutical development. European Medicines Agency.

EMA. (2006). ICH guideline Q9 on quality risk management. European Medicines Agency.

EMA. (2007). ICH guideline Q10 on pharmaceutical quality system. European Medicines Agency.

Hollyman, D., Stefanski, J., Przybylowski, M., Bartido, S., Borquez-Ojeda, O., Taylor, C., Yeh, R., Capacio, V., Olszewska, M., Hosey, J., Sadelain, M., Brentjens, R. and Rivière, I. (2009). Manufacturing Validation of Biologically Functional T Cells Targeted to CD19

Antigen for Autologous Adoptive Cell Therapy. *Journal of Immunotherapy*, 32(2), pp.169-180.

Wang, X. and Rivière, I. (2016). Clinical manufacturing of CAR T cells: foundation of a promising therapy. *Molecular Therapy - Oncolytics*, 3, p.16015.

B. Programs Written for Image Analysis

```
/// Crop out scale bar
//setTool("rectangle");
makeRectangle(0, 0, 1280, 958);
run("Crop");
/// Filter to removed excess image noise
run("Median...", "radius=2");
/// Remove background and convert to black and white
run("Subtract Background...", "rolling=25 sliding");
setAutoThreshold("Li dark");
//run("Threshold...");
//setThreshold(24, 255);
setOption("BlackBackground", false);
run("Convert to Mask");
run("Invert LUT");
// Seperate overlapping pores
run("Watershed");
/// Measure "Feret's diameter" of pores
run("Set Measurements...", "area perimeter feret's display redirect=None decimal=3");
run("Analyze Particles...", "size=1-Infinity pixel exclude summarize add");
roiManager("Show All");
roiManager("Measure");
```

Figure B.1. Program written to assess pore diameter and area in polymer A. Annotations are preceded with "///". Program was ran on Fiji image analysis software.

```
/// Create duplicate
run("Duplicate...", "title=Copy.tif");
/// Convert to 8-bit image
run("8-bit"); Convert to 8-bit
/// Subtract backgroung
run("Subtract Background...", "rolling=50");
/// Apply gaussian blur filter
run("Gaussian Blur...", "sigma=2");
/// Identify cells through highlighting fluorescence maxima
run("Find Maxima...", "prominence=2 output=[Single Points]");
/// Count cells (summarise maxima's)
run("Analyze Particles...", "summarize add");
```

Figure B.2. Program written to count T-cells bound to polymer A from fluorescent confocal images on Fiji image analysis software. T-cells were stained with CellTracker™ Red CMTPX Dye. Annotations are preceded with "///". Program was ran on Fiji image analysis software.

```
/// Crop out scale bar
//setTool("rectangle");
makeRectangle(1, 0, 639, 478);
run("Crop");
/// Filter to remove excess image noise
run("Median...", "radius=2");
/// Remove background and convert to black and white
run("Subtract Background...", "rolling=25 sliding");
setAutoThreshold("Li dark");
//run("Threshold...");
//setThreshold(24, 255);
setOption("BlackBackground", false);
run("Convert to Mask");
run("Invert LUT");
/// Seperate overlapping prores
run("Watershed");
/// Measure "Feret's diameter" of pores
run("Set Measurements...", "area perimeter feret's display redirect=None decimal=3");
run("Analyze Particles...", "size=1-Infinity pixel exclude summarize add");
roiManager("Show All");
roiManager("Measure");
```

Figure B.3 Program written to assess pore diameter and area in porous polymer B. Annotations are preceded with "///". Program was ran on Fiji image analysis software.

```
/// Link together images to stack
run("Concatenate...", "all_open open");
/// Convert to 8-bit image
run("8-bit");
/// Set image scale
run("Set Scale...", "distance=441 known=200 unit=µm global");
/// Set stack time intervals as 10 seconds
run("Properties...", "channels=1 slices=1 frames=180 pixel_width=0.4535147 pixel_height=0.4535147 voxel_depth=0.4587156 frame=[10 sec] global");
/// Run TrackMate plugin
run("TrackMate");
```

Figure B.4. Program written to stack multiple time-lapse confocal images of T-cells interacting with polymer B on Fiji image analysis software. Annotations are preceded with "///". Program was ran on Fiji image analysis software.

C. Fluorescence Confocal Microscopy Staining Controls

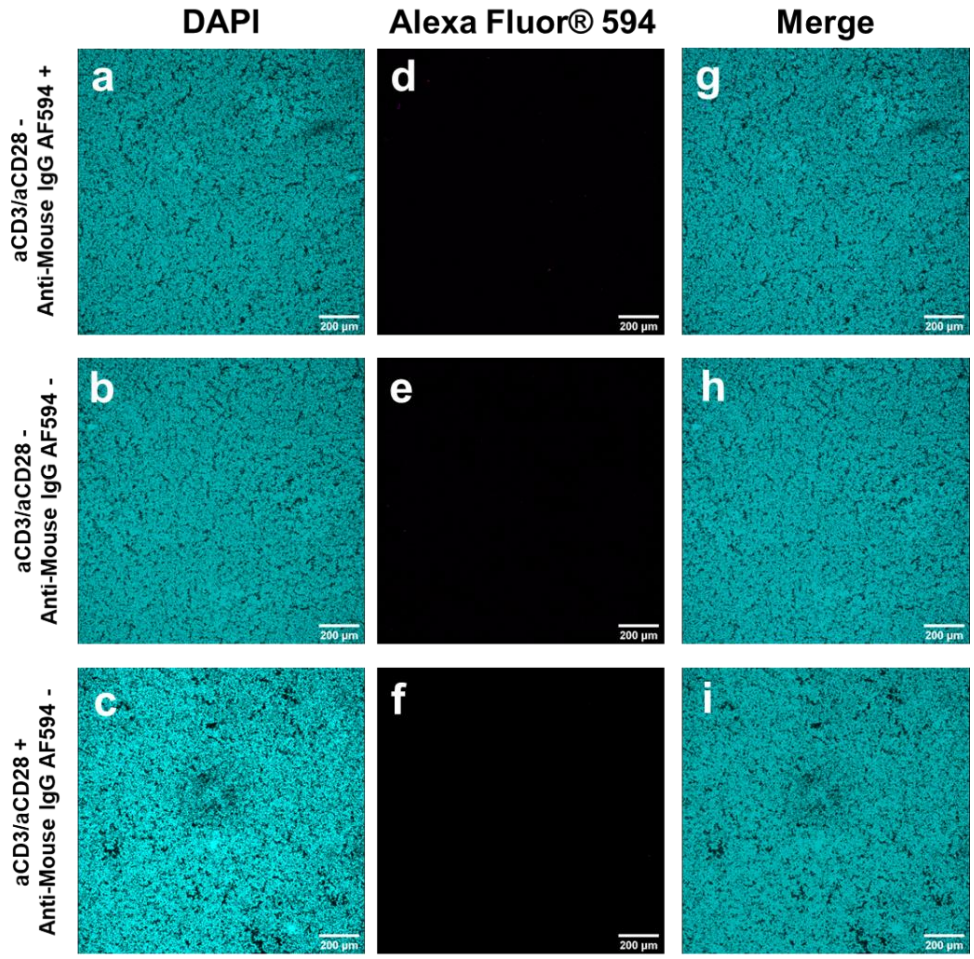

Figure C.1. Controls for the antibody attachment visualisation of polymer A. 3D fluorescent confocal microscopy images. **a - c.** Polymer A, visualised through the DAPI channel, pseudo-coloured cyan. **d - f.** Excitation = 594 nm, emission = 493 nm, used to visualise Alexa Flour® 594. **g - i.** Merged Channels. All images show a top view. Scale bars = 200 µm. Top row images (**a, d, and g**) show polymer samples that did not have aCD3 and aCD28 attached and have been incubated with anti-murine Alexa Flour® 594. Middle row images (**b, e, and h**) show polymer samples that did not have aCD3 and aCD28 attached and were not incubated with anti-murine Alexa Flour® 594. Bottom row images (**c, f, and i**) show polymer samples that had aCD3 and aCD28 attached and were not incubated with anti-murine Alexa Flour® 594.

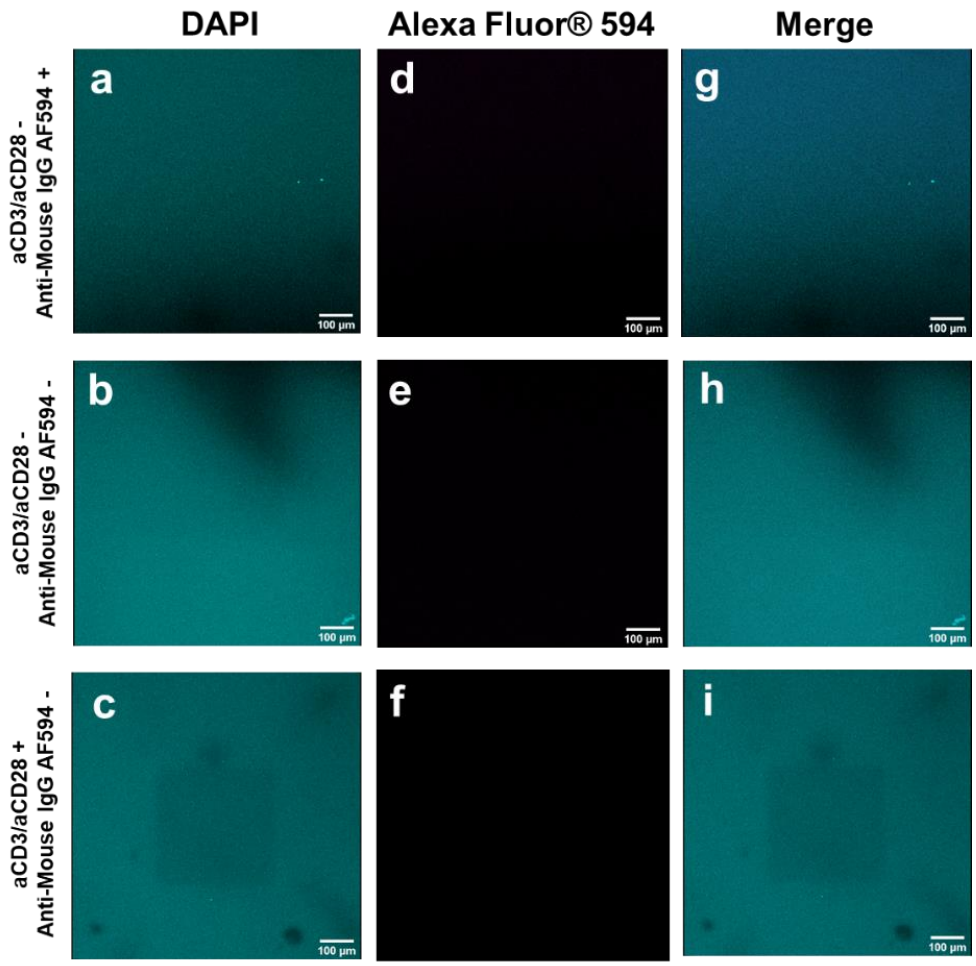

Figure C.2. Controls for the antibody attachment visualisation of non-porous polymer B. 3D fluorescent confocal microscopy images. **a - c.** Non-porous polymer B, visualised through the DAPI channel, pseudo-coloured cyan. d. e. and f. Excitation = 594 nm, emission = 493 nm, used to visualise Alexa Flour® 594. **g - i.** Merged Channels. All images show a top view. Scale bars = 100 µm. Top row images (**a, d,** and **g,**) show polymer samples that did not have aCD3 and aCD28 attached and have been incubated with anti-murine Alexa Flour® 594. Middle row images (**b, e,** and **h**) show polymer samples that did not have aCD3 and aCD28 attached and were not incubated with anti-murine Alexa Flour® 594. Bottom row images (**c, f,** and **i**) show polymer samples that had aCD3 and aCD28 attached and were not incubated with anti-murine Alexa Flour® 594.

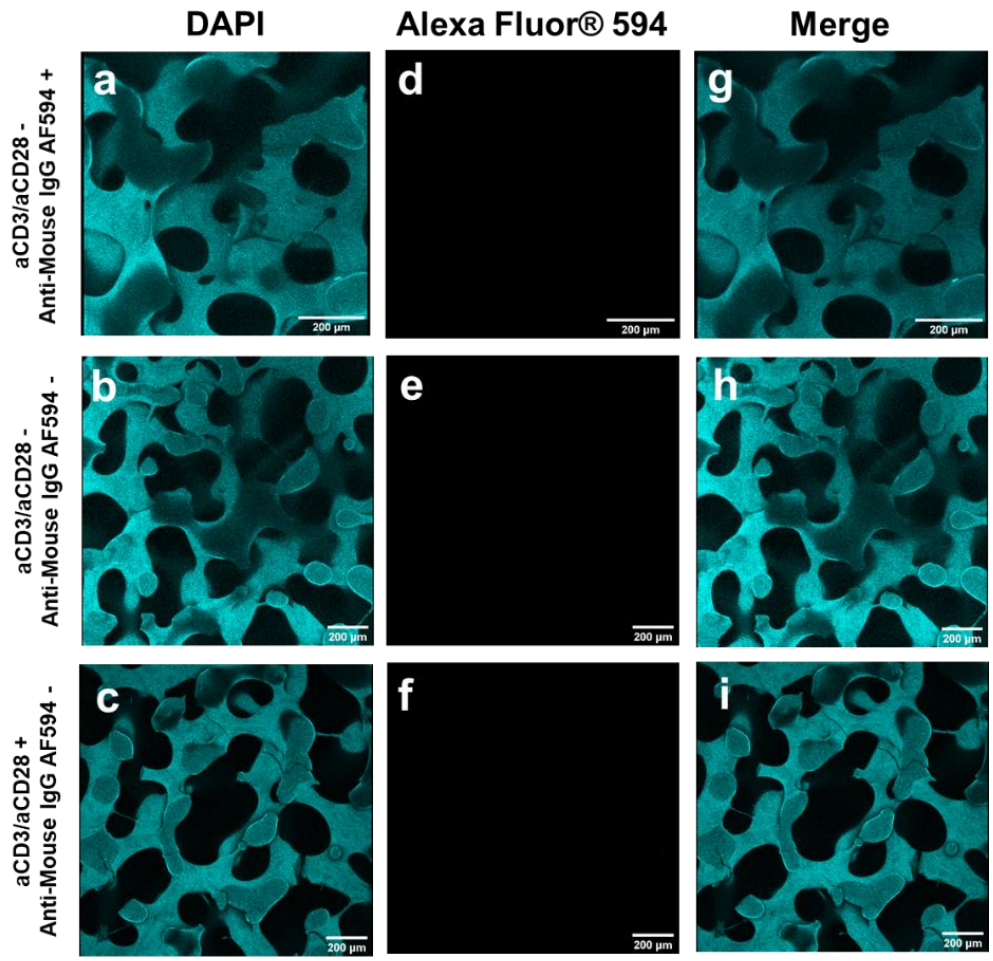

Figure C.3. Controls for the antibody attachment visualisation of porous polymer B. 3D fluorescent confocal microscopy images. **a - c.** Porous polymer B, visualised through the DAPI channel, pseudo-coloured cyan. **d - f.** Excitation = 594 nm, emission = 493 nm, used to visualise Alexa Flour® 594. **g - i.** Merged Channels. All images show a top view. Scale bars = 200 µm. Top row images (**a, d,** and **g**) show polymer samples that did not have aCD3 and aCD28 attached and have been incubated with anti-murine Alexa Flour® 594. Middle row images (**b, e,** and **h**) show polymer samples that did not have aCD3 and aCD28 attached and were not incubated with anti-murine Alexa Flour® 594. Bottom row images (**c, f,** and **i**) show polymer samples that had aCD3 and aCD28 attached and were not incubated with anti-murine Alexa Flour® 594.

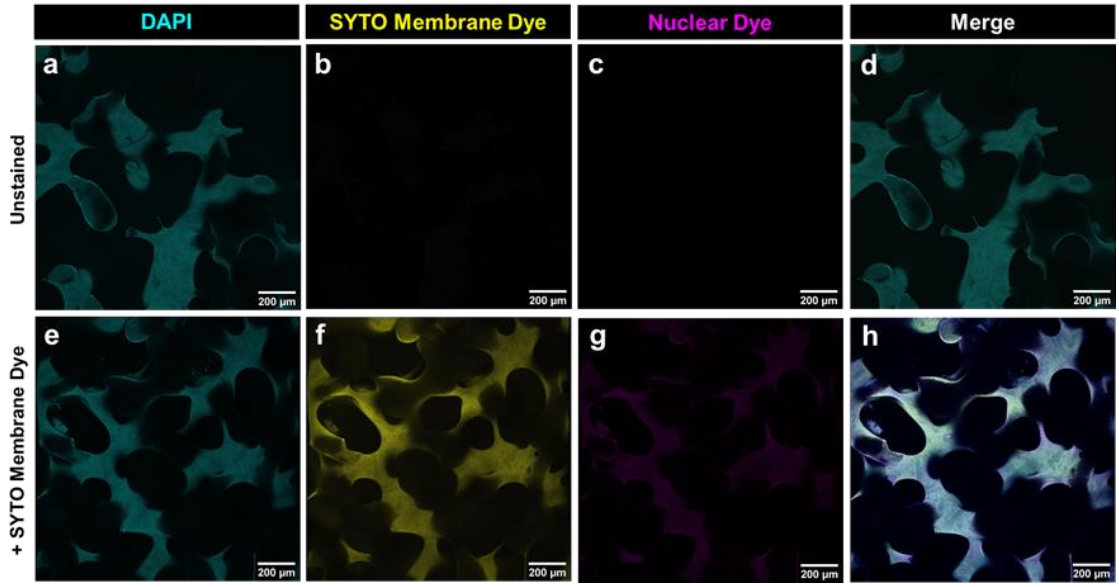

Figure C.4. Controls for T-cell visualisation on an aCD3/aCD28 polymer scaffold. 3D fluorescent confocal microscopy images. **a** and **e.** Porous polymer B visualised through the DAPI channel, pseudo-coloured cyan. **b** and **f.** Excitation = 561 nm, emission = 604 nm, used to visualise SYTO™ Deep Red Nucleic Acid Stain, pseudo-coloured yellow. **c** and **g.** Excitation = 633 nm, emission = 683 nm, used to visualise CellTracker Red CMTPX Dye, pseudo-coloured magenta. **d** and **h.** Merged channels. **a** - **d.** aCD3/aCD28 polymer scaffold with no additional stains added. **e - h.** aCD3/aCD3 polymer scaffold incubated with SYTO™ Deep Red Nucleic Acid Stain. Absorbance of dye resulted in the fluorescence of the scaffold in other channels, consequently, T-cells were identified through fluorescence in the membrane and nuclear dye channels combined with absence of fluorescence in the DAPI channel as detailed in **Section 7.3.2.7.** Scale bars = 200 µm.

D. Positive Controls for Apoptosis Assays

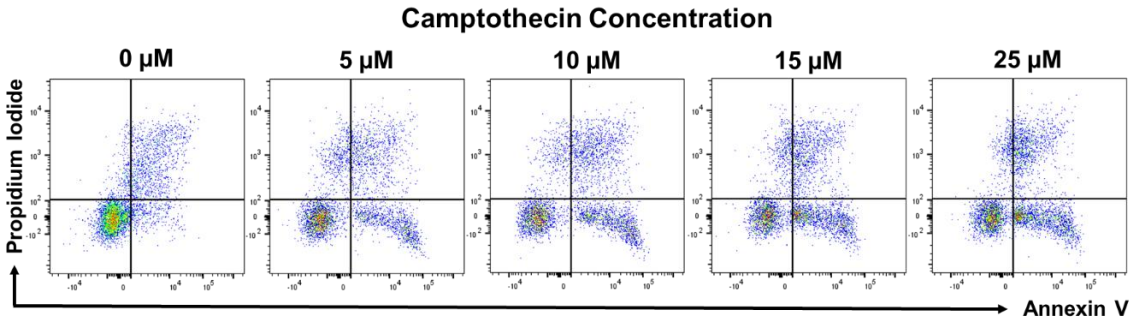

Figure D.1. Positive control for apoptosis assay performed with Jurkat T-cells. Jurkat T-cell cultures were incubated with varying concentrations of camptothecin - a known apoptosis inducer - for 6 hours before being subject to an apoptosis assay. T-cells were stained with propidium iodide and annexin V.

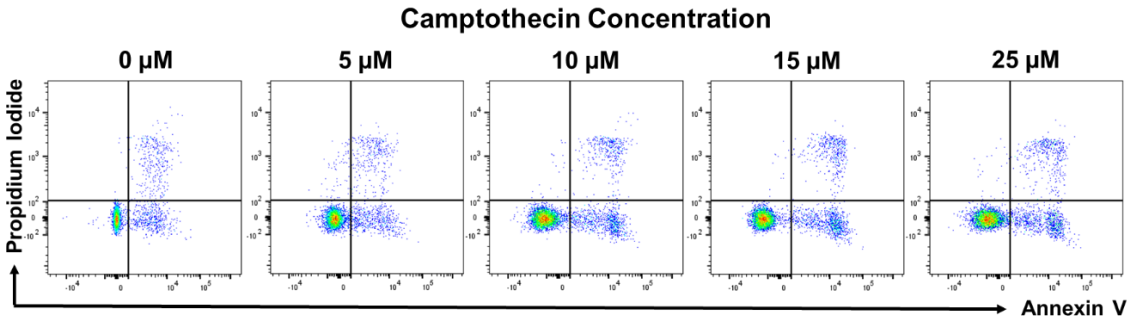

Figure D.2. Positive control for apoptosis assay performed with primary human T-cells. Primary human T-cell cultures were incubated with varying concentrations of camptothecin - a known apoptosis inducer - for 6 hours before being subject to an apoptosis assay. T-cells were stained with propidium iodide and annexin V.

E. Unstained and Isotype Controls for Flow Cytometry

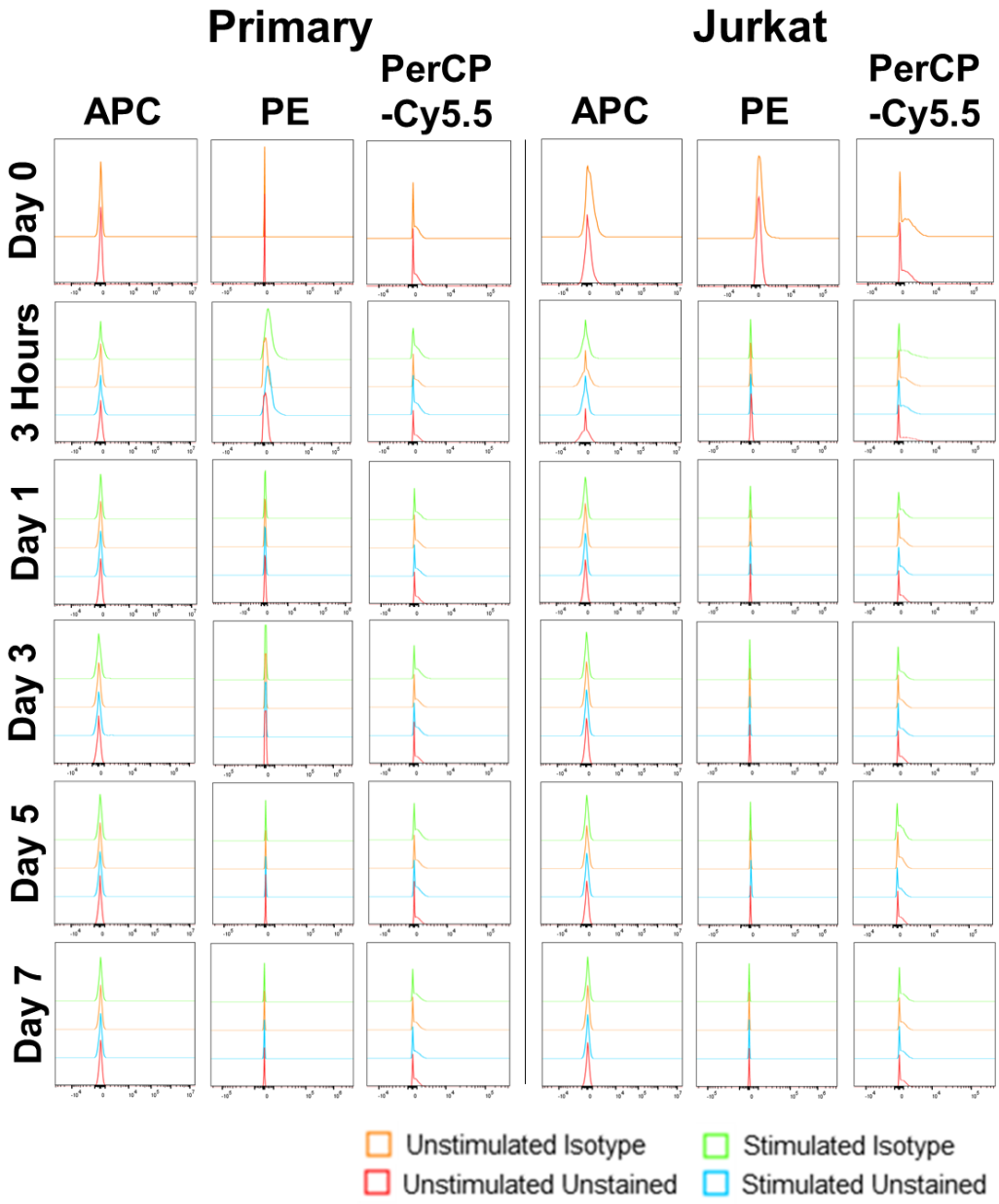

Figure E.1. Unstained and isotype controls for the comparison of activation markers on primary and Jurkat T-cells. Isotype controls were stained with: IgG1κ-APC; IgG1κ-PE; IgG1κ-PerCP-Cy5.5.

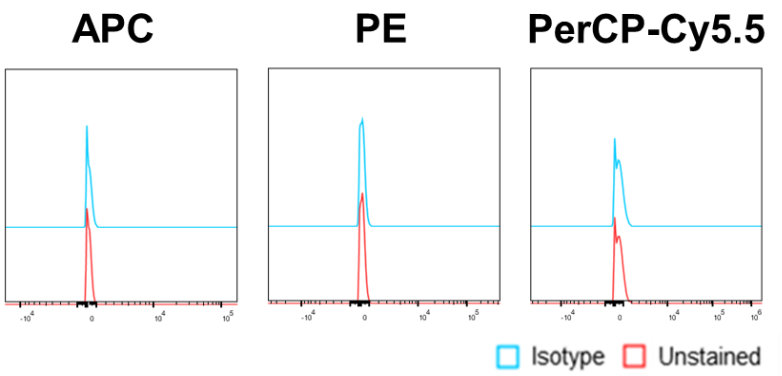

Figure E.2. Unstained and isotype controls for the assessment of activation markers expressed on T-cells exposed to aCD3/aCD28 polymer A. Isotype controls were stained with: IgG1κ-APC; IgG1κ-PE; IgG1κ-PerCP-Cy5.5.

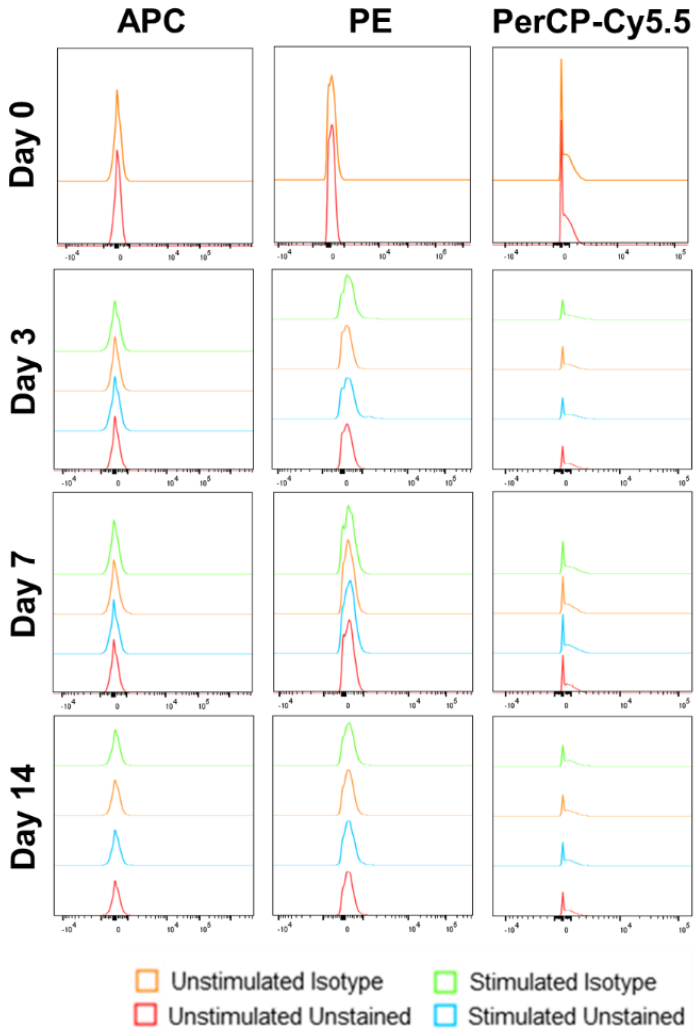

Figure E.3. Unstained and isotype controls for the assessment of activation markers expressed on T-cells exposed to non-porous aCD3/aCD28 polymer B. Isotype controls were stained with: IgG1κ-APC; IgG1κ-PE; IgG1κ-PerCP-Cy5.5.

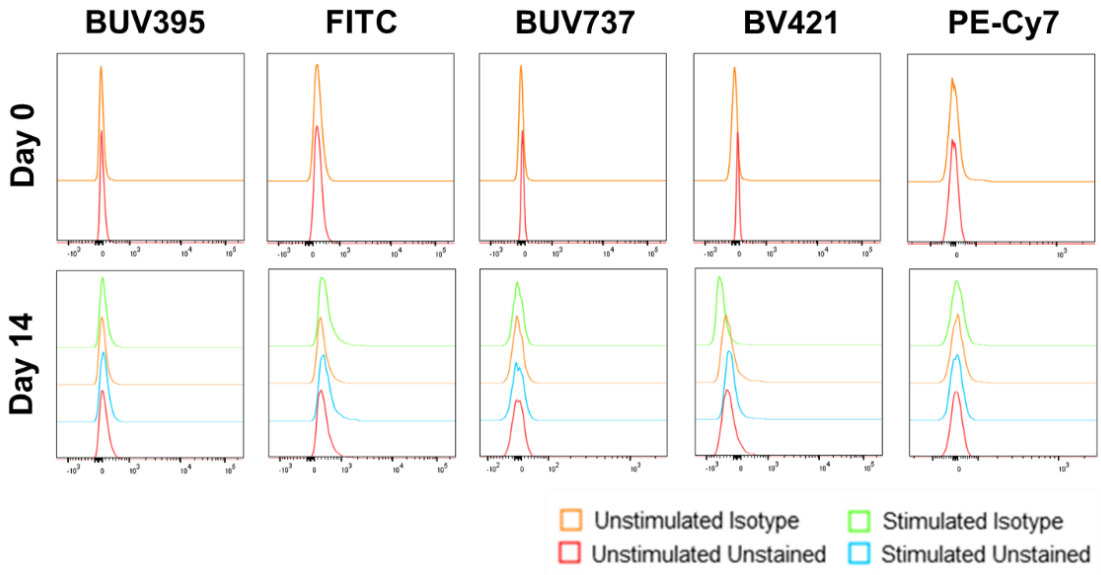

Figure E.4. Unstained and isotype controls for the classification of T-cells populations in cultures expanded with non-porous aCD3/aCD28 polymer B. Isotype controls were stained with: IgG1κ-BUV395; IgG1κ-FITC; IgG1κ-BUV737; IgG2a-BV421; IgG2a-PE-Cy7.

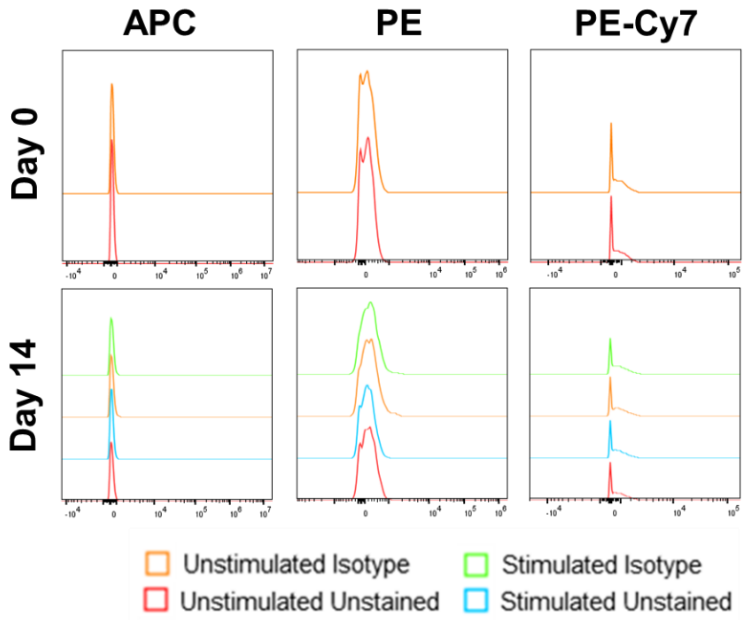

Figure D.5. Unstained and isotype controls for the assessment of exhaustion markers expressed on T-cells expanded with non-porous aCD3/aCD28 polymer B. Isotype controls were stained with IgG1κ-APC; IgG1κ-PE; IgG1κ-PE-Cy7.

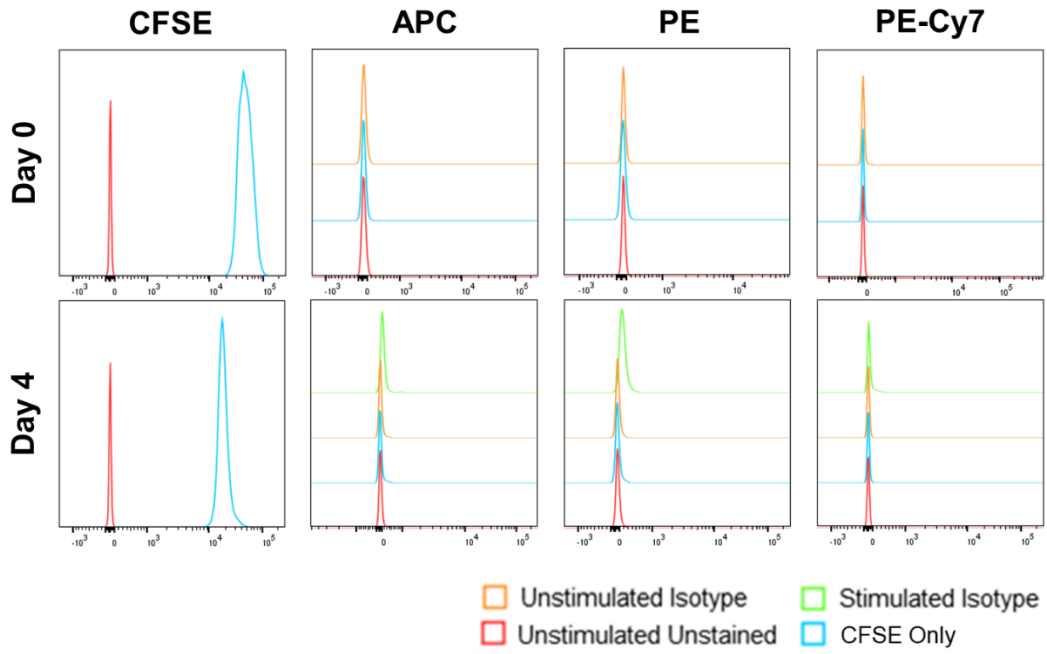

Figure E.6. Unstained and isotype controls for the classification of T-cells populations in the early stages of expansion with non-porous aCD3/aCD28 polymer B. Isotype controls were stained with: IgG1κ-APC; IgG1κ-PE; IgG1κ-PE-Cy7. CFSE only were T-cells that had been pre-stained with carboxyfluorescein succinimidyl ester (CFSE).

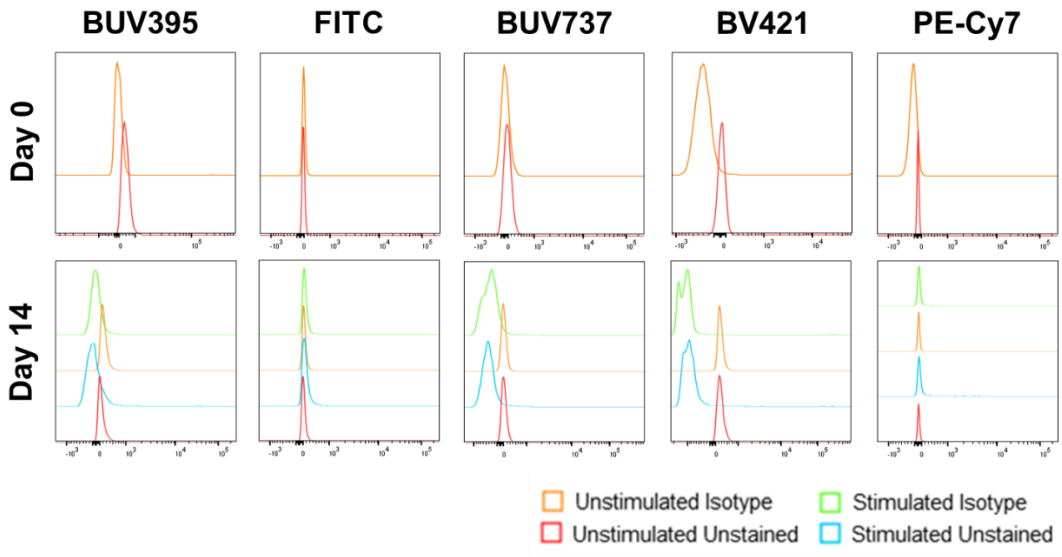

Figure E.7. Unstained and isotype controls for the classification of T-cells populations in cultures expanded with porous aCD3/aCD28 polymer B scaffolds. Isotype controls were stained with: IgG1κ-BUV395; IgG1κ-FITC; IgG1κ-BUV737; IgG2a-BV421; IgG2a-PE-Cy7.

F. Flow Cytometry Scatter Graphs and Histograms

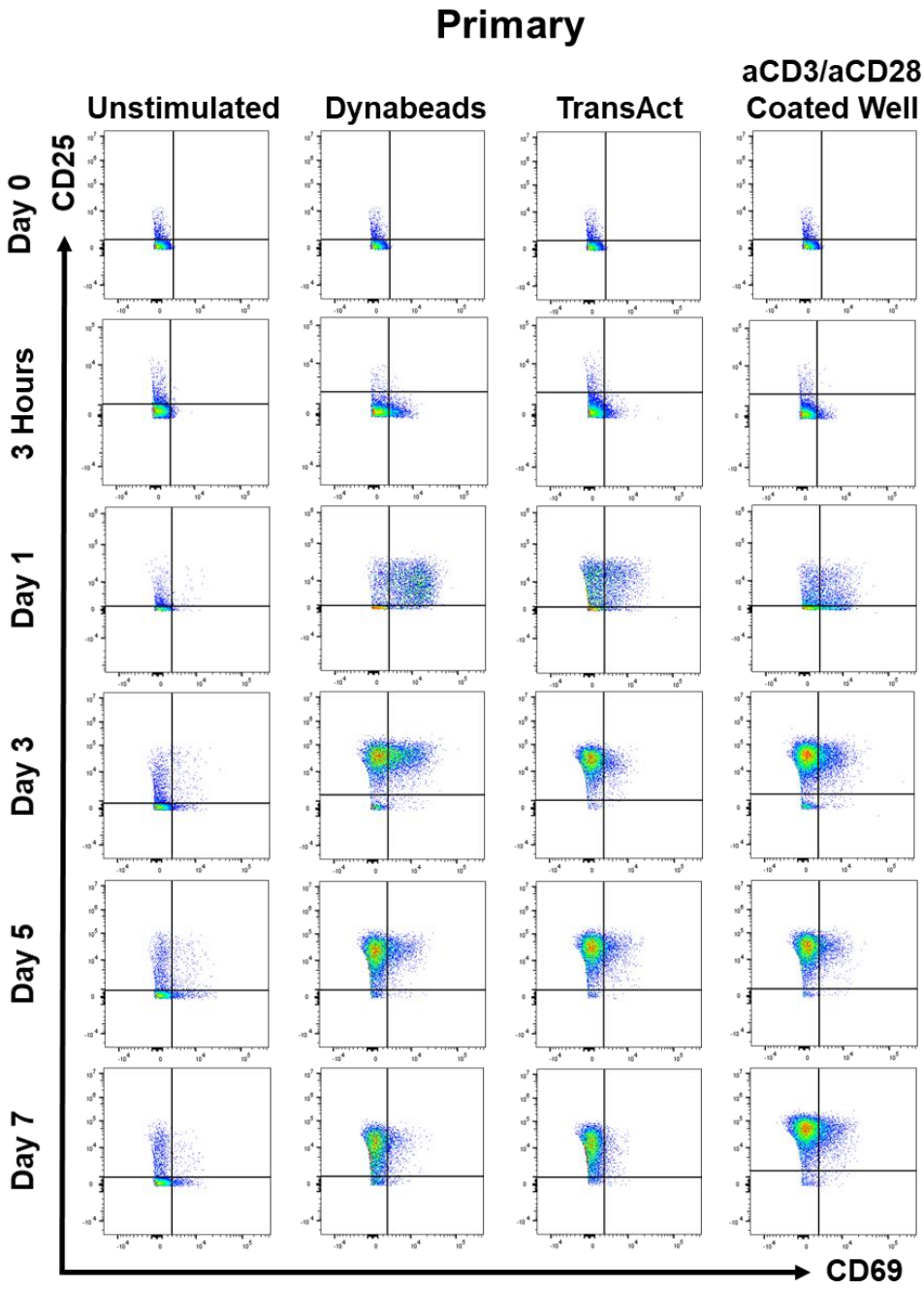

Figure F.1. Scatter graphs displaying the expression of activation markers CD69 and CD25 on primary T-cells stimulated with Dynabeads, TransAct, or an aCD3/aCD28 coated well. T-cells were stained with: fixable viability stain 520; CD3-APC; CD25-PE; CD69-PerCP-Cy5.5. Graphs are representative of n = 3.

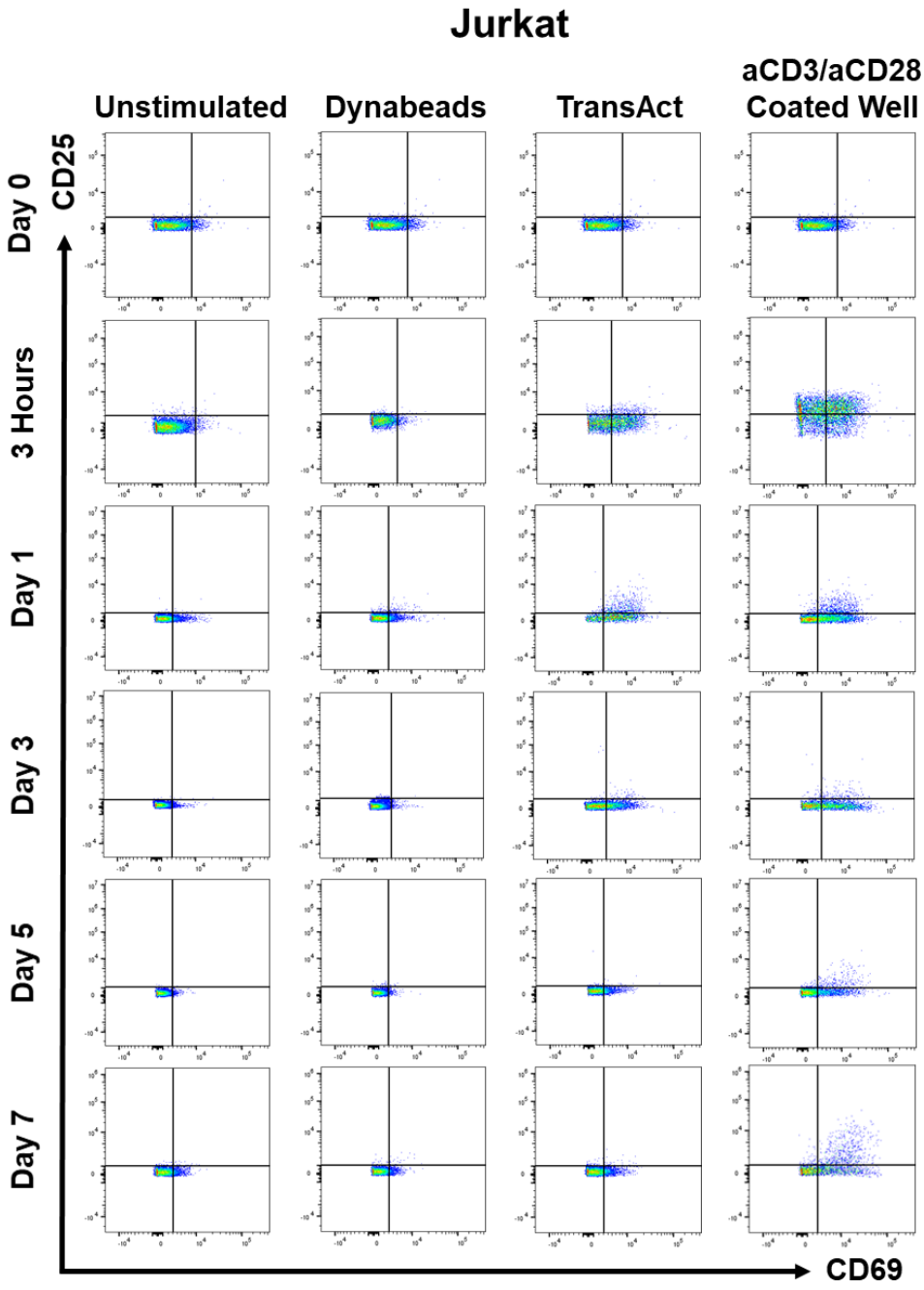

Figure F.2. Scatter graphs displaying the expression of activation markers CD69 and CD25 on Jurkat T-cells stimulated with Dynabeads, TransAct, or an aCD3/aCD28 coated well. T-cells were stained with: fixable viability stain 520; CD3-APC; CD25-PE; CD69-PerCP-Cy5.5. Graphs are representative of n = 3.

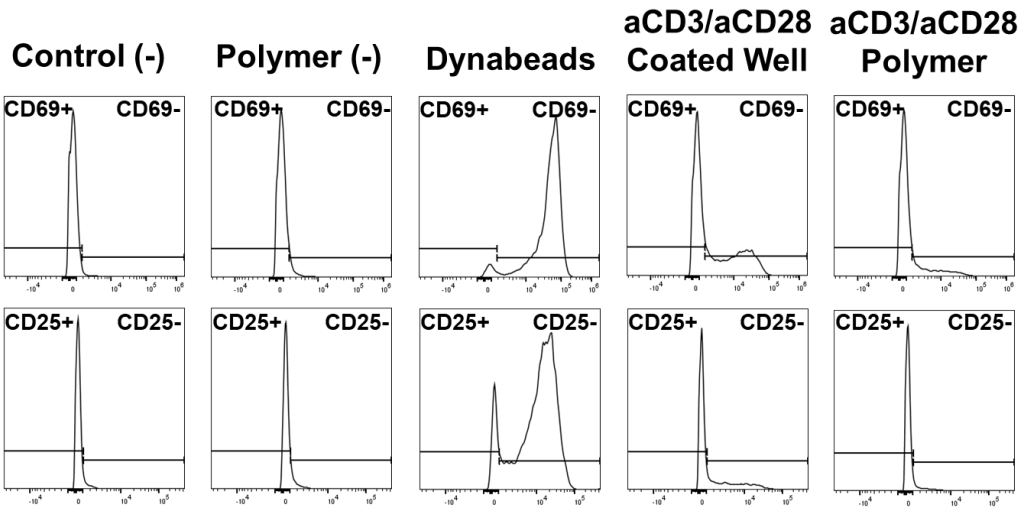

Figure F.3. Histograms displaying the expression of activation markers CD69 and CD25 on primary T-cells stimulated aCD3/aCD28 polymer A. T-cells were stained with: CD3-APC; CD25-PE; CD69-PerCP-Cy5.5. Graphs are representative of 3 donors, with 3 replicates each.

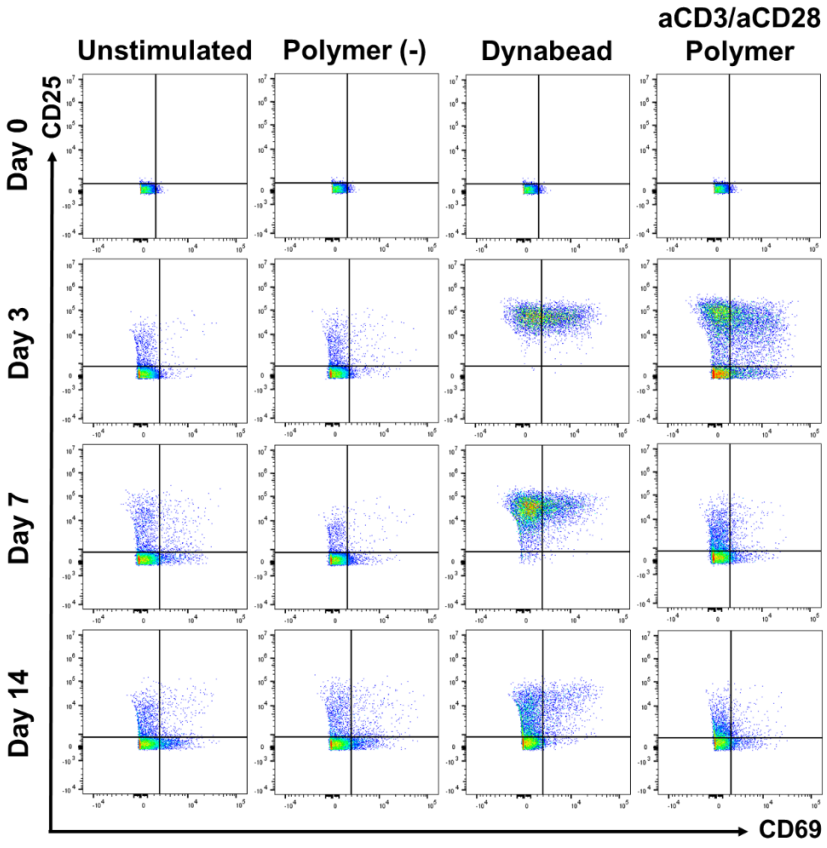

Figure F.4. Scatter graphs displaying the expression of activation markers CD69 and CD25 on T-cells stimulated with non-porous aCD3/aCD28 polymer B. T-cells were stained with: fixable viability stain 520; CD3-APC; CD25-PE; CD69-PerCP-Cy5.5. Graphs are representative of 3 donors, with 3 replicates each.

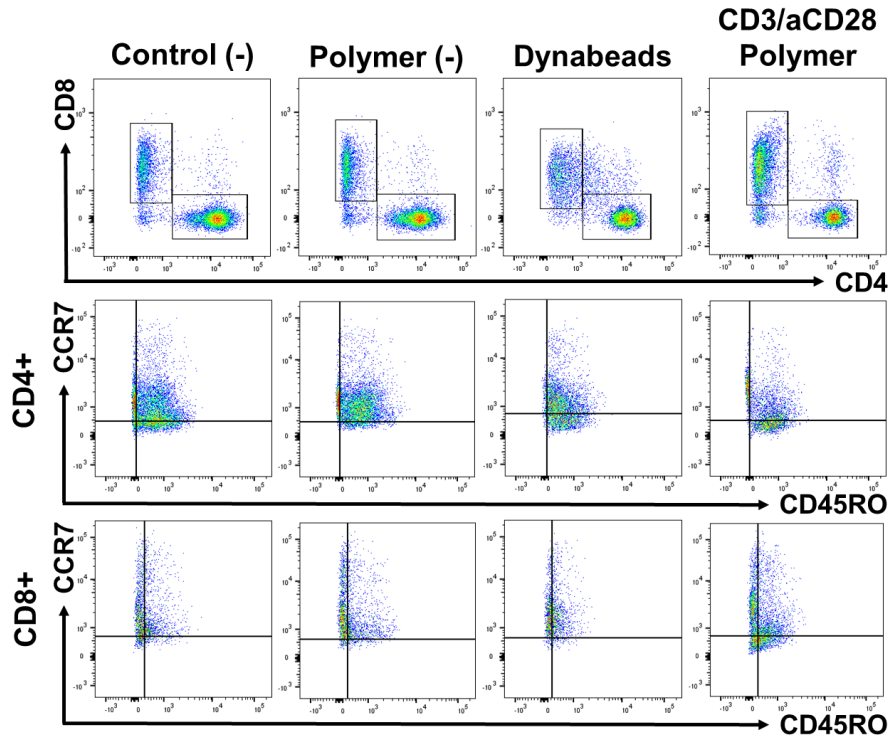

Figure F.5. Scatter graphs displaying the expression of markers for the classification of T-cell populations expanded with non-porous aCD3/aCD28 polymer B. T-cells were stained with: fixable LIVE/DEAD aqua; CD3-BUV395; CD4-FITC; CD8-BUV737; CCR7-BV421; CD45RO-PE-Cy7.Graphs are representative of 3 donors, with 3 replicates each.

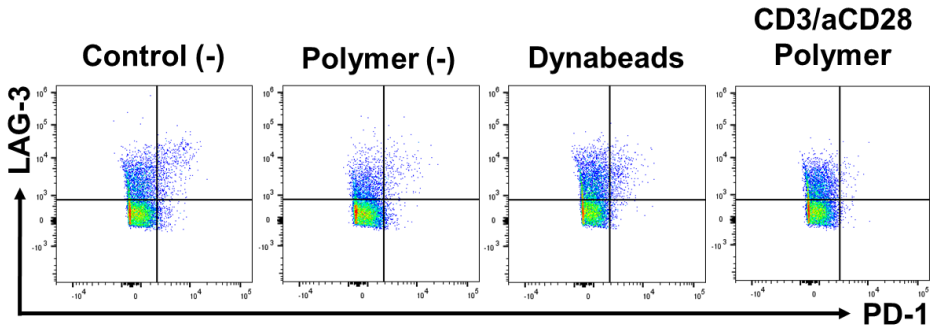

Figure F.6. Scatter graphs displaying the expression of exhaustion markers LAG-3 and PD-1 on T-cells stimulated with non-porous aCD3/aCD28 polymer B. T-cells were stained with: fixable viability stain 520; CD3-APC; LAG-3-PE; PD-1-PE-Cy7. Graphs are representative of 3 donors, with 3 replicates each.

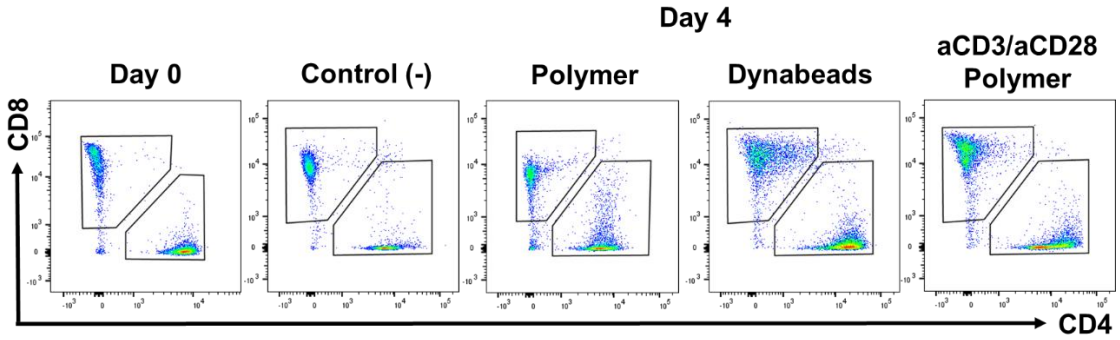

Figure F.7. Scatter graphs displaying the expression of markers for the classification of T-cell populations in the early stages of expansion with non-porous aCD3/aCD28 polymer B. T-cells were stained with: CD3-APC; CD4-PE; CD8-PE-Cy7. Graphs are representative of 3 donors, with 3 replicates each.

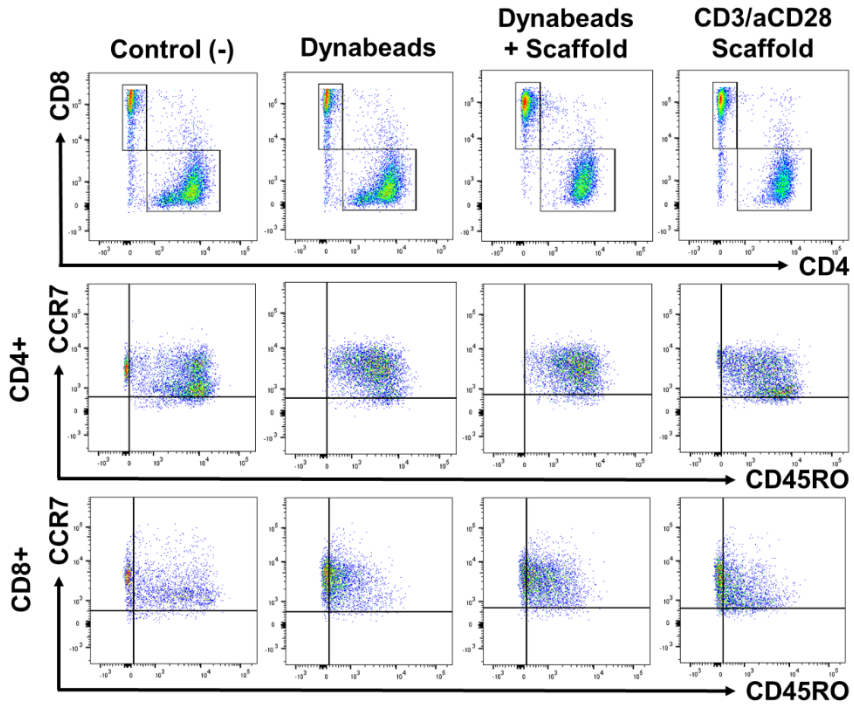

Figure F.8. Scatter graphs displaying the expression of markers for the classification of T-cell populations expanded with porous aCD3/aCD28 polymer B scaffolds. T-cells were stained with: fixable LIVE/DEAD aqua; CD3-BUV395; CD4-FITC; CD8-BUV737; CCR7-BV421; CD45RO-PE-Cy7. Graphs are representative of 3 donors, with 3 replicates each.

G. ELISA Standard Curves

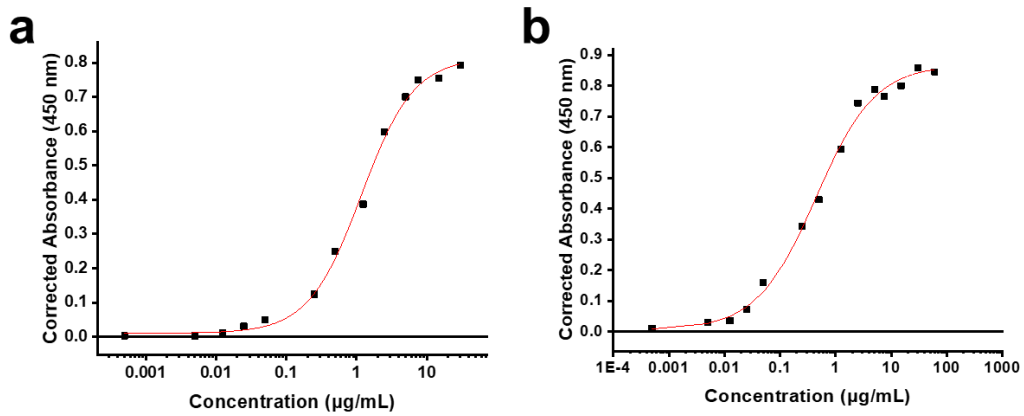

Figure G.1. Standard curves for aCD3/aCD28 ELISAs showing a four parameter logistic fit. a. Standard curve corresponding to **Figure 5.5a. b.** Standard curve corresponding to **Figure 5.5b.**

H. Control Culture Images of T-cells on Polymer B

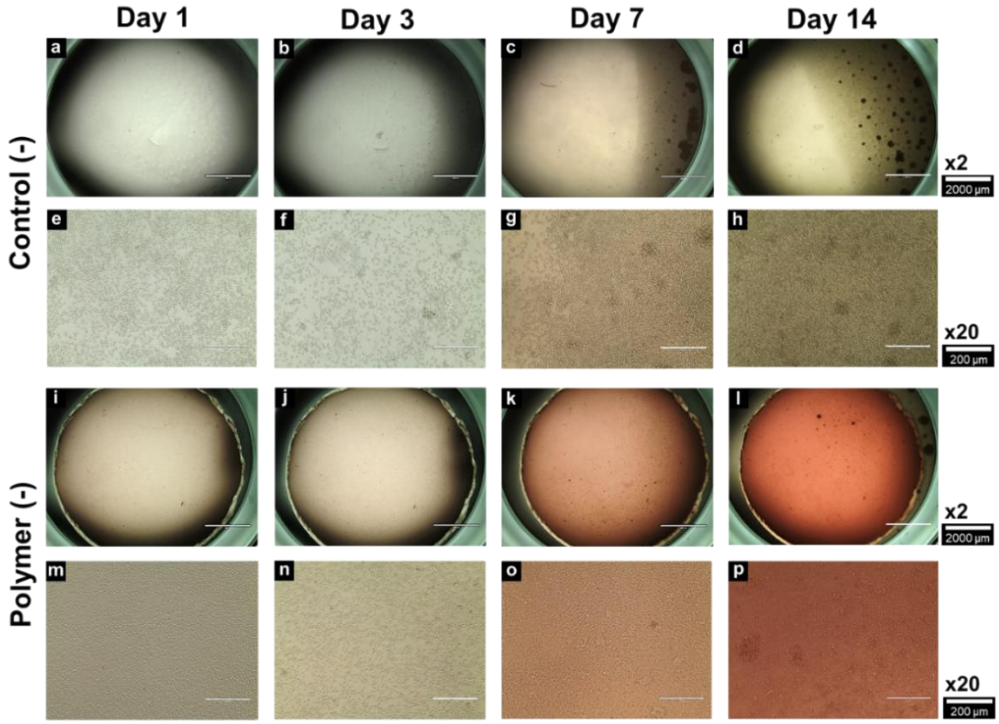

Figure H.1. Negative control images of T-cells stimulated with aCD3/aCD28 non-porous polymer B. Confocal images showing the culture morphology of T-cells in culture over 14 days. Unstimulated cultures with no addition (Control (-)) imaged at x2 (**a - d.** Scale bars = 2,000 µm), and x20 (**e - h.** Scale bars = 200 µm). T-cells in culture with polymer B without antibodies attached (Polymer (-)) imaged at x2 (**j - l.** Scale bars = 2,000 µm), and x20 (**m - p.** Scale bars = 200 µm). Images are representative of 3 donors, with 3 replicates each.

I. Preliminary Scale-up and Perfusion Attempt with an aCD3/aCD28 Polymer B Scaffold

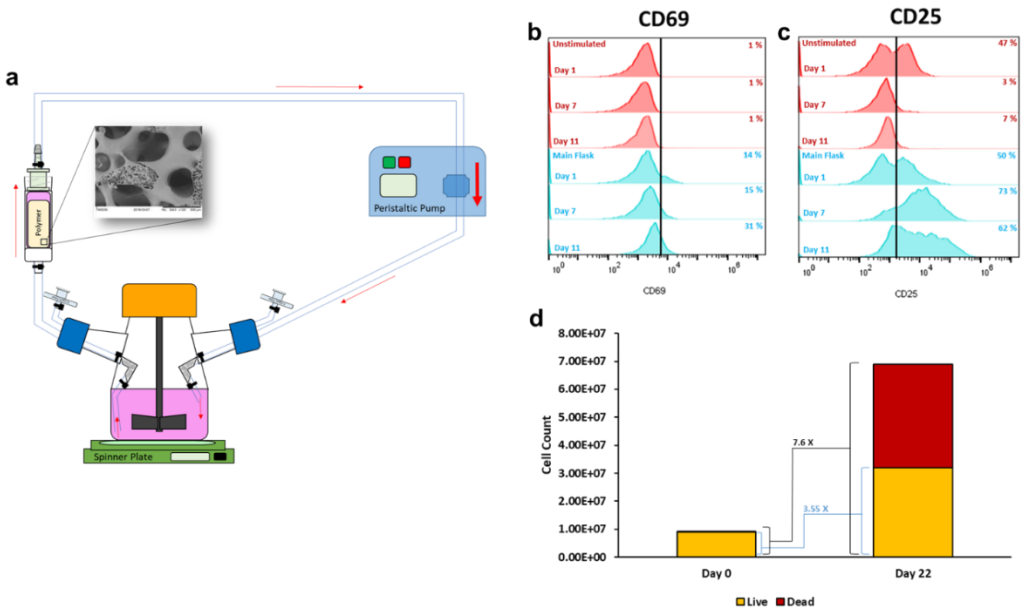

Figure I.1. Preliminary scale-up and perfusion attempt with an aCD3/aCD28 polymer B scaffold. a. Diagram of set-up. Porous aCD3/aCD28 polymer B scaffold is set with a plastic casing which is attached to a stirred flask via silicon tubing. Media and T-cells are repeatedly circulated from the stirred flask into the polymer scaffold using a peristaltic pump which is attached to the tubing. (**b** and **c**) Percentage of T-cells expressing activation markers CD69 (**b**) and CD25 (**c**). T-cells were harvested from the main flask during expansion. Increases in both markers were found. **d.** Expansion of T-cells at day 22 of culture. Total cell count gives a 7.6-fold expansion, however, when taking into account only live cells, the expansion is 3.6-fold.